Defense Nuclear Agency
Alexandria, VA 22310-3398

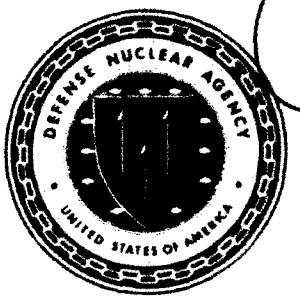

DNA-TR-92-37-V1

Chernobyl Doses

Volume 1—Analysis of Forest Canopy Radiation Response from Multispectral Imagery and the Relationship to Doses

Gene E. McClellan
George H. Anno
F. Ward Whicker
Pacific-Sierra Research Corp.
2901 28th Street
Santa Monica, CA 90405-2938

September 1994

"Original contains color plates: All DTIC reproductions will be in black and white"

Technical Report

CONTRACT No. DNA 001-87-C-0104

Approved for public release; distribution is unlimited.

Destroy this report when it is no longer needed. Do not return to sender.

PLEASE NOTIFY THE DEFENSE NUCLEAR AGENCY, ATTN: CSTI, 6801 TELEGRAPH ROAD, ALEXANDRIA, VA 22310-3398, IF YOUR ADDRESS IS INCORRECT, IF YOU WISH IT DELETED FROM THE DISTRIBUTION LIST, OR IF THE ADDRESSEE IS NO LONGER EMPLOYED BY YOUR ORGANIZATION.

DISTRIBUTION LIST UPDATE

This mailer is provided to enable DNA to maintain current distribution lists for reports. (We would appreciate your providing the requested information.)

☐ Add the individual listed to your distribution list.

☐ Delete the cited organization/individual.

☐ Change of address.

NOTE:
Please return the mailing label from the document so that any additions, changes, corrections or deletions can be made easily. For distribution cancellation or more information call DNA/IMAS (703) 325-1036.

NAME: _____

ORGANIZATION: _____

OLD ADDRESS	CURRENT ADDRESS
_____	_____
_____	_____
_____	_____

TELEPHONE NUMBER: ( ) _____

DNA PUBLICATION NUMBER/TITLE	CHANGES/DELETIONS/ADDITIONS, etc.) *(Attach Sheet if more Space is Required)*
_____	_____
_____	_____
_____	_____

DNA OR OTHER GOVERNMENT CONTRACT NUMBER: _____

CERTIFICATION OF NEED-TO-KNOW BY GOVERNMENT SPONSOR (if other than DNA):

SPONSORING ORGANIZATION: _____

CONTRACTING OFFICER OR REPRESENTATIVE: _____

SIGNATURE: _____

CUT HERE AND RETURN

DEFENSE NUCLEAR AGENCY
ATTN: IMAS
6801 TELEGRAPH ROAD
ALEXANDRIA, VA 22310-3398

DEFENSE NUCLEAR AGENCY
ATTN: IMAS
6801 TELEGRAPH ROAD
ALEXANDRIA, VA 22310-3398

DISCLAIMER NOTICE

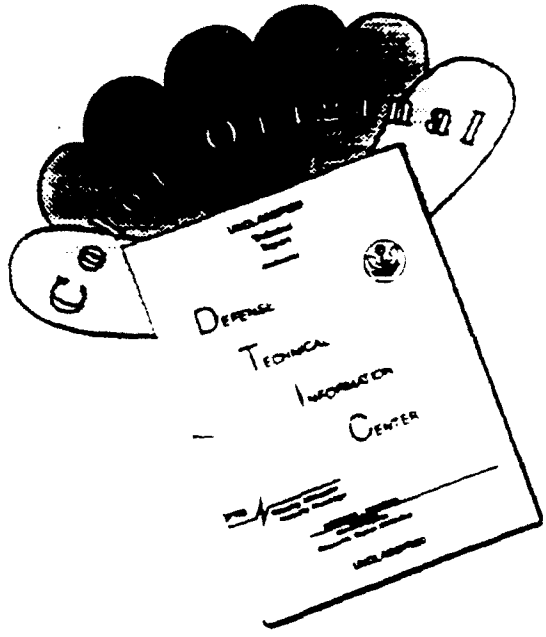

THIS DOCUMENT IS BEST QUALITY AVAILABLE. THE COPY FURNISHED TO DTIC CONTAINED A SIGNIFICANT NUMBER OF COLOR PAGES WHICH DO NOT REPRODUCE LEGIBLY ON BLACK AND WHITE MICROFICHE.

REPORT DOCUMENTATION PAGE

Form Approved
OMB No. 0704-0188

1. AGENCY USE ONLY (Leave blank)	2. REPORT DATE	3. REPORT TYPE AND DATES COVERED
	940901	Technical 870929 – 930930

4. TITLE AND SUBTITLE
Chernobyl Doses
Volume 1—Analysis of Forest Canopy Radiation Response from Multispectral Imagery and the Relationship to Doses

5. FUNDING NUMBERS
C - DNA 001-87-C-0104
PE - 62715H
PR - RM
TA - RH
WU - DH026130

6. AUTHOR(S)
Gene E. McClellan, George H. Anno, and F. Ward Whicker

7. PERFORMING ORGANIZATION NAME(S) AND ADDRESS(ES)
Pacific-Sierra Research Corp.
2901 28th Street
Santa Monica, CA 90405-2938

8. PERFORMING ORGANIZATION REPORT NUMBER
PSR Report 2251

9. SPONSORING/MONITORING AGENCY NAME(S) AND ADDRESS(ES)
Defense Nuclear Agency
6801 Telegraph Road
Alexandria, VA 22310-3398
RAEM/Kehlet

10. SPONSORING/MONITORING AGENCY REPORT NUMBER
DNA-TR-92-37-V1

11. SUPPLEMENTARY NOTES
This work was sponsored by the Defense Nuclear Agency under RDT&E RMC Code B4662D RM RH 00038 STRP 3500A 25904D.

12a. DISTRIBUTION/AVAILABILITY STATEMENT
Approved for public release; distribution is unlimited.

12b. DISTRIBUTION CODE

13. ABSTRACT *(Maximum 200 words)*

This volume of the report *Chernobyl Doses* presents details of a new, quantitative method for remotely sensing ionizing radiation dose to vegetation. Analysis of Landsat imagery of the area within a few kilometers of the Chernobyl nuclear reactor station provides maps of radiation dose to pine forest canopy resulting from the accident of April 26, 1986. Detection of the first date of significant, persistent deviation from normal of the spectral reflectance signature of pine foliage produces contours of radiation dose in the 20 to 80 Gy range extending up to 4 km from the site of the reactor explosion. The effective duration of exposure for the pine foliage is about 3 weeks. For this exposure time, the LD_{50} of *Pinus sylvestris* (Scotch pine) is about 23 Gy. The practical lower dose limit for the remote detection of radiation dose to pine foliage with the Landsat Thematic Mapper is about 5 Gy or 1/4 of the LD_{50}.

14. SUBJECT TERMS
Chernobyl, Dose, Forest Damage, Conifer Stress, Fallout, Change Detection, Ionizing Radiation, Multispectral Imagery

15. NUMBER OF PAGES
226

16. PRICE CODE

17. SECURITY CLASSIFICATION OF REPORT	18. SECURITY CLASSIFICATION OF THIS PAGE	19. SECURITY CLASSIFICATION OF ABSTRACT	20. LIMITATION OF ABSTRACT
UNCLASSIFIED	UNCLASSIFIED	UNCLASSIFIED	SAR

CLASSIFIED BY:

N/A since Unclassified.

DECLASSIFY ON:
N/A since Unclassified.

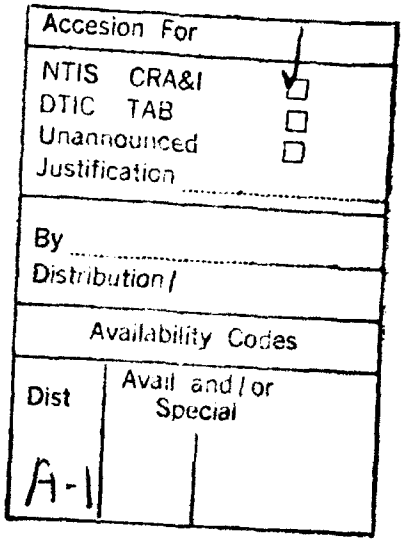

EXECUTIVE SUMMARY

This volume of the report *Chernobyl Doses* presents details of a new, quantitative method for remotely sensing ionizing radiation dose to vegetation. The method uses a time series of multispectral images taken from an orbital or airborne platform to reveal changes in spectral reflectance of foliage that has been exposed to radiation. The threshold of detection is about 1/4 of the median lethal dose (LD_{50}) of the dominant plant species .

Figure S-1 illustrates the sequence of events leading to detection of radiation dose. The effective duration of the vegetation exposure is determined by the radioactive decay rate of the fallout deposited on the foliage and the rate at which fallout is removed from the foliage by weathering. The accumulated dose during this exposure time causes biological damage at the cellular level in plant tissues. At high doses (several times the LD_{50}), radiation damage to multiple tissues kills vegetation in a short time, a matter of one or two weeks for pine trees. At lower doses, radiation damage to foliage is significant only for growth tissue at the tips of branches. Such damage takes more time to change the appearance of foliage. The dose dependence of the delay until the onset of observable foliage response provides the basis for remote detection of radiation dose.

Figure S-2 shows a map of the foliage doses received by the pine forest canopy near the site of the Chernobyl nuclear power station as derived from analysis of a time series of eleven Landsat Thematic Mapper images spanning a period from one year before to two years after the explosion of the Unit 4 reactor on April 26, 1986. Table S-1 shows the doses for the three contours drawn on the map as well as the dose range between contours and the total area within each contour.

Individual pixels, representing 25 m squares of pine forest, are color-coded according to the legend on the map, which shows the image number of first-observed, persistent deviation from normal of the spectral signature of the pixel. Table S-2 provides a conversion of this image number to a radiation dose range. The dose is quoted as a range since the first observable response may have occurred at any time during the interval between the date of the image showing first response and the date of the previous image. Black areas on the map are either not pine forest or were cleared of pine forest before showing a radiation response. Gray pixels on the map correspond to pine forest that appears normal at the end of the two year observation period. Although not indicated on the map, some of these pixels showed a transient radiation response corresponding to doses less than about 20 Gy.

The methodology developed during this effort and the resulting data contribute to an improved understanding of the effects of high levels of fallout radioactivity on vegetation and, especially, on the remote observation of radiation-induced foliage response and the extraction of dose estimates from those observations. The results aid in the understanding of the consequences to personnel of

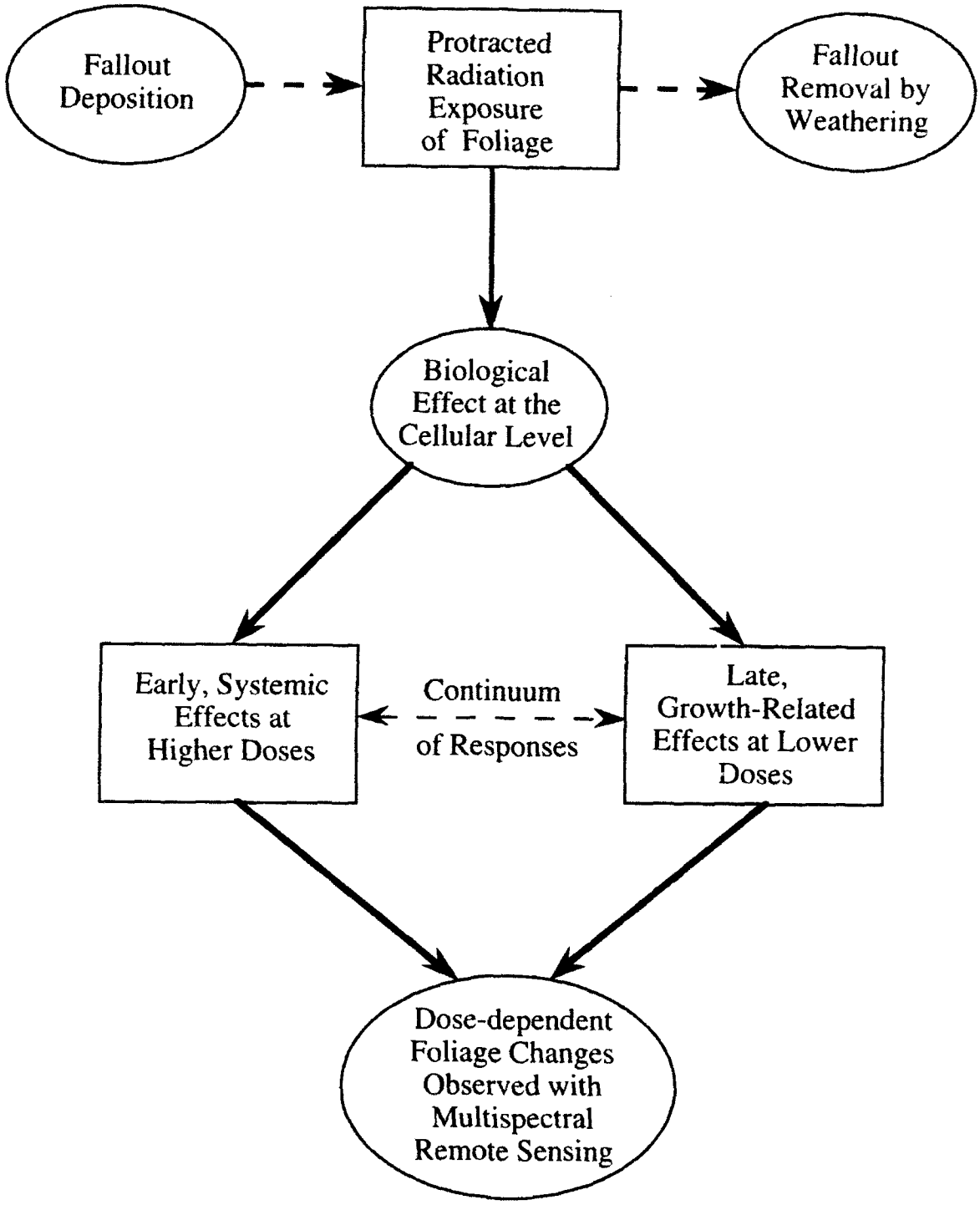

Figure S-1. Sequence of events that enables remote detection of the exposure of vegetation to ionizing radiation and calculation of the dose from the time of resulting foliage changes relative to the start of exposure.

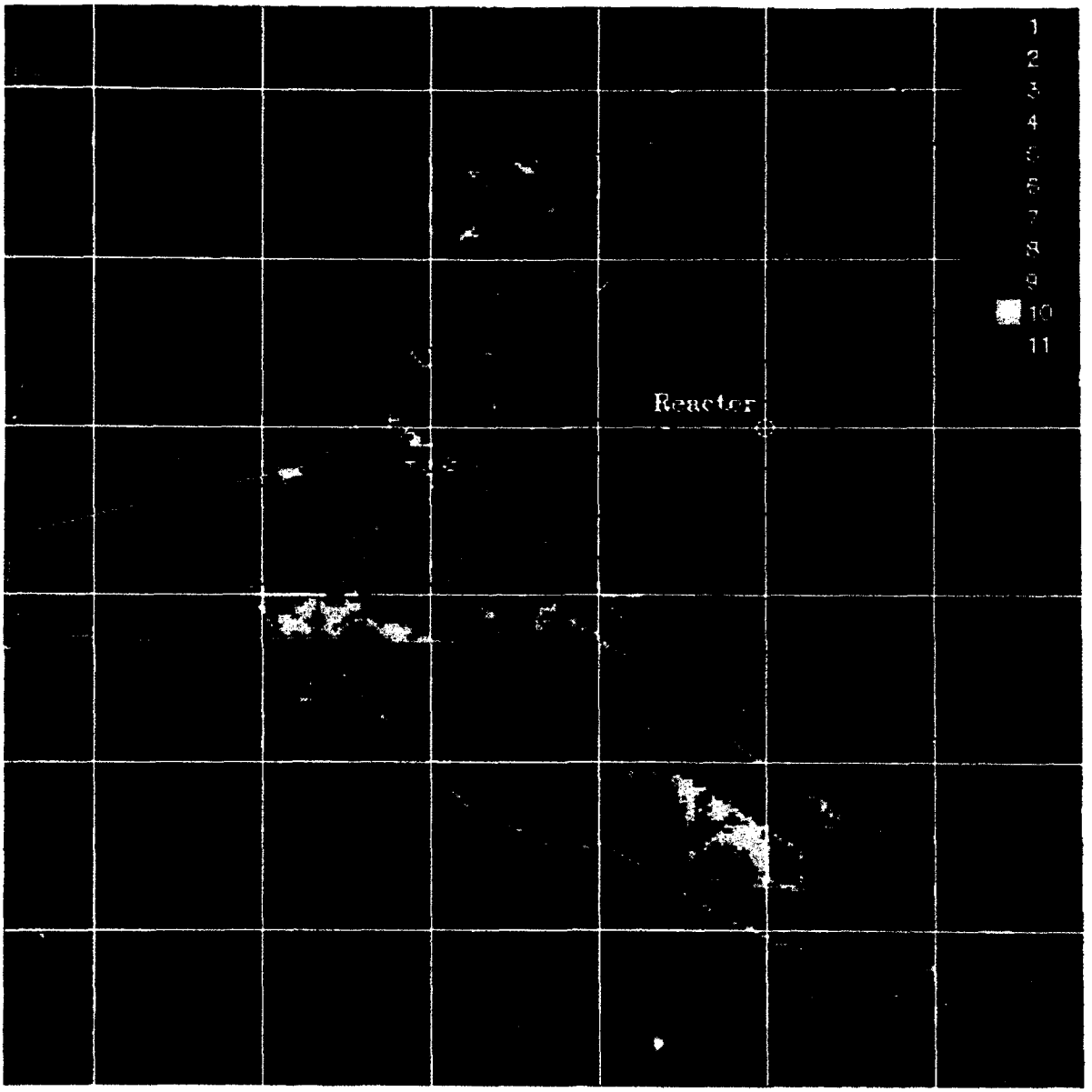

Figure S-2. Chernobyl radiation dose contours derived from foliage changes in pine forest canopy observed with the Landsat Thematic Mapper multispectral imaging device; 1 km grid lines originating at the Unit 4 reactor site. See Table S-1 for dose values.

in an area contaminated by radioactive fallout and the impact of vegetation on that

Table S-1. Description of contours drawn in Figure S-2.

ontour	*Pine foliage response time at contour (days)*	*Dose at contour (Gy)*	*Dose range within contour (Gy)*	*Cumulative enclosed area (km^2)*
Inner (blue)	35	54	54 - 80	0.8
Middle (green)	172	30	30 - 54	2.9
Outer (yellow)	499	20	20 - 30	14.5

The final section of this report lists recommendations for improving and extending the results presented herein. The recommendation of primary importance is the establishment of a cooperative effort with scientists of the former Soviet Union to compare the satellite data with ground studies made at specific locations within a few kilometers of the Chernobyl power plant. The comparison of the image analysis with other data in Section 8 is encouraging but only qualitative because of the unavailability of data with the temporal and spatial resolution of the satellite images. We believe better data exists (Gamache, 1993); furthermore, some of the affected forest is probably still standing. Histological examination of exposed pine trees observed in the imagery would be of great value both for interpreting the imagery and interpreting the histological data.

Table S-2. Pine foliage doses corresponding to first detected response at the times of the 9 postaccident images (Images 1 and 2 are preaccident).

Image number	*Time postaccident (days)*	*Dose (Gy)*
3	3	>133
4	12	80 - 133
5	28	59 - 80
6	35	54 - 59
7	172	30 - 54
8	220	28 - 30
9	380	23 - 28
10	499	21 - 23
11	763	18 - 21

PREFACE

This volume is the first of three volumes composing the final report to the Defense Nuclear Agency (DNA) for contract DNA001-87-C-0104, Chernobyl Doses. In addition to summarizing investigations carried out by Pacific-Sierra Research Corporation (PSR) under that contract, this volume presents the analytical work that connects satellite multispectral observations of pine forests around Chernobyl to the nuclear radiation dose received by the trees as a consequence of the reactor accident of 26 April 1986. Volume 2, *Conifer Stress Near Chernobyl Derived from Landsat Imagery*, describes the acquisition and processing of Landsat imagery of the area containing the Chernobyl Nuclear Reactor Station and presents the exploratory analysis of the imagery using PSR's proprietary Hyperscout™ change detection algorithm. Volume 3, *Habitat and Vegetation Near the Chernobyl Nuclear Reactor Station* presents a detailed exposition on the soils, climate, and vegetation of the Poles'ye region of the Ukraine and Belorussia with emphasis on the area around Chernobyl. This data provides background for interpretation of the satellite imagery.

The authors wish to acknowledge Frank Thomas of PSR who pointed out the possibility of observing radiation effects on vegetation near Chernobyl with multispectral imagery. They also wish to recognize the considerable computational expertise of Leigh Matheson of PSR who implemented the image processing and analysis described in this report and the skillful manuscript preparation by Kathy Howell. Dr. Gerald Gamache was helpful in providing data he obtained in Ukraine.

The authors wish to acknowledge the technical monitor of this project, Robert W. Young of DNA's Radiation Policy Division, for his support and encouragement during this work. Dr. Young was assisted first by Major Bruce West and then by Major Robert Kehlet. The authors also wish to acknowledge Dr. Marvin Atkins and Dr. David Auton of DNA whose interest made this work possible.

CONVERSION TABLE

Conversion factors for U.S. customary to metric (SI) units of measurement

To Convert From	To	Multiply
angstrom	meters (m)	1.000 000 X E-10
atmosphere (normal)	kilo pascal (kPa)	1.013 25 X E+2
bar	kilo pascal (kPa)	1.000 000 X E+2
barn	meter^2 (m^2)	1.000 000 X E-28
British Thermal unit (thermochemical)	joule (J)	1.054 350 X E+3
calorie (thermochemical)	joule (J)	4.184 000
cal (thermochemical)/cm^2	mega joule/m^2(MJ/m^2)	4.184 000 X E-2
curie	giga becquerel (GBq)*	3.700 000 X E+1
degree (angle)	radian (rad)	1.745 329 X E-2
degree Fahrenheit	degree kelvin (K)	$t_K=(t^\circ f + 459.67)/1.8$
electron volt	joule (J)	1.602 19 X E-19
erg	joule (J)	1.000 000 X E-7
erg/second	watt (W)	1.000 000 X E-7
foot	meter (m)	3.048 000 X E-1
foot-pound-force	joule (J)	1.355 818
gallon (U.S. liquid)	meter^3 (m^3)	3.785 412 X E-3
inch	meter (m)	2.540 000 X E-2
jerk	joule (J)	1.000 000 X E+9
joule/kilogram (J/Kg) (radiation dose absorbed)	Gray (Gy)	1.000 000
kilotons	terajoules	4.183
kip (1000 lbf)	newton (N)	4.448 222 X E+3
kip/inch^2 (ksi)	kilo pascal (kPa)	6.894 757 X E+3
ktap	newton-second/m^2 (N-s/m^2)	1.000 000 X E+2
micron	meter (m)	1.000 000 X E-6
mil	meter (m)	2.540 000 X E-5
mile (international)	meter (m)	1.609 344 X E+3
ounce	kilogram (kg)	2.834 952 X E-2
pound-force (lbf avoirdupois)	newton (N)	4.448 222
pound-force inch	newton-meter (N·m)	1.129 848 X E-1
pound-force/inch	newton/meter (N/m)	1.751 268 X E+2
pound-force/foot^2	kilo pascal (kPa)	4.788 026 X E-2
pound-force/inch^2 (psi)	kilo pascal (kPa)	6.894 757
pound-mass (lbm avoirdupois)	kilogram (kg)	4.535 924 X E-1
pound-mass-foot^2 (moment of inertia)	kilogram-meter^2 (kg·m^2)	4.214 011 X E-2
pound-mass/foot^3	kilogram/meter^3 (kg/m^3)	1.601 846 X E+1
rad (radiation dose absorbed)	Gray (Gy)**	1.000 000 X E-2
roentgen	coulomb/kilogram (C/kg)	2.579 760 X E-4
shake	second (s)	1.000 000 X E-8
slug	kilogram (kg)	1.459 390 X E+1
torr (mm Hg, 0°C)	kilo pascal (kPa)	1.333 22 X E-1

*The becquerel (Bq) is the SI unit of radioactivity; Bp = 1 event/s.

**The Gray (Gy) is the SI unit of absorbed radiation.

CONTENTS

CONTENTS (CONTINUED)

FIGURES

FIGURES (CONTINUED)

FIGURES (CONTINUED)

FIGURES (CONTINUED)

FIGURES (CONTINUED)

TABLES

TABLES (CONTINUED)

SECTION 1
INTRODUCTION

During an extreme radiation accident such as occurred at the Chernobyl nuclear power station on April 26, 1986, explosion and fire may cause lofting of radioactive aerosols and vapors from a few hundred meters to more than a kilometer into the air. Winds then transport the material away from the accident site. The aerosols settle to the ground, larger, heavier particles nearby and smaller, lighter ones farther away. The resulting terrestrial deposition of fallout particles occurs in a more or less continuous but irregular fashion, following local and regional weather patterns. The finest aerosols enter the global atmospheric circulation.

Much attention has been given to the regional and global patterns of fallout from the Chernobyl accident because of worldwide concerns for human radiation exposure and the entry of radio nuclides into the food chain. The primary health concern is the induction of cancers in the human population from the resulting low level radiation exposures. The doses at regional and global distances are far below the levels required to induce acute radiation sickness or cause visible changes in vegetation.

Locally, however, at the site of the reactor explosion and more than a kilometer downwind from the site, radiation doses from radio nuclide fallout were above lethal levels for humans. Symptoms of radiation sickness occurred in some accident victims within the first hour of exposure (Young, 1988). Early fatalities and causes of death have been reviewed as part of this project and described in an earlier report (Laupa and Anno, 1989).

The circumstance of one victim is of particular interest in the context of the analysis in this report. According to Barabanova and Osanov (1990), this person was 1.0 km downwind from the reactor at the time of the explosion, remained there for about an hour, and was exposed to both the radioactive plume and particles of fallout. According to Barabanova and Osanov, the individual was covered with black dust and received an estimated total gamma radiation dose of 12.7 Gy. The estimated beta radiation dose to the skin of his scalp, neck and upper body was 250-360 Gy at a depth of 7 mg/cm^2 and about 30 Gy at a depth of 150 mg/cm^2. He died on the 17th day after exposure.

As detailed in Section 6 of this report, the gamma dose alone for this victim is comparable to the median lethal dose (LD_{50}) for pine trees, which are only slightly less radiosensitive than humans. Beta dose will contribute further to vegetation damage depending on the depth of sensitive plant tissues. In addition, vegetation remains in the contaminated area and accumulates dose over a much longer exposure time than would mobile human beings who leave the area and are decontaminated.

Figure 1-1 shows the Chernobyl nuclear power station and immediate vicinity. The burning Unit 4 reactor (dark red dot) is circled and the approximate wind direction at the time of the reactor explosion is indicated by the arrow. The image was produced by merging data from a Landsat[1] Thematic Mapper image from April 29, 1986 with data from a SPOT[2] panchromatic image from May 1, 1986. The merged image combines the 10 m spatial resolution of the SPOT image and the wider spectral coverage of the 25 m resolution Landsat image. The area shown in the image is a square with 5 km sides oriented along the Landsat orbital path. The edge of the forest at the tail end of the arrow in Figure 1-1 is only a little over 1 km from the burning reactor, so the victim described by Barabanova and Osanov was near the forest. Exposure of the victim is presumably a lower limit to the exposure of the nearby forest.

Volume 3 of this report (Painter and Whicker, 1993) presents a description of the geography and vegetation of the Poles'ye region of Ukraine and Belarus where the Chernobyl nuclear power station is located. As is true in many other regions of the world, pines trees are the most radiosensitive (see, for example, Whicker and Fraley, 1974) of the large, widely occurring species of vegetation in this region. Thus, substantial effects on pine forest near the Chernobyl accident site are to be expected. Because the radiosensitivity of pines is comparable to that of humans, the study of such pine tree responses in a fallout radiation field, especially through remote sensing, is relevant to human operations in a radiation environment.

The area around the Chernobyl nuclear power station after the accident of 26 April 1986 provides a unique opportunity to observe the response of large scale plant communities to fallout radiation. In a review article, Whicker and Fraley (1974) quote only two studies involving realistic fallout exposures of plants. One (Murphy and McCormick, 1971) involved spreading feldspar particles coated with ^{90}Y on small plant communities on granite outcrops in the southeastern United States. The other (Rhoads and Platt, 1971) observed damage to desert vegetation receiving fallout from two small cratering explosions at the Nevada Test Site. Neither of these studies encompassed the size and variety of plant communities present at Chernobyl. No other studies involve the appropriate mix of beta and gamma exposure to foliage.

---

[1]Landsat is the United States' civil land remote sensing satellite system. Data is obtained from the Earth Observation Satellite (EOSAT) Company of Lanham, Maryland.

[2]The Système Probatoire d'Observation de la Terre (SPOT) satellite is operated by the French space agency Centre National d'Etudes Spatiales. Data is obtained from the SPOT Image Corporation, a U.S. subsidiary of the French company SPOT IMAGE.

Figure 1-1. Immediate vicinity of the Chernobyl nuclear power station with Unit 4 reactor (circled) still burning; arrow shows approximate wind direction when the reactor exploded.

Time plays several essential roles in the radiation response of a plant community (Whicker and Fraley, 1974), including:

1) duration of exposure (or dose rate),
2) season of exposure,
3) time for manifestation of injury,
4) repair and recovery times, and
5) time for development of secondary effects such as community succession.

Control areas are of primary importance in analyzing these time factors and in separating radiation-induced changes from naturally occurring ones. There should be multiple observations over at least one annual cycle of both the control and exposed vegetation. In addition, preirradiation observations of the experimental area are required to establish the initial condition of the exposed vegetation.

Fortunately, satellite multispectral imagery provides observations of both control areas and preirradiation observations of the area affected by the Chernobyl reactor explosion. Control areas are available within individual Landsat scenes outside the highly irradiated areas and are an integral feature of our analysis. Furthermore, both summer and winter preaccident scenes of the irradiated area are included. Finally, the 16-day revisit time for acquisition of Landsat scenes from the same satellite on the same path offers ample opportunity to obtain multiple cloud-free images over an annual cycle. The analysis reported here uses 7 images during the first year postaccident and 2 more during the following year. This time series of remote observations is a unique record of the spectral response of pine foliage to fallout radiation exposure. Section 2 outlines the procedure used in the remainder of the report to estimate dose to pine foliage from these images.

SECTION 2
REMOTE FALLOUT DETECTION THROUGH IMAGERY ANALYSIS

A substantial amount of forest within a few kilometers of the Chernobyl nuclear power station was heavily contaminated with radionuclides by the April 26, 1986 explosion of the Unit 4 reactor and the ensuing fire. Radiation doses to conifers in some areas were sufficient to cause discoloration of needles within four to five weeks. Other areas, receiving smaller doses, showed foliage changes six months to a year later. Although we do not have color photographs of the trees affected by the accident, Figure 2-1 shows typical dying pine foliage from landscape plantings in northern Virginia. One photo shows branches with needles dying only at the tips. The other shows part of a tree whose needles are completely dead except for a few isolated bunches of green needles. Healthy trees are located in the background. Progression from green to yellow-green to reddish orange to dry brown is typical of the death of pine foliage from many causes including exposure to ionizing radiation.

Multispectral imagery available from satellite sensors is especially suited for remote monitoring of such changes in vegetation since the changes affect both the visible and infrared reflectivity of foliage. A series of Landsat Thematic Mapper images spanning two years after the Chernobyl accident are analyzed for significant, accident-induced change in a companion document, Volume 2 (McClellan et al., 1992). Accident-related changes in foliage are apparent three days after the accident. Changes due to cleanup activities and the progression of foliage deterioration are present in images taken in the following months. Finally, delayed effects of low radiation doses on initially undamaged foliage were still appearing more than a year after the accident.

Pacific-Sierra Research Corporation's Hyperscout™ algorithm provided the analytical basis in Volume 2 for demonstrating significant, radiation-induced change in the forests around Chernobyl. The Hyperscout algorithm will detect image-to-image change, providing a measure of significance of change on a pixel-by-pixel basis. The algorithm analyzes reflectivity and emission changes occurring in the detection bands of the imaging device. Spectral signature, spatial distribution, and time dependence of the observed changes help identify stresses causing the change. The algorithm is especially useful when the induced change has a low signal-to-noise ratio and when general image variations such as seasonal illumination and annual vegetation cycles cause change that is not of interest. It operates on pairs of spatially registered images and is capable of useful results even

---

™ Hyperscout is a trademark of Pacific-Sierra Research Corporation.

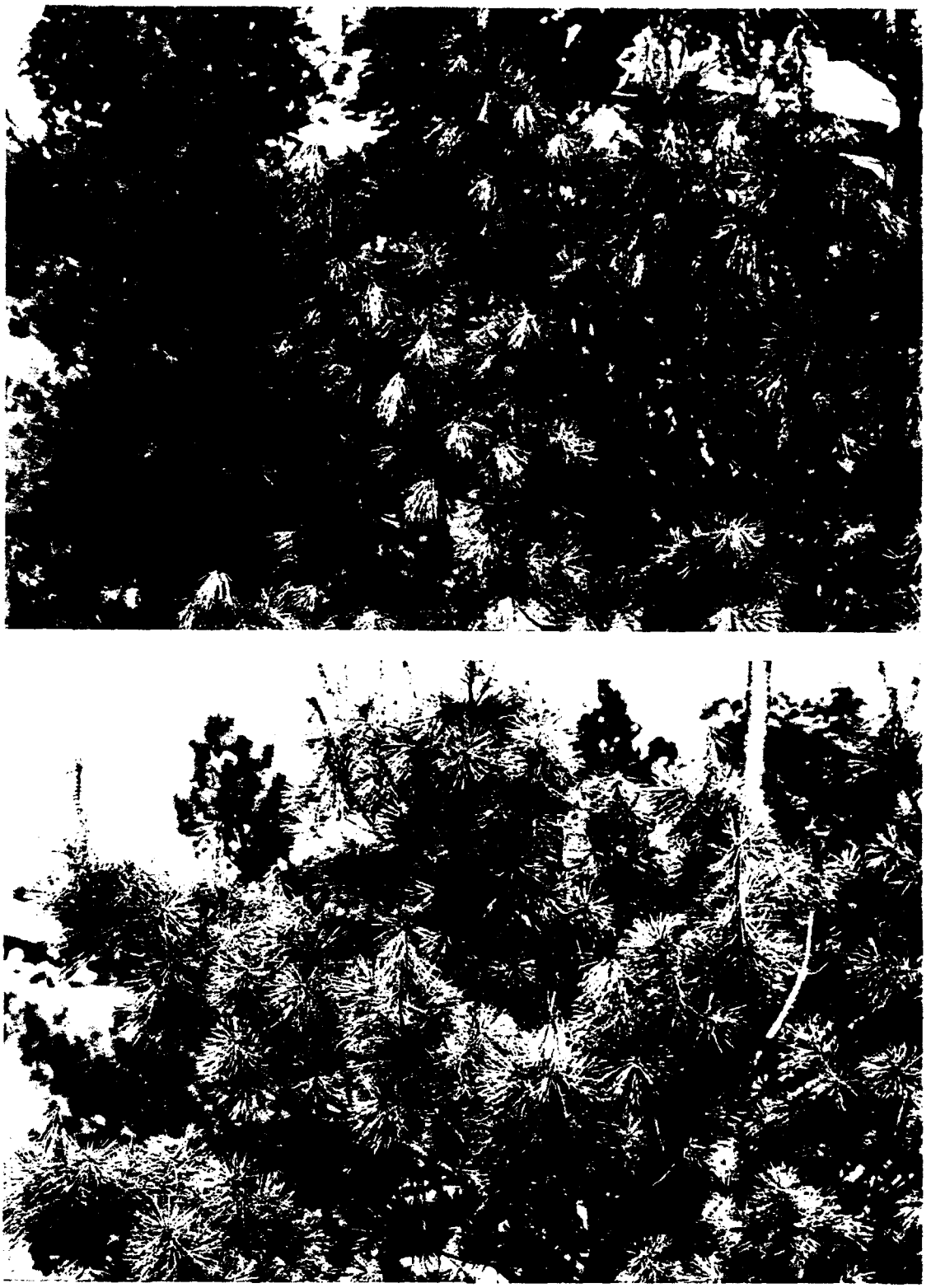

Figure 2-1. Typical coloration of dying pine foliage. Landscape setting; upper photo, branches almost completely brown with healthy trees in background; lower photo, only needles at tips of branches are brown.

when comparing images from different detectors. The sensitive nature of the Hyperscout algorithm enabled delineation of both the earliest changes in heavily exposed forest and the late-developing deterioration of less exposed forest.

Figure 2-2 shows an example of one of the Hyperscout stress maps (12 days postaccident) from Volume 2, with the area of affected forest nearest the reactor site circled. The Unit 4 reactor is marked with a white cross. The site marked is the brightest pixel of the fire visible in the Landsat image at 3 days postaccident (see Figure 1-1).

With guidance from the changes detected by the Hyperscout algorithm, this volume presents quantitative estimates of radiation dose to the pine foliage near the Chernobyl nuclear power station derived from remote Landsat imagery. The physical basis for detecting foliage stress with Landsat imagery is presented in Volume 2 and will not be repeated here. Quantitative dose estimation for the exposed conifers requires extracting the time of onset of observable radiation-induced foliage damage from the images for each pine forest pixel and combining this data with the relationship between dose and time of onset (time-to-response) of conifers for ionizing radiation.

Figure 2-3 outlines the remote sensing method for dose determination from multispectral images of pine forest. Similar considerations apply to other vegetation; however, pine trees are among the most radiation sensitive species of widely occurring vegetation. The first step indicated in Figure 2-3 is the determination of preaccident vegetation classes in the multispectral imagery, particularly, the identification of pixels that consist predominantly of pine trees. Generally, forested areas are readily apparent from their color, texture and location in false color images as presented in Volume 2. However, to optimize data quantity and quality it is necessary to classify individual pixels. Section 3 of this volume describes the procedure for quantitative determination of class membership on a pixel-by-pixel basis. Since a primary problem is the discrimination among coniferous, deciduous, and mixed coniferous-deciduous pixels, we use preaccident images from both summer and winter to achieve a reliable forest classification.

The extent to which tree foliage excludes a view of the ground from above is called canopy closure. If closure is high then satellite images will see mostly foliage. If closure is low then rocks, soil, and understory vegetation will dominate the image. We used a preaccident, late winter image (21 March 1986) with extensive snow cover to assist selection of areas with a high canopy cover of pine trees. The snow is a good discriminate for areas with low canopy cover or areas with a substantial number of deciduous trees. By eliminating these areas, we obtain a set of pixels containing a high canopy cover of pines that increases confidence in our dose estimates for these areas. Also, in this late winter image, the Pripyat River and its tributaries are mostly frozen. The resulting bright snow and ice along the river basin eliminates substantial misclassification that

Figure 2-2. Forest stress map for 8 May 1986 as presented in Volume 2. Accident-affected area circled. White cross is Unit 4 reactor site; Zone 36 Universal Transverse Mercator (UTM) coordinates about X = 298,275 m and Y = 5,697,175 m.

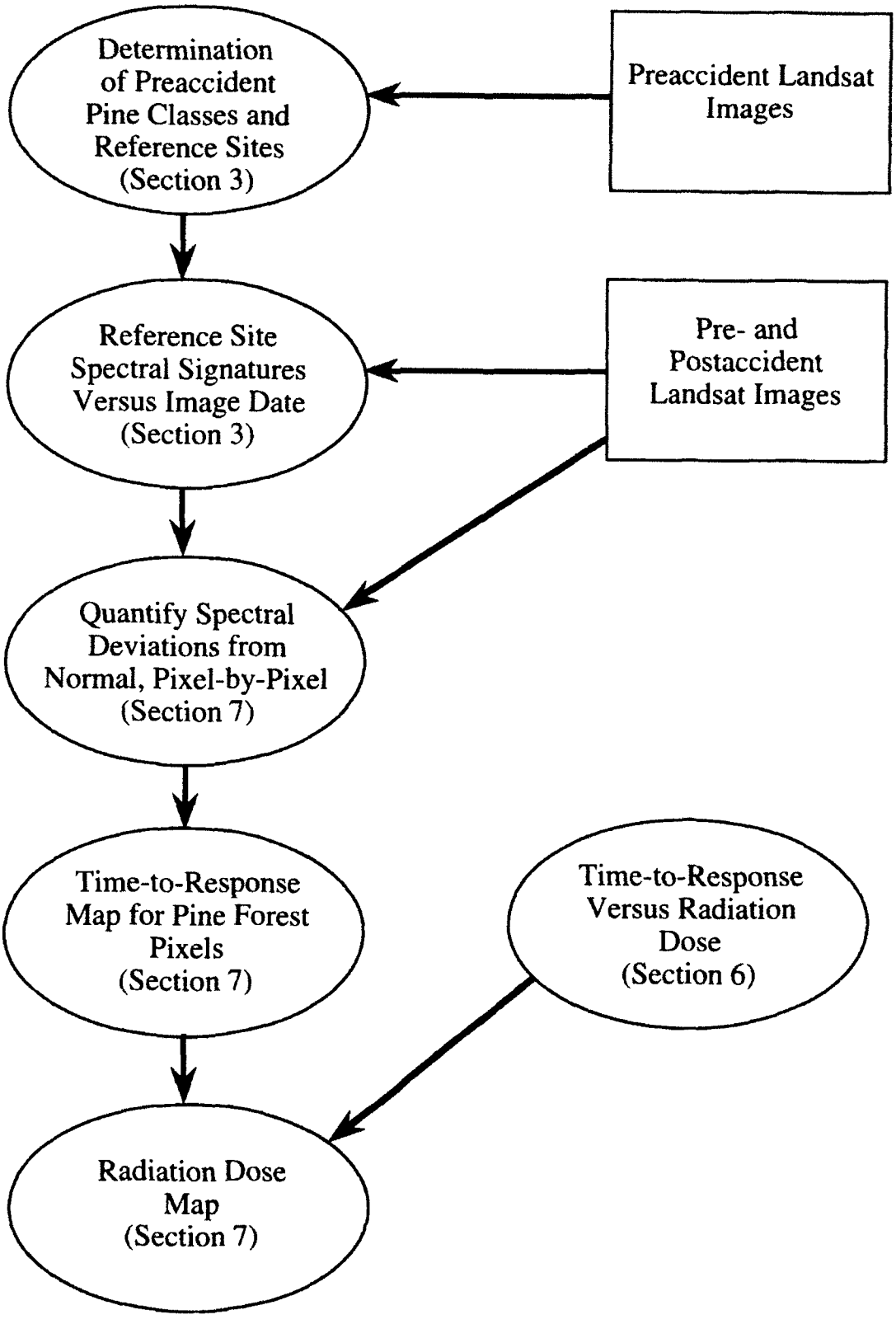

Figure 2-3. Method of radiation dose determination from remote multispectral sensing of pine forest.

occurred in our preliminary analysis (Volume 2) using only the summer image (6 June 1985) for determination of pine forest classes. In that analysis, many mixed pixels of dark water and deciduous vegetation at the rivers edge mimic the spectral response of pine forest . These misidentified pixels lead to the spurious indications of stress seen along the river in Figure 2-2.

The classification of pine forest is based on the location of a reference site for each class that contains on the order of one hundred contiguous pixels belonging to the class. The reference sites are defined by polygons at fixed geographic locations. These locations must be far enough from the reactor to be unaffected by radiation and must not be obscured by clouds or haze on any image. The mean spectral signature and its covariance matrix for each class on each date is determined from the pixels in these reference sites. This procedure is described in Section 3.

For many biological responses to radiation exposure, there is a dose-dependent delay between exposure and onset of the response. Such is the case for foliage damage in pine trees. We use the deviation of the spectral signal of each pine forest pixel from its class mean to detect significant change in foliage and, hence, estimate a time-to-response for areas of forest affected by the accident. Section 7 presents our time-to-response results.

The biological endpoint for these satellite observations is change of spectral reflectivity of the foliage. However, the endpoints most commonly reported in plant radiobiology literature are 100% lethality and 50% reduction in growth rate. There are no published reports, as far as we know, that provide controlled measurements of the spectral response of foliage to radiation exposure that can be directly correlated with other reported endpoints. Fortunately, though, there are sufficient visual observations reported for pine trees and sufficient reports of other vegetation stress responses to establish a plausible connection between pine tree response and multispectral detection. Section 6 discusses the connection made between reported endpoints and their relationship to spectral appearance from remote sensing. A functional relationship between time-to-response as determined from visible and infrared imagery and foliage dose is deduced.

Finally, in Section 7 the time-to-response map from the imagery and the relationship between radiation dose and time-to-response are combined to generate a map of estimated radiation dose to pine trees in the vicinity of the reactor explosion.

SECTION 3
HABITAT AND VEGETATION NEAR THE CHERNOBYL NUCLEAR POWER PLANT

This section summarizes the geography, soils, climate, native vegetation, and crops of the region surrounding Chernobyl and provides details on the analysis of Landsat imagery leading to the delineation of four classes of pine forest within a 38.4 km square area centered approximately on the Chernobyl nuclear power station.

Figure 3-1 is a regional map of the border area between the former Soviet republics of Ukraine and Belorussia (Belarus) stretching from Kiev in Ukraine to Gomel in Belorussia. The city of Chernobyl lies on the Pripyat River near the northwest corner of the Kiev Reservoir. The city of Pripyat is about 15 km further up the Pripyat River adjacent to the Chernobyl nuclear power station. The power station and its cooling pond are indicated by a small black rectangle labeled "Site of Chernobyl power station." Figure 3-1 provides the geographical framework for the regional description in Section 3.1 below.

Figure 3-2 is the earliest of the series of Landsat images analyzed in this report. It shows a north/south oriented rectangle about 58 km by 72 km. The upper left, or northwest, corner of the rectangle is clipped because the desired area was near the edge of the Landsat path on this date. The angle of the clipped portion corresponds to the angle of the satellite orbit relative to lines of longitude at this location. The Dnieper River and the Pripyat River both empty into the Kiev Reservoir at the lower right of Figure 3-2. Only the upper end of the reservoir is visible in the image as an indistinctly outlined dark area merging with the meandering river beds. The cooling pond of the nuclear power station appears as the large, black, footprint-like shape outlined in white along the Pripyat River. The north/south extent of the Landsat image of Figure 3-2 corresponds approximately to the north/south extent of the dashed circle on the map in Figure 3-1. This 30 km radius circle is the *danger zone* evacuated in the aftermath of the reactor explosion. A 38.4 km square subset of Figure 3-2 is selected for the ground cover analysis in Sections 3.2 through 3.5 below.

3.1 REGIONAL DESCRIPTION.

In the following regional description, we use the term Former Soviet Union (FSU) to denote the old Union of the Soviet Socialist Republics (USSR) but continue to use references to the names of the Soviet Socialist Republics (SSRs).

3.1.1 Geography.

The Chernobyl Nuclear Power Plant (NPP) and much of the area within 30 km around it are located in the Poles'ye region of the Ukrainian and Belorussian (Byelorussian, White Russian)

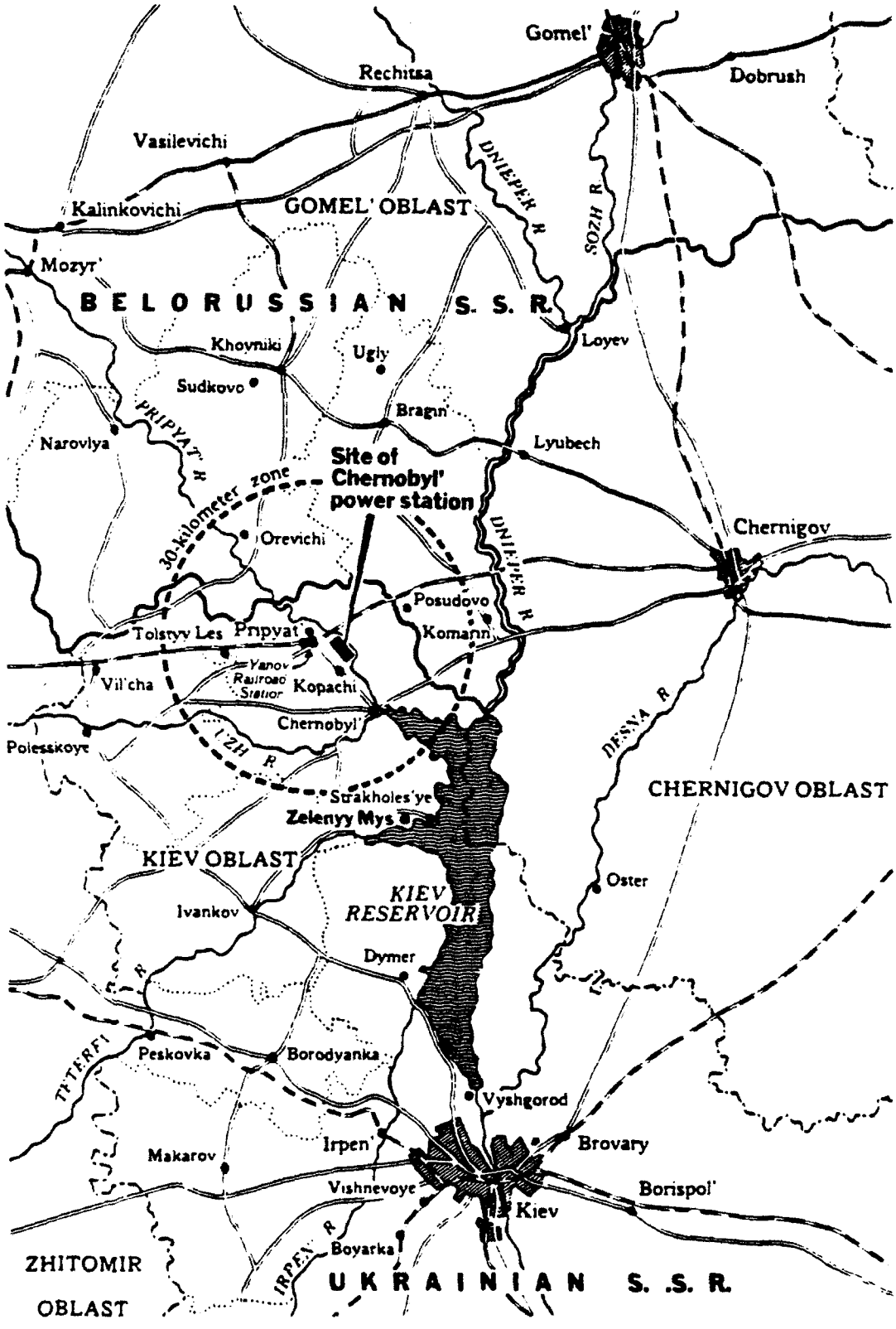

Figure 3-1. Regional map encompassing the 30 kilometer danger zone around the Chernobyl nuclear accident.

Figure 3-2. Landsat image of the confluence of the Dnieper and Pripyat Rivers at the upper end of the Kiev Reservoir. The sharply outlined black footprint shape is the reactor station cooling pond along the Pripyat River. [Thematic Mapper false color presentation (R,G,B) = (7,4,1) , 6 June 1985, geocoded, 1 degree longitude by 0.5 degree latitude.]

Soviet Socialist Republics. The power plant itself and the cities of Pripyat and Chernobyl are in the Ukrainian SSR. It lies at about 51°12'N longitude 30°8'E latitude.

The Poles'ye (Polesye, Poles'e, Poles'ya, Polesie, Polessie) lies in the Pripyat (Pripyat', Prip'at, Pripiat, Pripet) River basin and part of the Dnepr (Dnieper) River basin and includes the area called the Pripyat marshes or bogs. It is a vast lowland on the Russian platform, extending south to the Volyno-Podolsk Plateau (Keller 1927; Berg 1950; Fridland 1976; Lysenko and Golovina 1982). The relief from the center to the edges of the basin is only 55-100 m (Berg 1950; USSR 1987). Drainage is very poor and the ground-water table is usually high (Keller 1927; Berg 1950; Fridland 1976). The banks of the streams in the Poles'ye are very low (Keller 1927). In the spring and after heavy summer rains, streams overflow into areas between neighboring streams and water from one stream passes into another. The Poles'ye is often divided into three sections: the western, the central (or right bank--on the right bank of the Dnepr River), and the eastern (or left bank) (Golovina, et al., 1980; Lysenko and Golovina 1982). In the Ukraine, the central section is divided into the Kiev Poles'ye and the Zhitomir Poles'ye. The Kiev Poles'ye lies on the middle Dnepr slope, in the interfluve of the Pripyat and Teterev Rivers, extending east to the Dnepr River (Golovina, et al., 1980; Lysenko and Golovina 1982), and includes the Chernobyl NPP and the immediately area

3.1.2 Soils.

The soils in the Poles'ye formed in a humid climate on platform plains from a blanket of unconsolidated Quaternary fluvioglacial sand and loamy sand over and underlying a glacial moraine (Fridland 1976; Lysenko and Golovina 1982). The moraine itself is mostly loamy sand. Clay-loam lake deposits are rare and loesses even rarer (Lysenko and Golovina 1982). The parent materials are very boldery and gravely; fine particles are usually washed away (Golovina, et al., 1980). Glacial waters were active for along time during the formation of the parent material (Lysenko and Golovina 1982). The soils generally lack carbonates in the parent materials. The sandy soils of the Poles'ye are particularly vulnerable to erosion if plowed (Symons 1972). Some areas possess aeolian relief, often in the form of parabolic, west-facing dunes (Berg 1950; Fridland 1976). This significantly affects soil cover composition.

Most of the Poles'ye soils are poor in humus (USSR 1986). Soils in the western and central Poles'ye often have 1-1.5% humus and can have less than 1% (Krupskiy, et al., 1970). The soils generally have a low pH (Golovina, et al., 1980) and are low in available nutrients, including boron, zinc, phosphorus, potassium, and nitrate (Golovina, et al., 1980; Oleynik 1981; Lynsenko and Golovina 1982). There are large quantities of weakly podzolic sandy soils. Podzols develop under coniferous forests (Sukachev 1928; Berg 1950). The distribution of podzols is patchy in

the Poles'ye (Fridland 1976). Medium-podzolic sod loamy sandy soils have formed on moraine outcrops in the Kiev Poles'ye (Lysenko and Golovina 1982).

Much of the area is boggy. Bog soils receive excessive moisture for the greater part of the year, are sometimes covered with shallow water, and have poor drainage (Berg 1950). Much of the Poles'ye is low lying, with poor drainage, ideal for bogs (Keller 1927; Berg 1950). There are also sod-podzolic ("half-bog" or "meadow") soils (Berg 1950). Soils on flood plains may be bog, meadow, or podzols. Some parts of the Poles'ye contain "islands" of soils foreign to it (Berg 1950). One such island occurs on the Ovruch ridge (about 90 km west of Chernobyl). This ridge is 320 m above sea level and 60 m above the surrounding lowland.

Based on the soils map in the Ukrainian SSR Atlas (Anonymous 1962), the site of the Chernobyl nuclear power plant appears to be at or near the boundary of:

Type 1: Soddy-slightly podzolic sands and sandy-clayey soils.

Type 27: Sods and meadowlands, gleys, sandy loams, and loams.

It is likely that the coniferous forests near the site are on type 1 soils.

3.1.3 Climate.

The climate of the Poles'ye is influenced by maritime, continental, and local factors. Moisture from the Baltic Sea and the "great valley" region of Poland influences the Poles'ye (Borisov 1965; Szafer 1966). There is unrestricted passage of marine winds, unhindered by major land relief, so there is considerable marine influence on the climate.

A small local maximum of relative humidity, caused by the intensified evaporation of water of standing water, is noticed over the marshes of the Poles'ye(Borisov 1965). Bogs influence the local microclimate (Szafer 1966). These areas have high humidity, low temperature minima, evening and morning mists close to the soil surface, and frequent frosts. Forests also influence the microclimate (Szafer 1966). The mean air temperatures are lower than in the open, the daily temperature ranges are smaller, the snow cover is less, and winds are stilled.

In the Poles'ye, the minimum relative humidity at 1 pm in May is 50-55%. The mean humidity for June, July, and August is 56-60% (Borisov 1965). Mean temperatures in the region are -6 to -7°C in January, 6 to 7°C in April, 19° in July, and 7°C in October (Anonymous 1962). Absolute minimum temperatures are -30 to -35°C in January, while summer maximums range up to 40°C (Anonymous 1962). The growing season (days with mean temperatures above 5° C) is about 160-190 days (Anonymous 1962; Szafer 1966). It begins about April 11 and runs to about October 25 (Anonymous 1962). Summer precipitation exceeds that in winter by a factor of two (Borisov 1965). In any season, there is precipitation every 2-3 days. In the warm season (April-September), the amount of precipitation in the interior of the European FSU is much greater (350-500 mm) than on the coasts (200-300 mm) (Borisov 1966). During the cold half of the year

(November to March) in the central belt of European FSU, the precipitation amounts are 100-300 mm (Borisov 1965). A precipitation maximum is situated on the Pripyat and the upper reaches of the Dnepr and Western Dvina Rivers. The maximum precipitation in the Pripyat basin is 680-695 mm/year (Berg 1950). Precipitation diminishes eastward from the Pripyat (Borisov 1965). In the specific region of interest, mean precipitation is 500-600 mm/year, with around 180 days/year recording precipitation (Anonymous 1962). The mean intensity of precipitation amounts to 8-10 mm/hr in the central belt o the country (51-59°N) (Borisov 1965).

At 50°N, by the second 10-day period in November snow cover is normally continuous (Borisov 1965). In western European FSU, snow cover is usually continuous by the last 10 days in October or the first 10 days in November. According to Anonymous (1962), snow cover in the Chernobyl area usually lasts from mid-December to Mod-March. At 55°N 30°E, there are an average of 2.5 temporary snow covers before the onset of winter (Borisov 1965). In central European FSU, winter temperatures and precipitation are highly variable (Borisov 1965). Mean maximum snow depth is 10-30 cm. Continuous snow cover generally lasts about 80 days. Rivers and streams are generally frozen for about 100 days/year (Kendrew 1942).

3.1.4 Native Vegetation.

Most of Belorussia and Ukraine, including the Poles'ye, is in the Eastern European Vegetation Province (Takhtajan 1986). The northern, eastern and southeastern boundaries correspond to the distributions of *Quercus robur*[1] (English oak), *Acer platanoides* (Norway maple), and *Corylus avellana* (European filbert). The basic plant community types in the region are forests, woodlands or carrs, meadows, fens, and bogs.[2]. Many of these communities can grade into one another. Bog, meadow, and forest vegetation may occur on flood plains. Meadows may be transitional or ecotonal between bogs and forests. In poor sandy soils, peat bogs occupy the low areas, forests the more upland areas. Succession can progress from forest to bog or from bog to forest. Most bogs in central Europe are being drained (Walter 1978). The replacement vegetation is usually meadow grasses, birch, pine, or spruce. While the vegetation types to be discussed are specific to the Poles'ye, the species lists given are those known to occur in that type of vegetation in northern Ukraine, southern Belorussia, and/or adjacent areas in Poland. Information on both the vegetation

[1]Both Common and Latin names come from a number of literature sources. In order to eliminate synonyms and assure current nomenclature, the names in the **Flora of the USSR and the Flora Europaea** will be used for the final report.

of the Poles'ye and the species lists was synthesized from Keller 1927; Sukachev 1928; Wulff 1943; Berg 1950; Szafer 1966; Walter 1978; Oleynik 1981; and Takhtajan 1986.

The sandy riverine sections along river channels receive an annual sand deposit Berg (1950). The community lying closest to the stream is often a sedge-horsetail fen. The plants found in this type of habitat include *Equisetum arvense* (field horsetail), *E. variegatum*, *E. palustre* (horsetail or scouring rush), *Carex fusca*, *C. canescens*, *C. stellulata*, *C. dioica*, *C. flava* (sedges), *Eriophorum latifolium*, and *E. augustifolium* (cottongrass or cottonsedge).

Immense tracts of the Poles'ye are occupied by bogs. There are several types, but most are *Sphagnum* or peat bogs. These are dominated by sphagnum mosses, including *Sphagnum recurrum*, *S. fuscum*, *S. cuspitatum*, *S. medium*, *S. revellum*, *S. acutifolium*, *Hypnum schreberi*, and *H. crista-castrensis*. Such bogs also have *Eriophorum vaginatum* (sheathed cottongrass), *Carex pauciflora*, *C. limosa*, and *C. vaginata*, and the carnivorous plant *Drosera intermedia* (roundleaf sundew). The vegetation of reed-bulrush bogs include *Phragmites communis* (common reed), *S. lacuster* (bulrush), *Phalaris arundinacea* (canarygrass), *Calamagrostis neglecta* (reedgrass), *Typha angustifolia*, *T. latifolia* (cattails), *Carex vesicaria*, *C. gracilis*, *C. pseudocyperus*, *C. rostrata*. Sedge bogs often include *Carex filiformis* (large sedge), *C. vesicaria*, *C. pseudocyperus*, *C.rostrata*, *C. elata*, *C. gracilis*, *C. acutiformis*, *C. riparia*, *C. lasiocarpa*, *C. diandra*, *C. aespitosa*, and *C. omaskiana* (omskiana sedge) with *Deschampsia caespitosa* (tufted hairgrass) on hummocks. Sedge bogs are often found where *Alnus glutinosa* (European alder) has been cut. Transitional areas begin with either *Sphagnum* or sedge bogs and these can grade to alder, birch, birch-spruce, pine-birch, pine, and birch-aspen-conifer bogs.

There are two basic types of meadows, flood-plain (or wet) meadows and upland (or fresh) meadows. Flood-plain meadows may be inundated for some time each year, especially in late winter and early spring. These are found in river valleys and at the peripheries of shallow lakes. They often consist of secondary vegetation resulting from drainage of fens or bogs. The vegetation includes *Festuca ovina* (sheep fescue), *F. rubra* (red fescue), *F. pratensis* (fescue), *Agropyron repens* (quack- or conchgrass), *Poa pratensis* (Kentucky bluegrass), *P. annua* (annual bluegrass), *Phleum pratense* (timothy), *Agrostis stolonifera* (redtop), *Calamagrostis neglecta*, *Deschampsia caespitosa*, *Molinia coerulea*, *Carex panicea*, *C. caespitosa*, *Eriophorum neglecta*, and *Trifolium pratense* (red clover).

Fresh meadows generally are found in interstream areas, developing as secondary vegetation on cut or burned forest sites. Mowing is often used to prevent forest encroachment. They have a

---

[2]A fen is a constantly or frequently flooded area through which water flows. For simplification, the term "bog" includes marsh and swamp and is used to mean flooded areas having zero or very low rates of water flow.

moderate moisture supply which fluctuates widely but generally does not surface. These meadows are usually used as pastures or hay meadows and some of the plants, especially the legumes, may have been sown. The vegetation includes *Arrhenatherum elatius* (tall or false oatgrass), *Bromus mollis* (smooth brome), *Agrostis stolonifera*, , *P. trivialis* (bluegrass), *P. annua*, *Phleum pratense*, *Lolium perenne* (perennial rye grass), *Cynosurus cristatus* (crested dogtail), *Festuca pratensis*, *F. rubra*, *Agropyron repens*, *Phalaris arundinacea*, *Calamagrostis negecta*, *Alopecurus pratensis* (meadow foxtail), *Trifolium repens* (white clover), *T. pratense*, *T. hybridum* (Alsike clover), *T. incarnatum* (crimson clover), and *Medicago sativa* (lucerne or alfalfa).

There are several types of carrs (or woodlands). The plants in willow carrs include *Salix cinerea* (gray willow), *S. rosmarinifolia* (rosemary willow), *S. alba*, *S. fragilis*, *S. triandra*, *S. purpurea*, *S. rossica* (willows), *Alnus gutinosa*, *Fraxinus excelsior* (ash), *Betula laevis* (European birch), *Cornus alba* (Siberian or white dogwood), *Rosa* (rose) sp., and *Ribes nigrum* (black current). The plants in elm carrs include *Ulnus pedunculata* (Russian elm), *U. glabra* (Scotch elm), *Quercus robur*, and *Acer Platinoides*. Alder-ash carrs usually include *Alnus glutinosa*, *Fraxinus excelsior*, *Ulnus pedunculata*, *U. glabra*, *Acer platinoides*, *Carpinus betulus* (European hornbeam), *Festuca gigantea*, and *Agropyron Caninum* (wheatgrass).

The Kiev Poles'ye lies on the ecotone between the mixed coniferous-deciduous forest and the forest steppe. There are two basic mixed coniferous-deciduous forest types: Pine-oak forest and spruce-oak forest. The common steppe-forest of the area is oak-hornbeam. There are also some pine (bor) woodlands in the Poles'ye. It is unlikely that any virgin forests remain in eastern Europe (Walter 1978).

Quercus robur is the dominant in forest-steppe in the European USSR. It grows best in the southwestern part of the European FSU and in the Poles'ye. *Quercus robur* will not grow on strongly podzolic soils. It is commonly found on floodplains and often grows in mixed stands with *Pinus sylvestris* (Scotch, Scots, or common pine), *Picea abies* (European spruce), or *Carpinus betulus*. *Fagus sylvatica* (European beech) is sometimes a component in oak-hornbeam forests on richer soils.

Pinus sylvestris is a light-loving species, not tolerant of shade. It is not very exacting in soil and moisture requirements. It tolerates relatively poor soils and is often associated with bogs and "bor" soils. "Bor" forest is a type of sparse pine forest growing on sandy soil, dunes, etc. (Fridland 1976). The sandy forested areas, such as the parabolic, west-facing dunes, of the Poles'ye are usually covered with *Pinus sylvestris*, giving the region a "northern" appearance. The understory in pine (bor) woodland is often dune vegetation, including *Festuca ovina*, *F. rubra*, *Poa pratensis*, *Deschampsia caespitosa*, *Carex arenaria* (sand sedge), and *Trifolium arvense* (clover). When these forests are cut, the dune vegetation replaces them until there is a secondary pine growth. The understory in pine-oak forests often include *Betula laevis*, *Tilia cordata* (linden,

lime), *Populus tremula* (aspen), and *Corylus avellana*. *Pinus* trees in bogs are frequently stunted. Based on the maps in Anonymous (1962), common pine (*Pinus sylvestris*) is the most likely forest type in the immediate vicinity of the Chernobyl nuclear power plant.

Picea abies endures shade well but requires humid, relatively rich soils. Its southern limit runs through Kiev Poles'ye. Spruce-oak forests are probably occur mainly on "islands" of richer podzolic soils scattered in the Poles'ye. Near the southern limit of *Picea's* range, the most frequent understory species in spruce-oak forest are *Tilia cordata*, *Acer platanoides*, *Fraxinus excelsior*, *Ulnus pedunculata*, *Corylus avellana*, *Betula laevis*, and *Populus tremula*. Isolated *Pinus sylvestis* trees are also occasionally encountered in the spruce-oak type.

3.1.5 Crops.

Only about half of the area around Chernobyl is suitable for agriculture and much of it is in hay meadows and grazing land (*Trifolium* spp. and grasses) and only fodder crops, including corn (*Zea mays*) and fodder beets (*Beta Vulgaris*) (Symons 1972; USSR 1987). Winter wheat (*Triticum aestivum*), winter rye (*Secale cereale*), millet (*Panicum miliaceum*), winter and spring barley (*Hordeum vulgare*), oats (*Avena sativa*), flax (*Linum usitatissimum*), hemp (*Cannabis sativa*), sugar beets (*Beta vulgaris*), buckwheat (*Fagopyrum esculentum*), and potatoes (*Solanum tuberosum*) are all grown from human use in the southern part of the Byelorussian SSR and northern part of the Ukrainian SSR (Sanbur and Kovalenko 1969; Fullard 1972; Symons 1972; Dewdney 1982). However, these crops are not grown in the poorly drained, boggy parts of the Poles'ye (Dewdney 1982). At any one time, 12-17% of the land is being fallowed (Symons 1972).

3.2 *TASSELED CAP* TRANSFORMATION OF LANDSAT IMAGERY.

As a first step in the analysis of vegetation in Landsat imagery, it is useful to transform the spectral bands of the Thematic Mapper (TM) multispectral imaging sensor to a new spectral coordinate system that compresses the useful information into fewer bands and provides a physical interpretation of the transformed bands. We use the so-called *Tasseled Cap* transformation.

3.2.1 Description of the Tasseled Cap Transformation.

The Tasseled Cap (TC) transformation for the six reflective spectral bands of the Landsat Thematic Mapper imaging multispectral sensor was first described by Crist and Cicone (1984). It is a descendant of the Kauth-Thomas transformation developed for agricultural and vegetation scenes for the Multispectral Scanner (MSS) imaging device on earlier Landsat missions. The TC transformation is linear and preserves the Euclidean relationship of the pixel data contained in the six reflective TM bands. It is chosen so that most of the spectral-temporal variance in agricultural

and vegetation scenes is included in the first three TC bands. Furthermore, the linear combinations of the original TM band intensities that provide the first three TC band intensities are chosen so that the magnitude of each of the three has a physical interpretation with respect to vegetation and soils. Later Crist and coworkers (Crist et al., 1986), adjusted the fourth, fifth and sixth components of the tasseled cap transformation to maximize the correlation of the fourth component with atmospheric haze. Table 3-1 lists the resulting transformation coefficients. The coefficients are used according to the following example:

$$TC1 = 0.2909*TM1 + 0.2493*TM2 + \ldots + 10.3695,$$

where TCi represents the ith Tasseled Cap band intensity and TMi represents the ith Thematic Mapper band intensity.

Table 3-1. Original Landsat-5 TM Tasseled Cap coefficients (Christ et al., 1986).

Tasseled cap		*Coefficients*						*Additive*
Band	*Feature*	*TM1*	*TM2*	*TM3*	*TM4*	*TM5*	*TM7*	*Term*
TC1	Brightness	.2909	.2493	.4806	.5568	.4438	.1706	10.3695
TC2	Greenness	-.2729	-.2174	-.5508	.7221	.0733	-.1648	-0.7310
TC3	Wetness	.1446	.1761	.3322	.3396	-.6210	-.4186	-3.3828
TC4	Haze	.8461	-.0731	-.4640	-.0032	-.0492	.0119	0.7879
TC5	Fifth	.0549	-.0232	.0339	-.1937	.4162	-.7823	-2.4750
TC6	Sixth	.1186	-.8069	.4096	.0571	-.0228	.0220	-0.0336

Figure 3-3 illustrates the transformation from the Landsat TM images presented in Volume 2 to the tasseled cap images analyzed in this volume. The first four TC features have interpretations in terms of the physical features brightness, greenness, wetness and haze:

Brightness (Br).

Brightness is the overall reflectivity with band-by-band weighting; red (TM3) and near infrared (TM4) bands are emphasized; soils are generally brighter than vegetation; pines forest has a relatively low brightness compared to other vegetation.

Greenness (Gr).

Greenness is a basic vegetation index, dominated by the difference between the near infrared (TM4) and red (TM3) band intensities; chlorophyll and other plant pigments absorb red light but strongly reflect near infrared light giving foliage a high greenness value. In principle, the difference

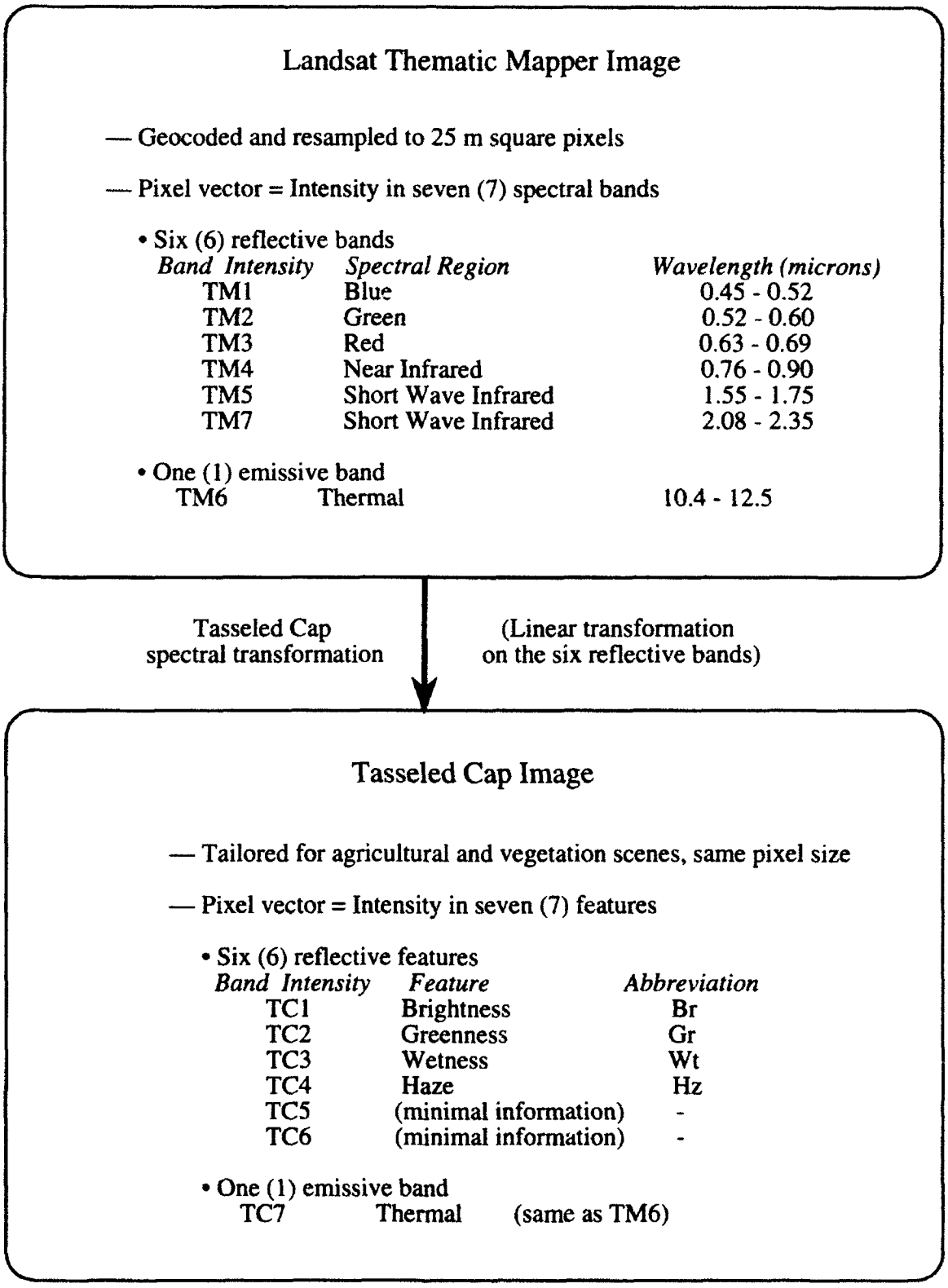

Figure 3-3. Illustration of the Tasseled Cap spectral transformation for Landsat Thematic Mapper images; transformation coeffcients are listed in Table 3-2.

between green light intensity and either blue or red provides a similar index. However, the contrast is higher between near infrared and red with the added benefit that atmospheric scattering introduces less background noise in the infrared than at the shorter visible wavelengths.

Wetness (Wt).

Wetness increases with soil and vegetation moisture content; it is predominately determined by the difference between the combined red/near infrared reflectivity (TM3 + TM4) and the combined short wave infrared reflectivity (TM5 + TM7); it is affected by absorption bands of water and structural effects related to foliage hydration; there is some contribution from shadowing which relates to vegetation height and stand density.

Haze (Hz).

Haze is aerosol scattering index that emphasizes the difference between blue light reflectance (TM1) and red light reflectance (TM3); Rayleigh scattering by small aerosols strongly scatters light at shorter (blue) wavelengths providing a large haze signal from clouds, mist, smoke and aircraft contrails; on clear days the largest "haze" signals come from urban/industrial surfaces, snow and ice.

Our image processing software (see Volume 2) requires band intensities in the range 0 to 255. We modified the tasseled cap transformation slightly to insure that all TC band intensities for the Landsat Chernobyl images fall in this range. Table 3-2 shows the resulting transformation coefficients. Band 1 requires a multiplicative scale factor of 1/2 applied to the corresponding coefficients in Table 3-1 to reduce its dynamic range below 255. Tasseled cap bands 2 through 6 require an additive term to eliminate negative values. These changes do not effect the linearity or physical interpretation of the TC transformation.

Table 3-2. Modified Tasseled Cap coefficients used in the present work to place all feature intensities in the range 0 to 255.

Tasseled cap		*Coefficients*						*Additive*
Band	*Feature*	*TM1*	*TM2*	*TM3*	*TM4*	*TM5*	*TM7*	*Term*
TC1	Brightness	.1455	.1247	.2403	.2784	.2219	.0853	5.2
TC2	Greenness	-.2729	-.2174	-.5508	.7221	.0733	-.1648	160.
TC3	Wetness	.1446	.1761	.3322	.3396	-.6210	-.4186	128.
TC4	Haze	.8461	-.0731	-.4640	-.0032	-.0492	.0119	64.
TC5	Fifth	.0549	-.0232	.0339	-.1937	.4162	-.7823	160.
TC6	Sixth	.1186	-.8069	.4096	.0571	-.0228	.0220	160.

Finally, we note that the Tasseled Cap transformation is named for the distinctive shape in the brightness-greenness plane of a scatter plot of crop and soil pixels from an agricultural scene.

3.2.2 Tasseled Cap Images of the Analysis Area.

The change detection analysis in Volume 2 covers a 12.8 km square area consisting of 512 x 512 pixels centered on the main westward trace of initial local radioactive deposition caused in the first hours by the reactor explosion and fire. For the analysis of radiation doses presented in this volume, we have extended the dimensions of the analysis area threefold to a 38.4 km square consisting of 1536 x 1536 pixels centered at the same spot. Thus, the area analyzed in Volume 2 is the central 1/9th of the area analyzed here.

Table 3-3 lists chronologically the 11 images analyzed and the time of each image relative to the day of the reactor explosion. References to date numbers or image numbers in this report are made according to this table.

Table 3-3. Landsat scenes analyzed and time of scene relative to reactor explosion.

Image/date number	*Date*	*Time relative to reactor explosion, Days*	
1	6/06/85	-324	(-10.7 months)
2	3/21/86	-36	(-5.1 weeks)
Day of Accident	4/26/86	-	
3	4/29/86	3	
4	5/08/86	12	
5	5/24/86	28	(4.0 weeks)
6	5/31/86	35	(5.0 weeks)
7	10/15/86	172	(5.6 months)
8	12/02/86	220	(7.2 months)
9	5/11/87	380	(1.04 years)
10	9/07/87	499	(1.4 years)
11	5/28/88	763	(2.1 years)

Figures 3-4 through 3-9 present the 11 TC-transformed images of the 38.4 km square area in chronological order. These false color images were produced by displaying the first three tasseled cap features, brightness, greenness and wetness in red, green and blue, respectively. For shorthand notation, we use (R,G,B) = (Br,Gr,Wt). Table 3-4 gives the geographic coordinates of the area included in the images in the Universal Transverse Mercator (UTM) coordinate system. As usual, north is up and east is the right in these images.

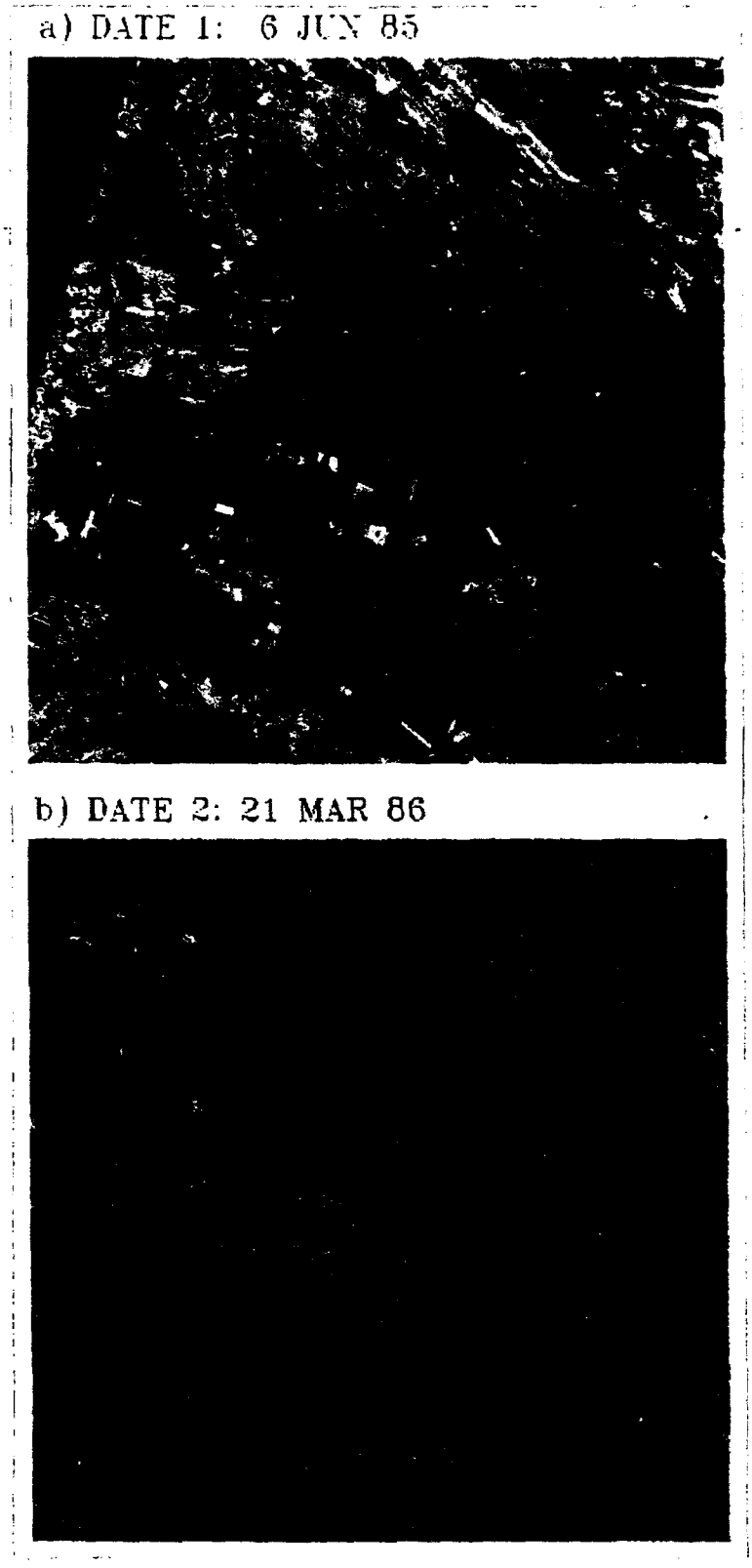

Figure 3-4. Tasseled Cap false color images, (R,G,B) = (Br,Gr,Wt) of 38.4 km square area around Chernobyl: a) early summer image one year preaccident and b) late winter image 5 weeks preaccident.

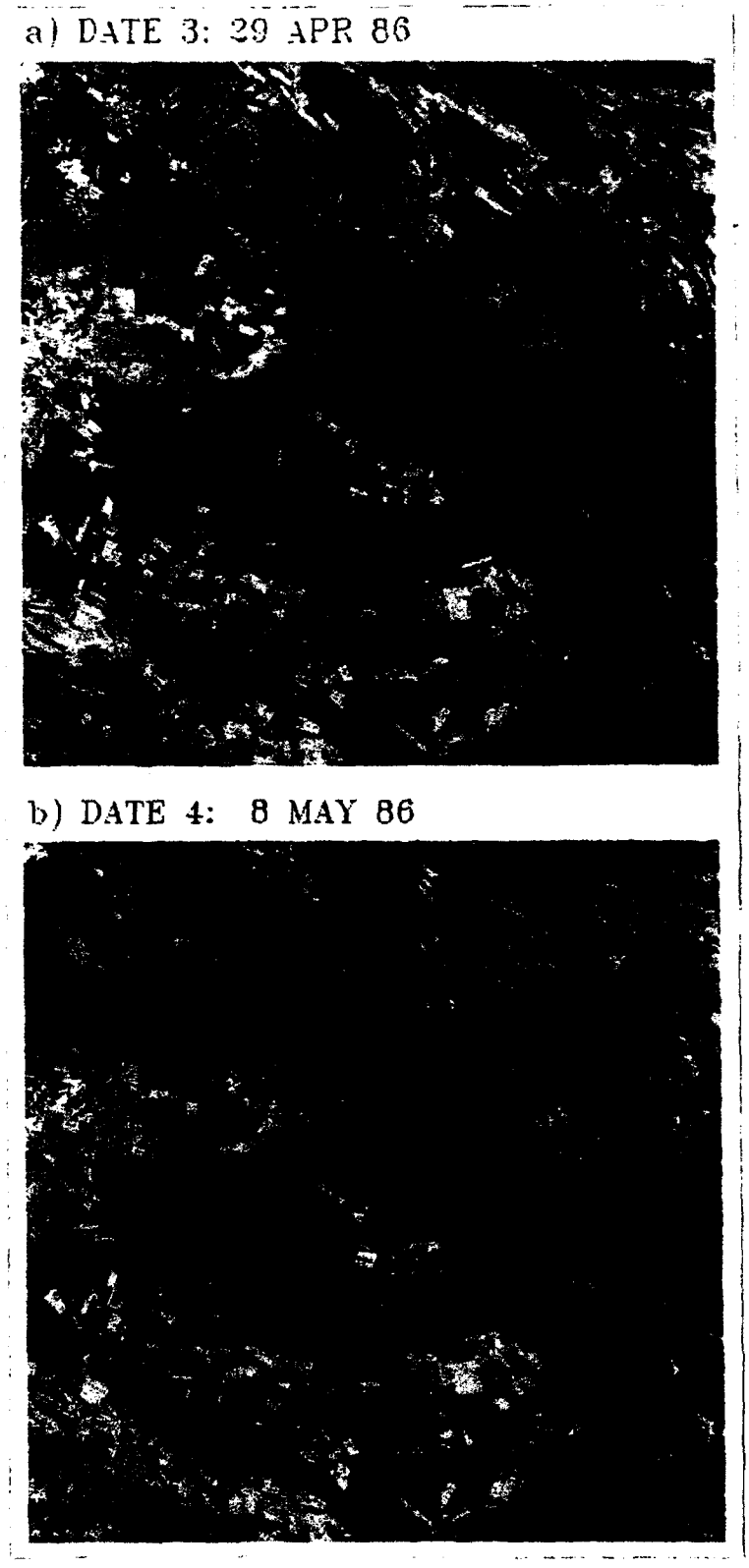

Figure 3-5. Tasseled Cap false color images, (R,G,B) = (Br,Gr,Wt) of 38.4 km square area around Chernobyl: a) 3 days postaccident and b) 12 days postaccident.

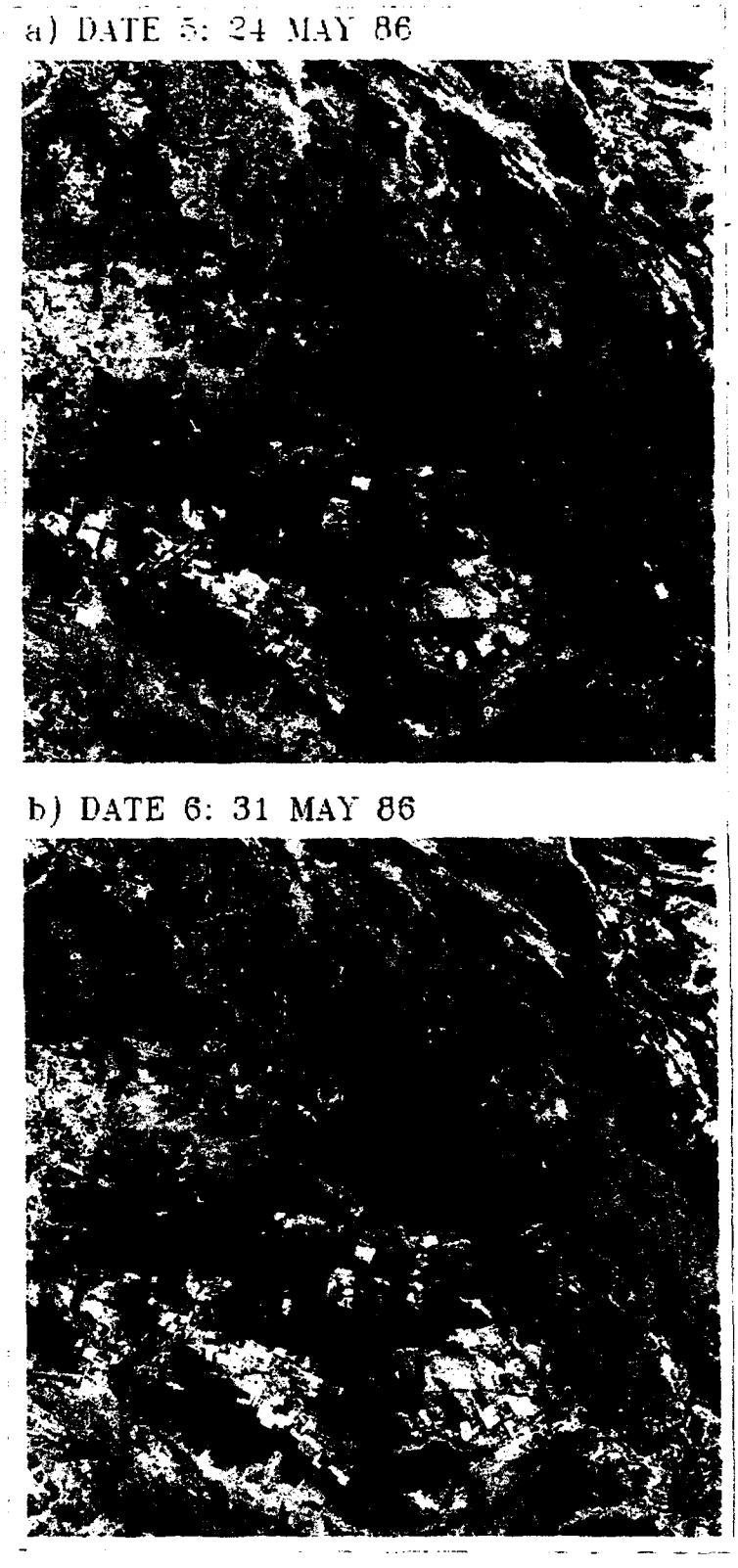

Figure 3-6. Tasseled Cap false color images, (R,G,B) = (Br,Gr,Wt) of 38.4 km square area around Chernobyl: a) 4 weeks postaccident and b) 5 weeks postaccident.

a) DATE 7: 15 OCT 86

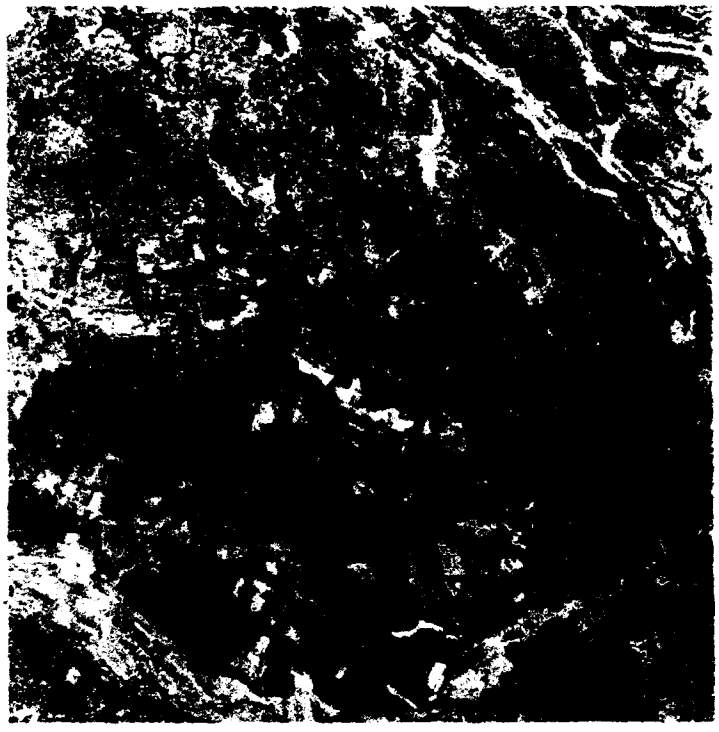

b) DATE 8: 2 DEC 86

Figure 3-7. Tasseled Cap false color images, (R,G,B) = (Br,Gr,Wt) of 38.4 km square area around Chernobyl: a) 5.6 months postaccident and b) 7.2 months postaccident.

a) DATE 9: 11 MAY 87

b) DATE 10: 7 SEPT 87

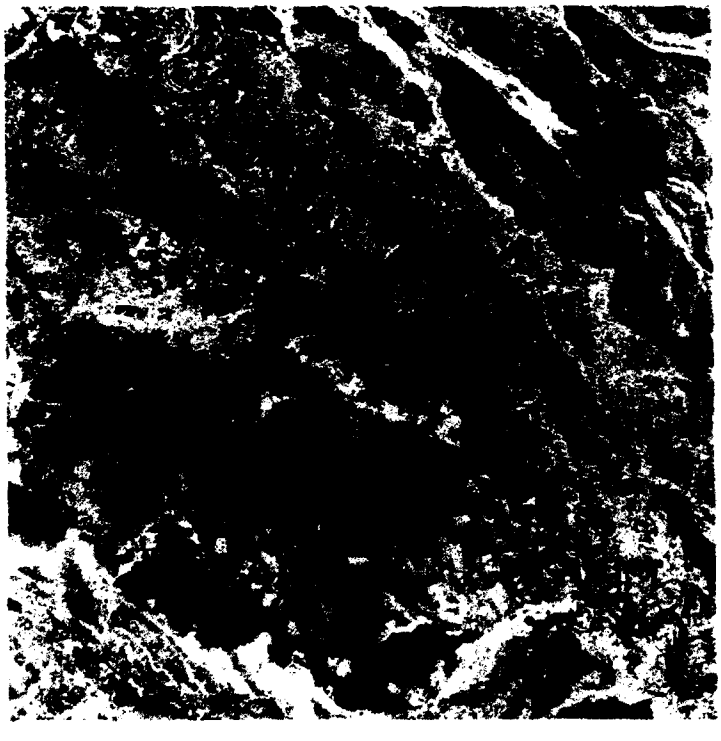

Figure 3-8. Tasseled Cap false color images, (R,G,B) = (Br,Gr,Wt) of 38.4 km square area around Chernobyl: a) 1 year postaccident and b) 1.4 years postaccident.

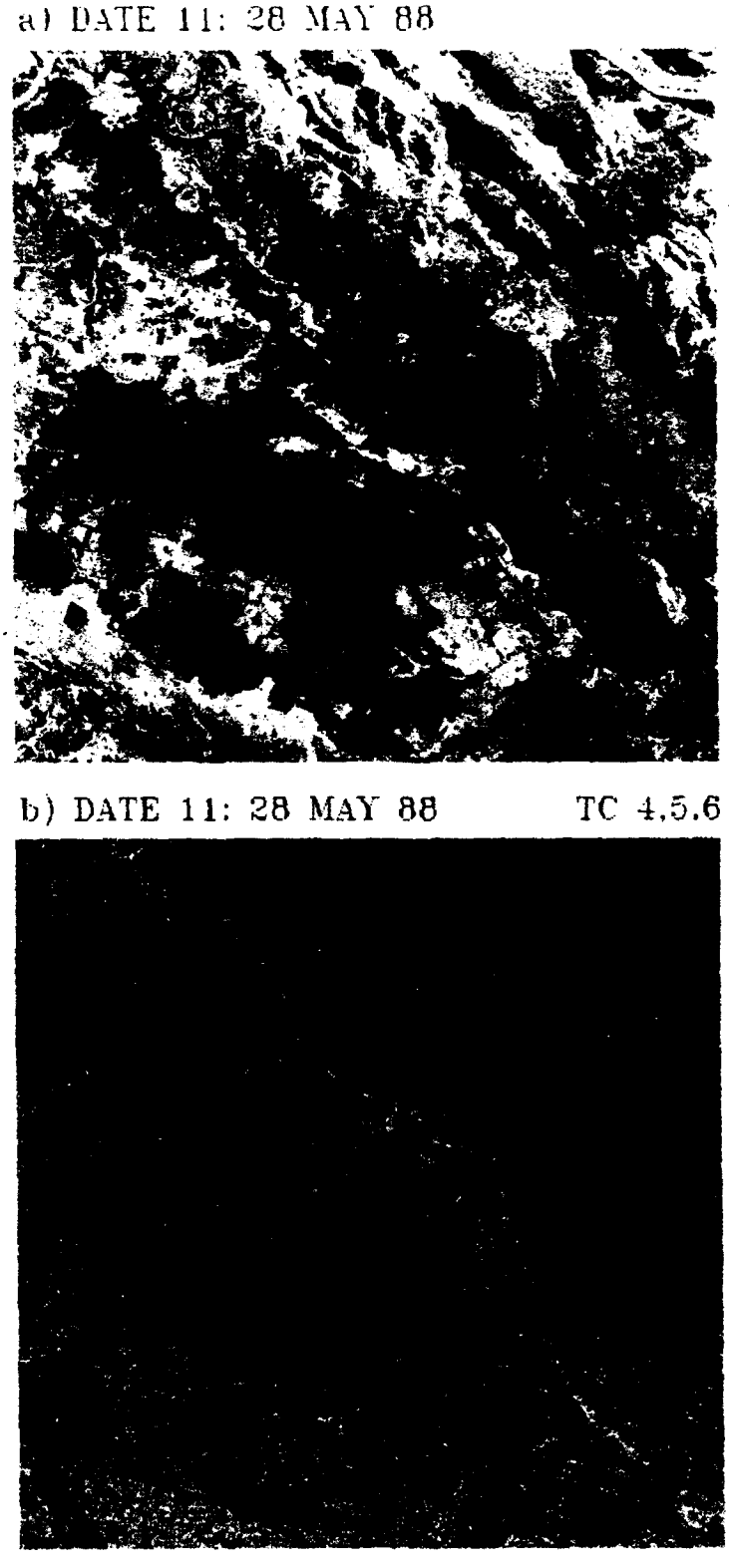

Figure 3-9. Tasseled Cap (TC) false color images of 38.4 km square area around Chernobyl 2.1 years postaccident: a) (R,G,B) = (Br,Gr,Wt) as in Figures 3-4 through 3-8 and b) (R,G,B) = (Hz,TC5,TC6), the last 3 components of the TC transformation.

Table 3-4. Coordinates (UTM, Zone 36) of the upper left corners of the corner pixels of the 1536 x 1536 pixel area analyzed in this report.

Corner pixel	*X (meters)*	*Y (meters)*
Upper left	277,100.	5,714,900.
Upper right	315,475.	5,714,900.
Lower left	277,100.	5,676,525.
Lower right	315,475.	5,676,525.

Date 1, shown in Figure 3-4a, is a summer image one year before the nuclear accident. This image is used as the reference image for the change detection analysis presented in Volume 2. The red patches in Figure 3-4a are mostly soil in agricultural fields. The Chernobyl nuclear power station at the upper left of the cooling pond and the city of Pripyat also show as red. These areas have high brightness, low greenness, and low wetness in the TC spectral coordinate system. The darker, mostly bluish areas to the lower left (southwest) of the cooling pond are areas of predominately coniferous forest. Portions of the forest have been cleared for farmland. The lighter, more greenish areas sometimes grading into the coniferous forest are predominately deciduous vegetation.

Date 2, shown in Figure 3-4b, is a late winter image taken five weeks before the accident. Ice and snow have high brightness, low greenness, and high wetness and appear magenta in the image since (R,G,B) = (Br,Gr,Wt). The Pripyat River is frozen over and residual snow cover is apparent bordering the areas of coniferous forest, which are now the strongest green areas of the image. Clearings in the coniferous forest are snow covered even though farmland is not. This observation suggests that the snowfall is not recent. It is likely that the floor of the forest is snow covered but the canopy is snowless. The snow cover will then show through from the satellite perspective wherever pine trees are thinner. This observation from the image implies that in areas of high TC greenness, TC brightness and wetness provide a measure of coniferous canopy closure.

Date 3, shown in Figure 3-5a, is three days after the accident. There are more bare fields on this date than on Date 1 since it is earlier in the growing season. Likewise, deciduous areas have greened somewhat, but there is only moderate contrast between the evergreen and deciduous areas. Dates 4, 5, and 6, shown in Figures 3-5b, 3-6a, and 3-6b, respectively, are range from 12 days to 5 weeks after the accident. By the end of May (Date 6), the contrast between evergreen and deciduous vegetation has returned to the higher level of Date 1 a year earlier.

Date 7, shown in Figure 3-7a, is apparently after the autumn leaf senescence since the greenness of the deciduous vegetation has dropped dramatically. Date 8, shown in Figure 3-7b, is in December after the accident. It is similar to Date 2 except that the Pripyat River is not frozen and there is no snow cover.

Dates 9 and 10 are shown in Figure 3-8. They are 1.0 and 1.4 years after the accident, respectively. Date 11, shown in Figure 3-9a, is 2.1 years postaccident. The cessation of agriculture in the analysis area after the accident is apparent from the absence of any fields with bare soil after Date 6 (31 May 1986). Such fields show up as bright red areas because of the high brightness of most bare soils. The red fields in the images before Date 6 are fading as cultivated fields are overtaken by indigenous vegetation.

On the other hand, the increasing size of the red area around the reactor station on Dates 9, 10, and 11 shows land, including forests, being cleared as part of the radiation decontamination effort. On close examination, Date 7 shows earlier forest clearing along a road that crosses the trace of highest fallout deposition about 2 km west of Reactor Unit 4. The analysis of radiation response must account for these cleared areas and avoid mistaking cleared forest for radiation damaged trees.

Figure 3-9b shows the other three bands of the Tasseled Cap image for Date 11 presented as (R,G,B) = (Hz,5,6). The lack of contrast in this image relative to the first three bands of the same image presented in Figure 3-9a illustrates how the Tasseled Cap transformation includes most of the pixel variance for vegetation scenes in the first three bands. The largest contrast in Figure 3-9b is between the urban/industrial area and the cooling pond, for which the Tasseled Cap transformation was not optimized.

In summary, the Tasseled Cap images for Dates 1 through 11 as shown in Figures 3-4 through 3-9 provide the data for all analysis in this volume.

3.3 PRELIMINARY CLASSIFICATION OF EVERGREENS.

This subsection describes the preliminary classification of vegetation in the 38.4 km square analysis area aimed at the identification of pixels in the image dominated by pine forest. We first define areas of evergreen vegetation and then use an unsupervised clustering algorithm (see, for example, Duda and Hart, 1973) in TC space to group the pixels into spectrally-related classes.

3.3.1 Selection of Evergreen Pixels.

In order to provide good discrimination between coniferous and deciduous forest, we construct a composite image from the preaccident images of 21 March 1986 (late winter) and 6 June 1985 (early summer). Table 3-5 shows the band structure of the composite image. We refer to this winter/summer composite image as COMP21 since it is generated from Dates 2 and 1.

Table 3-5. Band structure for the winter/summer composite image, COMP21, generated from Dates 2 and 1.

COMP21 Band	*Tasseled cap band(date number)*	*Tasseled cap feature name*
1	Br(2)	Winter brightness
2	Gr(2)	Winter greenness
3	Wt(2)	Winter wetness
4	Br(1)	Summer brightness
5	Gr(1)	Summer greenness
6	Wt(1)	Summer wetness
7	Th(1)	Summer thermal

An obvious difference between coniferous and deciduous forest is that coniferous forest has moderate greenness in both winter and summer while deciduous forest has high greenness in summer and low greenness in the winter. Figure 3-10 exploits this contrast by displaying winter greenness and summer greenness as the complementary colors green and magenta, respectively, in the same image. Evergreen vegetation, including coniferous forest, appears in varying shades of bright green. Deciduous vegetation appears magenta.

Because the presentation colors in Figure 3-10 are complementary, pixels that have equal relative greenness in summer and winter appear as a shade of gray. Very dark shades of green are associated with the cooling pond, the power station, and some cultivated fields. Other cultivated fields appear nearly white. The Pripyat River and its meandering stream bed are nicely defined across the diagonal of the image. The river flows from upper left to lower right. The smaller Uzh River flows to the right across the lower portion of the image, dipping temporarily off the lower edge before emptying into the Pripyat River at the lower right corner of the image. Although it is not readily visible in Figure 3-10, the city of Chernobyl lies on the right bank of the Pripyat River along the north side of the Uzh River.

The false color presentation of COMP21 in Figure 3-10, interpreted in the context of regional information presented in Section 3.1, clearly indicates the presence of the large contiguous areas of pine forest in the vicinity of the Chernobyl nuclear power station, especially to the west in the direction of the main trace of early fallout deposition. To maximize the amount of data, we want to find all pixels (25 m by 25 m each) whose ground cover is dominated by pine trees. The method of classifying individual pixels based on their spectral signature is discussed in Volume 2. In short, we find a representative set of pixels, called a reference site, which defines the mean vector

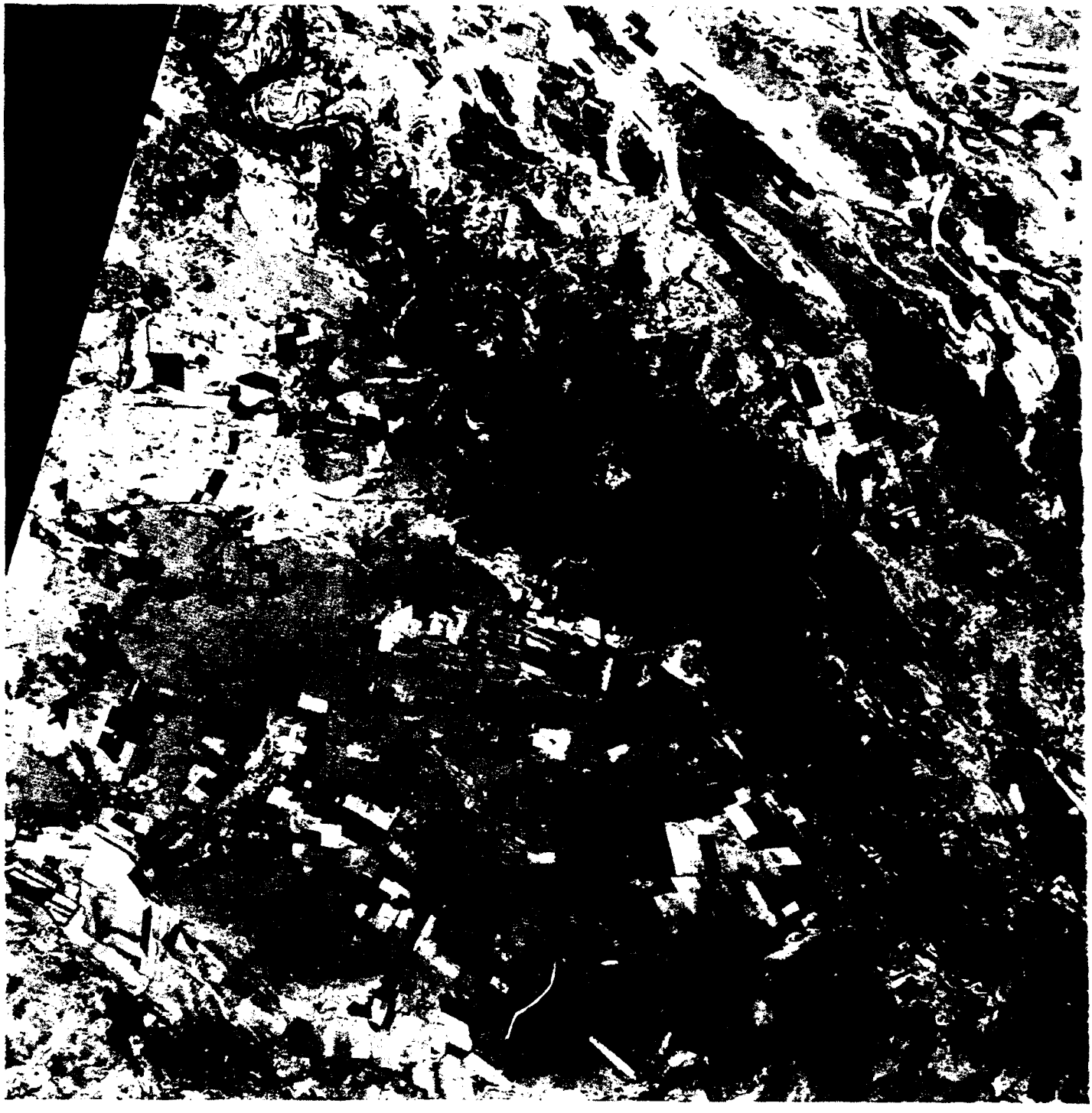

Figure 3-10. Evergreen vegetation appears bright green and deciduous and annual vegetation appears magenta in this false color presentation of COMP21 with (R,G,B) = (5,2,5).

and the covariance matrix for the spectral signature of each vegetation class of interest. Maximum likelihood is then used to assign pixels to the various classes.

Figure 3-11 outlines the procedure for defining classes of evergreen vegetation occurring in the 38.4 km square analysis area. The procedure described in Figure 3-11 is a preliminary classification and need not account for all pixels in the image. In fact, to limit the complexity of the task, it is best to preselect pixels of the general type needed for the final analysis. Therefore, we limit our preliminary classification to pixels of evergreen vegetation.

The selection of evergreen pixels is based on ranges of brightness, greenness, and wetness from the winter scene of Image 2. The ranges are listed in Figure 3-11. These ranges were chosen after examination of histograms of values of brightness, greenness and wetness for identifiable areas in Image 2. The ranges were adjusted to cut out areas of water, ice, snow, soil, urban/industrial areas, and deciduous vegetation while keeping all pixels with a moderate to high value of wintertime greenness.

As mentioned in Section 3.2.2, because of snow cover on the forest floor, TC brightness and wetness provide a measure of canopy closure in areas of coniferous forest. By inspection, we found that the wetness intensity value increased from about 146 to about 184 as the canopy closure varied from maximum (presumably near 100%) to zero. The wetness value for snow and ice was distributed mostly between 184 and 216, with a tail extending to 255.

Figure 3-12b shows the set of pixels that pass the brightness, greenness, and wetness cuts defining evergreen pixels as shown in Figure 3-11. These evergreen pixels are marked in green over a gray-scale background image. This figure should be compared with Figure 3-10 to judge the effectiveness of the evergreen cuts. Notice that very few pixels in the agricultural fields or in the bottom land along the river passed the evergreen criteria. Most importantly, the obvious magenta areas in Figure 3-10 corresponding to deciduous or annual vegetation do not appear in the set of evergreen pixels.

For the purpose of contrast, Figure 3-12a shows the same presentation as Figure 3-10 except that the roles of winter and summer greenness are reversed. The resulting false color image displays deciduous areas in bright green and evergreen areas in magenta.

3.3.2 Unsupervised Clustering of Evergreen Pixels.

As a first step toward identifying pine forest pixels in the analysis area, we use the first six bands of the winter/summer composite image COMP21 to divide the evergreen pixels into a manageable number of spectrally-related classes. Manual examination of the shape and structure of the evergreen pixel distribution in the six-dimensional spectral hyperspace is difficult, so we use an unsupervised clustering algorithm to divide the structure into ten neighborhoods or clusters.

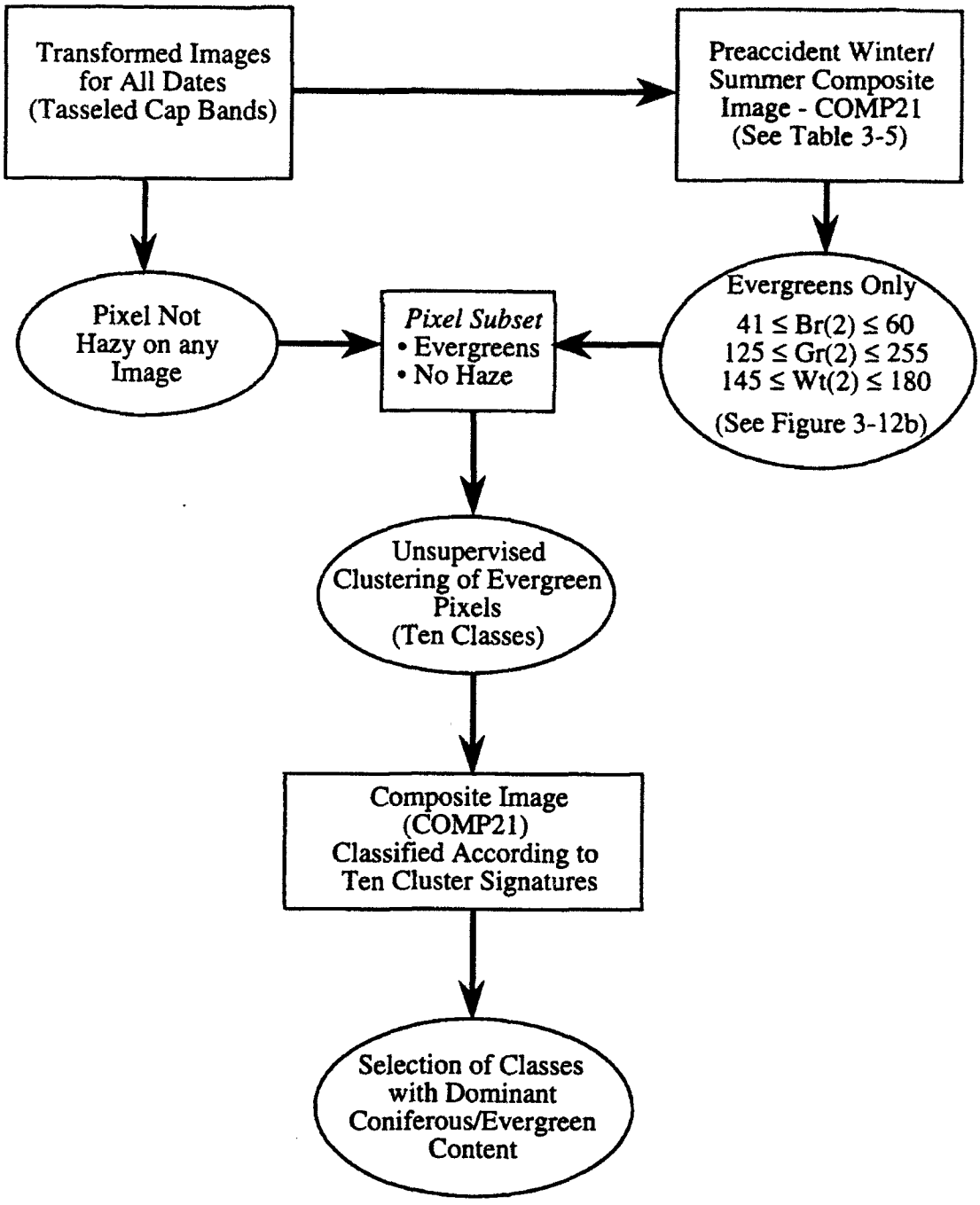

Figure 3-11. Procedure for classifying evergreen vegetation.

a) Deciduous in green

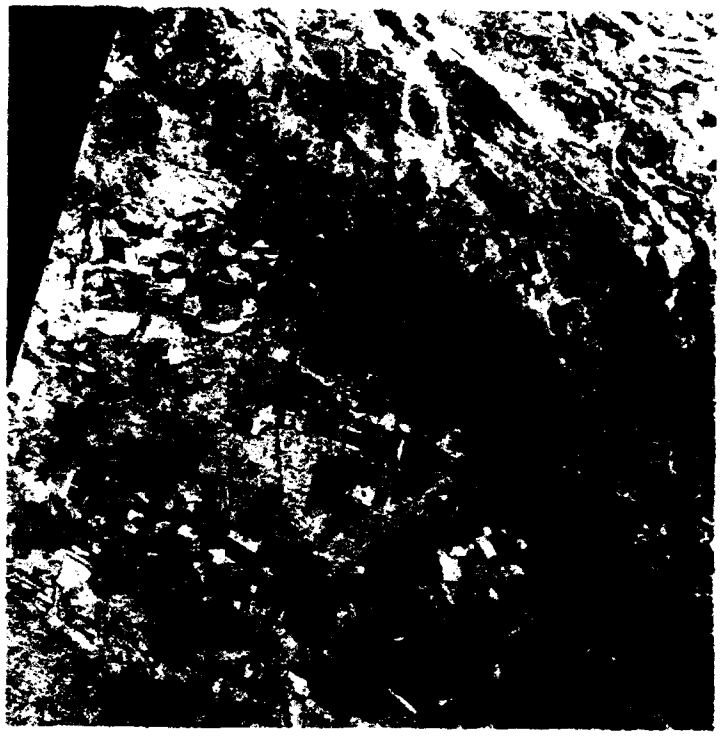

b) Evergreen areas

Figure 3-12. a) Like Figure 3-10 except color reversal (R,G,B) = (2,5,2) displays deciduous or annual vegetation in bright green and evergreens in magenta, and b) areas passing the evergreen criteria of Figure 3-11 shown in green.

The avoidance of pixels affected by clouds and haze is discussed in Section 3.4 below. Since Image 1 and, hence, COMP21 contains significant clouds in the lower third of the image, we use the haze mask from Section 3.4 to avoid affected pixels in the subset used for unsupervised clustering.

For unsupervised clustering, we use the ISODATA algorithm, which stands for "Iterative Self-Organizing Data Analysis Technique" (Tou and Gonzalez, 1974). The multipass algorithm is based only on the spectral signature of each pixel and not on that of its spatial neighbors in the image. The algorithm begins with a selected number (ten in this case) of class mean intensity vectors spaced evenly along a straight line through the region occupied by the evergreen pixels. On the first pass of the algorithm, all pixels are assigned to the class with the nearest mean. Each class mean is then moved to the mean value of the pixels assigned to it. On the next pass, class assignments of all pixels are reevaluated and adjusted based on distances to the new means. The process is repeated until subsequent iterations produce changes in pixel assignments less than a specified percentage. The method is reasonably nonparametric and is not biased toward any spatial location on the image. Results are also reasonably independent of the initial placement of means.

The mean pixel vector and the covariance matrix of the resulting ten classes from the unsupervised clustering of evergreen pixels were used to classify all pixels of the COMP21 image. Examination of the spectral signatures of the ten classes and the spatial distribution of pixels assigned to each class resulted in the elimination of four of the ten as either only marginally evergreen or lacking in contiguous areas of significant size. The spectral signatures of the remaining six classes, numbered 3 through 8 are displayed in Figure 3-13 along with the spectral signatures of the two forest classes used in the preliminary analysis of Volume 2. Detailed listings of the spectral signatures appear in Appendix D.

3.3.3 Identification of Evergreen Classes.

The spectral signatures of the six classes retained from the unsupervised clustering are best distinguished from one another in Figure 3-13 by the plot of Band 5 versus Band 4 (CHAN 5 versus CHAN 4) of the COMP21 image. This is a plot of summer greenness versus summer brightness. The spectral signatures organize into two branches emanating from Class 5. The 4/3 branch extends to higher brightness and lower greenness and the 6/8 branch extends to both higher brightness and greenness.

Similarity to the Forest1 and Forest2 signatures from the analysis of Volume 2 shows that the 4/3 branch corresponds to the large areas of coniferous forest evident in Figure 3-10. Class 5 is pine forest with the highest canopy closure and the least component of deciduous trees since it has the lowest brightness of all the classes in both summer and winter and the highest greenness in the winter.

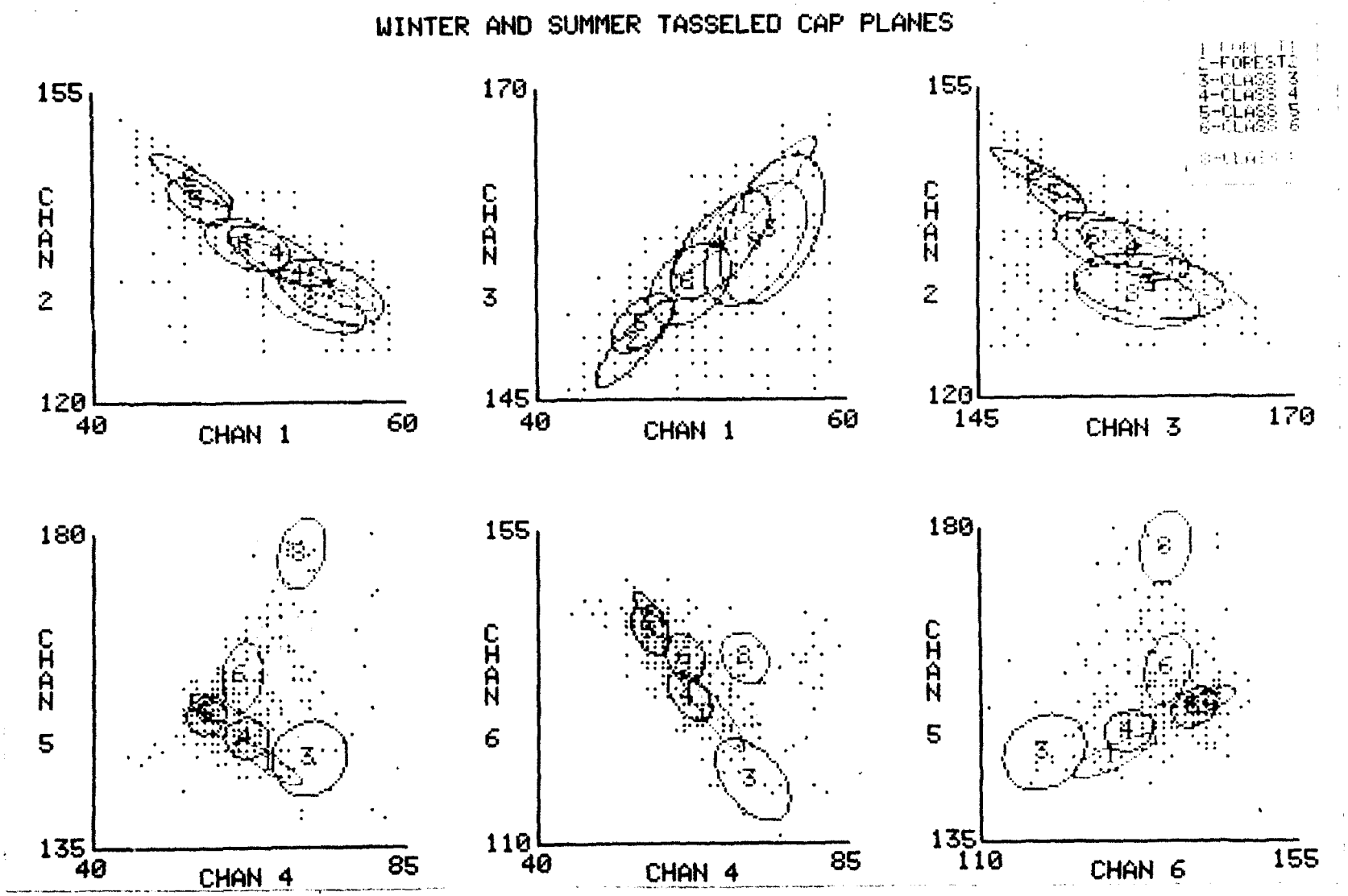

Figure 3-13. Spectral signatures of selected classes from the unsupervised clustering of evergreen pixels. One standard deviation ellipses for each class overlay a scatter plot of the evergreen pixels. Signatures labeled Forest1 and Forest2 correspond to Sites 3 and 4, respectively, as defined in Volume 2. (CHAN # refers to COMP21 band numbers as listed in Table 3-5.)

Class 3 has lower greenness and higher brightness than Class 5 in both summer and winter; it apparently consists of similar pine trees with lower canopy closure (less dense foliage) but no significant component of deciduous trees which would increase the greenness feature in summer. The signature of Class 4 lies between Classes 5 and 3 in both summer and winter, indicating that it consists of the same pine trees with intermediate canopy closure. Thus, the 5/4/3 class sequence is apparently due to varying canopy closure of similar trees.

Class 6 is adjacent to Class 5, the high density pine forest. In the winter it has essentially the same spectral signature as Class 4 and so may be inferred to contain about the same density of pine trees as Class 4. On the other hand, Class 6 has a higher greenness in summer than Class 6, indicating that the pine trees in Class 6 are interspersed with deciduous trees.

Class 8 is most removed from Class 5 along the 6/8 branch in the summer brightness/greenness plane. The very high summer greenness value indicates a dominant component of deciduous or annual vegetation. On the other hand, the winter greenness value still indicates a significant evergreen component. Three possibilities are sparse pine trees in deciduous forest, evergreen shrubs or vines as understory in deciduous forest, and evergreen shrubs with other deciduous or annual vegetation. In exploratory calculations, we found clear examples of interspersed pixels of Class 6 and Class 8 where Class 6 showed definite radiation response and Class 8 did not. Also, by association with water patterns in the image, Class 8 apparently tends toward lower lying areas. We assume for further analysis that Class 8 contains few or no pine trees. A reference site for Class 8 is defined and Class 8 is retained in the pixel classification procedure, however, to minimize the number of Class 8 pixels that might otherwise be mistaken for Class 6.

Class 7 lies near the 6/8 branch of the summer spectral signatures between Class 6 and Class 8. With respect to of its spatial distribution, Class 7 tends to occur at the edges of Class 6 and to have no significantly sized areas of its own. We assume that it consists of mixed pixels rather than a primary forest type. We do not include it in further analyses because of the lack of a spatially homogeneous reference site.

3.4 REFERENCE SITES FOR PINE FOREST CLASSES.

Figure 3-14 outlines the procedure for selecting a single reference site for each of the retained classes of evergreen vegetation. The starting point is the winter/summer composite image with pixels classified according to the signatures of the classes from the unsupervised clustering described in Section 3.3.2. Using an interactive mode of the image processing software, polygons are drawn around several representative areas of contiguous pixels for each of the retained evergreen classes (3,4,5,6, and 8). These homogenous polygons are candidates for class reference sites.

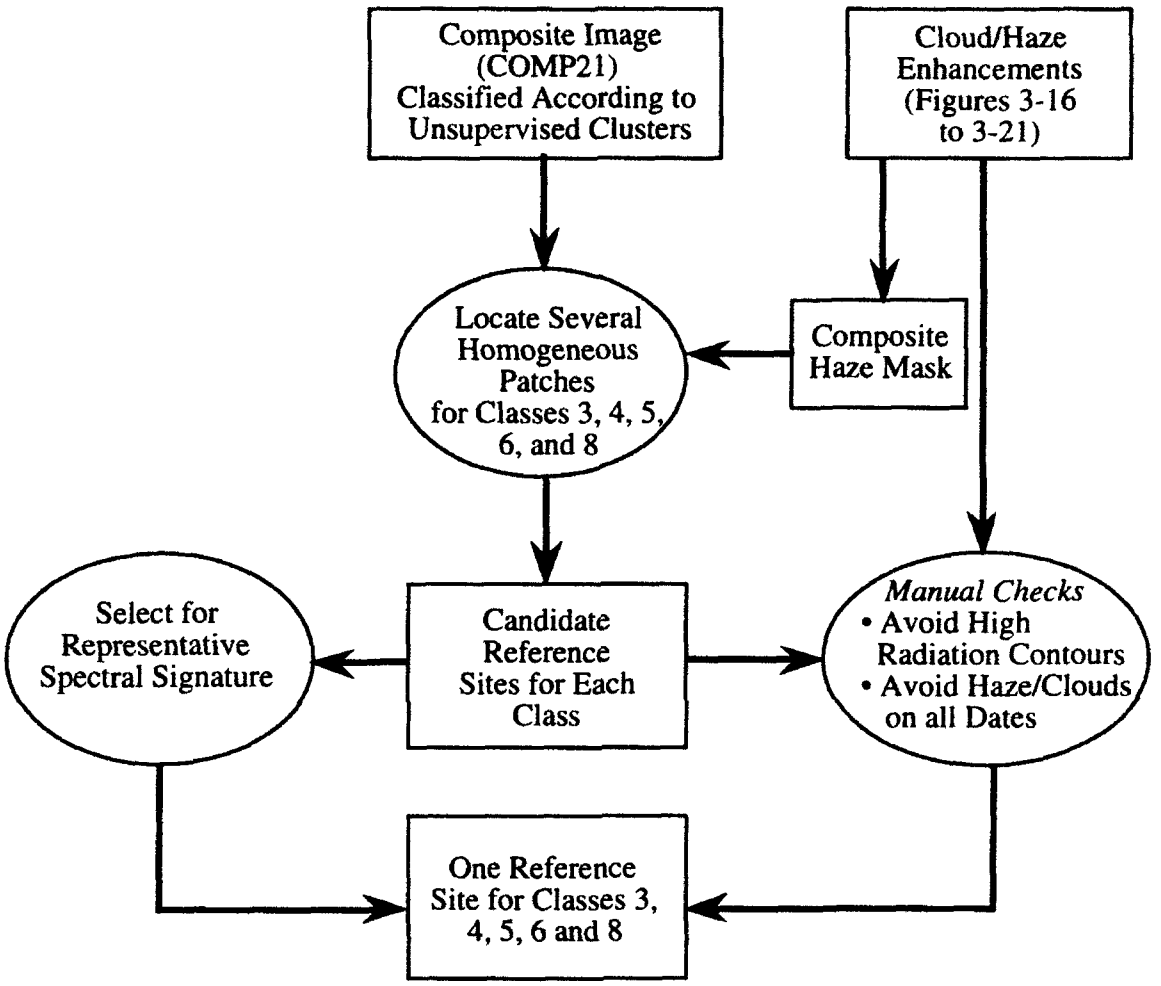

Figure 3-14. Procedure for selecting one good reference site for each coniferous/evergreen class.

The reference sites will be used to define the normal spectral signature of each pine forest class on each image date analyzed. As such, the reference sites must not be obscured by clouds or haze on any date and must not be significantly affected by radiation exposure on any date. Guidance from the forest response and radiation contours reported in Volume 2 is used to avoid areas of forest showing radiation damage. Images enhanced to show clouds and haze are used to insure a clear view of each reference site on each image.

3.4.1 Avoidance of Clouds and Haze.

Figure 3-15 shows a cloud and haze enhanced image for Date 1. The presentation shows clouds and hazy areas in blue and all other areas in shades of yellow and gray. The use of complementary colors (here, blue and yellow) follows the same principle used to contrast summer and winter greenness in Figure 3.10. The cloud and haze enhancement contrasts the Tasseled Cap haze band with the thermal band from the same date. The TC haze band, as discussed in Section 3.2, provides a high signal from the aerosols in clouds and haze and a generally lower signal from land and water surfaces. On the other hand, the thermal band provides a high signal from land surfaces warmed by the sun and a lower signal from clouds and haze, which are at the usually cooler temperature of the atmosphere. Display of the haze signal in blue and the thermal signal in yellow results in good definition of clouds and any nonuniform haze as shown in Figure 3-15.

Figures 3-16 through 3-21 show the cloud and haze enhanced images for each date. Only Dates 1, 3, 5, 6, 9, and 10 have significant clouds or nonuniform haze. As indicated in the procedural diagram of Figure 3-14, the cloud/haze enhancements are used in two ways. First, we construct a composite *haze mask* for the full set of images. A threshold value for the TC haze feature is determined for each of the six images with clouds or haze such that pixels in obvious areas of clouds and haze always exceed the threshold. With these thresholds, we create a single numerical mask that marks each pixel of the analysis area that is affected by clouds or haze on one or more dates. This haze mask is used during the selection of candidate reference sites to limit consideration to areas that are clear of clouds or haze on all dates.

Second, the individual cloud/haze enhancements are used in the final choice of a single reference site for each class to double check that the chosen site is always free of clouds and haze. This step is accomplished by plotting the polygons of the candidate reference sites directly on the cloud/haze-enhanced images.

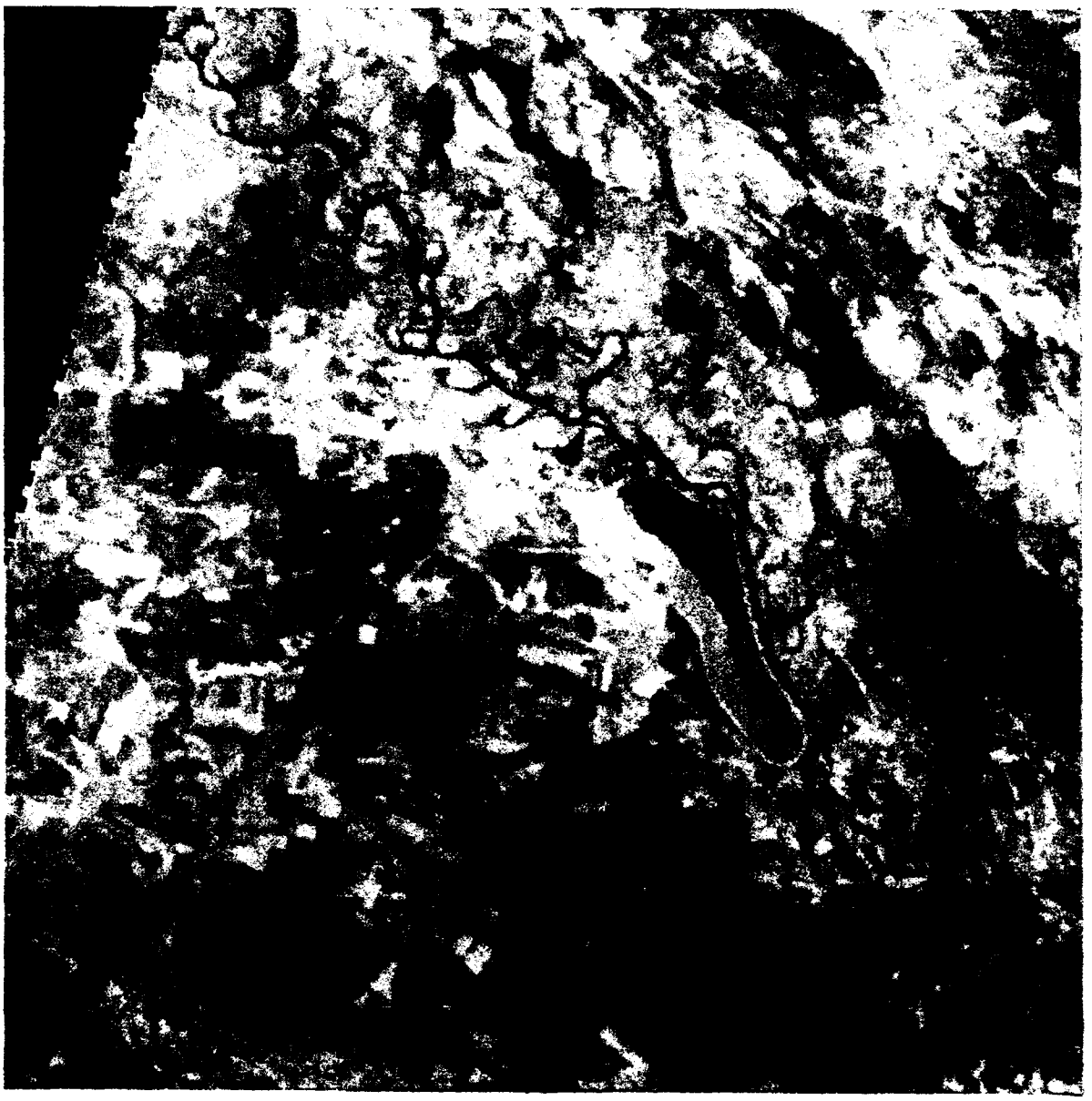

Figure 3-15. Cloud/haze enhancement for Date 1 for the 38.4 km square analysis area, (R,G,B) = (Th,Th,Hz). Clouds appear blue, warm areas yellow. Thermal gradient appearing as variation in yellow shade of the cooling pond shows counterclockwise flow of water around central barrier.

a) Training site locations

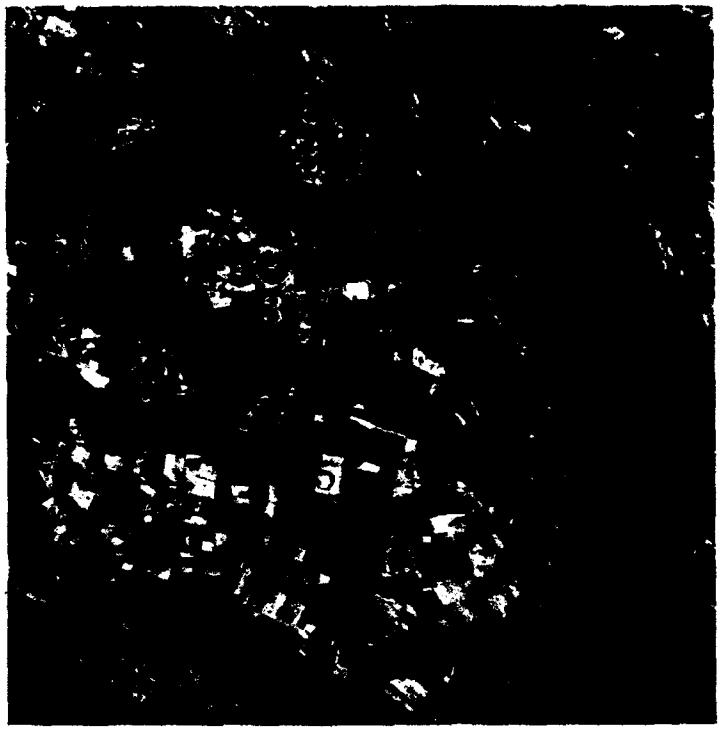

b) Date 1: 6 JUN 85

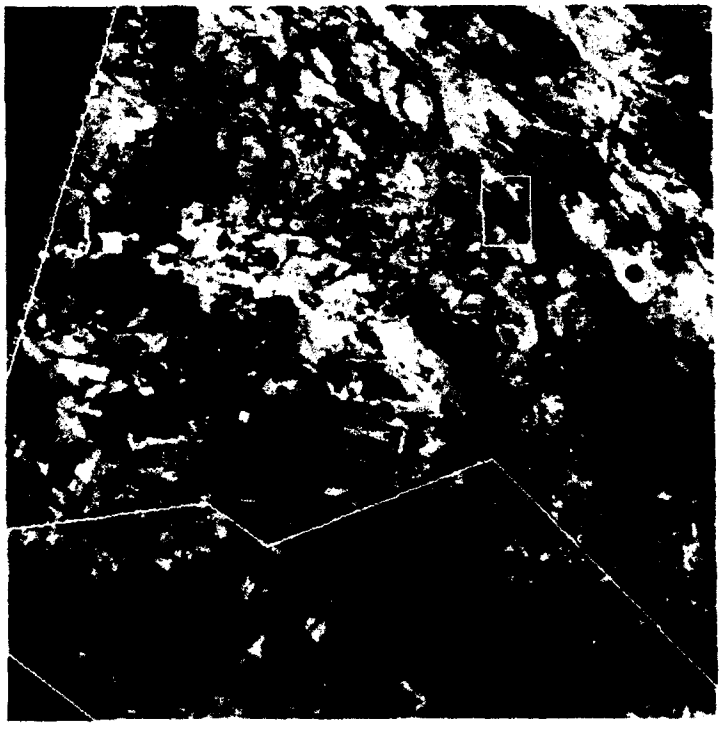

Figure 3-16. a) Reference (control) site locations for Classes 3, 4, 5, 6, and 8 in the 38.4 km analysis area and b) cloud/haze enhancement for Date 1 showing three polygons used for classification merger described in Section 3.5. Red dots are reference site locations.

a) Date 2: 21 MAR 86

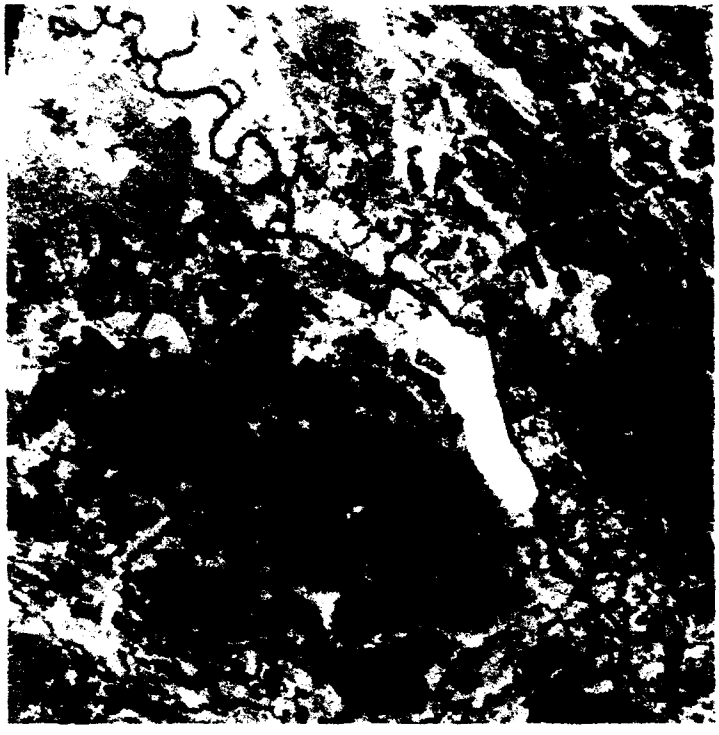

b) Date 3: 29 APR 86

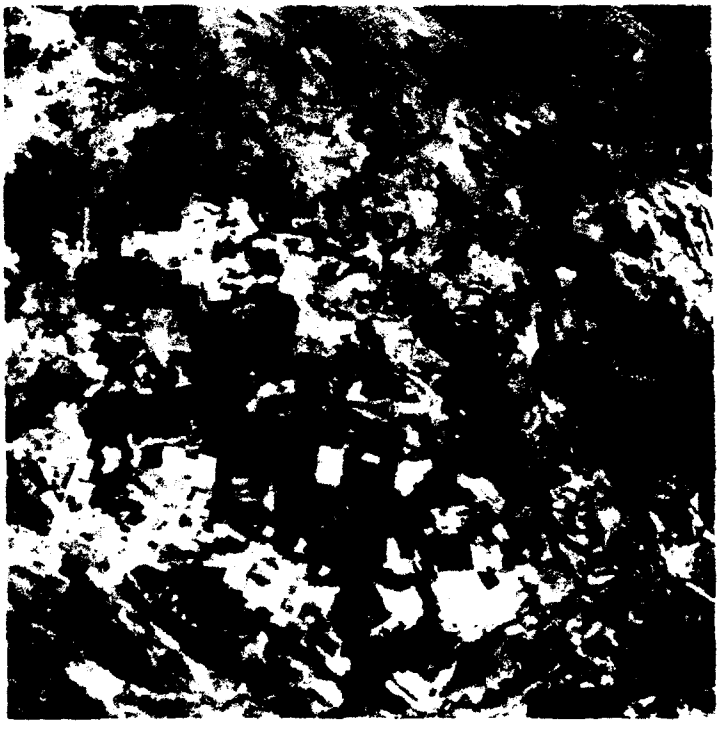

Figure 3-17. Cloud/haze enhancements for a) Date 2 and b) Date 3. Only Date 3 has clouds. Red dots are reference site locations.

a) Date 4: 8 MAY 86

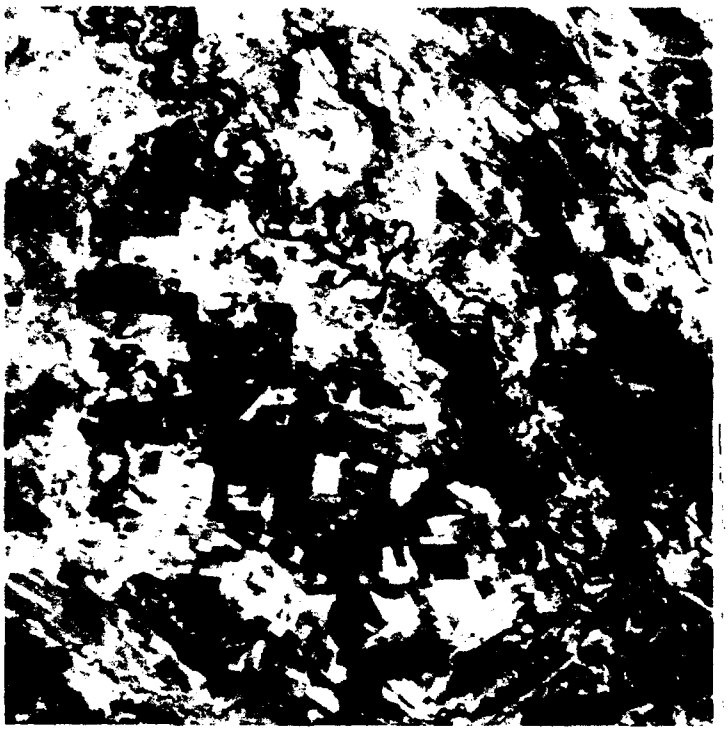

b) Date 5: 24 MAY 86

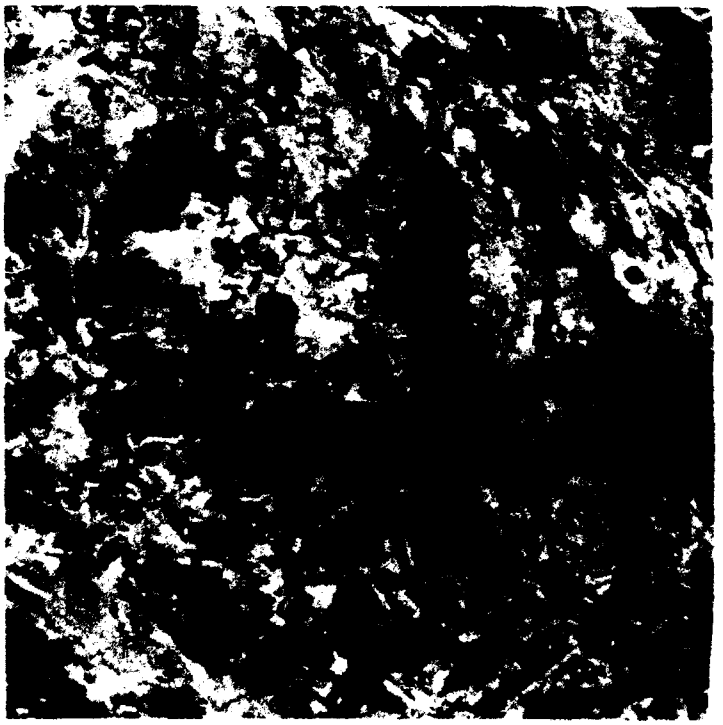

Figure 3-18. Cloud/haze enhancements for a) Date 4 and b) Date 5. Only Date 5 has clouds. Red dots are reference site locations.

a) Date 6: 31 MAY 86

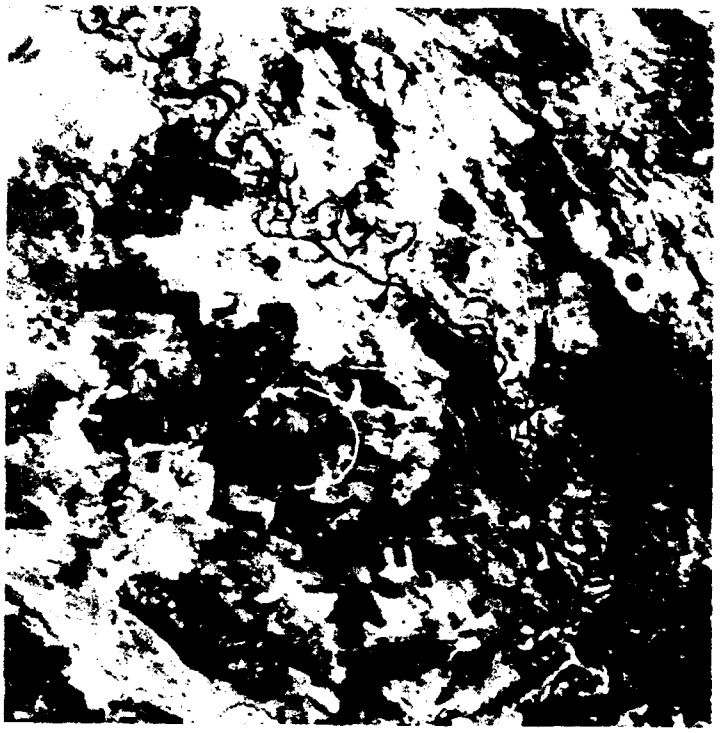

b) Date 7: 15 OCT 86

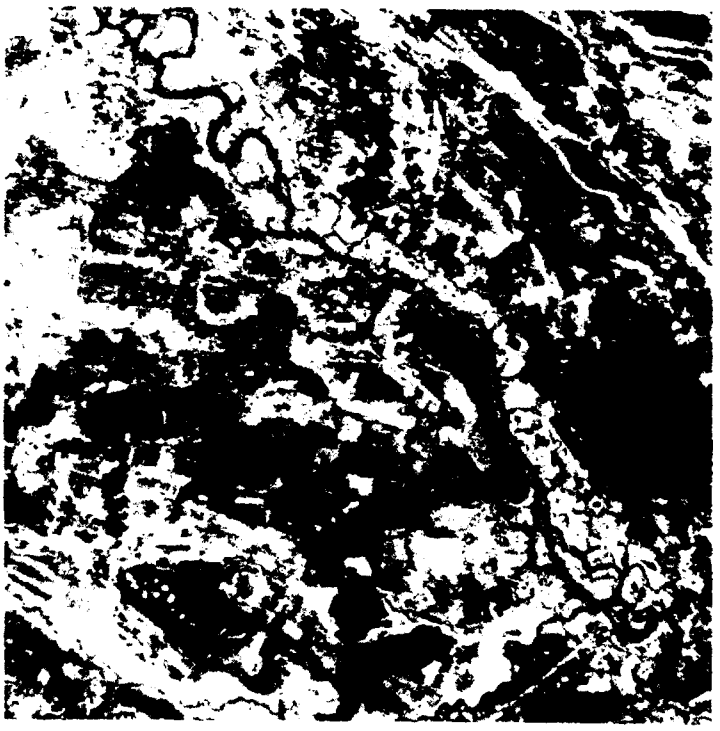

Figure 3-19. Cloud/haze enhancements for a) Date 6 and b) Date 7. Only Date 6 has clouds. Red dots are reference site locations.

a) Date 8: 2 DEC 86

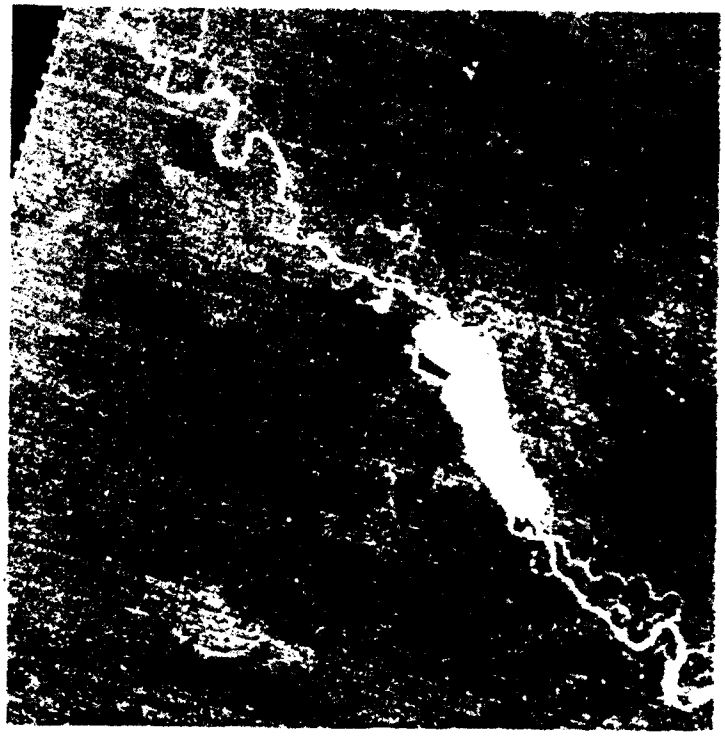

b) Date 9: 11 MAY 87

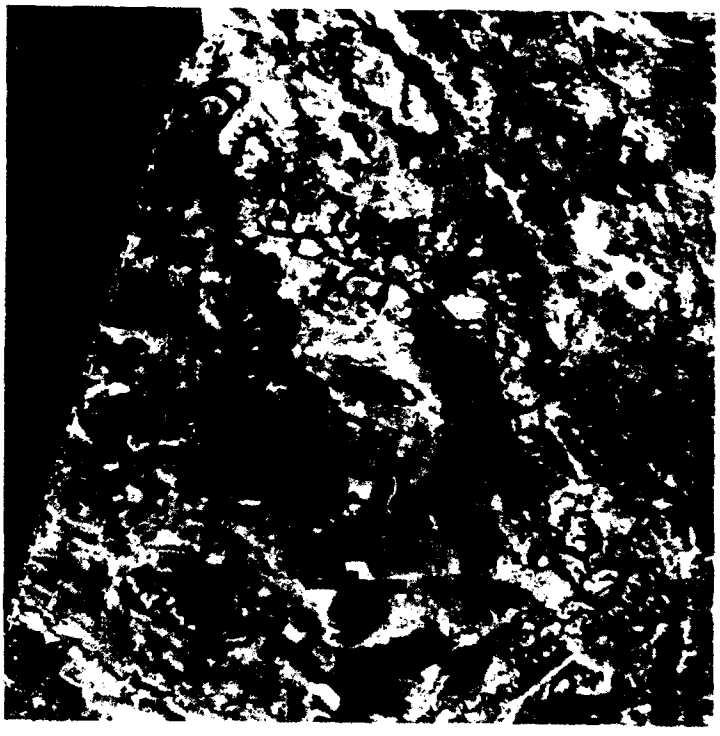

Figure 3-20. Cloud/haze enhancements for a) Date 8 and b) Date 9. Only Date 9 has clouds. Reference Sites 5, 6 and 8 have been moved on Date 9 to avoid a faint jet contrail.

a) Date 10: 7 SEP 87

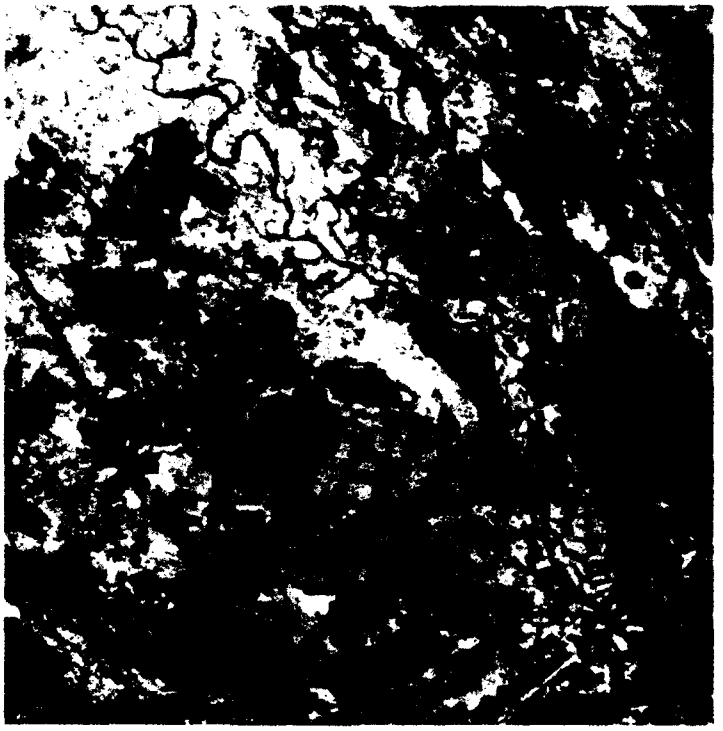

b) Date 11: 28 MAY 88

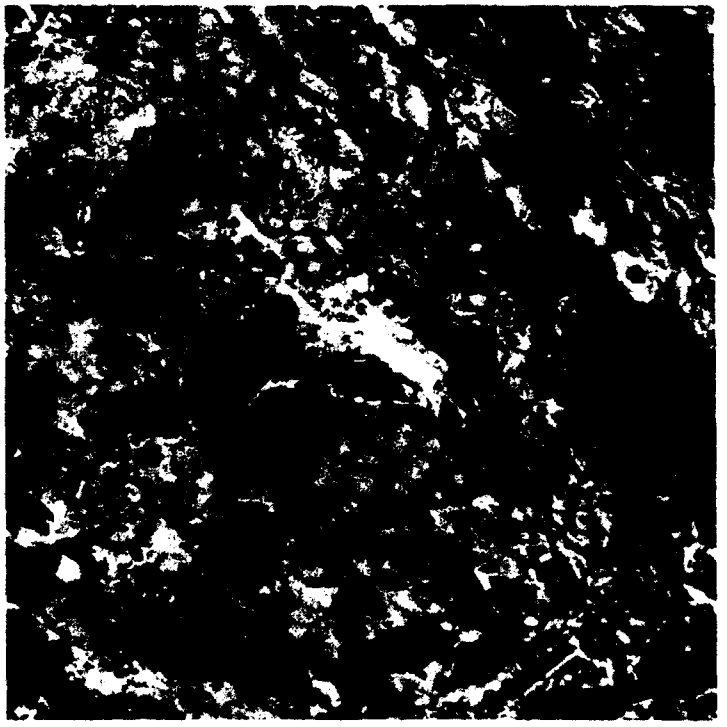

Figure 3-21. Cloud/haze enhancements for a) Date 10 and b) Date 11. Neither date has clouds, but Date 10 has a jet contrail. Red dots are reference site locations.

3.4.2 Representative Spectral Signatures.

During the final selection of reference sites, the spectral signature of each site is examined to insure that it is truly representative of its class. This step is accomplished by plotting the spectral signatures of each of the candidate sites with the signature of the overall class as in Figure 3-13.

3.4.3 Sites Chosen.

Figure 3-16a shows the final choice of primary reference sites for Classes 3, 4, 5, 6, and 8 overlaying a gray-scale image of the analysis area. On this image, the actual size and shape of each reference site is displayed as a patch inside a circle labeled with the class number of the reference site. Included on the cloud/haze enhancements in Figures 3-16 through 3-21 for each of the eleven image dates are five red dots marking the location of the reference sites. For better visibility, the red dots on the enhanced images are larger than the actual reference sites.

The primary reference sites shown in Figure 3-16a are used on all images except Date 9. On this date, the primary Reference Sites 5 and 8 are slightly obscured by the remnants of a jet contrail. Site 5 is moved to a nearby patch in the same forested area and Site 8 is moved across the river to a similar site. Finally, primary Reference Site 6 is off the edge of the available image on Date 9. It is also moved across the river to a similar site on this date. Reference Sites 3 and 4 are unchanged. Site 3 is near, but safely outside, the contrail. Note that a very well defined, presumably newer, jet contrail appears in the image on Date 10. Date 5 shows hints of a contrail along the same flight path. Date 5 also has a broader diffuse band passing north/south over the reactor cooling pond. It may be an old contrail or a thin cloud.

3.4.4 Other Impacts of Clouds and Haze.

The enhanced images show that Dates 2, 4, 7, 8, and 11 are entirely free of clouds over the analysis area. These images presumably have varying degrees of atmospheric haze from one date to another, but the haze is uniform over each image and does not impact the radiation response analysis.

The occurrence of occasional scattered clouds on the other image dates is tolerable in our analysis even though the presence of a cloud over a forested area in an image causes an apparent deviation from normal of the obscured pixels. We avoid difficulties with the apparent deviation due to clouds by requiring persistence from date to date in the detection of radiation-induced response. Because the percentage of cloud cover is low and because we have several cloud-free images, there is no case where coincidence of cloud cover in successive images mimics damaged forest.

It is interesting to note in passing that the thermal signals from the reactor cooling pond represented by the shades of yellow in Figures 3-16 to 3-21 show that after the explosion of Unit

4, the other three reactors were turned off on Dates 3 through 6. At least one reactor was operating on Date 7 (October 1986) and thereafter through Date 11.

3.5 PREACCIDENT PINE FOREST CLASSIFICATION MAP.

The classification of evergreen pixels in the winter/summer composite image COMP21 requires extracting the spectral signature of the reference sites for Classes 3, 4, 5, 6, and 8 from COMP21. These spectral signatures consist of the mean pixel intensity vector and its covariance matrix for each reference site. With this information, the likelihood that a pixel belongs to each class is calculated. The pixel is assigned to the class with the highest likelihood as long as a threshold value is exceeded. Pixels below the threshold value are not assigned to any class. We used the first six bands of COMP21 for the signatures and the maximum likelihood assignment to classes. These six bands are the brightness, greenness, and wetness for winter and summer as listed in Table 3-5. The maximum likelihood method is discussed further in Section 5.1 of Volume 2.

Because Image 1 is missing one corner and is also affected by clouds as illustrated in Figure 3-15, the pixel classification from COMP21 is not satisfactory for the whole analysis area. The areas of unacceptability are outlined in white by three polygons in Figure 3-16b. Fortunately, Image 4 from 12 days after the accident is cloud free and can provide a substitute summer component for a composite winter/summer image. We have constructed such a composite called COMP24 according to Table 3-5 by substituting Date 4 for Date 1. Although technically not a preaccident composite, COMP24 serves as a reasonable substitute since the areas of unacceptability in COMP21 are far enough from the reactor station to show no radiation effects by Date 4. The final classification uses COMP21 where acceptable and COMP24 elsewhere.

The procedure for generating the final pixel preaccident classification map is illustrated in Figure 3-22. COMP24 is classified using spectral signatures from its own reference sites in the same way as COMP21. Classifications from COMP21 and COMP24 are merged by using the COMP21 pixel assignments everywhere except within the three polygons displayed in Figure 3-16b where assignments from COMP24 are used.

Figure 3-23 displays the final pine forest classification on a pixel-by-pixel basis for the central 512 x 512 pixel section of the analysis area. Classes 3, 4, 5, and 6 are color-coded according to the labeled squares in the figure. Unassigned pixels are represented by a gray-scale image taken from Date 4 to provide spatial background for the classification map. Figure 3-24 provides the same display at a lower magnification for the full analysis area using the same color code. Class 8, although used in the maximum likelihood pixel assignments, is not represented in Figures 3-23 and 3-24 because it is presumed to have negligible pine tree content as discussed in Section 3.3.3.

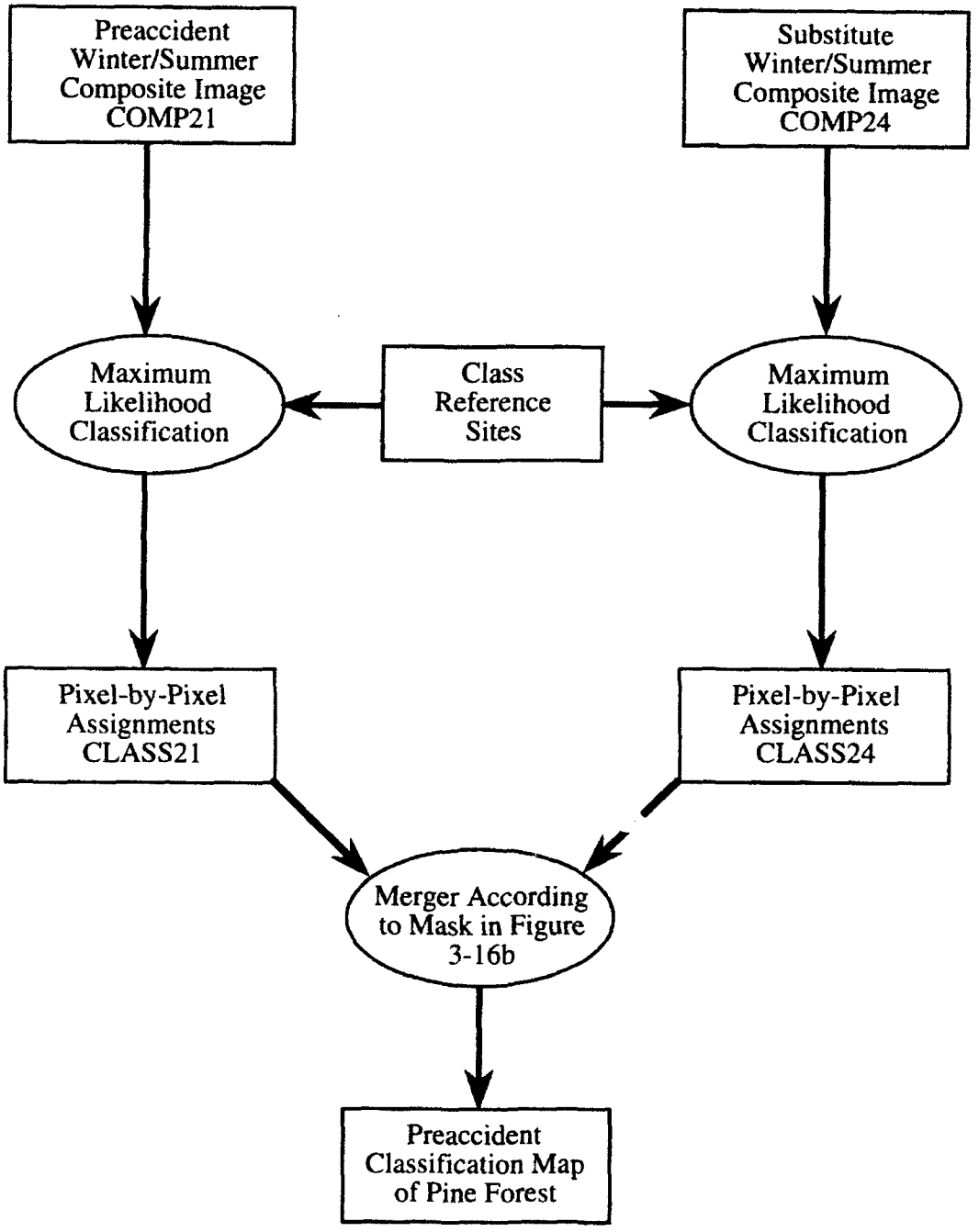

Figure 3-22. Procedure for generating final preaccident classification of pine forest.

Table 3-6 defines the pine forest classes based on the discussion in Section 3.3.3. According to Section 3.1, the pine trees are likely to be *Pinus sylvestris* (Scotch pine).

Table 3-6. Pine forest classes.

Class number	*Tree composition*
3	Predominately pines, low canopy closure
4	Predominately pines, moderate canopy closure
5	Predominately pines, high canopy closure
6	Mixed pines and deciduous, pine density like Class 4
8	Believed to contain very few pine trees

Figures 3-23 and 3-24 show that the highest density pine trees (Class 5 in dark green) are in the large areas of forest southwest of the reactor site. These same areas have large sections of the moderate density pine forest (Class 4 in light green). Mixed forest (Class 6 in cyan) tends to occupy the borders of these areas. Large areas of mixed forest occur near the southern edge of the analysis area in Figure 3-24. The patches of pine forest directly west of the reactor station within a few kilometers are dominated by Classes 3, 4, and 6 with essentially no high density pine stands. Likewise, across the Pripyat River in the northeast corner of the analysis area, there is little Class 5 forest.

In conclusion, Classes 3, 4, 5, and 6 are used in Section 7 for the analysis of radiation dose response after the explosion of Unit 4 at the Chernobyl nuclear power station.

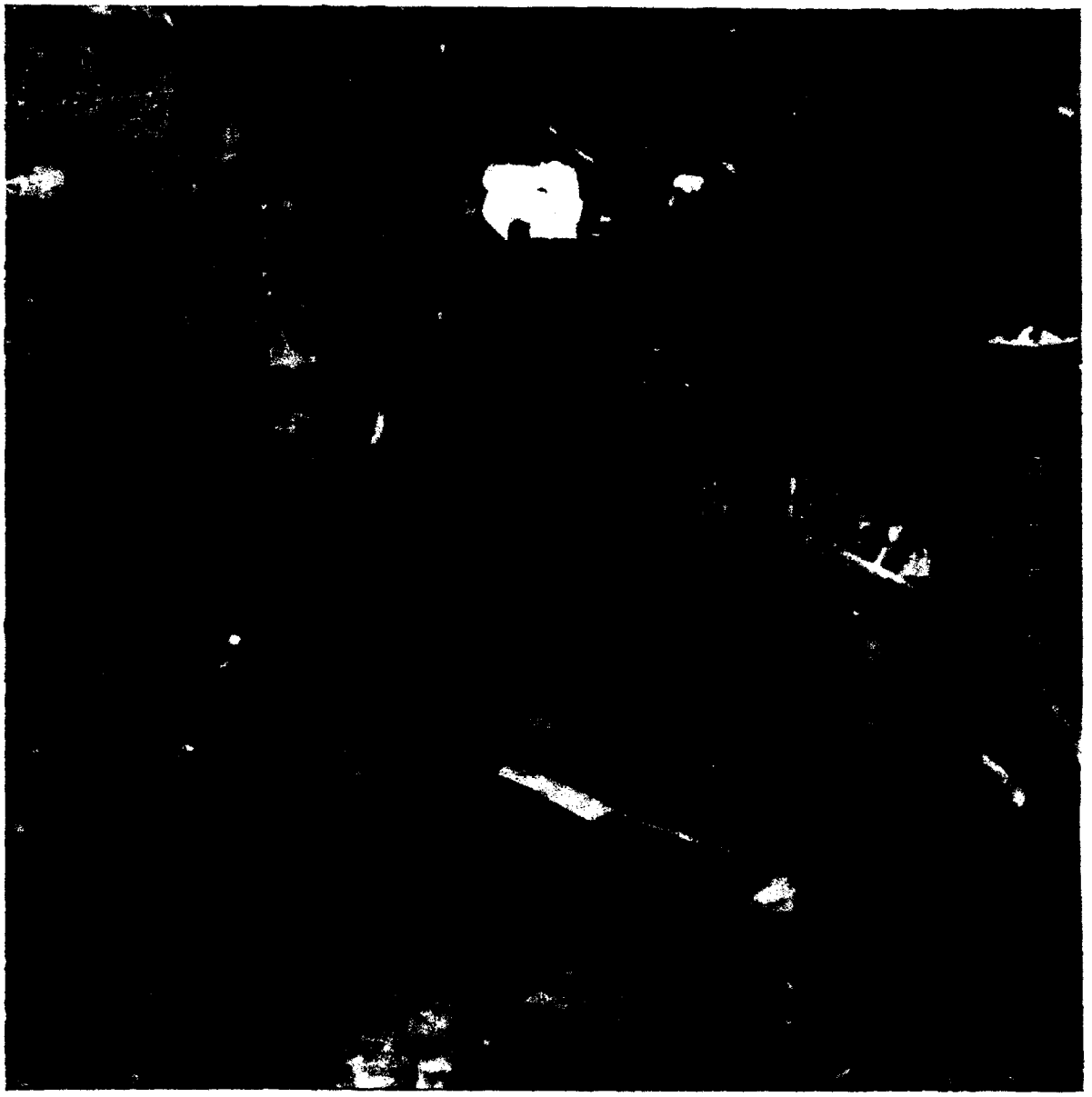

Figure 3-23. Final preaccident classification of pine forest for the 12.8 km square area analyzed in Volume 2. Class numbers according to Table 3-6.

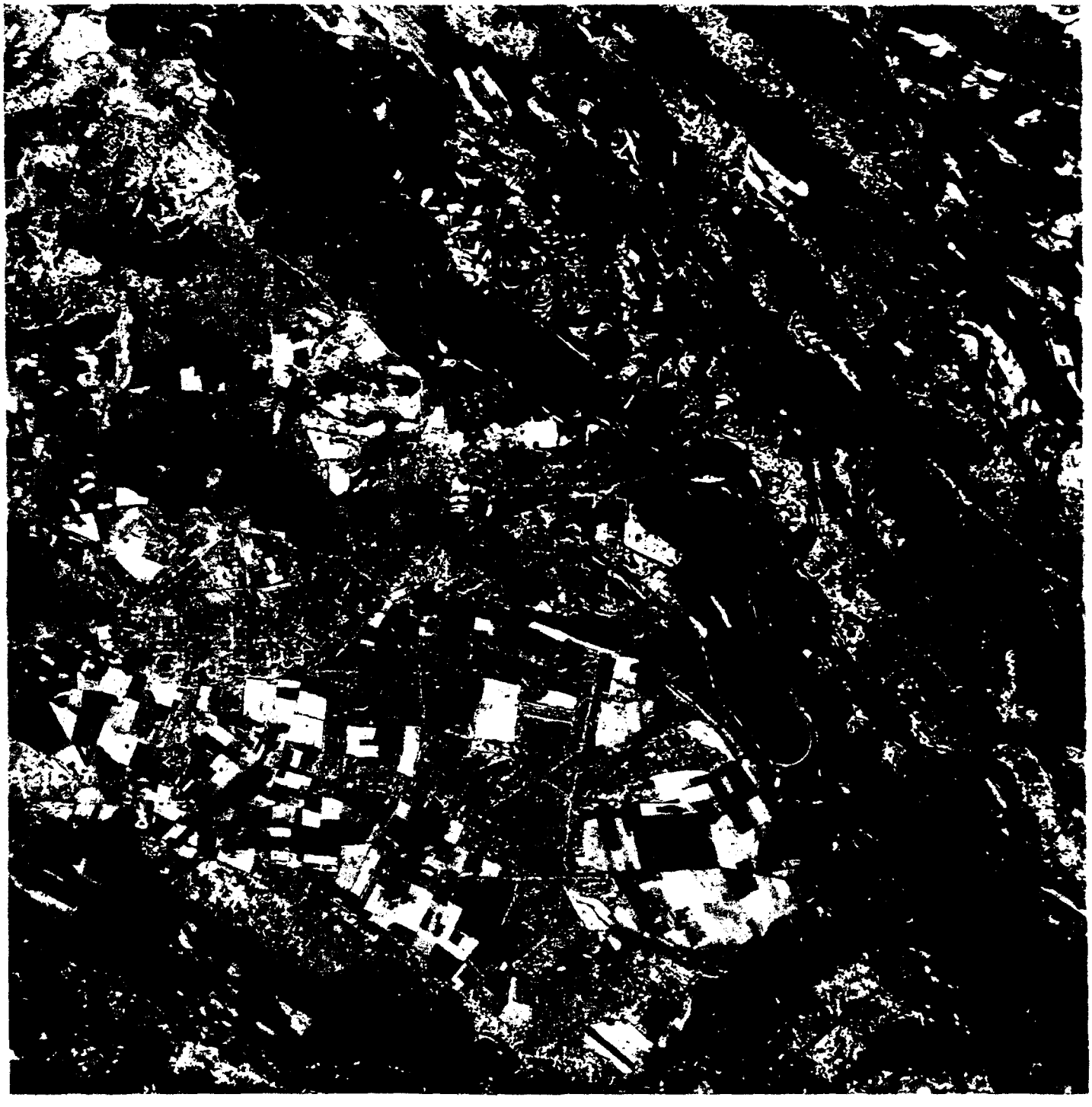

Figure 3-24 Final preaccident classification of pine forest for the full 38.4 km square analysis area. Class color code same as in Figure 3-23.

SECTION 4
RADIONUCLIDE FALLOUT FROM THE CHERNOBYL ACCIDENT

This brief section summarizes the release, deposition, and composition of radioactive fallout from the Chernobyl accident.

4.1 RELEASE AND DEPOSITION.

The most reliable description of the daily radionuclide release from Chernobyl is provided in Table 4.13 of Annex 4 of USSR (1986). Some 24% of the total release occurred on April 26, 1986. During the next five days (4/27-5/1), the release dropped considerably, declining each day. From 5/2 to 5/5, the release rate increased again, peaking on 5/5 to a level roughly 2/3 that on April 26. Then, successful mitigative efforts reduced releases on 5/6 and afterward to levels insignificant in comparison to the releases over the first 10 days.

During the initial 10-day release, the primary wind direction changed almost daily. On April 26, the wind was toward the west. During the ensuing nine days, it shifted in clockwise fashion toward the north, then the east, the south, and southwest (Izrael, Petrov and Severov, 1987; NEA, 1987). This indicates that fallout deposition to the west of the reactor occurred primarily on April 26. The report of Izrael, Petrov and Severov (1987) strongly suggests an instantaneous spread of radioactive debris directly to the west immediately after the explosion. Continuing releases over the next 24-36 hours appeared to have been spread in directions ranging from southwest to northwest. There appears to have been no westward plume during the 10-day release after 12 noon on April 27th. This information indicates that the source term relevant to the westward-extending plume can be described as an acute (< 1 day) deposition episode occurring early in the day on April 26.

4.2 RADIONUCLIDE COMPOSITION.

The radionuclide composition of the close-in fallout can be approximated by the discharges reported by the Soviet experts (USSR, 1986). The primary radionuclides listed by the Soviets include ^{131}I, $^{134, 137}Cs$, ^{99}Mo, ^{95}Zr, $^{103, 106}Ru$, ^{140}Ba, $^{141, 144}Ce$, $^{89, 90}Sr$, and ^{239}Np. Several of these radionuclides have short-lived radioactive daughters in equilibrium with them, which should be add to the list (DOE, 1987). These daughter products include ^{99m}Tc, ^{95}Nb, ^{106}Rh, ^{140}La, ^{144}Pr, and ^{90}Y. In addition, measurements of airborne radioactivity outside the Soviet Union indicated the presence of ^{133}I in large quantities (Lange, Dickerson and Gudikson, 1987), so this radionuclide was also added to the list for our dose rate analysis. It is possible, and is in fact likely, that radionuclide fractionation within the debris occurred after the material escaped to the atmosphere (DOE, 1987); thus the radionuclide composition of fallout debris could differ

somewhat from that reported by the Soviets. A major effect is the condensation of volatile radionuclides such as ^{131}I, ^{132}Te, and ^{137}Cs onto refractory particles (DOE, 1987). However, this is a kinetic process subject to complexities of time, space, microphysics, and meteorological conditions not specifically addressed in this effort. Therefore, in the absence of specific information relative to the dominant, westward plume, it is assumed that the relative quantities of radionuclides in the fallout that affected the vegetation are the same as those reported by the Soviet experts (USSR, 1986), with the addition of radioactive daughter products and ^{133}I, as noted above. These radionuclides are used for dose and dose rate calculations in Section 5 and Appendix A where tables of relative quantities and radioactive properties are provided.

SECTION 5
RADIOBOTANICAL AND DOSIMETRIC CONSIDERATIONS

This section discusses radiobotanical and dosimetric considerations regarding the observation and interpretation of radiation damage to pine forest. Tree characteristics such as age, morphology, and annual growth cycles play an important role. The interplay of ionizing particle range and depth of sensitive tissues in trees determines how the forest responds to the distribution of fallout. Detailed calculations are required to judge the relative importance of beta and gamma radiation for the induction of observable foliage response. As with most biological systems, the response of pine trees to radiation exposure depends not only on dose but on the rate at which the dose is delivered. Finally, specific characteristics of the radionuclide mix and how it was released during the Chernobyl accident influence the course of radiobotanical response.

5.1 TREE CHARACTERISTICS RELEVANT TO RADIATION DAMAGE.

Our satellite imagery analysis and reports such as that of Bohlen (1987) leave little doubt that the predominant radiobotanical effects were observed on pine trees. The dominant species of pine in the area is assumed (Painter and Whicker, 1993) to be Scotch (or common) pine, *Pinus sylvestris*. Figure 5-1 shows an example of a six-foot Scotch pine grown commercially in Maryland that was cut down in December. The date of the Chernobyl accident, 26 April 1986, suggests that the trees were in the spring growth phase. In this phase the trees are probably the most radiosensitive to acute or short-term irradiation (Woodwell and Sparrow, 1963). On average, the growing season begins about 11 April in the region (Anonymous, 1962).

The radiobiological response of pines is also affected by the age and size of the trees, with seedlings being the most radiosensitive and large, healthy trees the least sensitive (Sparrow, Schwemmer and Bottino, 1971; Sparrow, Rogers and Schwemmer, 1968; McCormick, 1967). Tree dimensions and leaf density are also important in the context of understanding the fallout exposure scenario. Higher and denser tree canopies initially retain more of the fallout particles on foliage (Chamberlain, 1970), also, the lesser is the gamma radiation exposure from fallout on the ground surface (Beck and de Planque, 1968).

It is most likely that irradiation of pine apical and lateral meristems at Chernobyl from fallout on the foliage was due primarily to beta particles rather than gamma photons based on a variety of dosimetric studies in the past (Aleksakhin, Tikhomirov and Kulikov, 1970; Broido and Teresi, 1961; Mackin, Brown and Lane, 1971; Kantz, 1971; Rhoads et al., 1969). Even though the relative biological effect (RBE) of beta and gamma radiation is similar (~1), the distinction is important because the beta radiation dose rate from fallout on foliage is expected to differ significantly from that of gamma radiation due to fallout on the ground; and, it is well known that

dose rate is a very important modifier of the radiobiological response (Sparrow, Schwemmer and Bottino, 1971). The dose rate versus time for beta and gamma exposures differ because 1) as time passes, fallout particles are lost by weathering from foliage (and concurrently build up on the ground) and 2) the decay schemes depend on radionuclide species and radiation energy spectra.

Figure 5-1. An example of Pinus sylvestris. A six-foot specimen cut and photographed in December in Maryland.

No precise information was available for this study on the average height, foliar density, or age of the radiation-affected pines near Chernobyl. However, a forest is not usually referred to as "forest" unless most of the trees are relatively mature, and several published accounts do refer to "forest" (Asmolov et al., 1987; Bohlen, 1987). In addition, photo-pictorial documents of the accident's environs reveal mature trees in the background. Therefore, in this analysis we assume that most affected trees were mature and averaged 12 to 15 m in height. This assumption is consistent with a study (Painter and Whicker, 1993) of the area surrounding the Chernobyl

Nuclear Plant where the pines can be 20-30 m in height on solid soil but can be stunted to only 6 to 8 m high in the bogs that exist in the vicinity.

We also assume that the canopy was sufficiently dense to intercept initially 50% or more of the fallout particles. This assumption is consistent with a calculated mean green biomass (dry weight) of at least 2 kg/m^2 for boreal forests (Rodin, Bazilevich and Rozov, 1975). Using the Chamberlain (1970) filtration model and a conservative foliar interception constant of 0.4 m^2/kg (Whicker and Kirchner, 1987), the predicted foliar interception fraction is 1-exp(-0.4 x 2.0) = 55%.

5.2 BETA RADIATION EXPOSURE OF PINE MERISTEMS.

To address the question of whether beta exposures could be significant for pines, we consider the geometry of pine needles and meristems. If there were a sufficient thickness of nondividing tissue to protect the meristem by absorbing the beta energy, then the dominant exposure mode would be gamma radiation. This issue involves a review of the histology of pines, as well as an assessment of the beta particle energies of the radionuclides composing the fallout. According to Biatobok and Zelawski (1976), the shoot apices (within which reside the dividing cells of the meristematic tissue) vary considerably in shape and dimensions depending on the stage of ontogenetic and annual development. However, the larger apices in *Pinus ponderosa* (which has similar apex morphology to *Pinus sylvestris*), are about 500 µm in diameter and 120 µm in height. These apices are usually surrounded by scales some 200-500 µm thick. While some airborne particles might find their way underneath these scales and lie in direct contact with the apex, most particles would settle on the outer surfaces of the scales, and their beta particles would have to traverse this layer to reach the meristem.

From the descriptions and photomicrographs of longitudinal sections of *Pinus sylvestris* apices in Biatobok and Zelawski (1976: pp. 207-209), we estimate that the mean distance through nondividing tissue that a beta particle would have to traverse in order to reach the meristem would be about 400 µm, with a lower limit of 100 µm and an upper limit of about 1200 µm. If the tissues were fully hydrated (as they should be in late April), the tissue density would be about 1.0 g/cm^3.

The range of a beta particle having an initial kinetic energy of 0.2 Mev is 0.04 g/cm^2 (Public Health Service, 1960) or 400 µ in water. Thus, beta particles having energies exceeding 0.2 Mev should, on average, be able to penetrate into the meristem of Scotch pines if the radionuclide is in contact with the scales directly over the apex. All of the radionuclides under consideration in this report have beta transformation energies in excess of 0.2 Mev; they range from 0.41 to 4.83 Mev (Public Health Service, 1960). Indeed, many of these beta particles exceed 0.5 Mev and would be able to traverse well over 1200 µm of unit density material, which would likely correspond to the

upper limit of protection afforded by the nondividing tissue. We conclude from the probable dimensions of the Scotch pine apices and the energies anticipated of beta particles from the predominant fallout radionuclides, that beta particle exposure must be considered in the total doses received by the pine trees around Chernobyl. Radiation transport calculations are presented in Appendix A for dose depths relevant to both needles and meristematic tissue.

5.3 BETA VERSUS GAMMA EXPOSURE.

Evidence from published reports is cited in this subsection to implicate beta particles as the dominant exposure mode for the apical meristem of pine trees. Estimates of the ratio of the beta-dose to the gamma-dose components for various parts of the upper canopy appropriate for pine forests near the Chernobyl nuclear power plant, however, require models and calculations specifically designed for that purpose. Such calculations are presented in Appendix A and discussed in Section 5.3.2 below.

5.3.1 Values from the Literature.

Theoretical calculations by Osanov, Tissen and Radzievsky (1969), show that beta depth doses from a mixture of ^{239}Pu fission products at 0.04 g/cm^2 range from 16 to 61 rad/day per μCi/cm^2, depending on time after fission (which affects the radionuclide mix and hence the beta energy distribution). These values are 0.13 to 0.38 of the beta exposure at a depth of only 0.005 g/cm^2 (50 μm).

Other theoretical considerations by Broido and Teresi (1961), show that for equal fallout depositions on skin and the soil surface, "the β-dose at the surface of a contaminated individual would be approximately forty times the γ-dose measured 1 m above the contaminated surface" (assumed to be of infinite extent). Elevating the individual to a height 12 to 15 m above the surface (as is the case for pine meristems of the upper canopy), would decrease the gamma exposure rate due to the ground surface fallout to roughly one half that at 1 m (Beck and de Planque, 1968). The γ-dose component to the skin (or foliage) due to the fallout on the skin would be approximately the same as that 1 m above the ground. β-radiation from ground surface fallout does not contribute to exposure in the upper canopy since the air between the ground and 10 m up is equivalent to about 1 cm of water and further shielding is provided by the lower branches. Finally, the estimated β-to-γ exposure ratio is about 40:1.5 or 27 for equal deposition on the foliage and on the ground.

Actual measured doses to vegetation from close-in fallout debris at the Nevada Test Site showed that beta doses exceeded gamma doses by more than an order of magnitude (Kantz, 1971). In this case, the vegetation comprised shrubs about 25 cm above the soil. In the same setting at the Nevada Test Site, Rhoads et al. (1969), demonstrated that mortality of desert vegetation was caused by beta particles rather than gamma radiation.

Finally, the world-renowned Russian radioecologist, R. M. Aleksakhin (Aleksakhin, Tikhomirov, and Kulikov, 1970) has the following to say about beta radiation damage to trees of the coniferous forest:

"On the basis of data obtained in a study of global fallout, it has been established that the coefficient of primary retention of the most important fission fragments in middle-aged plantings is not less than 40% - in dense conifer plantings radioactive substances may be completely retained."

"-- the duration of the period of half-purification (weathering half-time) may fluctuate from two weeks in plantings purged well by the wind and washed by precipitation to three or four months in dense coniferous plantings."

"--the highest radiation doses (from fallout) will be obtained by the crowns of woody plants in the topmost layer"

"--the needles and buds are comparable in size with the run length of β particles -- and all cells of these tissues prove to be accessible to β radiation --- a considerable portion of the β energy will be absorbed in meristematic tissue"

"-- with radioactive contamination of the crowns, the main contribution to the radiation dose of meristematic tissues will be made by β radiation."

"-- radiation on the crowns in the topmost layer -- will exceed by ten or more times the radiation dose of mammals -- under the forest canopy."

5.3.2 Calculations.

An estimate of the dose of radiation from fallout must account for 1) the spectrum of radiation emitted by the radionuclide mix, 2) the transport of radiation from source to exposed foliage, and 3) the relative exposure rates of beta and gamma particles within the pine tissue. Appendix A presents detailed calculations for specific geometrical arrangements of fallout source and foliage accounting for these factors. Additionally, quantitative estimation of the relative importance of beta and gamma ray exposures of pine tree tissues requires a model for the distribution of fallout in the forest. This distribution involves the initial arrangement of fallout radioactivity at the end of the deposition episode and the time dependent redistribution caused by weathering.

First, we consider the distribution of fallout at the end of the deposition episode. Figure 5-2 illustrates a simple model for visualizing the distribution of fallout particles in the forest. We will not treat horizontal gradients of fallout concentration in our calculations so horizontal movement caused by wind is neglected. Fallout particles stick (adhere) with some probability when they encounter a surface within the canopy. This probability varies with particle size, shape, composition and the nature of the encountered surface. The overall fraction of radioactivity that is

retained in the canopy at the end of the deposition episode is the foliar interception fraction, f, discussed in Section 5.1.

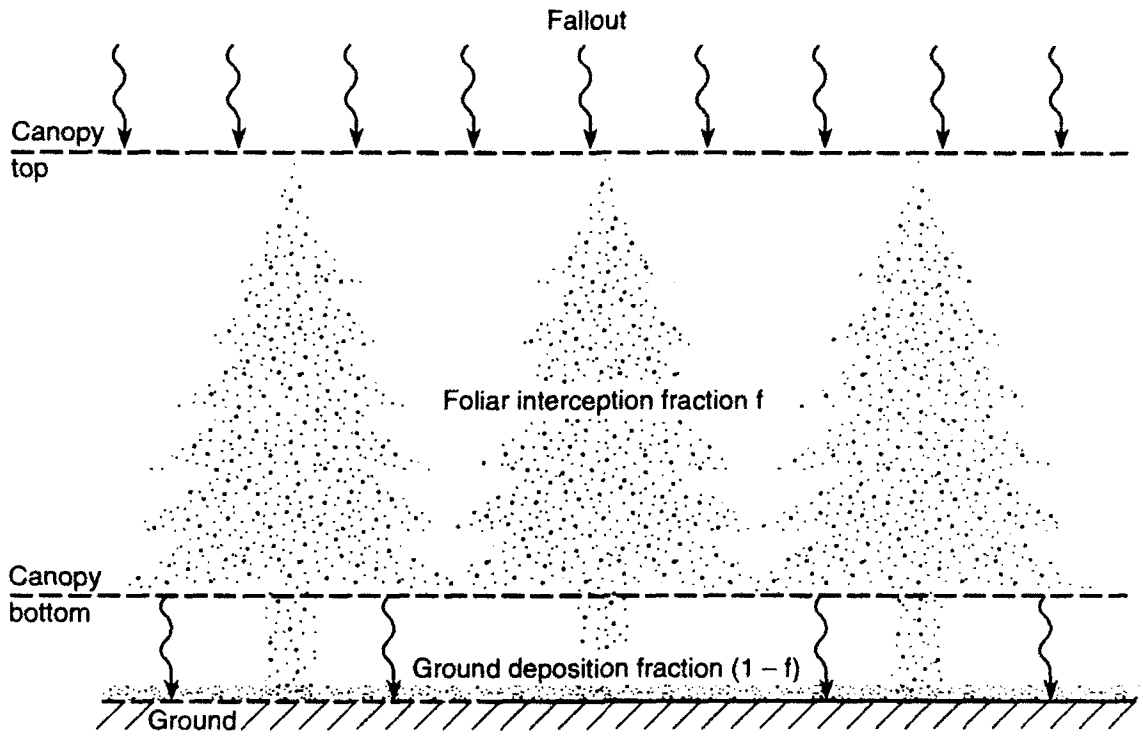

Figure 5-2. Illustration of fallout distribution described by a foliar interception fraction with neglect of winds.

The fraction (1-f) of the incident fallout radioactivity not intercepted by foliage is assumed to fall uniformly on to the floor of the forest. Thus, the two sources of radioactivity are the fallout assumed to be uniformly distributed in the foliage and the fallout deposited on the ground. We refer to these two sources as the canopy source and the ground source, respectively. We assume that the canopy and ground sources have the same radionuclide composition so that both emit the same spectra of gamma and beta radiation.

In Appendix A, the canopy source is further divided into two contributions to improve calculational accuracy. The first consists of fallout particles in direct contact (deposited on) the surface of the foliage element under consideration. The second is the fallout deposited on all other foliage throughout the canopy volume. Calculations for the first contribution, called the foliage contact source, use an estimated surface density of fallout on the foliage element. Calculations for the second contribution, referred to as the canopy volume source, use a mean volume density of

fallout distributed uniformly throughout the canopy. For the transport of radiation from the ground source and from the canopy volume source, the canopy mass (exclusive of tree trunks) is approximated by its mean density over the volume of the horizontal layer occupied by the canopy.

Table 5-1 summarizes the ratio of beta radiation doses to gamma radiation doses for the foliage contact source and the canopy volume source. The dose due to the foliage contact source is overwhelmingly due to beta radiation for all the dimensions of foliage elements chosen. The homogenized canopy volume source produces beta dose rates that are two or three times larger than the gamma dose rates at the same location.

Table 5-1. Ratio of beta to gamma doses to foliage calculated from the results of Appendix A for fallout retained in the canopy.

	Foliage Contact Source	
Dimensions of foliage element		
Radius (ρ) (cm)	*Length (2l) (cm)*	*β/γ dose ratio at center of element*
0.04	4.5	58.8
0.04	9.0	59.1
0.0625	9.0	46.3
0.10	4.5	34.7
0.15	9.0	25.
0.40	2.0	8.5
	Canopy Volume Source	
Dose point at:	middle of canopy	3.2
	top of canopy	2.0

In order to estimate the beta to gamma dose ratio for the total absorbed dose to a foliage element, doses from all radiation components are summed including the ground source. A model for relative densities of the fallout sources is specified and results from Appendix A are utilized calculate total reference dose rates or doses for foliage elements.

The complications from the wind-driven, horizontal component of fallout motion and the finite size of forested areas are neglected. The calculated dose rates to the foliage are referenced to the same amounts of radioactive fallout distributed throughout the canopy mass and on the ground surface below at the end of the deposition episode. Accordingly, on the basis of a unit source density, reference dose rates to the canopy are calculated for 1 β-particle or γ-ray per cm^2-sec on the ground surface and 10^{-3} β-particles or γ-rays per cm^3-sec within the canopy volume, based on

vertical thickness of 10 m for the canopy. For summing dose contributions at a given dose point, the canopy volume source density is scaled in proportion to the foliar intercept fraction f. The ground fallout source is scaled in proportion to (1-f).

An appropriate model for the areal source density for fallout material in surface contact with foliar canopy components is less straightforward to formulate than for ground surface fallout underneath. Complicating factors include the geometry of canopy components, the aerodynamic behavior of particle trajectories in the canopy, the effective adherence of particles that make contact with canopy component surfaces, and weathering influences.

In the absence of definitive information regarding the contact source density, we examine the effect of varying the density between the unit incident fallout density and one tenth of that value. The value of the initial foliar intercept fraction, f = 0.6, is taken from Kerr et al. (1971) to be consistent with the average foliage density used for transport calculations in Appendix A. Also, this value is close to that of 0.55 estimated in Section 5.1. Table 5-2 summarizes the dose rate per unit source for the various sources and dose points from Appendix A. Summing the doses over beta and gamma sources scaled appropriately for each dose point gives the dependence of the beta to gamma dose ratio as a function of the contact source density in the assumed range for each of the foliage elements.

Figure 5-3 shows the variation of the beta to gamma dose ratio with contact source density for selected foliage elements at the top of the canopy. Since the dose from the contact source at the center of the thinner foliage elements is dominated by beta radiation, the beta to gamma ratio for these elements is strongly affected by the assumed contact source density factor. Thicker elements are less influenced by the contact source strength because the beta penetration to their centers is suppressed.

It is likely that the adherence probability and, hence, the contact source density varies from one part of the foliage to another and is surely close to one for areas of the pine branches that are sticky to the touch, which are quite common. Smoother surfaces such as the needles are likely have a lower adherence probability. Also, there is some reduction in fallout flux as it filters through to lower canopy levels. *We assume that a value of 0.5 for the contact source density factor is reasonably representative and use it for all further calculations.*

With the assumption of a contact source density factor of 0.5 and an initial foliar intercept fraction of 0.6, Figure 5-4 shows how the beta to gamma dose ratio changes with weathering. Just after deposition, the ground fraction is 0.4; it increases as weathering effects move fallout particles from the canopy to the ground. The values plotted in Figure 5-4 for foliage elements of various radii located at the top and middle of the canopy are calculated with the assumption that

Table 5-2. Dose rate per unit source for various sources and dose points. Reference canopy volume source density is taken equal to the unit ground source density spread over the assumed 10 m canopy height.

	Dose point	*Beta dose rate ($cGy/h \times 10^7$)/unit source*	*Gamma dose rate ($cGy/h \times 10^7$)/unit source*
Unit Ground Source	12 m	-	10.1
1(β or γ)/cm^2 - sec	7 m	-	16.9
	1 m	185[a]	29.4
Reference Canopy	12 m	33.4	16.5
Volume Source	7 m	66.9	20.6
10^{-3}(β or γ)/cm^3-sec	1 m	-	16.5[b]
	Radius of foliage element (cm)		
Unit Contact	0.04	302.	5.13
Source, Cylindrical	0.0625	236.	5.10
Geometry	0.10	173.	4.98
1(β or γ)/cm^2 - sec	0.15	124.	4.95
	0.40	32.0	3.78

[a]Based on β / γ dose ratio of 6.3 according to Barabanova and Osanov (1990).

[b]Assumed equal to the value at the 12 m dose point.

weathering lowers the canopy retention for both the foliage contact source and the canopy volume source in unison and that the ground fraction increases accordingly. Weathering of the ground fallout into the earth is neglected.

As discussed in Section 5.2, the most sensitive growth tissues of the pine are located in the apical meristems at the tips of branches (and roots) and are typically less than 0.10 cm below the surface of the foliage elements. Figure 5-4 shows that the calculated beta to gamma ratio for these tissues is greater than six in both the middle and upper canopy before the effects of weathering. Even when half the intercepted fallout has moved to the ground (ground fraction = 0.7), the ratio is still above four. These calculations confirm the assertions in the literature as reported above that beta doses dominate for the most sensitive growth tissues of the pine.

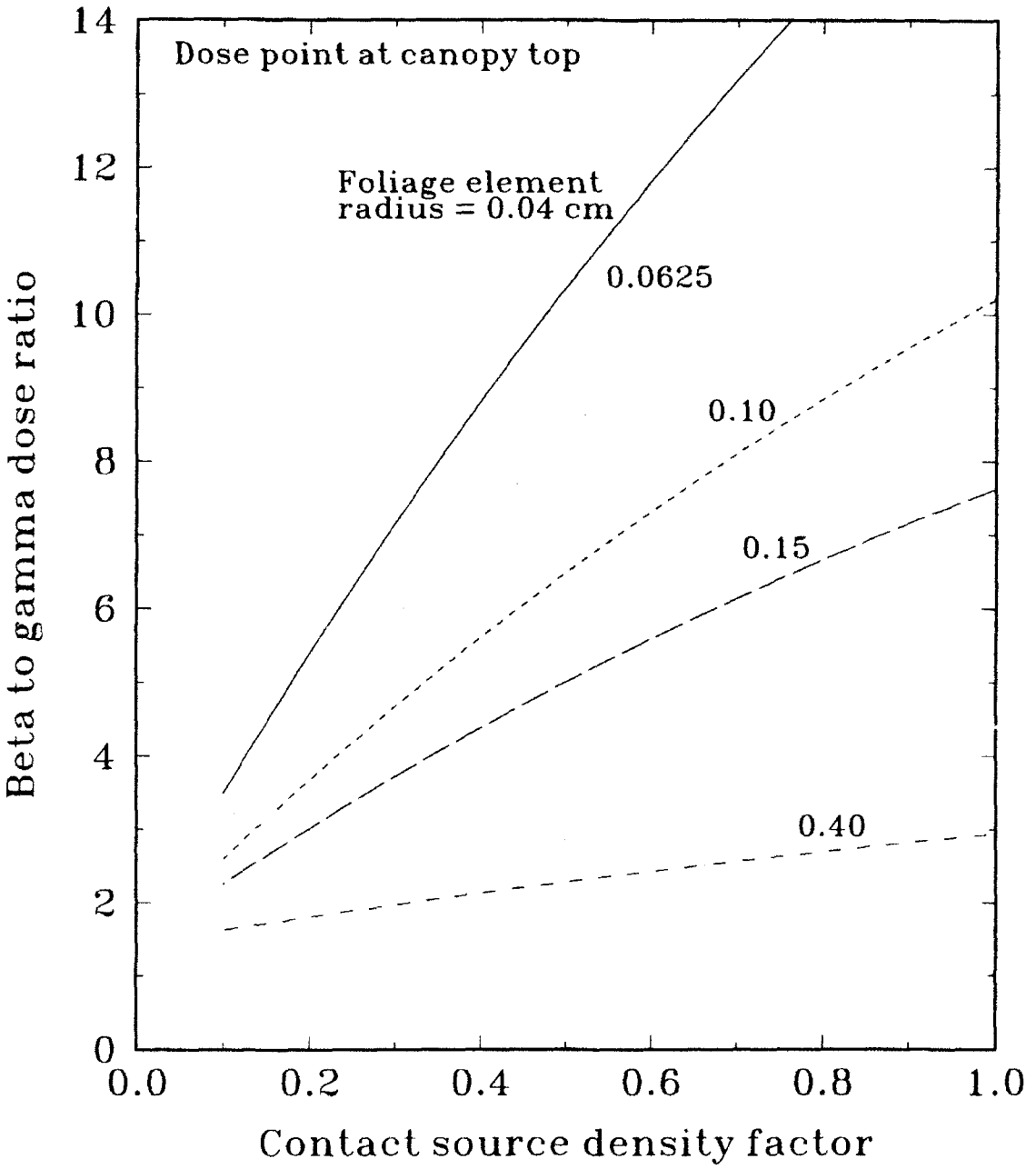

Figure 5-3. Beta to gamma dose ratio versus contact source density relative to unit areal density of incident fallout. Curves are for various radii of foliage elements located at the top of the canopy.

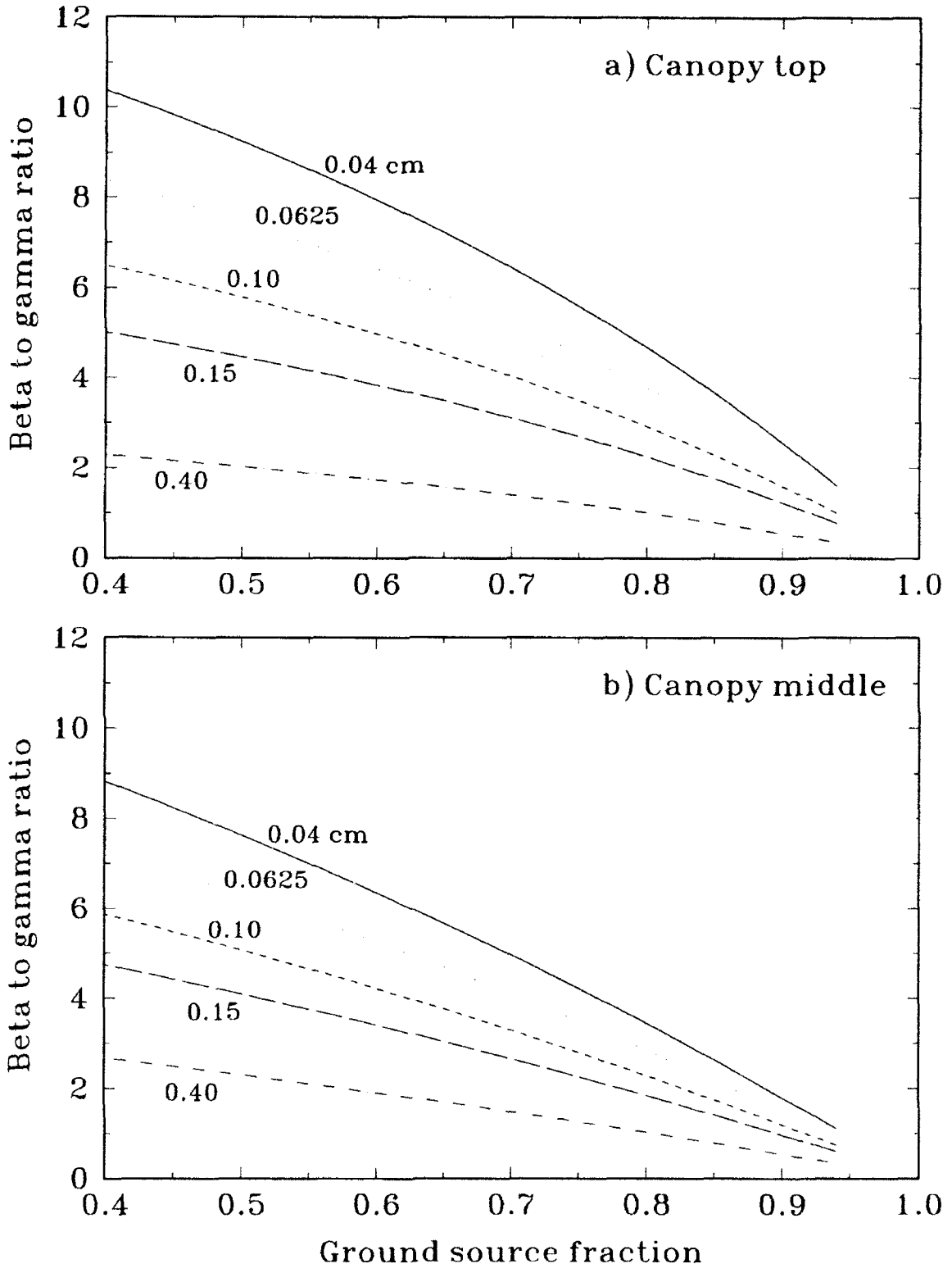

Figure 5-4. The beta to gamma dose (dose rate) ratio at the center of cylindrical foliage elements of various radii at a) the top of the canopy and b) the middle of the canopy.

Lateral meristematic tissue, which is located in the cambium and provides for growth in the diameter of branches, may be better protected from beta radiation than the apical meristems. However, Figure 5-4 shows that tissues as deep as 0.4 cm still have beta to gamma ratios larger than two until substantial weathering has taken place. Figure 5-3 shows that lowering the assumed contact source density factor from 0.5 to 0.1 has only a weak influence on the beta to gamma ratio for such deep tissues.

We conclude that beta doses are much more important than gamma doses for the sensitive growth tissue in the apical meristems of pine trees. At doses below the LD_{50}, the dominant effect of radiation is on the apical meristems. Established growth is outwardly unaffected. Thus, visible affects may not show up until the growing season when the lack of viable apical meristems inhibits new growth. We expect that late developing effects from these relatively low doses are likely to be associated with high beta to gamma ratios for the causative dose.

For doses much higher than the LD_{50}, however, trees can be completely dead in a matter of a few weeks. Radiation response in this short time requires more than just sterilization of the growth tissue. The broader systemic effects associated with acute mortality (involving irradiation and response of all canopy foliar components) may be more influenced by penetrating gamma radiation. It is likely that early death of a tree from large doses is associated with lower beta to gamma ratios (but still not lower than one or two as discussed above) than for later occurring foliage deterioration at lower doses.

5.4 DOSE RATE EFFECTS.

It has long been recognized that the radiobiological response to a given dose depends on the time over which the dose is delivered. This dependency is sometimes caused by subcellular repair which is more effective if the exposure is protracted. In other cases, if exposure times are short compared to the cell division cycle time, high dose rates are clearly more damaging than low dose rates because of reduced recovery time during irradiation. This is particularly true in physiologically active plants which may have greater recovery potential than dormant plants. In the case of chronic or long-term exposures however, somewhat different patterns may emerge. For example, dormant plants might show a greater effect from a long-term irradiation exposure than do actively-growing individuals; the dormant cells can accumulate a higher total dose and repair mechanisms may be less efficient (Whicker and Fraley, 1974).

Most of the research on the effects of radiation on pines has involved either acute (< 1 day) or chronic (> 1 year) exposures, with constant dose rates applied over the specified period. Unfortunately, neither of these dose rate regimes match the exposure of the pines at Chernobyl. The likely exposure conditions and mix of radionuclides at Chernobyl would have produced a

declining dose rate with time. The rate of decline was too slow to allow the exposure to be considered acute, but was too rapid to approximate a chronic exposure.

We have dealt with this dilemma by estimating a credible dose rate versus time curve for the westward plume at Chernobyl. From the integral of such a curve, one can estimate the length of a comparable constant-rate exposure. Knowing the length of a constant-rate exposure that would be comparable to Chernobyl, one can examine the more relevant literature to estimate the dose-response relationship. A few studies on short-term (8-30 day) constant rate exposures of pines have been conducted (e.g., Monk, 1966; McCormick, 1967; Pedigo, 1963; Miller, 1968; and Platt, 1963). These studies involved pine species other than *P. sylvestris*; however, the chromosome characteristics of *P. sylvestris* are similar to those of pines in general and there is not a great deal of variation among the pines in radiosensitivity (Sparrow, Rogers and Schwemmer, 1968). In addition, dose rate effects *per se* have been studied (e.g., Sparrow, Schwemmer and Bottino, 1971; Amiro, 1986) and these data will also be considered in the development of the dose-response algorithm.

5.5 DOSE RATE SCENARIO FOR CHERNOBYL.

Because the larger part of the dose to pine meristems is assumed to have been delivered by beta particles, a normalized beta dose rate function is estimated from the list of radionuclides and their decay rates, the relative quantities released, the total beta transformation energies, and an assumed rate of weathering from the foliage. The relative beta dose rate (BDR) at time t (in days) is:

$$BDR = \sum_i R_i E_i \exp(-k_i t) \qquad (5.1)$$

where:

R_i = Estimated abundance proportion of nuclide i, MCi (USSR, 1986)

E_i = Energy of beta transformation of nuclide i (Public Health Service, 1960)

k_i = Effective loss rate constant of nuclide i, $k_i = \lambda_p + \lambda_w$, where λ_p = physical decay constant and λ_w = weathering rate constant, 0.0495/day (Hoffman and Boes, 1979)

The normalized beta dose rate (NBDR) is calculated from:

$$NBDR(t) = \frac{BDR(t)}{BDR(t = 1)} \qquad (5.2)$$

Table 5-3. Calculation of normalized beta dose rate (BDR) versus time assuming all dose from beta particles on foliage, all fallout on t = 1 day.

				BDR						
Nuclide(i)	*R*	*E*	*k*	*1d*	*2d*	*4d*	*8d*	*16d*	*32d*	*64d*
^{131}I	7.3	0.97	0.1360	6.180	5.400	4.110	2.390	0.8040	0.0910	1.18E-3
^{132}Te	1.3	0.41	0.2600	0.411	0.317	0.188	0.066	0.0080	0.0001	—
^{134}Cs	0.5	2.05	0.0500	0.975	0.927	0.839	0.687	0.4610	0.2070	4.18E-2
^{137}Cs	1.0	1.18	0.0495	1.123	1.069	0.968	0.794	0.5350	0.2420	4.97E-2
$^{99}Mo + ^{99m}Tc$	3.0	1.38	0.2980	3.073	2.281	1.257	0.382	0.0350	0.0003	—
$^{95}Zr + ^{95}Nb$	3.8	2.05	0.0600	7.336	6.909	6.128	4.820	2.9830	1.1420	1.67E-1
^{103}Ru	3.2	0.77	0.0670	2.304	2.155	1.885	1.442	0.8440	0.2890	3.38E-2
$^{106}Ru + ^{106}Rh$	1.6	3.57	0.0510	5.428	5.158	4.658	3.798	2.5260	1.1170	2.18E-1
$^{140}Ba + ^{140}La$	4.3	4.83	0.1040	18.720	16.870	13.700	9.038	3.9330	0.7450	2.67E-2
^{141}Ce	2.8	0.58	0.0710	1.513	1.409	1.222	0.920	0.5220	0.1670	1.73E-2
$^{144}Ce + ^{144}Pr$	2.4	3.32	0.0520	7.564	7.181	6.472	5.256	3.4670	1.5090	2.86E-1
^{89}Sr	2.2	1.46	0.0630	3.016	2.832	2.497	1.940	1.1720	0.4280	5.70E-2
$^{90}Sr + ^{90}Y$	0.2	2.81	0.0495	0.535	0.509	0.461	0.378	0.2550	0.1150	2.37E-2
^{239}Np	1.2	0.73	0.3450	0.620	0.439	0.220	0.127	0.0035	—	—
^{133}I	15.9	1.83	0.8470	12.470	5.350	0.983	0.033	—	—	—
Σ				71.270	58.810	45.590	32.070	17.5500	6.0520	0.922
Σ (normalized to t = 1 d)				1.000	0.820	0.640	0.450	0.2500	0.0850	0.013

$BDR = \sum [R_i E_i \exp(- k_i t)]$

R = Estimated release, MCi (USSR, 1986)

E = Energy of beta transformation (Public Health Service, 1960)

k = $\lambda_p + \lambda_w$ (λ_p = physical decay constant; λ_w = weathering constant 0.0495/day)

The values for R_i, E_i, k_i and BDR(t) for each radionuclide (see Section 4) is summarized in Table 5-3. The normalized beta dose rates (NBDR) are plotted through 60 days in Figure 5-5. For comparison, there are also shown a normalized gamma dose rate curve based on aerial surveys (Asmolov et al., 1987) and a normalized gamma exposure rate curve that is calculated for the list of radionuclides in Table 5-3. In the latter calculation, the relative gamma dose rate (GDR) for radionuclides on the ground is estimated from:

$$GDR = \Sigma\ R_i\ G_i\ \exp(-\lambda_{pi}\ t) \qquad (5.3)$$

where:

R_i = is the same quantity as in Equation 5.1

G_i = gamma dose factor for nuclide i in μR/hr per mCi/km^2 (Beck, 1980)

λ_{pi} = physical decay constant for nuclide i

As with the BDR, the GDR values were normalized to 1.0 at t = 1 day. Table 5-4 summarizes the calculations for the normalized gamma exposure rate curve.

Inspection of Figure 5-5 reveals that the estimated dose rate curve for the beta component is very similar to the aerially-measured gamma component for the first two weeks, after which the beta curve declines more rapidly. The shapes of the calculated and measured gamma exposure rate curves are similar after the first two weeks. It is not clear exactly how the aerial measurements were made. If they were taken just above the forest canopy and if a large fraction of the fallout was initially retained by the canopy, then the aerially-measured curve would include a beta component and should resemble the calculated beta curve for the first couple of weeks, since both would be affected by foliar weathering (λ_w) as well as the mix of radionuclides. The more likely situation is that the aerial measurements were taken sufficiently above the canopy to avoid turbulent propeller down wash that might disturb measurement . If this were the case, the measurements would be largely of gamma radiation. As the fallout material weathered from the foliage and accumulated on the ground, the aerial measurements would be expected to more closely approach the calculated gamma component arising from the soil, and this seems to be the case. The somewhat widening increase with time between the measured curve (dashed) and that from gamma emitters "on soil" (solid) could reflect weathering, both from the foliage to the ground and from migration of fallout into the soil over time. Based on this discussion, it appears that the relative shapes of the three curves in Figure 5-4 are compatible with the essential facts and with plausible assumptions we have made.

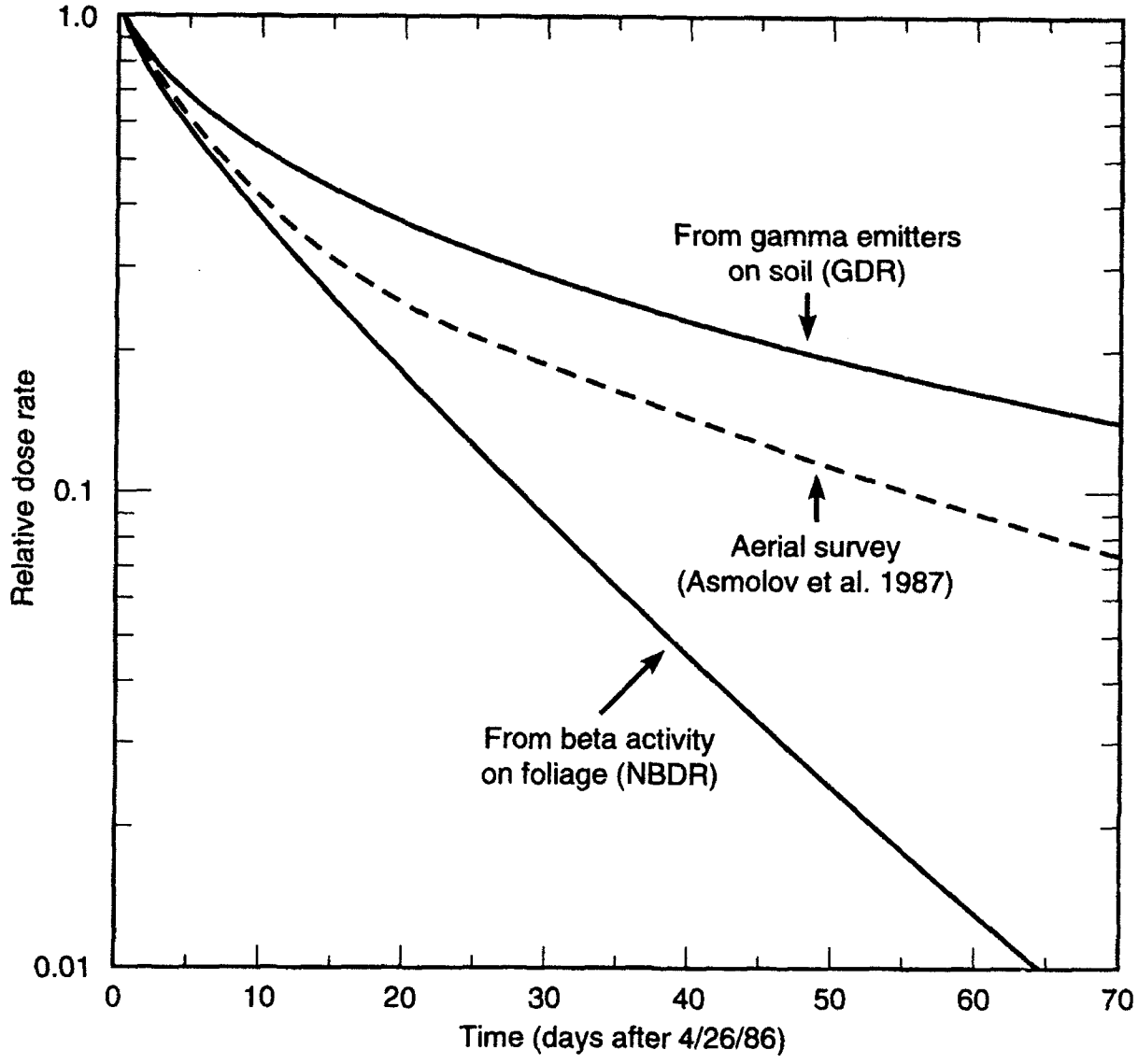

Figure 5-5. Calculated dose rates (normalized to 1.0 at t = 1 day) from gamma radiation emanating from fallout on the soil and from beta activity on the foliage.

Table 5-4. Calculation of normalized gamma dose rate (GDR) versus time assuming all dose from gamma emitters on the ground and all fallout on t = 1 day.

Nuclide(i)	R	G	λ_p	GDR 1d	2d	4d	8d	16d	32d	64d
^{131}I	7.3	6.32E-3	0.0866	4.23E-2	3.88E-2	3.26E-2	2.31E-2	1.15E-2	2.88E-3	1.81E-3
^{132}Te	1.3	3.38E-3	0.2100	3.56E-3	2.89E-3	1.90E-3	8.19E-4	1.53E-4	5.30E-6	6.90E-9
^{134}Cs	0.5	1.18E-2	9.24E-4	5.90E-3	5.89E-3	5.88E-3	5.86E-3	5.81E-3	5.73E-3	5.56E-3
^{137}Cs	1.0	4.32E-3	6.3E-5	4.32E-3	4.32E-3	4.32E-3	4.32E-3	4.31E-3	4.31E-3	4.30E-3
$^{99}Mo + ^{99m}Tc$	3.0	4.51E-3	2.48E-1	1.06E-2	8.24E-3	5.02E-3	1.86E-3	2.56E-4	4.84E-6	—
$^{95}Zr + ^{95}Nb$	3.8	1.61E-2	1.07E-2	6.05E-2	5.99E-2	5.86E-2	5.62E-2	5.16E-2	4.34E-6	3.09E-2
^{103}Ru	3.2	5.25E-3	1.78E-2	1.65E-2	1.62E-2	1.57E-2	1.46E-2	1.26E-2	9.51E-3	5.38E-3
$^{106}Ru + ^{106}Rh$	1.6	1.56E-3	1.88E-3	2.49E-3	2.49E-3	2.48E-3	2.46E-3	2.42E-3	2.35E-3	2.21E-3
$^{140}Ba + ^{140}La$	4.3	3.57E-2	5.41E-2	1.45E-1	1.38E-1	1.24E-1	9.96E-2	6.46E-2	2.72E-2	4.81E-3
^{141}Ce	2.8	7.25E-4	2.13E-2	1.99E-3	1.95E-3	1.86E-3	1.71E-3	1.44E-3	1.03E-3	5.19E-4
$^{144}Ce + ^{144}Pr$	2.4	3.37E-4	2.44E-3	8.07E-4	8.05E-4	8.01E-4	7.93E-4	7.78E-4	7.48E-4	6.92E-4
^{239}Np	1.2	2.56E-3	2.95E-1	2.29E-3	1.70E-3	9.44E-4	2.90E-4	2.74E-5	2.45E-7	—
^{133}I	15.9	1.00E-2	0.7970	7.17E-2	3.23E-2	6.56E-3	2.71E-4	—	—	—
Σ				3.67E-1	3.13E-1	2.12E-1	2.12E-1	1.56E-1	9.72E-2	5.45E-2
Σ (normalized to t = 1 d)				1.00	0.85	0.71	0.57	0.43	0.26	0.15

$GDR = \Sigma [R_i G_i \exp(- \lambda_{pi} t)]$

R = Estimated release, MCi (USSR, 1986)

G = Gamma dose factor, μR/hr per mCi/km^2 (Beck, 1980)

λ_p = Physical decay constant

None of the three dose rate curves in Figure 5-5 would produce an "acute" exposure. Of the three, the beta dose rate curve declines the most rapidly and hence provides the shortest effective duration of exposure. The beta curve is considered the most plausible representation of the actual dose rate curve experienced by meristems of the damaged pines; its time-integral is plotted in (Figure 5-6). An exposure following this curve produces 50% of the total exposure in nine days and some 80% of the exposure in 21 days. A subjective estimate of the exposure time at a constant rate that would produce a similar biological response is about 21 days. Note that from day 2 to day 12, when nearly 50% of the dose has been delivered, the dose rates of the constant rate and calculated beta rate curves are quite similar. We assume that the lower dose rates for the constant-rate exposure for the first few days would be roughly compensated for by the higher dose rates after day 12. After 20-30 days, the additional cumulative exposure from fallout is probably not very significant in terms of biological response.

From this analysis, we surmise that experiments in which constant-rate exposures are delivered to mature pines for periods ranging from roughly 2 to 4 weeks during the early growing season should produce dose-response relationships comparable to those for the Chernobyl forest.

5.6 Summary.

Important results from Section 5 regarding the radiobotanical response of the pine forests near the Chernobyl accident include:

1) beta radiation doses are expected to dominate gamma doses by at least a factor of six for late foliage responses (after months) induced by doses less than the LD_{50},

2) beta radiation dose contributions are expected to be at least one or two times the gamma contribution for large doses that cause tree mortality within a matter of weeks or days,

3) the effective exposure time for foliage doses from beta radiation near the power station determined by the decay of radionuclides and weathering of fallout from the foliage is estimated to be about 3 weeks, and

4) results of constant dose rate experiments with pines exposed during their growing seasons for periods of 2 to 4 weeks may be used to interpret the observed responses at Chernobyl.

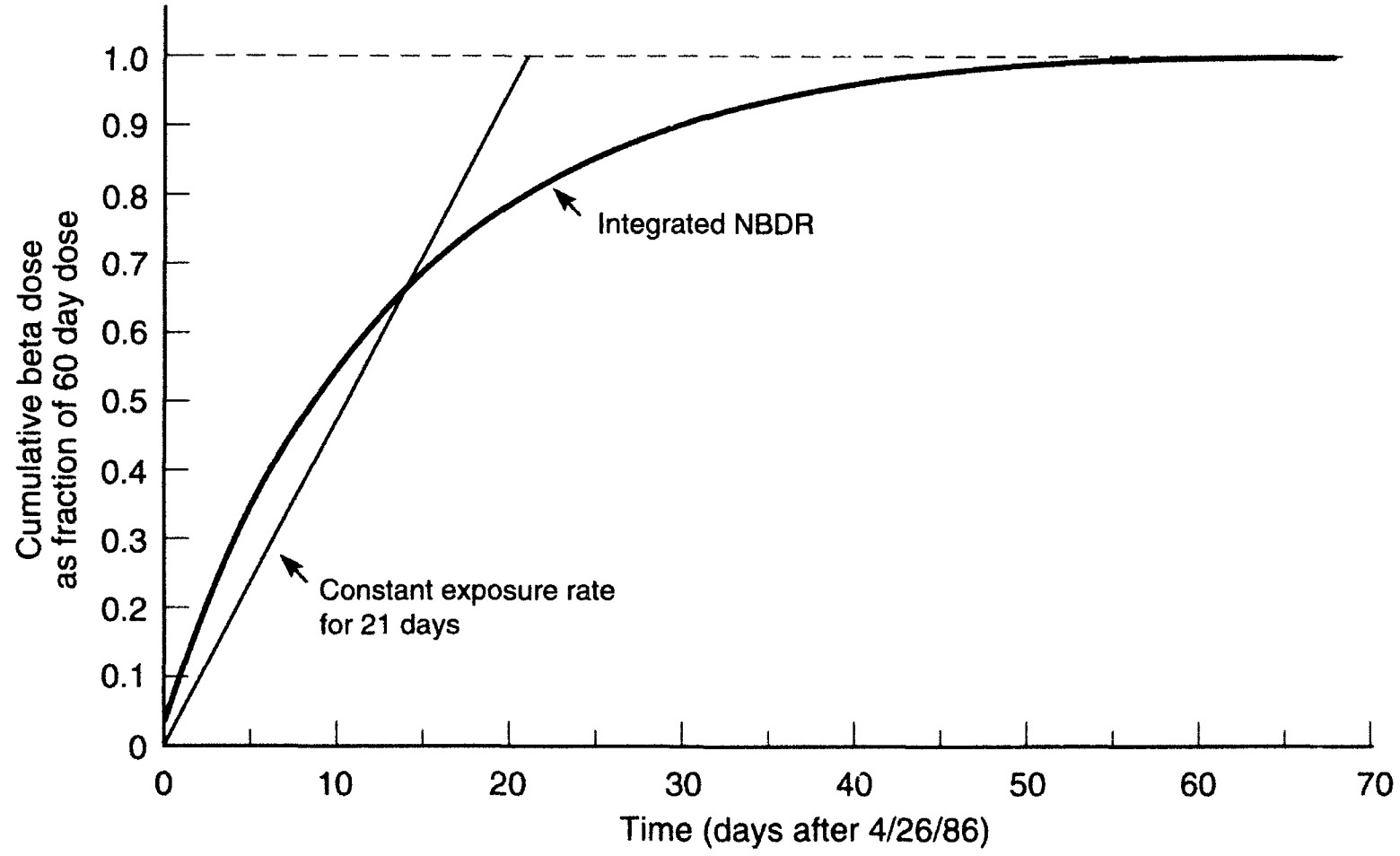

Figure 5-6. Integral of the beta dose rate curve in Figure 5-4 and a constant rate curve that should produce a similar biological response.

SECTION 6
DOSE-RESPONSE RELATIONSHIPS FOR PINE TREES

Based on a review of radiobotanical literature for pine tree response to ionizing radiation exposure, this Section examines the dependence of pine tree response on dose and dose rate and the relationship between time-to-response and dose for short term exposures relevant to the Chernobyl accident. A quantitative relationship is derived relating the time of earliest detection of response in multispectral imagery to the dose received by pine trees.

6.1 LITERATURE REVIEW.

Stress to foliage changes its spectral reflectance in various wavelength bands. Temperature, water content and leaf pigments largely determine the observed spectrum. Reflectance changes observed in the tree canopy in response to radiation stress are probably primarily due, initially, to a reduction in photosynthesis and an increase in dark respiration (Ursino, Moss, and Stimac, 1974). These effects are caused by damage to shoot apical meristems which retards growth and function of photosynthetic tissues (Bostrack and Sparrow, 1969). Eventual death of trees likely results from starvation brought about by a critical reduction in the amount of photosynthetic tissue (Bostrack and Sparrow, 1970). Thus, dying and dead trees should reveal a progressive decline in the amount of green tissue and water content of the foliage. As the foliage dries and falls from the branches, reflectance should become progressively similar to open fields or even to bare ground if the understory vegetation is sparse. The rate of progression of these changes is expected to depend on dose and season of the year. Because of the nature of these changes, it is appropriate to focus on mortality and growth reduction as the damage endpoints likely to be revealed by satellite images.

Based upon measured chromosome characteristics, Sparrow, Schwemmer, and Bottino (1971) estimated the acute LD_{50} exposures for 82 woody plants, including 13 species of pine. The predicted LD_{50} exposure for *Pinus sylvestris* was 620 R. The comparable values for the other pines ranged from 410 to 770 R, with an overall mean of 615 ± 97 (1 s.d.) R. These values were all for a 16 hour constant rate exposure. Sparrow, Schwemmer, and Bottino (1971) also provide some data on the total dose required to produce an LD_{50} for a given constant rate exposure time. The data were not developed from pines, but pines are expected to behave similarly. The relevant data are plotted in Figure 6-1 relative to the LD_{50} for a 16-hour constant rate exposure. Unfortunately, the data do not reflect exposure times over 36 hours. A linear extrapolation to exposure times of 2-4 weeks, however risky, predicts LD_{50} values for Scotch pines of 1300-1500 R.

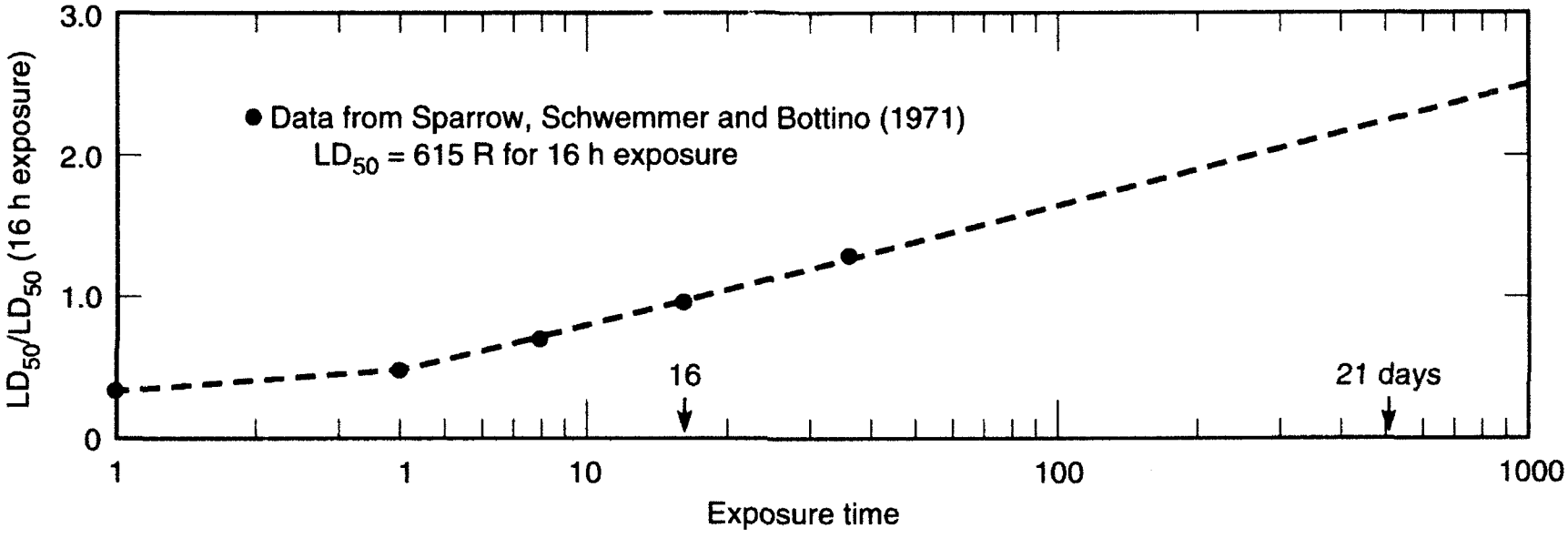

Figure 6-1. Relationship of LD_{50} doses at various constant rate (CR) exposure times in hours to those for 16-hour CR exposures.

Sparrow, Schwemmer, and Bottino (1971) also indicate that a fallout decay simulation (FDS) treatment is comparable to an 8-hour constant rate exposure. However, this is based on experiments in which the decay rate followed the $t^{-1.2}$ relationship with 1 hour as the initial reference time. In this case, the exposure rate at 1 hour would be 16 times that at 10 hours. There is no indication, to our knowledge, that the initial dose rates at Chernobyl were that much higher than the 10-hour dose rates. This would require a very acute deposition of fresh fission products (as from a weapon explosion) with no prior inventory buildup of longer-lived fission products as would be expected with used reactor fuel.

The study by Miller (1968) appears quite relevant because it involved a 29-day constant rate gamma exposure to *Pinus palustris* trees during the month of April. Sixty percent of the population survived an exposure of 2,100 R. Complete mortality occurred within three months at 8,700 R or greater. We estimate the LD_{50} to be about 2,600 R from a plot of survival versus total exposure. Noticeable (~ 12%) mortality occurred at an exposure of 700 R. A 50% reduction in growth was observed at approximately 500 R. In Miller's study, 29-day irradiations of nearby plots were also conducted in summer, fall, and winter. The LD_{50} for the summer and fall irradiations was only slightly higher than that of the spring irradiation. In the case of growth reduction, the spring, summer and fall irradiations gave nearly identical results. In winter, the pines were considerably more resistant.

Monk (1966) also studied the response of *Pinus palustris* to a constant rate gamma exposure. In this study, the trees (which were 5 years old) were exposed for 16 days in mid-May. A 50% reduction in growth was observed at 400 R, a value similar to that reported by Miller (1968). The exposure required to kill all the trees by the end of the growing season was about 9,300 R, again similar to the Miller (1968) study. Data on partial mortality were not reported.

A third study of *Pinus palustris* was carried out by McCormick (1967). In this case, the forest was exposed at a constant rate for 8.3 days during August. All these pines < 5 years of age receiving 800 R or more died within 4 months. Older trees (up to 12 year old) required 2,800 R for complete mortality. This forest also contained some *Pinus ellottii*. All individuals of this species receiving > 300 R died and a clear relationship between plant size and radiosensitivity was observed. In all cases, the larger trees were more resistant. Microenvironmental changes were also observed at various exposure levels. In areas receiving > 2,000 R, temperature gradients were more like those of open fields than forests.

The effects of mixed neutron-gamma radiation in air emanating from the Lockheed Aircraft Corporation reactor in northern Georgia on *Pinus taeda* and *P. rigida* were studied by Platt (1963) and Pedigo (1963). Most of the exposures were delivered in a 2-week period in June 1959 and a 3-week period in August 1960, so the dose rate regime should be relevant to Chernobyl. After the June irradiation, pines receiving more than 7,500 rads turned reddish-brown within a few days and

were dead within a few weeks. Those receiving about 5,000-6,000 rads took much longer (up to 8-10 months) to die. Doses of about 1,000-3,000 rads caused death of terminal buds, inhibited reproduction and growth, and reduced photosynthesis, but caused little mortality. A complication in this Lockheed reactor study was the presence of neutrons, which may have an RBE greater than 1, but we have no data to assess this effect for pine mortality or growth. The gamma/neutron dose ratios reported in Platt (1963) ranged from 0.5:1 to 3.0:1, depending on location. If the neutron RBE is greater than 1 for these effects, the doses of pure gamma radiation needed to produce the same effects would be higher.

Donini (1967) studied the histological response of five year old *Pinus pinea* and *P. halepensis* to various total doses and dose rates. From such data, the relationship of dose rate to total exposure time to produce plant death was estimated. The exposure times ranged from 25 to 380 days for *P. halepensis*. Both curves plotted as a straight line on a log-log scale and were thus extrapolated back to a 20-day exposure period. This yielded a lethal total exposure of 860 R for *P. halepensis* and 3,000 R for *P. pinea*. These species have nuclear volumes of 1,000-1,100 μm^3 (Donini, 1967), from which one would predict acute (16 hr) LD_{50} values of roughly 700 R (Sparrow, Rogers, and Schwemmer, 1968). The large discrepancy in radiosensitivity between the two species is puzzling in view of their similar nuclear volumes. Nevertheless, it is evident that to produce an LD_{50} a 2-3 week irradiation requires a somewhat to much larger dose than does a 16-hour exposure.

A nine-day gamma exposure in autumn of a pine birch stand in the Soviet Union resulted in an LD_{100} for pine of 5,000-6,000 rads (Karaban et al., 1978). The threshold dose for obvious damage to the buds and needles was about 800 rads.

Two excellent chronic gamma irradiation studies on pine forests were carried out by Woodwell and Rebuck (1967) and by Amiro and Dugle (1985). Unfortunately, it is not possible to infer from their data lethal doses to pines subjected to 2 to 3-week exposures. Nevertheless, both of these studies support the concept that prolonged exposures are less effective than acute ones. Approximately 80% mortality to *Pinus rigida* was observed after 7,000 R was delivered over an 11-month period (Woodwell and Rebuck, 1967). A total dose of 8,000 rad over a period of about 2 years produced significant (~ 80%) mortality in *Pinus banksiana* (Amiro and Dugle, 1985).

One year old *Pinus sylvestris* seedlings were exposed to various constant exposure rates for 150 days in Canada (Sheppard, Thibault, and Guthrie, 1982). Needle growth at 17 rad/day essentially terminated after 60 days with a total dose of about 1,000 rad. Relationships in Klechkovskii, Polikarpov, and Aleksakhin (1973) indicate that this dose would need to be about 1,700 rad to cause severe growth inhibition and result in total lethality of the population. The ratio in radiosensitivity for seedlings relative to adult trees is reported by McCormick (1967) to be about

3.5 for *P. palustris*, so that a dose of about 6,000 rad delivered over 60 days should kill all adult Scotch pines if *P. sylvestris* shows the same ratio.

A study by Amiro (1986) on 2 year old *Pinus banksiana* seedlings examined the effects of both dose rate and total dose on the relative growth of the plants. Converting his multiple regression predictive equation to the units used in this report:

$$RG = 1.072 - (2.303 \times 10^{-4})\, D - (2.369 \times 10^{-3})\, D/t$$

where:

RG = growth rate relative to controls

D = total dose in rad

t = time of the exposure in days

The third term in the equation above is the dose rate factor. For an exposure time of 21 days and a measurable growth response of RG = 0.8, this equation predicts a dose of ~ 800 rad. A severe growth inhibition (RG = 0.2) is predicted for a dose of 2,500 rad. If this dose corresponds to 0.6 of the LD_{100} (Klechkovskii, Polikarpov, and Aleksakhin, 1973), the LD_{100} would be about 4,200 rad for a 21-day exposure.

6.2 ANALYSIS OF DOSE RATE DATA.

We have plotted the relevant data from the literature review discussed above such that all estimates can be given some weight in developing a dose rate or exposure duration relationship for assessing the pine tree damage in the Chernobyl forest. The total dose required to produce three endpoints of damage is plotted against the duration of the constant-rate exposure in Figure 6-2. The LD_{100} represents the minimum dose required to produce 100% mortality to the pines, while the LD_{50} represents the lethal dose to 50% of the population. The GR_{50} represents a 50% reduction in growth rate, relative to controls. Generally, lethal effects were scored within the current growing season for exposure periods < 60 days. In the case of the longer exposure periods, the effects were generally scored within 1-3 years after the start of irradiation. Growth rate effects were usually scored within the current growing season for exposure periods < 60 days. The lines in Figure 6-2 are drawn by eye.

The point estimates of the dose required to produce the three endpoints of damage for a 21-day exposure period as read from Figure 6-2, along with uncertainty bounds, are listed in Table 6-1. The uncertainty bounds are subjective, but they include a 1-week uncertainty in the effective exposure period at Chernobyl, as well as the scatter in the data. The suggested uncertainty bounds are within a factor of 1.8 of the best point estimate. Because the data are based

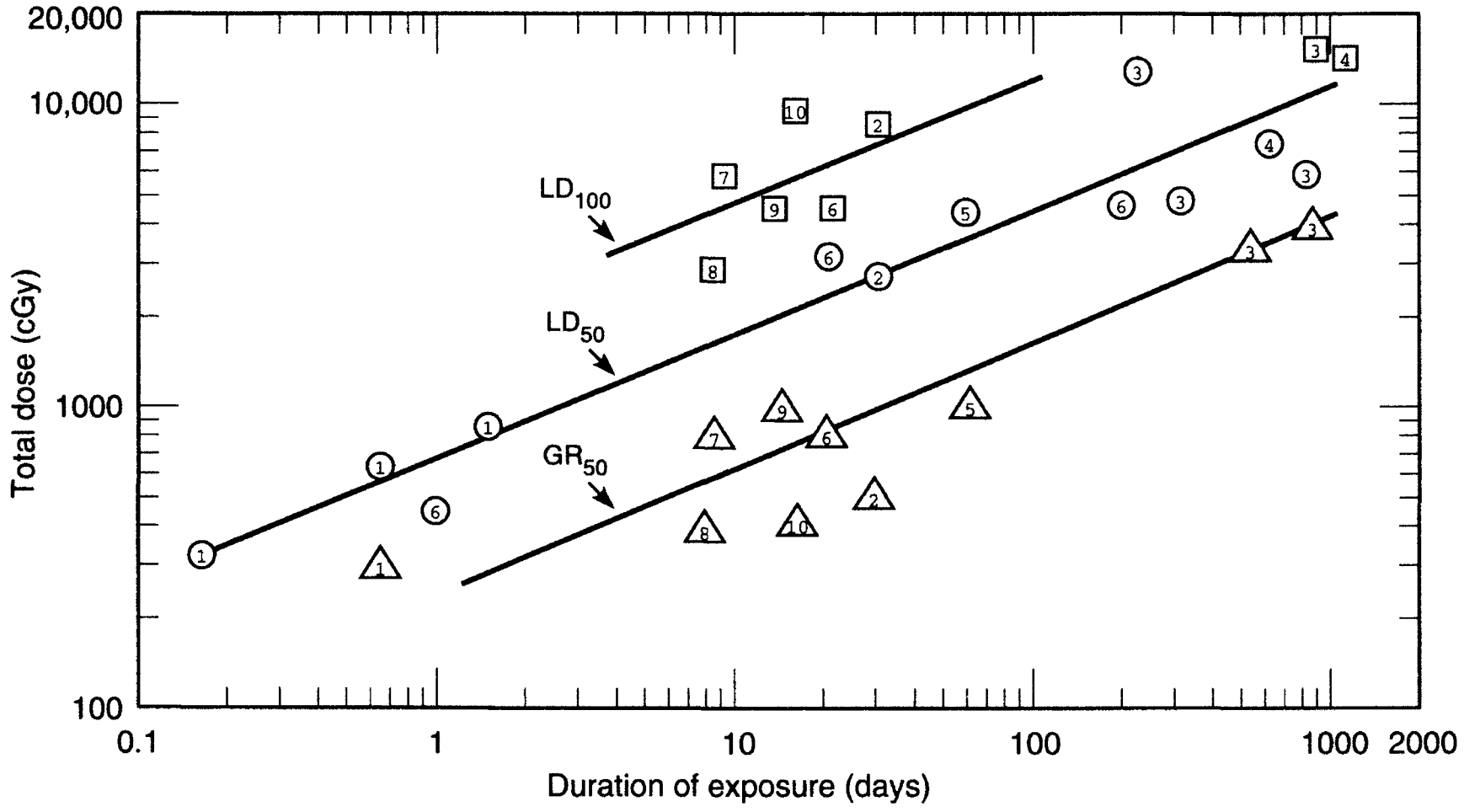

Figure 6-2. The relationship of total dose to duration of constant rate exposure for various endpoints of damage to pines. The LD_{100} represents complete mortality; the LD_{50} is 50% mortality; and the GR_{50} means a 50% reduction in growth rate. Squares represent data for the LD_{100}; circles the LD_{50}; and triangles the GR_{50}. Numbers represent the authors: 1 = Sparrow, Schwemmer, and Bottino (1971); 2 = Miller (1968); 3 = Woodwell and Rebuck (1967); 4 = Amiro and Dugle (1985); 5 = Sheppard, Thibault, and Guthrie (1982); 6 = Amiro (1986); 7 = Karaban *et al.* (1978); 8 = McCormick (1967); 9 = Platt (1963); 10 = Monk (1966).

on short-term exposures (< 60 days) received in the early growing season, the endpoints in Table 6-1 should be reached by the end of the growing season in late September or early October.

Table 6-1. Estimated total doses to produce three endpoints of damage to pines for an exposure period of three weeks (assumed equivalent to the effective exposure period at Chernobyl). The upper and lower bounds consider the scatter in the data from the literature, as well as a 1-week uncertainty in the effective equivalent exposure period.

	Required Dose (rad)		
Endpoint[a]	Best Estimate	Lower Bound	Upper Bound
LD_{100} (complete mortality)	6,000	3,300	10,800
LD_{50} (50 percent mortality)	2,300	1,300	4,100
GR_{50} (50 percent growth reduction)	800	440	1,400

[a]Endpoint observed by the end of the growing season.

We judge that the maximum stress indicated by satellite image processing would correspond roughly to the LD_{100}. Stress at the GR_{50} level is probably not detectable. At the GR_{50}, the vegetation will be hydrated, green, and functional, even though growth rate and reproduction are impaired. The LD_{50} is about a factor of 2.6 lower than the LD_{100} and roughly a factor of 2.9 higher than the GR_{50}. The LD_{50} will be detectable by satellite image processing certainly by the time half the trees are dead.

6.3 TEMPORAL PROGRESSION OF DAMAGE.

Most of the relevant studies on the effects of short-term radiation exposure on pines failed to score the vegetation frequently enough to document the rate of progression of the damage. In most cases, the damage was simply scored at the end of the growing season, and sometimes the following season. Fundamental radiobiological considerations would suggest that the rate of progression of damage should increase with total dose and dose rate, and also with the rate of mitotic activity.

The study by Platt (1963) is one of the more helpful with regard to time-progression of damage. Quoting from this author:

> "Within one week after the June irradiation, pine trees receiving doses of 7,500 rads or more began to turn a brilliant orange-red and died within a few weeks. Those receiving about 4,000 rads took much longer to die."

Multiple regression analyses of data from this study indicated that needle production in pines was a complex function of time after exposure, dose, and time-dose interactions. The work by Miller (1968), also one of the more relevant studies, showed that 100% mortality occurred within three months in pines receiving > 8,700 R. Unfortunately the time to death for pines receiving even higher exposures was not reported.

Pedigo (1963) reported noticeable effects within a few days in pines receiving a 2-week exposure of 8,000 rads or more. Significant mortality was recorded within one week after the exposure for pines receiving > 12,000 rads, but not until about 100 days after exposure for pines receiving 9,000 rads.

In the case of McCormick's (1967) study (an 8-day exposure in August), the older pines receiving 2,800 R took about four months to die. No additional trees died during the subsequent two years of the study.

Using the limited database, Figure 6-3 shows the approximate time required to reach the LD_{100} or the GR_{50} of pines for short-term (8 to 30-day) exposure periods plotted against total dose. The lines are drawn subjectively. The GR_{50} is offset from the LD_{50} by a factor of 7.5, as was the case in Figure 6-2. Considering the scatter in the data and other neglected variables such as growth stage, temperature, and moisture availability, we estimate that the uncertainty in the time to reach the endpoint is roughly a factor of 2. The curve would predict that very high doses (> 12,000 rad) would be required for prompt (< 1 week) mortality. Doses on the order of 1500 rad or more could cause growth impairment within a few days.

6.4 DOSE VERSUS TIME-TO-RESPONSE FOR MULTISPECTRAL DETECTION.

The reports of Monk (1966), Pedigo (1963), Platt (1963), and Miller (1968) provide visual descriptions and other data on pine tree response to radiation that allow qualitative estimation of the detectability of radiation response using Landsat Thematic Mapper images. These four reports are applicable for trees at least five years old and for springtime exposures lasting from two to four weeks. Table 6-2 lists data extracted from these reports.

For various combinations of absorbed dose and time since start of exposure, Table 6-2 repeats with minimal paraphrasing the description of damage found in the indicated Reference. The qualitative estimate of multispectral detectability for each dose/time combination in Table 6-2 is based on the descriptions of damage and the authors' experience with vegetation analysis using multispectral imagery. Factors considered include:

1) leaf senescence in deciduous trees is easily detected, so dead pine trees with brown needles will be easily detected,

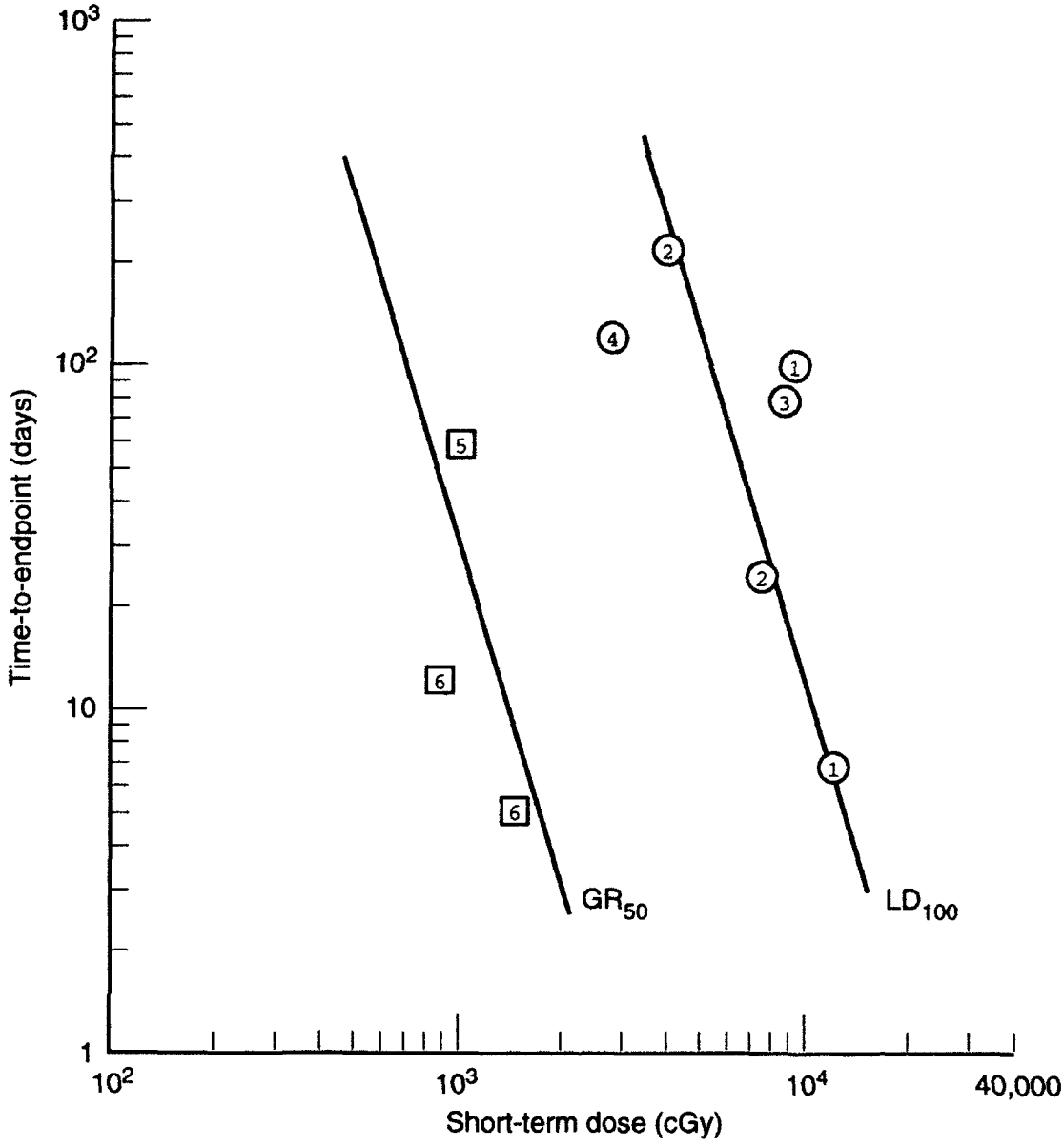

Figure 6-3. The time required to reach the LD_{100} or GR_{50} versus short-term (8-30 day) dose. Circles represent data for the LD_{100}; squares are data for the GR_{50}. Numbers represent the authors: 1 = Pedigo (1963); 2 = Platt (1963); 3 = Miller (1968); 4 = McCormick (1967); 5 = Sheppard, Thibault and Guthrie (1982); and 6 = Amiro (1986).

2) new growth needles and old growth needles on pine trees have a different color to the eye and have infrared spectral reflectivities that differ by 50% to 80% through the growing season (Wolfe and Zissis, 1978), and

3) minor variations in needle color or number will be masked by pixel-to-pixel fluctuations in canopy cover and residual misregistration of pixels.

Table 6-2. Detectability by multispectral remote sensing of radiation damage to pine trees for spring exposures as a function of time since start of exposure and dose. Exposure duration of two to four weeks.

Dose (Gy)	*Time since start of exposure (days)*	*Estimate of multispectral detectability*[a]	*Description of damage*[b]	*Reference*[c]
3.	330	×	No visible evidence of damage, terminal and lateral growth are 60-65% of normal	3
3.5	90	×	All trees alive, 85% survival of terminal buds, terminal growth 70% of normal	4
5.	142	×	Terminal buds alive, stem elongation reduced	1
11.6±1.7	142	×	Terminal buds dead, proliferation of lateral bud formation with subsequent growth	1
20.	20 (16 - 23)	×	No unusual needle fall	2
7.	90	□	12% survival of terminal buds, terminal growth 15% of normal, 50% survival of lateral buds, 10% of trees dead (may not be distinguishable from normal variations in canopy cover)	4
25.	280	□	First effects	2
30.	199	□	First effects	2
45.	20 (16 - 23)	□	Trees shed needles produced during first flush	2
80.	7	□	First signs of color, trees began to turn reddish brown	2
20.	390	■	Pines that had received more than 2000 rads were markedly affected	3
21.	90	■	0% survival of terminal buds, no terminal growth, 40 % of trees dead	4
32 ± 6	142	■	Trees alive but terminals dead, no lateral development	1
40.	270	■	Dead 8 to 10 months following an exposure greater than 4000 rads	3
42.	90	■	90% of trees are dead	4
45.	390	■	13 months following irradiation, pines that had received more than 4000 to 5000 rads were dead	3
75.	28	■	Began to turn a brilliant orange-red and died within a few weeks	3

Table 6-2. Detectability by multispectral remote sensing of radiation damage to pine trees for spring exposures as a function of time since start of exposure and dose. Exposure duration of two to four weeks. (Continued)

Dose (Gy)	*Time since start of exposure (days)*	*Estimate of multispectral detectability*[a]	*Description of damage*[b]	*Reference*[c]
87.	90	■	All trees dead at this dose and higher	4
93.	142	■	Trees dead, minimum lethal exposure (at this time) was 9261 R.	1
120.	16	■	Brilliant red-brown, coloring completed	2

[a]Detectability with Landsat Thematic Mapper (judgment of authors):

- × no, unlikely.
- □ maybe, uncertain,
- ■ yes, very likely,

[b]"Dead" means no green needles whatsoever; terminal and lateral refer, respectively, to the ends and sides of branches; terminal and lateral buds both contain apical meristem.

[c]References:

1. Monk (1966). 17 day exposure to ^{137}Cs γ-radiation; starting 11 May 1965, about one month after pine shoot elongation had begun; five-year-old longleaf pine (*Pinus palustris*).

2. Pedigo (1963): 14 day irregular exposure to output of Lockheed air-shielded reactor, n:γ ranging from 1:1.7 to more than 3:1; dominant exposure during second week starting about June 14, 1959; loblolly pine (*Pinus taeda*) forest containing trees with trunks up to at least 12" in diameter.

3. Platt (1963): Report based on same experiment as Reference 2 (Pedigo, 1961).

4. Miller (1968): 29 day exposure to ^{137}Cs γ-radiation; starting April 6, 1966, "at the very beginning of the growing season;" 8-year-old longleaf pine (*Pinus palustris*).

Figure 6-4 provides a graphical presentation of the detectability estimates from Table 6-2 with different symbols representing the three categories of detectability. Both dose and time since start of exposure should be considered as independent variables in Figure 6-4. The detectability data divides the dose/time plane into three regions corresponding to the three categories of detectability.

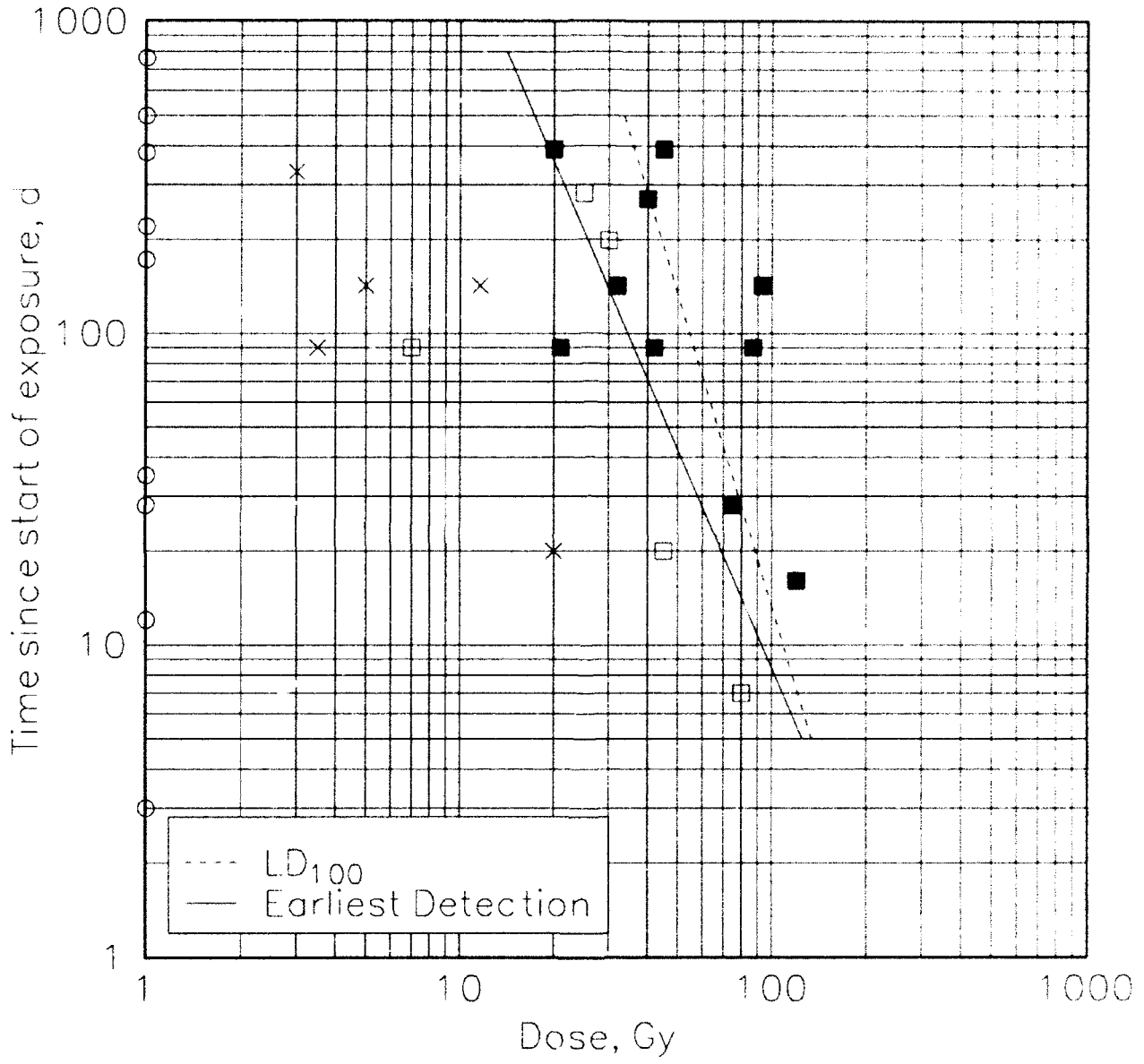

Figure 6-4. Detectability of the radiation response of pine trees using multispectral imagery. Solid squares, likely; open squares, uncertain; x's, unlikely. Circles correspond to Chernobyl image dates. Curves explained in text.

Although the data is somewhat sparse, the general outlines of the three regions are apparent in Figure 6-4.

Figure 6-4 includes the LD_{100} line from Figure 6-3 for reference. Because *dead* in the literature is defined as having no green needles, it is clear that any patch of forest lying along or to the right of the LD_{100} line will be detectable with the multispectral images of the Thematic Mapper. The other straight line in Figure 6-4 is hand-selected to approximate the boundary between the *likely* and *uncertain* estimates of detectability from Table 6-2. We assume that this line is a reasonable estimate of the relationship between dose and the time of earliest detectable response. This choice is conservative on the high side. A controlled experiment might reveal that multispectral analysis will detect responses well into the *uncertain* region of the dose/time plane. It seems unlikely that the line of earliest detectability would be much closer to the LD_{100} line.

We assume for the present analysis that the relationship between dose and time of first detectable response is linear on a log-log plot, that is, the relationship follows a power law. The factor likely to cause the biggest deviation from the assumed linearity is the seasonal variation in detectability arising from the spectral contrast between new and old needles. Consider a patch of pine trees that has received a dose at the beginning of the growing season large enough to kill most buds but not enough to significantly affect old growth. According to data presented by Miller (1968) such a dose would lie in the range of 7 to 15 Gy for a 4 week exposure in April. During the growing season, the appearance of unexposed trees is dominated by new growth, which would be absent from the exposed trees. Consequently, in multispectral imagery, unexposed and exposed trees would differ according to the spectral contrast between new and old needles. This contrast would fade after the growing season with the onset of cold weather as new needles on the unexposed trees assume the spectral reflectivity of mature growth. The contrast presumably returns the following growing season as radiation damage again is manifested by inhibited growth and mortality of some trees. Thus, in this intermediate dose range, the contrast between exposed and unexposed trees and, hence, the detectability of response, probably goes through a maximum toward the end of the first growing season and a minimum during the following winter.

This potential fluctuation in the detectability of pine tree radiation response in the intermediate dose range is represented by the *s*-shaped, dotted curve in Figure 6-4. Detectability occurs at a dose minimum 3 to 5 months after the start of exposure (during August or September) and then moves back to higher doses 7 to 9 months after the start of exposure (December to March). Although this fluctuation in detectability may influence the interpretation of our results, we nevertheless approximate the earliest detectability with a straight line in Figure 6-4 since the detectability data is sparse and we do not have late summer satellite observations to interpret.

The times of the 9 postaccident images relative to the day of the Chernobyl accident are indicated by the circles along the left edge of Figure 6-4.

Figure 6-5 presents a regression analysis intended to quantitatively estimate the boundary between the *likely* and *uncertain* estimates of detectability from Table 6-2. The data for the regression is selected from Figure 6-4 by taking the left-most occurrences (lowest dose for a given time interval) of the *likely* category and all of the points in the *uncertain* category. The data at 90 days has been excluded in both cases since we do not have an image of Chernobyl at that time and because of the probable temporary increase in detectability at the end of the growing season discussed above. Finally, the data at 142 days does not have a point in the *uncertain* category, so one has been interpolated halfway between the *likely* and *unlikely* points. Time of observation is taken as the independent variable and the dose as the dependent variable for the regression analysis. The regression line with 68% confidence band is plotted in Figure 6-5. The regression line is given by

$$D = 198\, t^{-0.365} \qquad (6.1)$$

where t is the time of first detectable response in days since start of exposure and D is the estimated dose in Gray. This relationship is our best estimate for detectability with remotely sensed multispectral imagery. It does not apply to close visual inspection of trees nor to growth measurement, both of which would reveal response at lower doses and earlier times.

Table 6-3 provides evaluations of Equation 6.1 for the postaccident image dates analyzed in this report. Equation 6.1 is based on data ranging from only 1 week to 1 year. Values for times outside this range are extrapolations as noted in Table 6-3 and are subject to additional uncertainty.

Table 6-3. Dose estimates according to Equation 6.1 for a first detected response corresponding to the times of the 9 postaccident images presented in this report.

Image number	*Time postaccident (Days)*	*Estimated dose (Gy)*	
3	3	133.	(extrapolation)
4	12	80.	
5	28	59.	
6	35	54.	
7	172	30.2	
8	220	27.6	
9	380	22.6	
10	499	20.5	(extrapolation)
11	763	17.6	(extrapolation)

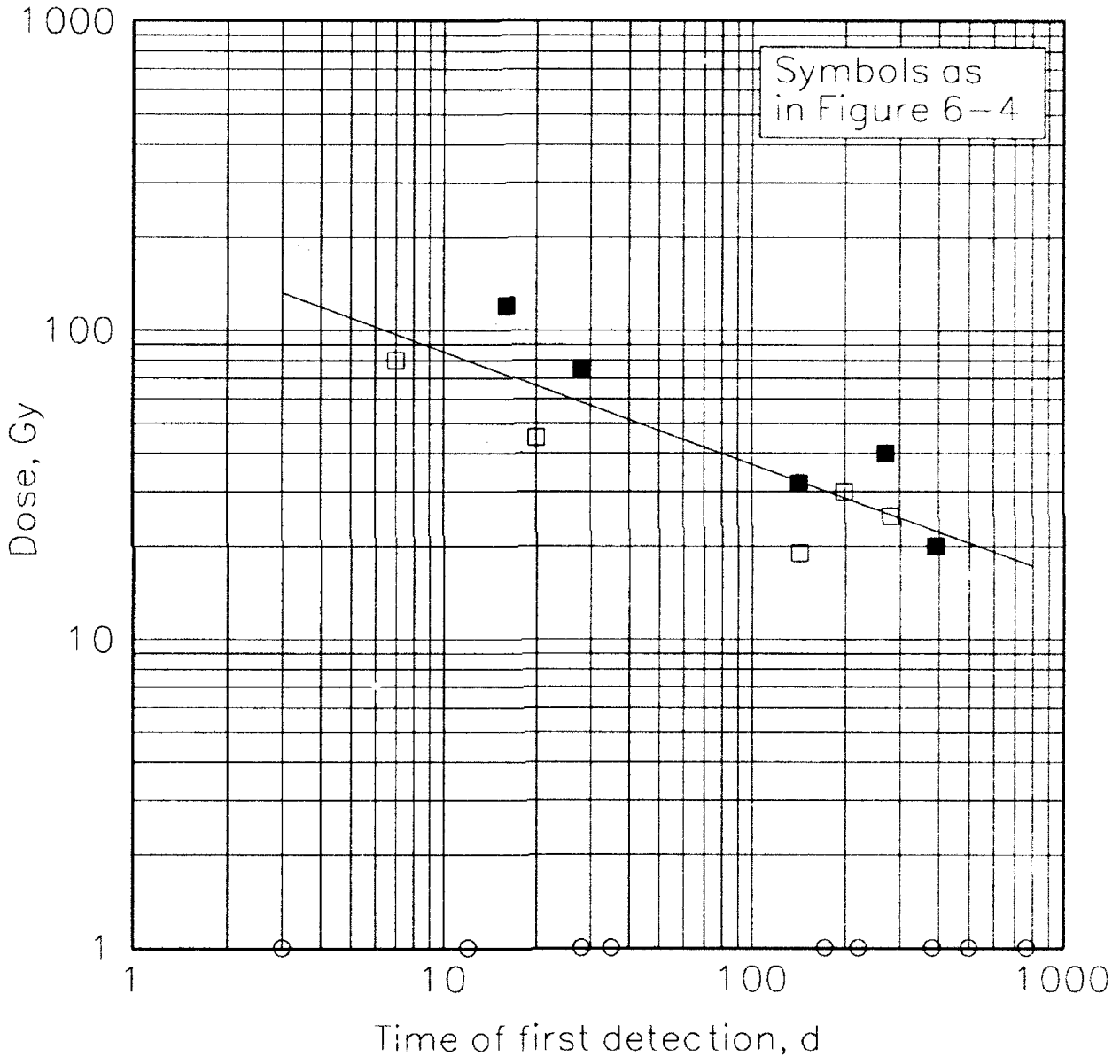

Figure 6-5. Regression line with 68% confidence band for the relationship between dose and time of earliest detection relative to the start of exposure for two- to four-week, springtime exposures.

In conclusion, Equation 6.1 represents the relationship between total absorbed dose and the time of first detected response relative to the start of exposure. This relationship is used for the dose estimates presented in this report. It is based mostly on gamma dose.

SECTION 7
DOSE DETERMINATION FOR CHERNOBYL FORESTS

This section maps estimated radiation doses to pine forest near the Chernobyl nuclear power station through an analysis of a time series of Landsat Thematic Mapper (TM) images for two years following the Chernobyl accidental nuclear reactor explosion. The first subsection describes a method for defining spectral deviation from normal for a pixel known to belong to a given class and presents such deviations based on the 11 Tasseled Cap images of Chernobyl and the 4 pine forest classes with reference (or control) sites for each class as given in Section 3. The second subsection discusses the progression of forest clearing during postaccident cleanup operations. The third subsection describes the calculation of time-to-response on a pixel-by-pixel basis for pine forest showing radiation response and discusses the correlation with radiation dose to foliage. The fourth subsection presents two alternative methods for generating dose contours from the satellite data. The final subsection discusses the resulting dose maps and summarizes results from this section.

7.1 SPECTRAL DEVIATION FROM CLASS.

Section 3 describes the procedures used to map four preaccident classes of pine forest based on pixel-by-pixel classification of spectral reflectivity. Each class of pine forest is represented by a reference site containing on the order of 100 contiguous pixels. Each pixel encompasses a 25 m by 25 m square of forest and is represented by a vector of spectral intensity values transformed to the Tasseled Cap coordinate system. The vector components measure the average spectral features of all trees and other surfaces within the pixel that are visible from above. In addition, each pixel vector has noise components due mainly to atmospheric scattering of light into the line of sight of the pixel.

In this subsection, we establish the basis for detecting the average radiation response of the pine trees in a pixel by quantifying the deviation of each pixel vector from normal, defined as the mean vector of the reference (or control) site for the class to which the pixel belongs. The deviation for each pixel is expressed as a *Mahalanobis vector*. The deviations for the pine forest within a few kilometers of the Chernobyl nuclear reactor station are presented in a color format designed to show deviations in Tasseled Cap brightness, greenness, and wetness for each date analyzed.

7.1.1 Mahalanobis Distance and the Mahalanobis Spectral Deviation Vector.

Figure 7-1 illustrates a cluster of pixels from a class reference site using two axes of the Tasseled Cap coordinate system. Each pixel is represented by a point plotted according to the components of its spectral intensity vector **x**. For calculational purposes, we assume that each cluster of pixels may be reasonably approximated by a multivariate normal distribution. The resulting hyperelliptical distribution in general has its principle coordinate axes tilted with respect to the Tasseled Cap axes and has unequal variance along the principle coordinate axes.

The spectral deviation of a pixel **x** from its class is expressed by the deviation vector $\mathbf{d} = \mathbf{x} - \mu$, where μ is the mean vector of the class reference site. In order to have a consist meaning for the spectral deviation from class to class, the deviation vector must be expressed in standard units. The method that we use is explained in Appendix B. For each class of pine forest, a normalizing matrix **N** is used to convert the deviation vector **d** to a *Mahalanobis vector* **m** by the transformation

$$\mathbf{m} = \mathbf{N}\,\mathbf{d}. \tag{7.1}$$

The matrix **N** is calculated from the covariance matrix of the class reference site as described in Appendix B.

The normalization of each pixel deviation according to Equation 7.1, transforms the set of deviations for the reference site to a distribution with unit variance in all directions. By definition, the deviations have a mean of zero. The magnitude of the Mahalanobis vector, called the *Mahalanobis distance* (Duda and Hart, 1973), measures the distance of a pixel from its class mean in standard units. It is the multivariate equivalent of the normal deviate z customarily used with a univariate standard normal distribution.

The Mahalanobis distance is used to determine the significance of the deviation of a pixel from its class mean. To define significant deviation, a threshold is set such that any pixel with Mahalanobis distance greater than the threshold is judged to have moved significantly away from it class through the action of some factor not affecting the class in general. Since the Mahalanobis distance is expressed in standard units, we can use the same threshold for deviations with respect to all classes.

7.1.2 Scaled Mahalanobis Distances and Vectors.

The image processing software used for the present analysis stores only 8 bit intensity values, that is, integers ranging from 0 to 255. Calculations are done with floating point arithmetic, but 8 bit numbers are used to store results in image format and for color display of images. For

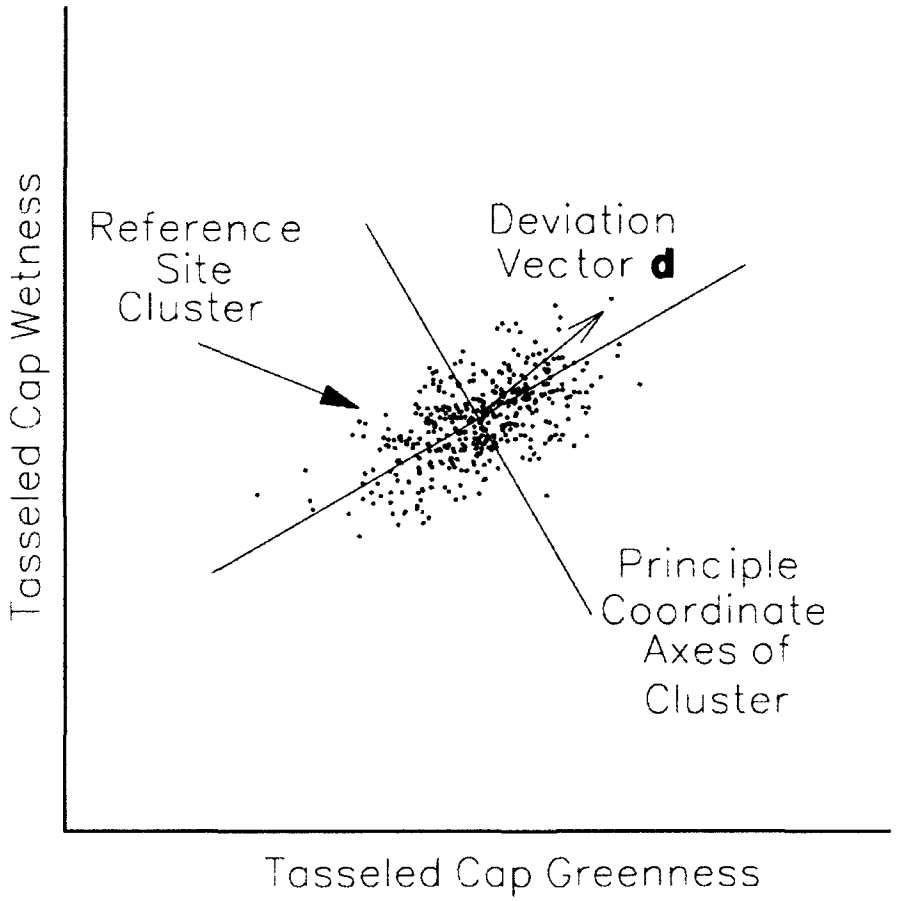

Figure 7-1. Two-dimensional illustration of the cluster of points formed by the pixel intensity vectors of a forest reference site. See Appendix B for the normalization procedure used to express deviations of pixels from the cluster center in standard units.

convenience, a scaled Mahalanobis vector **v** and a scaled Mahalanobis distance s are defined according to

$$\mathbf{v} = 4\,\mathbf{m} + 128\,\mathbf{i} \tag{7.2}$$

and

$$s = 4\,|\mathbf{m}|, \tag{7.3}$$

where **i** is a vector with all components are equal to one. The dimensionality of the scaled Mahalanobis vector **v** is equal to the number of spectral bands being utilized in the analysis and can range from one up to the original number of bands in the multispectral image. The scale factor of 4 in both equations scales the values such that in one dimension, a standard deviation becomes four units. In other words, the scaled Mahalanobis distance s is expressed in integer multiples of 0.25 standard deviations. This resolution is sufficient since deviations of one or two standard deviations, expressed here as 4 or 8 units, are below the level of significance. A full scale deviation of 255 corresponds to 255/4 = 63.75 standard deviations, a dynamic range that is quite sufficient for present purposes.

The scaled Mahalanobis vector **v** has an additive term of 128 on each of its components to shift the mean value from zero to 128, the center of the 8 bit scale. In this way, the cluster of scaled deviations for a reference site forms a spherical distribution at the center of the hypercube of possible deviation vectors with 8 bit components. The cluster has a standard deviation of 4 along each axis. Again, the only purpose of the scaling defined by Equations 7.2 and 7.3 is to accommodate the 8 bit data scale.

The analysis of vector deviations in this report uses only three components from the Tasseled Cap transformed images, namely, brightness, greenness, and wetness. Figure 7-2 illustrates a scaled cluster for a class reference site using these three dimensions. The value of the scaled Mahalanobis distance s from Equation 7.3 corresponds to the radial displacement of a pixel from the center of the cluster in Figure 7-2. It is used to judge the significance of a deviation independently of the combination of feature changes causing the deviation. A threshold is chosen such that any deviation greater than the threshold is flagged as significant. Following the usual procedures of statistical analysis, the threshold must be set high enough that the random occurrence of deviations above threshold on the tail of the multivariate distribution for normal forest as illustrated in Figure 7-2 does not interfere with the detection of the spatial pattern of deviations caused by radiation exposure.

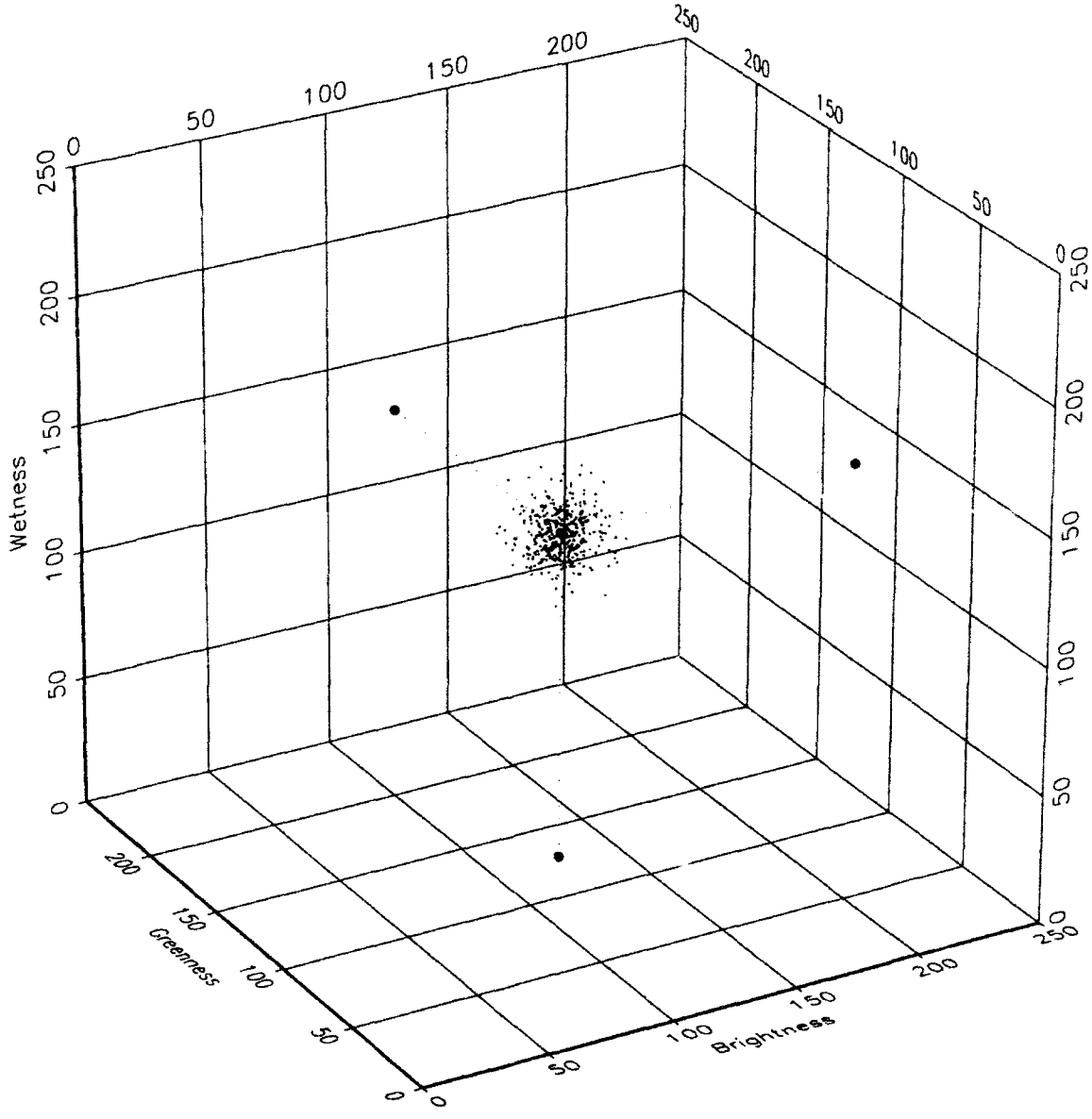

Figure 7-2. The cluster of scaled Mahalanobis vectors for a pine forest class reference site using the first three features of the Tasseled Cap spectral transformation. (Cluster enlarged for clarity.)

The scaled vector deviation **v** in Equation 7.2 specifies the direction of the deviation in the three-dimensional space, that is, it tells how much each of the Tasseled Cap features deviates from normal. It may be used to distinguish deviations with specific spectral signatures. It particular, the Mahalanobis vector is used in this report to detect pine forest that was cleared as part of the decontamination effort after the Chernobyl accident.

7.1.3. Spectral Deviations for the Chernobyl Images.

We have calculated both vector and scalar spectral deviations according to Equations 7.1-3 and Appendix B for all pixels in the 38.4 km square analysis area presented in Section 3 belonging to the four pine forest classes defined in Figure 3-24. Figures 7-3 and 7-4 provide a color graphic presentation of the vector deviations for a 4.4 km by 4.8 km area near the reactor station. The upper left panel in Figure 7-3 shows the four pine forest classes color-coded as in Figure 3-23 and superimposed on a gray-scale background image of the area for spatial orientation. The other five panels of the same size show the vector deviations for the pine forest pixels on the first five image dates; for clarity, no background image is include. The five panels are numbered according to the image/date numbering scheme of Table 3-3. Figure 7-4 shows the vector deviations in the same area for the last six image dates.

The color graphic presentation of vector deviations in Figures 7-3 and 7-4 is generated by displaying the components of the scaled Mahalanobis vector (Equation 6.2) for Tasseled Cap brightness, greenness, and wetness in the red, green, and blue channels, respectively, of the color images. The process can be visualized in the color space of the display images with the aid of Figure 7-2 by replacing each Tasseled Cap label on the axes with the corresponding red, green, or blue display intensity. The scale of gray levels (equal intensities of red, green, and blue) from black to white stretch along the diagonal of the color space from the origin (0,0,0) to (255,255,255).

The cluster corresponding to a class reference site is centered at midscale (128) on each of the color channels. The resulting display is gray at the middle of the intensity scale, halfway between black and white. A patch of forest with negligible deviations from the class mean would appear as nearly uniform gray in Figure 7-3. Since the pixels of normal forest have random deviations from the class mean as illustrated in Figure 7-2, normal forest will appear to be speckled with pastel colors lying near the midlevel gray point.

The three reference bars along the right edge of Figures 7-3 and 7-4 show the appearance of normal distributions like that of Figure 7-2 with standard deviations of 4, 6, and 8 units along each axis as indicated by the number in each bar. Note that only the intensity of color fluctuations and not their spatial scale is different in the three reference bars. By definition, reference sites for the

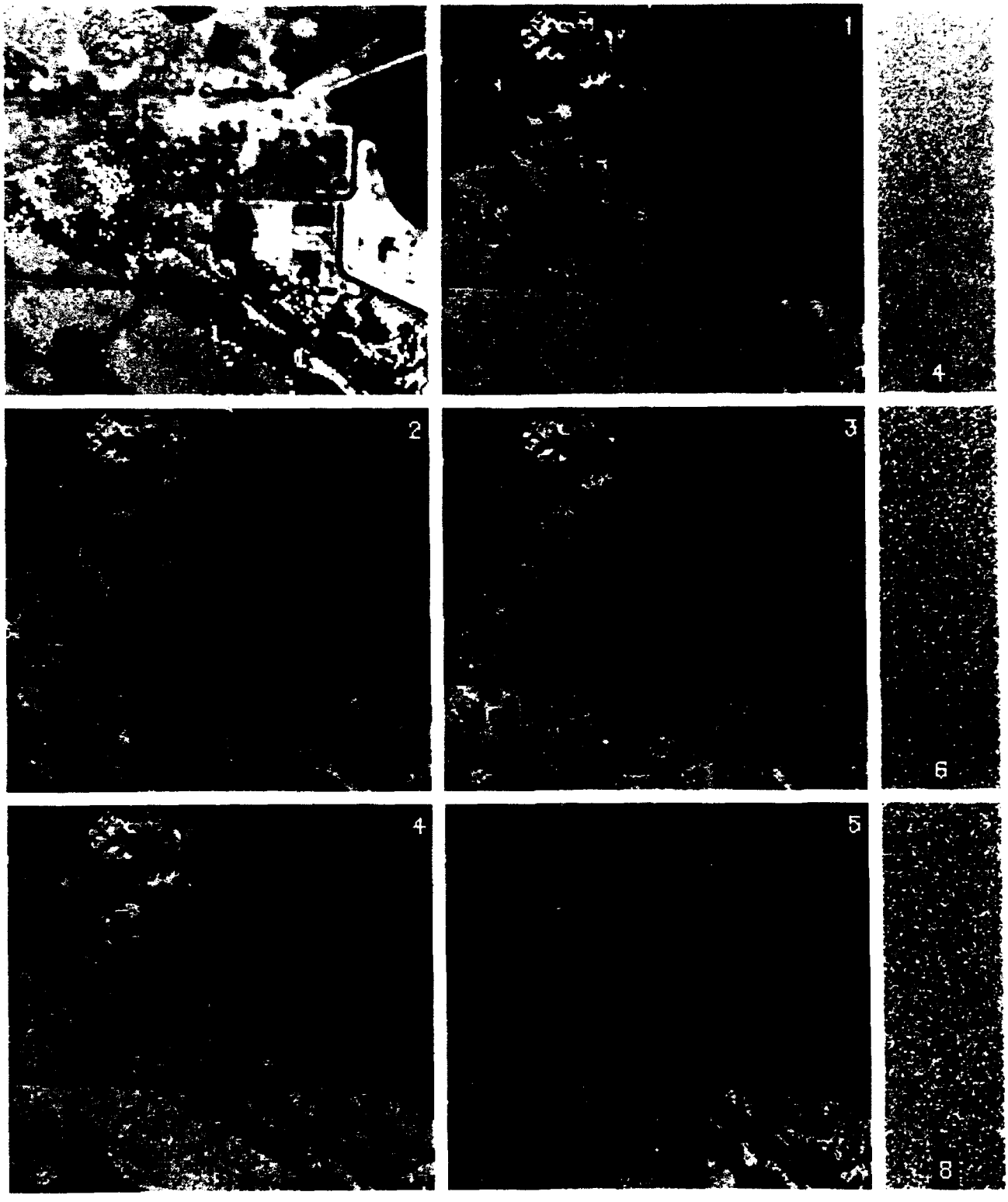

Figure 7-3. Color graphic presentation of the scaled Mahalanobis deviation vectors for pine forest on Dates 1 to 5 (194 by 177 pixel area). Upper left panel shows forest classes (see Figure 3-23). Three reference bars along right edge illustrate appearance of normal forest.

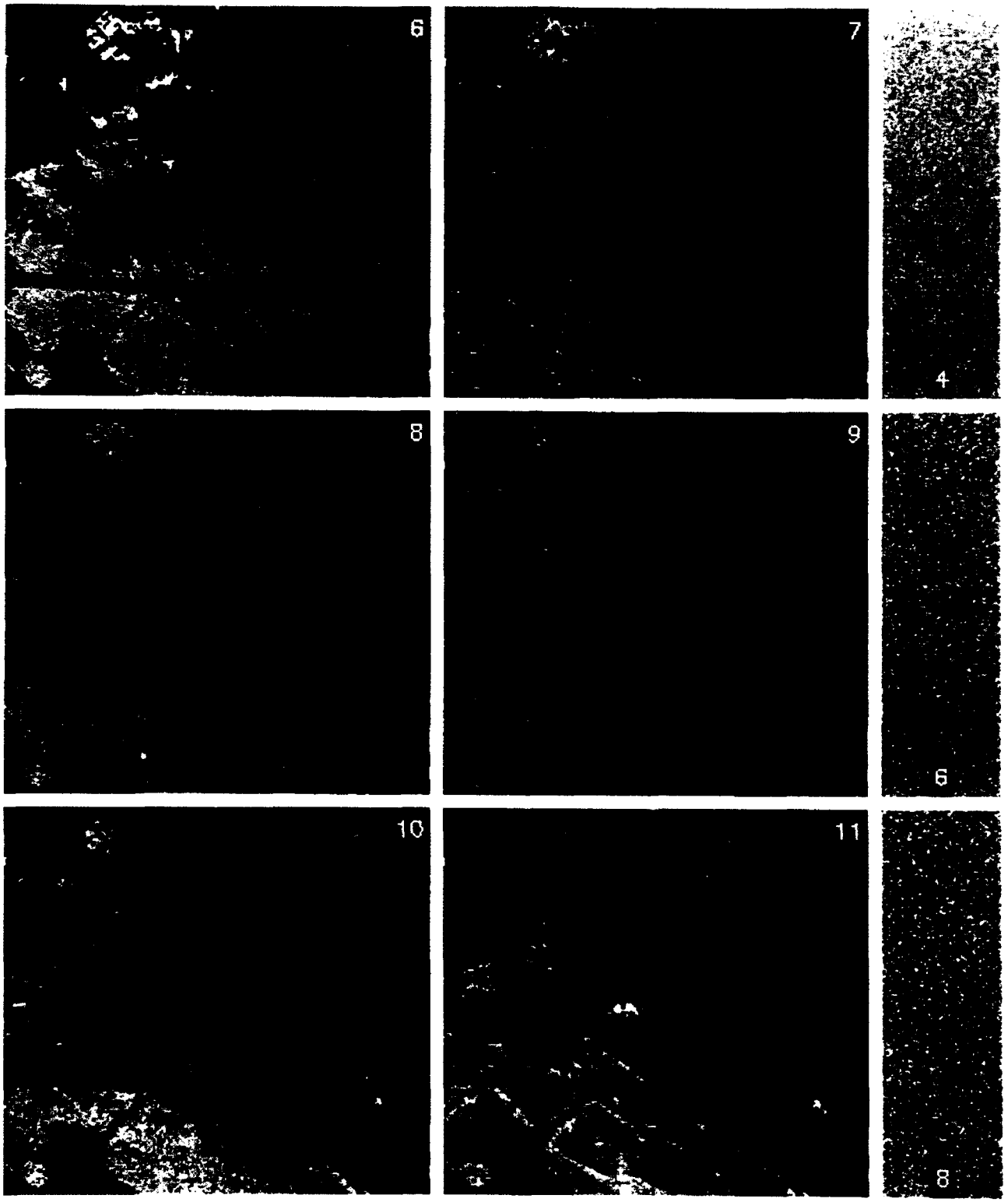

Figure 7-4. Color graphic presentation of the scaled Mahalanobis deviation vectors for pine forest on Dates 6 to 11 (194 by 177 pixel area). Three reference bars along right edge illustrate appearance of normal forest.

pine forest classes will appear like the upper bar with a standard deviation of 4 units along each color axis. The reference bars with standard deviations of 6 and 8 are included since geographically separated patches of normal forest may have additional random variance not present in the corresponding reference site.

Examination of the Date 1 spectral deviations as represented by the speckled gray patterns of the color graphic display in Figure 7-3 shows no significant difference from the reference bars as expected since Date 1 was before the reactor accident and is used to define the forest classes. Date 2, the preaccident winter image, is also reasonably close to the reference bars as it should be.

The strongest deviations in Date 3 of Figure 7-3 are the magenta patches caused by clouds which have high brightness and wetness with low greenness. The resulting mixture of red and blue with negligible green gives the magenta color.

Figure 7-4 clearly shows the progression of increasingly significant disturbance of the pine forest as a result of the reactor accident. By Date 9, strong red patches show forest that has been cleared for operational purposes and for radioactive decontamination These areas are expanded by Date 10. Some of the ground cover on these cleared areas has changed by Date 11 as evidenced by the shift from red to magenta. The red line through the large forest patch in the lower third of this image area is probably the disturbance caused by the construction of a ground water barrier as discussed in Appendix C. It first appears in the images on Date 7 (October 1986) with an additional segment on Date 9 (May 1987).

Not much forest clearing had been done by Date 7. There were no clouds on this date. The spectral deviations of the pine forest show a strong radiation response as the brown and orange swath across the middle of the left half of the image area. This swath corresponds to the westward trace of initial fallout deposition from the reactor explosion. Additionally, the irregular patch of forest at the top of the image area on Date 7 shows a radiation response with a somewhat different spectral signature as evidenced by the magenta hue in Figure 7-4. This response of the irregular patch has diminished on the winter image of Date 8 but returns the following year on Dates 9 and 10.

According to the data and discussion in Section 6.4, this fluctuation in detectability of the radiation response of the irregular patch suggests a short term total dose to the canopy in the 10 to 20 Gy range. The magenta hue on Date 7 indicates a reduction in greenness relative to normal pines, corresponding to a lack of new growth during the summer after the accident. As the new growth on unexposed pines matures, the winter image of Date 8 shows almost no difference between the exposed patch and normal forest. The shift to an orange hue by Date 10 indicates that many pines have died by that time.

Although it may not be apparent because of the resolution and fidelity of color reproduction of this report, the forest along the westward trace of fallout shows a widening response on Dates 4 through 6. This widening is demonstrated by the change detection analysis in Volume 2 of this report (McClellan et al., 1992). It is also apparent when the deviation images of Figures 7-3 and 7-4 are displayed on a high resolution color monitor of an image processing system. Because of limitations of color reproduction, further analysis of radiation response in this report is based on numerical analysis of the scaled Mahalanobis deviation vectors and distances.

7.2 DEVIATIONS CAUSED BY FOREST CLEARING.

In the detection of radiation-induced spectral deviations, clearing of forest must not be interpreted as severe radiation response. Figure 7-5 shows a map of pine forest that was present postaccident through May 1986 but appears to have been cleared (bulldozed) by the date of the image number indicated in the figure. The figure includes 1 km grid lines originating at the reactor (Unit 4). Clearing activity west of the reactor station seems to be mainly for decontamination. The earliest clearing is near the elbow in the main road about 1.5 km west and 0.5 km south of the reactor site where the road crosses the main trace of fallout deposition. Appendix C includes an eyewitness description by a man who walked along this road on the morning of the accident. He encountered a band of graphite flakes crossing the road and reported that the forest later "came under the ax."

The large area in green in Figure 7-5 located 1.5 km east and 2 km south of the reactor site was cleared between December 1986 and May 1987. This area shows no apparent radiation response before being cleared and so is presumed to have been cleared for operational reasons. The spectral signature of this area on Date 9 is used to define cleared forest on all dates. For this purpose, the scaled Mahalanobis vector is used as described in Section 7.1.2. A representative scaled Mahalanobis vector for cleared forest is calculated on Date 9 from a sample of pixels from the large cleared area. The vector is then normalized to provide a unit vector pointing in the direction of spectral deviation of cleared forest relative to normal forest. A forest pixel on any date is designated as cleared if the dot product of its scaled Mahalanobis deviation vector with this unit vector exceeds a threshold. The threshold is set high enough to eliminate spurious indications of clearing for isolated pixels and to avoid classifying radiation-damaged forest as being cleared.

Table 7-1 lists the areas of newly cleared pine forest on the various dates in Figure 7-5. These areas are lower limits to the amount of vegetation actually cleared since Figure 7-5 includes only pixels belonging to one of the four classes of pine forest defined in Section 3. The listed areas include the pixels along the path cleared through the forest 3 km south of the reactor for the construction of a ground water barrier as described in Appendix C.

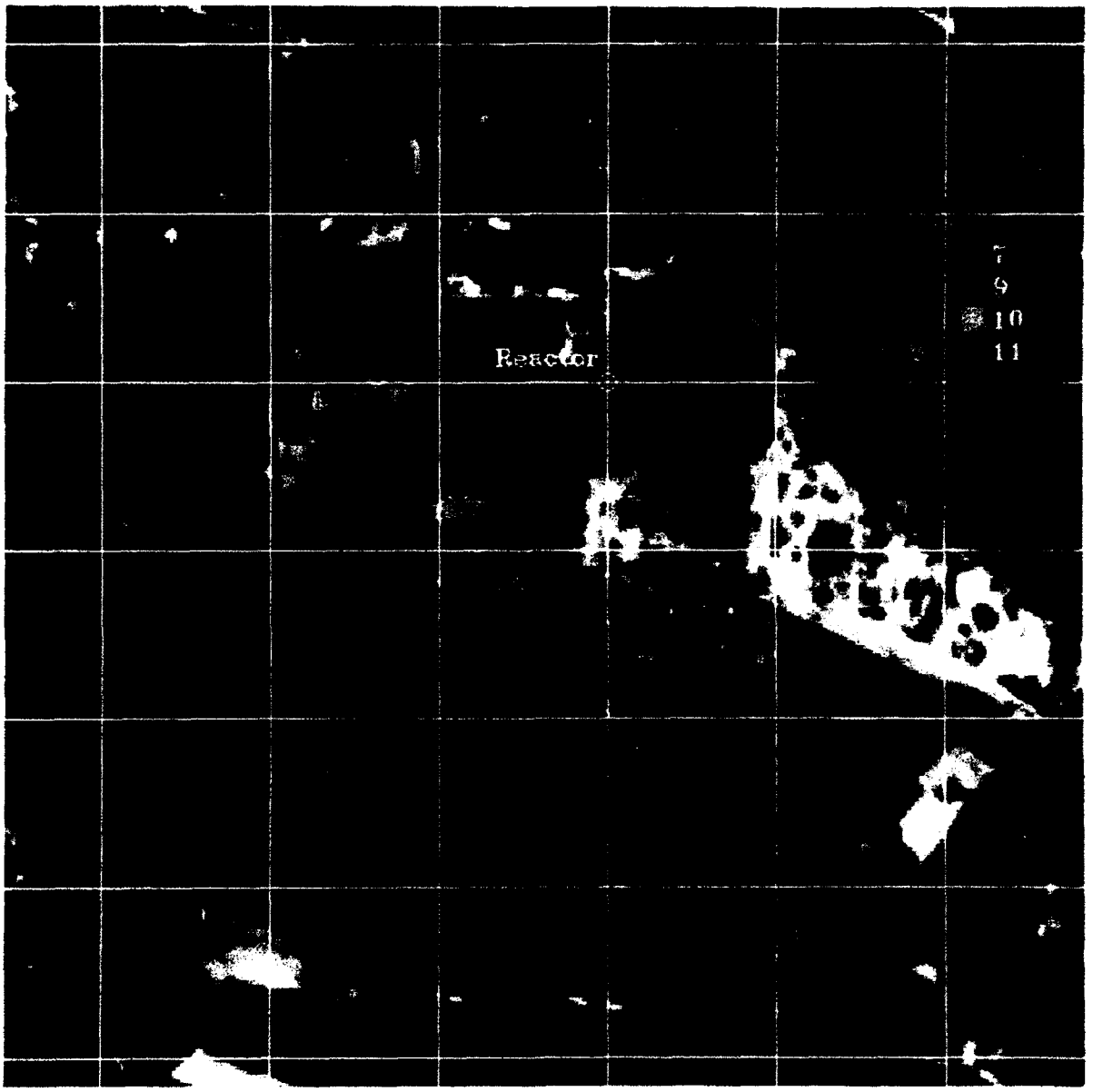

Figure 7-5. Forest cleared (bulldozed) after the Chernobyl acident is color coded by the date number of the first observed clearing. Grid lines are spaced by 1 km with an intersection at the Unit 4 reactor.

Table 7-1. Area of pine forest near the Chernobyl nuclear reactor station cleared by the listed image date. Clearing of other vegetation not included.

Image Number	*Date*	*Number of Pixels Cleared*	*Area (ha)*	*Cumulative Area (ha)*
7	15 Oct 86	5	0.3	0.3
8	2 Dec 87	0	0.0	0.3
9	11 May 87	1115	69.7	70.0
10	7 Sep 87	493	30.8	100.8
11	28 May 88	410	25.6	126.4

7.3 TIME-TO-RESPONSE FROM IMAGERY.

The time-to-response for the foliage comprising a single pixel is derived from the onset of significant, persistent deviation of the spectral signature of the pixel from normal the spectral signature of the class to which the pixel belonged before the accident. The time-to-response for the foliage in the pixel is the time difference between this response and the time of the accident, that is, time-to-response is measured relative to the start of radiation exposure.

Significant deviation from normal on a given date is judged by the scaled Mahalanobis distance of a pixel relative to its class mean as described in Section 7.1.2. A threshold distance is set for each date so that any pine forest pixel with scaled Mahalanobis distance exceeding threshold is flagged as having a significant deviation on that date. The procedure is equivalent to using a multivariate z score to judge the significance of an observed deviation. The Mahalanobis distance is calculated in 3 dimensions using the intensity values for Tasseled Cap brightness, greenness, and wetness. Thresholds of 20 to 24 are low enough to give good detection of the radiation-induced spatial patterns of change described in Volume 2 of this report and high enough to minimize the random occurrence of isolated pixels exceeding threshold at large distances from the reactor site.

In addition, a neighborhood-dependent algorithm for threshold comparison is used to improve the signal-to-noise ratio for detecting radiation response. In this algorithm, the Mahalanobis distance for each pixel is replaced by the magnitude of the average Mahalanobis vector of the pixel and any of its eight neighboring pixels that are also pine forest. The vector average reduces the influence of slight registration errors from image to image as well as noise from other sources. To take advantage of this noise reduction, the threshold for each pixel is scaled by the inverse of the square root of the number of pixels being averaged. That is, when a pine pixel at the center of a

3 by 3 square patch of pixels has N - 1 neighbors in the patch that are also pine forest, the pixel is flagged as having a significant deviation if

$$\left| \frac{\sum_{i=1}^{N} v_i}{N} \right| > \frac{T}{N^{1/2}} \tag{7.4}$$

where v_i is the scaled Mahalanobis distance of the *i* th pine forest pixel in the 3 by 3 patch and T is the threshold value for a single pixel. A form of Equation 7.4 that is more efficient for calculations is

$$\left| \sum_{i=1}^{N} v_i \right|^2 > N T^2 \tag{7.5}$$

Figure 7-6 illustrates the algorithm for the determination of time-to-response given that significant deviations have been flagged in each image and lists the threshold T used for each image. The algorithm is based on finding the first significant deviation that persists for the same pixel on all subsequent image dates. The deviation must precede any indication that the forest in the pixel has been cleared. Any pixel that does not contain pine forest, or is cleared of forest before any indication of radiation response, yields no data regarding radiation exposure. Such pixels are assigned a code of zero and will become black background in response maps presented as images in this report. Any pixel that appears normal (does not exceed threshold) on Date 11, the last image of the series, has no persistent response by definition and is coded as normal forest with no radiation response. Such forest pixels yield a null response and are coded to appear gray in response or dose images. These areas show where fallout contamination was too low to produce lasting visible damage to the foliage of pine trees. A pixel that shows a first persistent deviation from normal on Date n is coded with the value n to indicate the date of first observed response. Of course, the first "observable" response will have actually occurred sometime between this date and the previous image date.

The requirement of a persistent response over two years has the disadvantage of eliminating responses to low doses where the trees recover normal appearance within two years. On the other hand, the requirement has two major advantages. The first, and of most practical importance, is the elimination of spurious responses caused by clouds, jet contrails, and local haze patterns occurring on a single date. The second advantage is further reduction of noise signals that are uncorrelated from date to date. These advantages derive from the fact that several of the images in

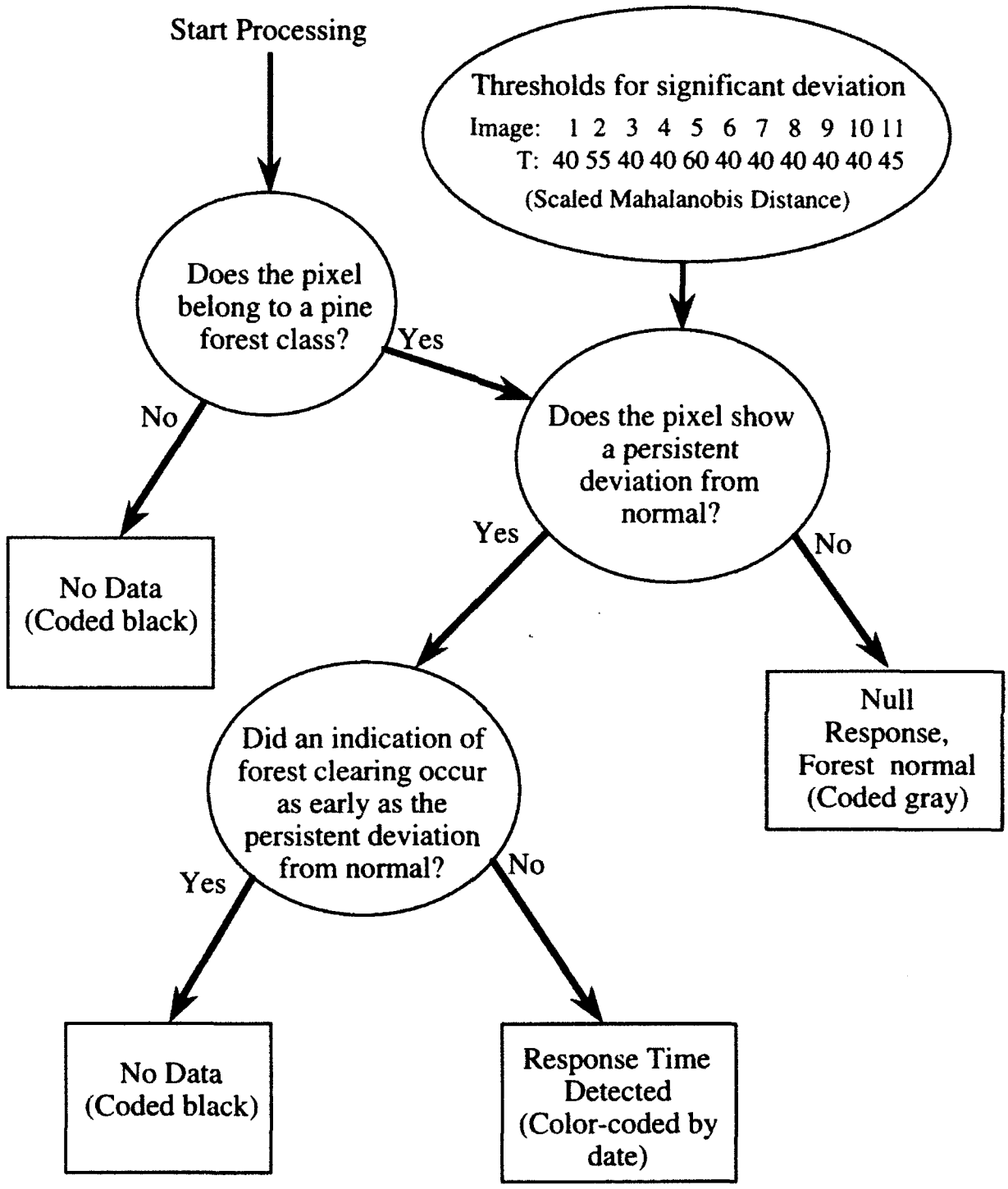

Figure 7-6. Algorithm for determination of time-to-response for radiation-damaged foliage on a pixel-by-pixel basis. Parenthetical remarks refer to presentations in response time figures.

the series are cloud free and none of the images have extensive cloud cover, so the probability of a persistent response at a given location due to a combination of clouds and random noise is nil. Since the last date (Date 11) has no subsequent image for establishing persistence, the threshold used for Date 11 is set higher than that of the other images to reduce spurious responses on that date.

Figure 7-7 presents results for the date of first observed radiation response according to the algorithm of Figure 7-6. The date number of response for each pixel is color-coded according to the legend in the image. Table 6-3 lists the date numbers and corresponding estimated foliage doses according to the analysis of published data presented in Section 6. No persistent responses exceed threshold on the preaccident Dates 1 and 2 or on postaccident Date 3. Only two pixels in the central blue area of Figure 7-7 have responses on Date 4. The main early response in Figure 7-7 is for Dates 5 and 6, four to five weeks after the accident date. Since the responses could have started immediately after Date 4 at 12 days, the dose for the blue area is estimated to be between 54 and 80 Gy according to Table 6-3. Surrounding the blue area and extending further to the west is a dark green area showing first observed response on Date 7 (October 1986). The estimated dose for this area is 30 to 54 Gy. The yellow-green and yellow areas have first observed response between Dates 8 and 10 with estimated doses in the 20 to 30 Gy range.

Note that the irregular patch of forest in the upper middle of Figure 7-7 shows only a few pixels with persistent responses, beginning on Dates 9 and 10 with estimated dose in the 20 to 28 Gy range. The irregular patch consists mostly of gray pixels, indicating a dose less than about 18 Gy. As pointed out in Section 7.1.3, this area shows a transient response maximizing on Date 7 (October 1986) and disappearing over the winter. As discussed in conjunction with Figure 6-4, this transient response is likely to be associated with doses in the range of 7 to 15 Gy. *The response of this irregular patch shows that the multispectral detection technique for pine tree radiation response could be extended to doses below 20 Gy if the analysis accounted for transient as well as persistent responses.*

A small, vertically oriented, rectangular group of about 20 pixels just to the right of the irregular patch shows a solid response on Date 7 for an estimated dose of 30 to 54 Gy. Figure 7-5 shows that this same group of pixels was cleared between Dates 9 and 10. The group is 1.2 km west and 1.3 km north of the reactor site. Figure 7-5 shows that the irregular patch of forest discussed above is located 2 km west and 1.5 km north of the reactor site and had not been cleared as of Date 11 (May 1988). The patch is at the eastern edge of Pripyat. If these trees are still standing, they would provide a good retrospective sample on which to perform histological studies to correlate with the responses and estimated doses derived from satellite images.

The path cut through the largest patch of gray, normal forest in the lower part of Figure 7-7 is associated with a ground water barrier several kilometers long and 30 - 35 m deep constructed to

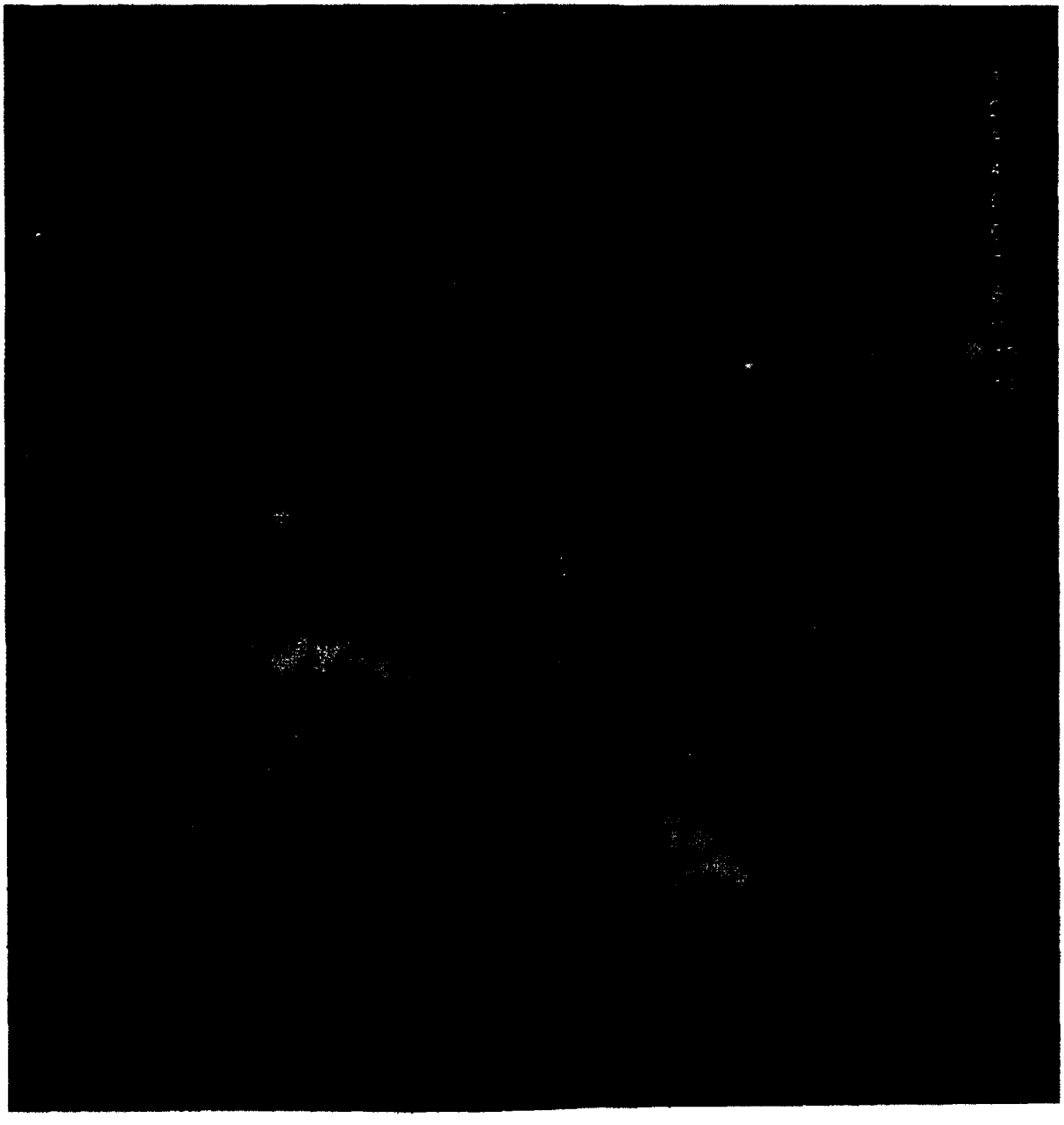

Figure 7-7. Date of onset of persistent deviation from normal of pine forest pixels according to algorithm of Figure 7-6; 6.4 km square area. See Table 6-3 for corresponding dose estimates. No responses occur for the preaccident Dates 1 and 2 or for Date 3 three days postaccident.

impede the migration of radionuclides in the ground. The presence of the ground water barrier apparently affects the pine trees adjacent to the path, especially on the southwest side. The trees show significant deviations from normal extending further from the barrier as time progresses between 1 and 2 years after the accident. These indications of stress are probably not due to radiation damage to the foliage. They may indicate a ground water effect on the health of the root systems of the trees not involving any radiation damage.

7.4 FOLIAGE DOSE MAPS.

Two procedures have been used to construct dose contours from the data on time to first response for pine trees shown in Figure 7-7. The first method uses shape of gamma dose rate contours measured aerographically as guidance for the hand-drawn contours wherever satellite image data is sparse or nonexistent. The second method uses a numerical relaxation technique to generate smoothed contours from the satellite image data alone in an area with sufficient data for analysis.

7.4.1 Dose Map with Hand-Drawn Contours.

Figure 7-8 shows the time-to-response data from the satellite image analysis with three hand-drawn radiation dose contours. Table 7-2 lists the total area enclosed by each contour and the dose range of the area inside each contour.

Table 7-2. Description of contours drawn in Figure 7-8.

Contour	*Time of observed response (image number)*	*Dose within contour (Gy)*	*Cumulative enclosed area (ha)*	*(km^2)*
Inner (blue)	5 and 6	54 to 80[a]	82.	0.8
Middle (green)	7	30 to 54	287.	2.9
ter (yellow)	8, 9 and 10	20 to 30	1450.	14.5

r limit set by the sparsity of response on Date 4.

tours in Figure 7-8 are hand-drawn starting in the westward trace of highest fallout here there is sufficient data from pine forest response to draw the contours as tween areas with different dates of first observed response. The intent is to draw ooth contours along the average boundary between different dates of response. urse, scattered pixels with response dates that do not match the contours. These

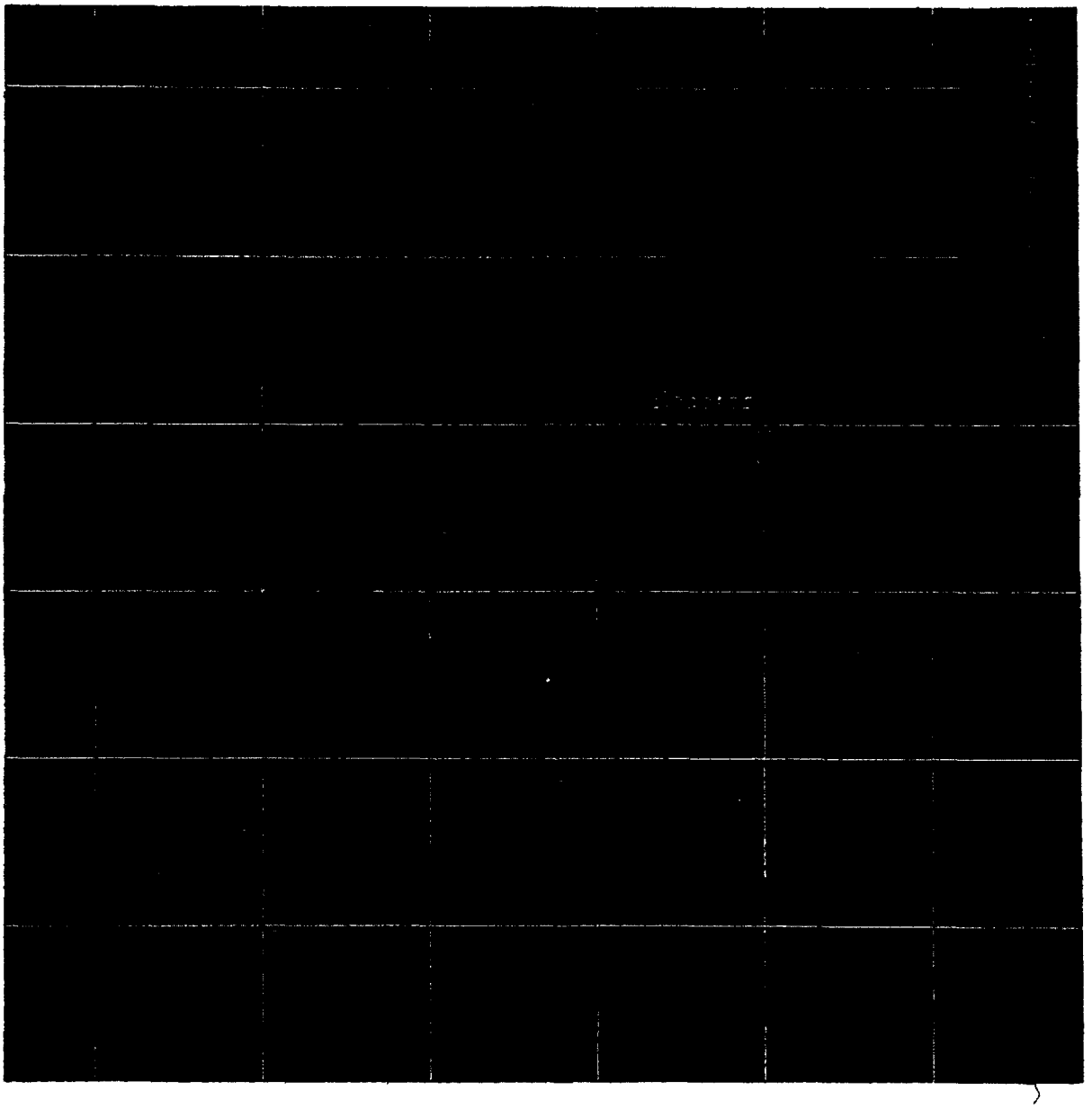

Figure 7-8. Time to first observed response with 1 km grid and three hand-drawn dose contours. See Table 7-2 for dose ranges.

variations presumably are caused by nonuniformity in fallout deposition and by noise in the detection process. The contour segments drawn where there is image data are extended around the reactor where there is no image data following the shape of published gamma dose rate contours measured a year after the reactor explosion (Asmolov et al., 1987). These Soviet-supplied contours are described in Volume 2 of this report (McClellan, 1992). Note the contours in Volume 2 and the outer contour in Figure 7-8 have been extended across the reactor cooling pond to approximate the situation in the absence of the body of water.

Since the contours in Figure 7-8 are derived from observations of pine tree response, they represent an estimate of the dose at any location that would be received by a patch of pine forest at that location. The relationship of this dose to the dose that would be accumulated by some other detector can be estimated from the results of the radiation transport calculations of Appendix A. In particular, Section 8 discusses the relation between the pine tree dose and the gamma dose 1 m above the ground under the canopy.

The extrapolation of the contours around the reactor in Figure 7-8, based on gamma dose rate contours, is uncertain because of the difference between in situ pine forest response and that of the gamma detectors one year after the accident. As discussed in Section 5, the pine forest canopy responds mainly to the dose accumulated during the first few weeks after the reactor explosion with a beta contribution at least as large as the gamma contribution. On the other hand, the curves of Asmolov et al. (1987) show the gamma activity a year after the explosion affected by weathering effects and cleanup activities. Because of this difference, it is of interest to consider a method of generating contours from the pine tree response alone.

7.4.2 Iterative Smoothing of the Dose Map.

Figure 7-9 illustrates an iterative numerical relaxation method for smoothing of the dose map. About 3 km^2 is cut from the area of highest radiation response in Figure 7-8. The upper left panel in Figure 7-9 shows the date of first observed response for this area following the color code of Figure 7-8. Gray pixels indicating forest that is normal on Date 11 are assigned date value 12. The lower right panel shows the result of the relaxation method with date numbers of first observed response used as the numerical value assigned to each pixel.

On each iteration, the response date number for each pixel not containing pine forest is replaced by the average date number (taken as a continuous variable) of its four nearest neighbor pixels. Values for pine forest pixels in the initial data set are held fixed at their initial values to provide boundary conditions for the relaxation solution. Relaxation of values at the border of the cut out area use a neighborhood average excluding pixels outside the border. This choice lets the value at

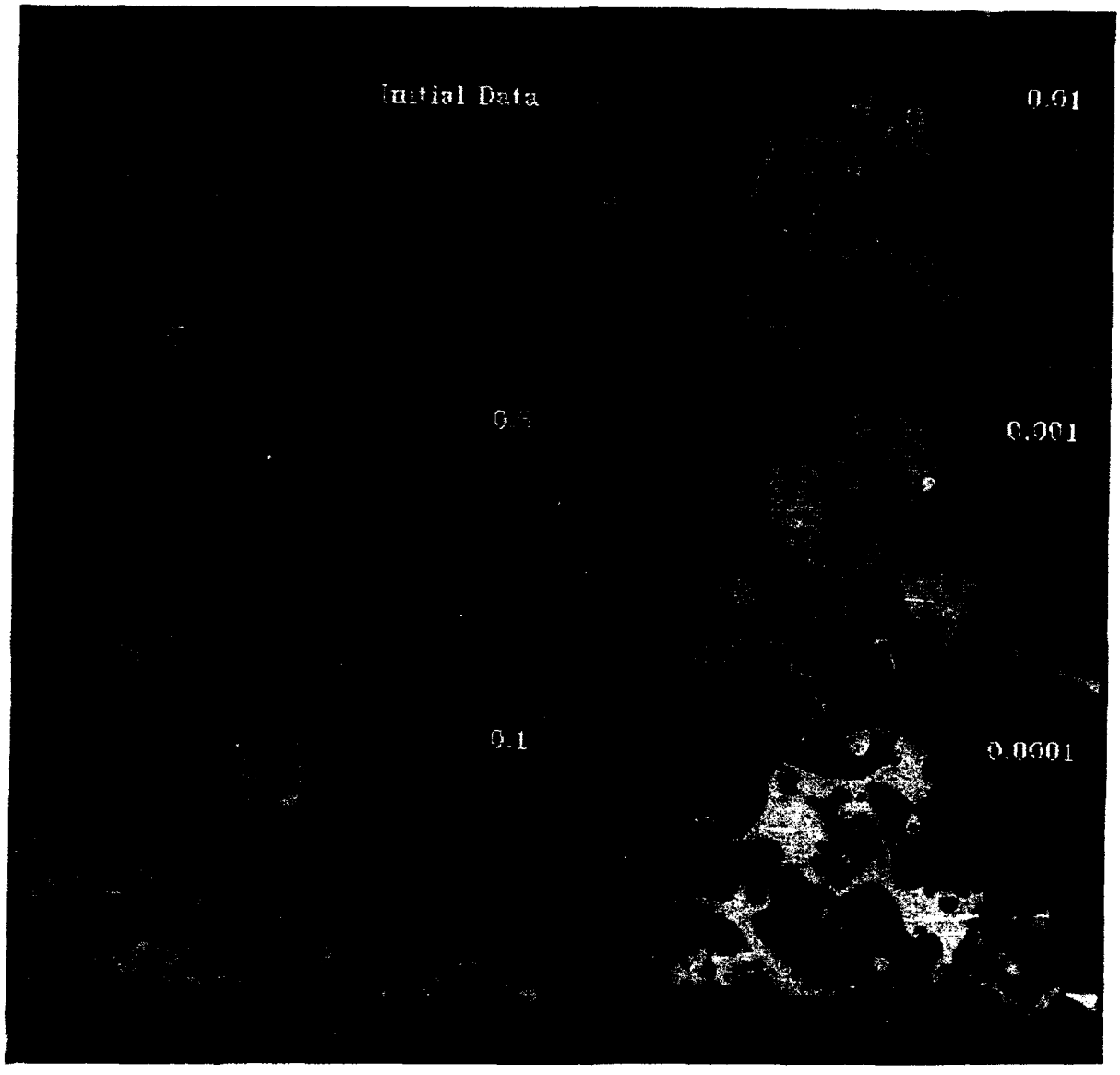

Figure 7-9. Series of intermediate stages leading to a smoothed map of date of first observed response by numerical relaxation as described in the text.

the border float according to the influence of the nearest pine forest pixels in the initial data set without requiring a definite value at the border. Pixels with no value (displayed as black) in the initial data set are initialized with date value zero. Iteration of the map until the value in every pixel changes by less than 0.0001 from the previous iteration gives the lower right panel in Figure 7-9. Stopping the iteration when all changes are below 0.5 and other intermediate values indicated in the figure gives the full series shown in Figure 7-9. For practical purposes, stopping the iteration when changes are less than 0.001 is good enough.

This numerical relaxation technique converges to a solution of Laplace's equation,

$$\nabla^2 n = 0 \tag{7.6}$$

where n is the date of first observed response treated as a continuous variable. In electrostatics, Laplace's equation describes the spatial variation of the electric potential in a region of uniform electrical conductivity. The pixels in the initial data set used as fixed boundary conditions correspond to areas held at a fixed voltage by an external source of electrical potential. There is no physical reason why the radioactivity level in a wind-driven fallout field should satisfy Laplace's equation. The numerical relaxation technique is simply a convenient tool for smoothing the dose map.

Figure 7-9 shows substantial small scale variation caused by isolated pixels in the initial data set. Furthermore, Figure 7-9 gives a map of date of first response rather than dose. Figure 7-10 addresses both of these issues. Based on the success of the relaxation solution in Figure 7-9, Figure 7-10 uses a larger area of data. To reduce small scale variations, isolated pixels in the initial data set are ignored as boundary conditions and allowed to vary in the relaxation calculation. Next, before relaxation, the date numbers in the initial data set are replaced by radiation doses according to Table 6-3. Iteration proceeds until fractional changes in all dose values drop below 0.001, then the pixels are assigned to dose bands and colored according to Table 7-3.

Figure 7-11 displays the smoothed contours from Figure 7-10 with a gray-scale image of the area. Both Figures 7-10 and 7-11 include one kilometer grid lines originating from the site of the Unit 4 reactor. The site of the reactor is chosen as the brightest pixel from the reactor fire visible on 26 April 1986 (Date 3), three days after the explosion. The Zone 36 UTM coordinates of the upper left hand corner of this pixel are X = 298,275 m and Y = 5,697,175 m as determined by the geocoding of our Landsat image data (see Volume 2).

Figure 7-10. Smoothed dose contours from pine foliage response using numerical relaxation of dose values from individual pine forest pixels inside the white border; 1 km grid lines. See Table 7-3 for estimated dose bands.

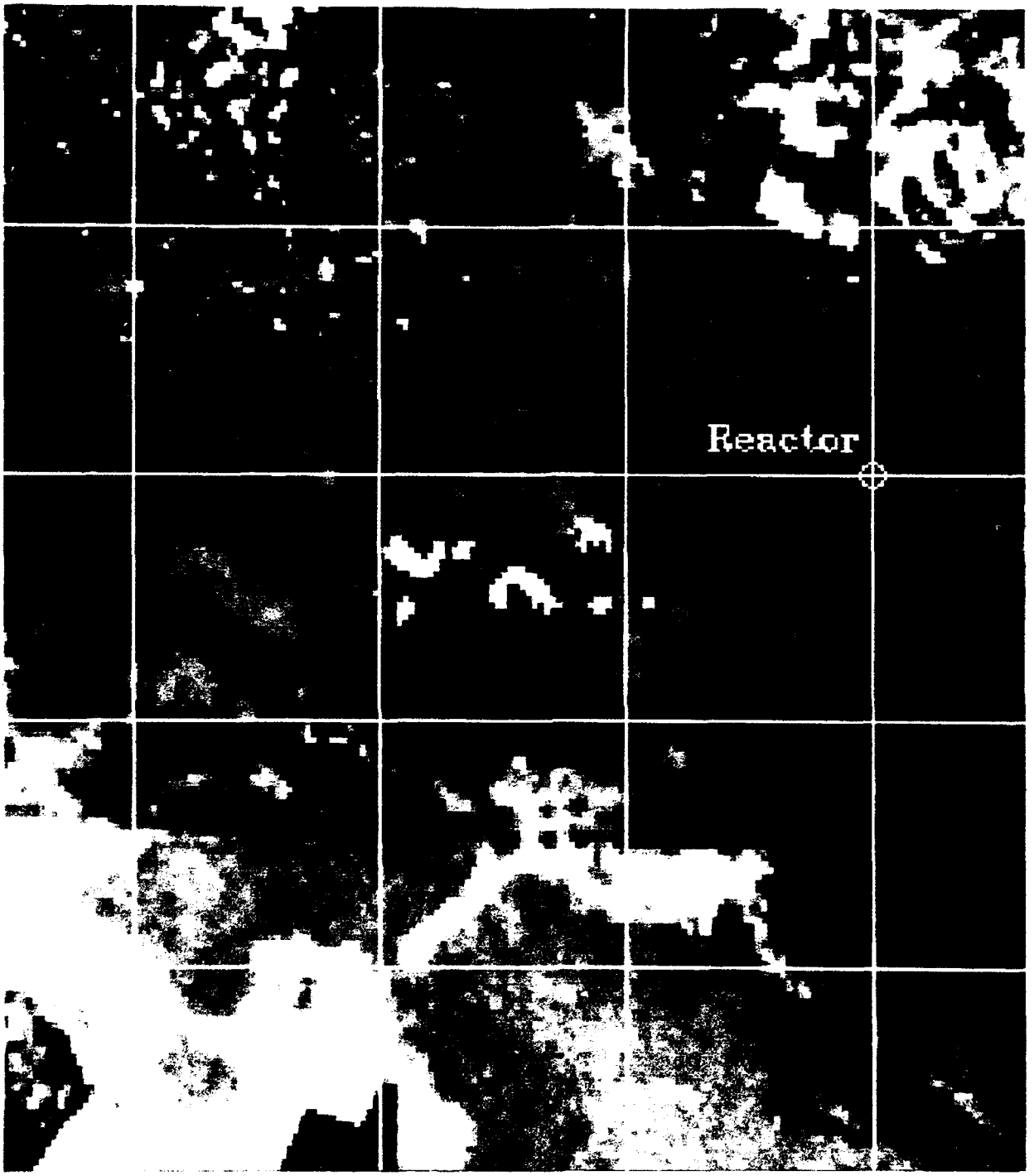

Figure 7-11. Smoothed dose contours from Figure 7-10 displayed with a gray-scale background of the western end of the Chernobyl nuclear power station; 1 km grid lines. See Table 7-3 for estimated dose bands.

Table 7-3. Dose bands and affected areas for the smoothed radiation contour maps of Figures 7-10 and 7-11. Areas are within the relaxation area (white boundary of Figure 7-10) only.

Color	*Dose band (Gy)*	*Band area (ha)*	*Cumulative area (ha)*
Red	> 94	0.1	0.1
Yellow	54 to 94	9.1	9.2
Green	35 to 54	16.8	26.0
Cyan	23 to 35	86.1	112.1
Blue	13 to 23	353.8	465.9

The smoothed contours produced by the relaxation method appear too irregular and sometimes discontinuous in the central area. For example, the yellow areas in Figure 7-11 with a dose range from 54 to 94 Gy originate mainly from the observed responses on Dates 5 and 6. The appearance of this data in Figure 7-8 (within the inner contour), suggests that all of the area between the yellow patches in Figure 7-11 probably received at least as much dose as the yellow patches themselves. However, because of the wide spacing of the three main areas of response on Dates 5 and 6, the relaxation method allows the influence of more distant pixels to lower the interpolated dose between the yellow patches. Although hot spots do occur in fallout fields, the spacing of the yellow patches in Figures 7-10 and 7-11 would not be expected in this situation and is clearly an artifact of the spacing of the patches of pine forest in the initial data set.

Except for the exaggerated irregularities induced by the patchiness of pine forest in the initial data set, the smoothed contours of Figure 7-11 seem reasonable. For example, the western outline of the outer most dose band (blue, 14 -26 Gy) in Figure 7-11 has the same general shape as the outer most, hand-drawn contour (yellow, 20 - 30 Gy) in Figure 7-8.

The relaxation method has the advantage of providing smoothed radiation dose contours without reference to other data and free of human bias. It has the disadvantage that it does not account for the physical transport properties of wind blown fallout patterns and tends to generate dose contours having the same spottiness as the pine forest spatial distribution. With further study, it might be possible to modify the relaxation method to better approximate true fallout patterns.

7.5 SUMMARY.

Both methods presented in Section 7.4 for generating maps with dose contours or bands from the pixel-by-pixel pine tree response data have advantages and disadvantages. Both provide a qualitative description of the likely initial fallout deposition pattern, but both must be used with care if quantitative extrapolations of dose outside the existing areas of pine forest are required. The most reliable results are the actual pixel-by-pixel dose estimates obtained through interpretation of the date of first observed response (Figure 7-7 or 7-8) with the dose and time-to-response relationship from Figure 6-5 or Table 6-3, keeping in mind that response observed on a certain date means that the actual first *observable* response may have occurred any time in the interval bracketed by the date of first observed response and the previous image date. The dose estimate for the pixel lies in the interval defined by the doses for the two dates from Table 6-3. Accordingly, the dose bands in Table 7-3 were obtained using the geometric mean of the dose for the first observed response and the dose for the preceding date.

The following list summarizes findings from this section:

1) Pixel spectral deviations for pine forest canopy relative to the average spectral signature of a pine forest class may be used on a pixel-by-pixel basis to detect foliage radiation response in multispectral imagery (Figures 7-3 and 7-4).

2) Time to first observed response for persistent spectral deviations over an annual cycle may be used to map pine canopy doses (Figure 7-7) near and above the LD_{50}, about 23 Gy for a three week exposure.

3) Mapping of dose responses significantly below the LD_{50} requires interpretation of temporal variation in detectability of spectral deviations caused by the annual growth cycle. It is likely that transient responses may be detected down to 10 or even 5 Gy.

4) Dose estimates at distances of 1 to 2 km downwind of the reactor site and from 30 to 54 Gy at 2 to 3 km downwind (Figure 7-8) from the Landsat multispectral imagery for pine forest canopy along the main westward trace of initial fallout deposition from the Chernobyl reactor explosion range from 54 Gy to 80 Gy . These doses estimates are based on the equivalent gamma dose that produces the same foliage spectral response as the actual mixed beta and gamma doses received by the foliage.

SECTION 8
DISCUSSION

This section discusses the pine forest foliage doses derived from the satellite imagery in relation to data from the former Soviet Union regarding three types of measurements: 1) doses and responses of trees near the Chernobyl nuclear power plant, 2) aerographic and ground surveys of gamma dose rates following the accident, and 3) exposures of accident victims. A final subsection discusses uncertainties in the derivation of foliage doses from the satellite imagery.

8.1 COMPARISON WITH MEASUREMENTS OF FOREST DAMAGE.

The only quantitative exposure and response data we have for trees within a few kilometers of the Chernobyl nuclear power station has been obtained by Gamache (1993) through visits with Ukrainian scientists (Sobdovych et al. 1992). Table 8-1 lists this data, which refers to forest with edge about 1 km from the Unit 4 reactor site. This distance corresponds to the boundary of the nuclear power station on the west side. We are fortunate to have this information although some uncertainty remains regarding the data. For example, it is tempting to assume that the subject forest is west of the reactor site along the main trace of fallout deposition, but there are also forest patches northwest, southwest, and south of the reactor site that are not much more than 1 km away. The forest reportedly consisted of pine trees but Table 8-1 implies an LD_{50} of 49 Gy, above the upper bound in Table 6-1 for pine trees suffering a few week exposure. Figure 6-2 indicates that an effective exposure time of about four months would be required to increase the LD_{50} for pines to 49 Gy; however, our image analysis shows significant response along the main trace after only one month.

Table 8-1. Results of forest damage by radiation for an area with edge about 1 km from the site of the Unit 4 reactor explosion (Sobdovych et al., 1992, courtesy of Gamache, 1993).

Distance from edge of forest (m)	*Calculated absorbed dose (Gy)*	*Tree crown damage (%)*	*Degree of harm*	*Recovery of trees (%)*
0 (Edge of forest nearest reactor)	100	100	Completely dry wood	0
35	65	50	Very strong damage	10 - 15
90	49	20 - 30	Medium	50
350	5	<10	Small	100

In addition, Table 8-1 lacks an indication of the time at which the listed endpoints were observed. Presumably, the percent of crown damage must have been observed well before the percent recovery of trees since 50% lethality of trees would be inconsistent with only 20 - 30 % crown damage if both endpoints were observed at the same time. Also, the nature of the calculated absorbed dose is not known to us. In particular, does it include dose from beta radiation and to what tissue and depth does it correspond?

The precipitous drop reported for the dose 350 m from the edge of the forest also needs explanation. Given that the plume from the initial explosion and fire rose more than a kilometer (Appendix C) and that the forest location is only 1 to 1.5 km from the reactor site, it would be surprising to have such a sharp gradient in dose within 250 to 350 meters along the main trace of initial deposition. Such a drop would be more likely, however, in moving off the trace laterally. Another possibility is that the reported forest is not on the main trace but was contaminated later in the 10 day release sequence by a plume that remained near the ground and was rapidly absorbed as it moved through the forest canopy. In the absence of accurate position information, the data in Table 8-1 cannot be directly compared with the satellite data.

In spite of the unknown factors, it is encouraging that the doses listed in Table 8-1 are of the same order of magnitude as the doses from the analysis of the satellite image data listed in Table 7-2 and 7-3. The attempt at comparison strongly emphasizes the need for well documented ground measurements at specific times and with locational accuracy and resolution comparable to the 25 m spatial resolution of the imagery.

8.2 COMPARISON WITH AEROGRAPHIC SURVEYS OF DOSE RATE.

Following the Chernobyl accident, frequent aerographic and surface measurements were made by the Soviets to determine and monitor the gamma field dose rates surrounding the nuclear reactor station. These measurements provide spatial contours and decay rates of the gamma dose rate within the area of our satellite observations. Utilizing the Soviet data, this subsection calculates integrated gamma ray doses for the three week period following the accident and compares these to the pine forest doses extracted from the satellite image data. The ratio of the pine foliage dose to the gamma dose one meter off the ground is compared to the same ratio derived from the calculations of Appendix A.

8.2.1 1-Meter Gamma Dose Rates for the Close-in Area.

Figure 8-1 shows plots of gamma dose rate versus contaminated area based on measurements referenced to two dates, May 29, 1986 and May 1, 1987. The area on the abscissa is that enclosed by a given isodose-rate contour. Accordingly, dose rates within a given area are larger than that at the contour bounding it. The Soviet dose rate data are given only for close-in areas greater than

about 2 km^2. Therefore, estimates down to 0.8 km^2 are based on extrapolation indicated by the dashed part of the curves in Figure 8-1.

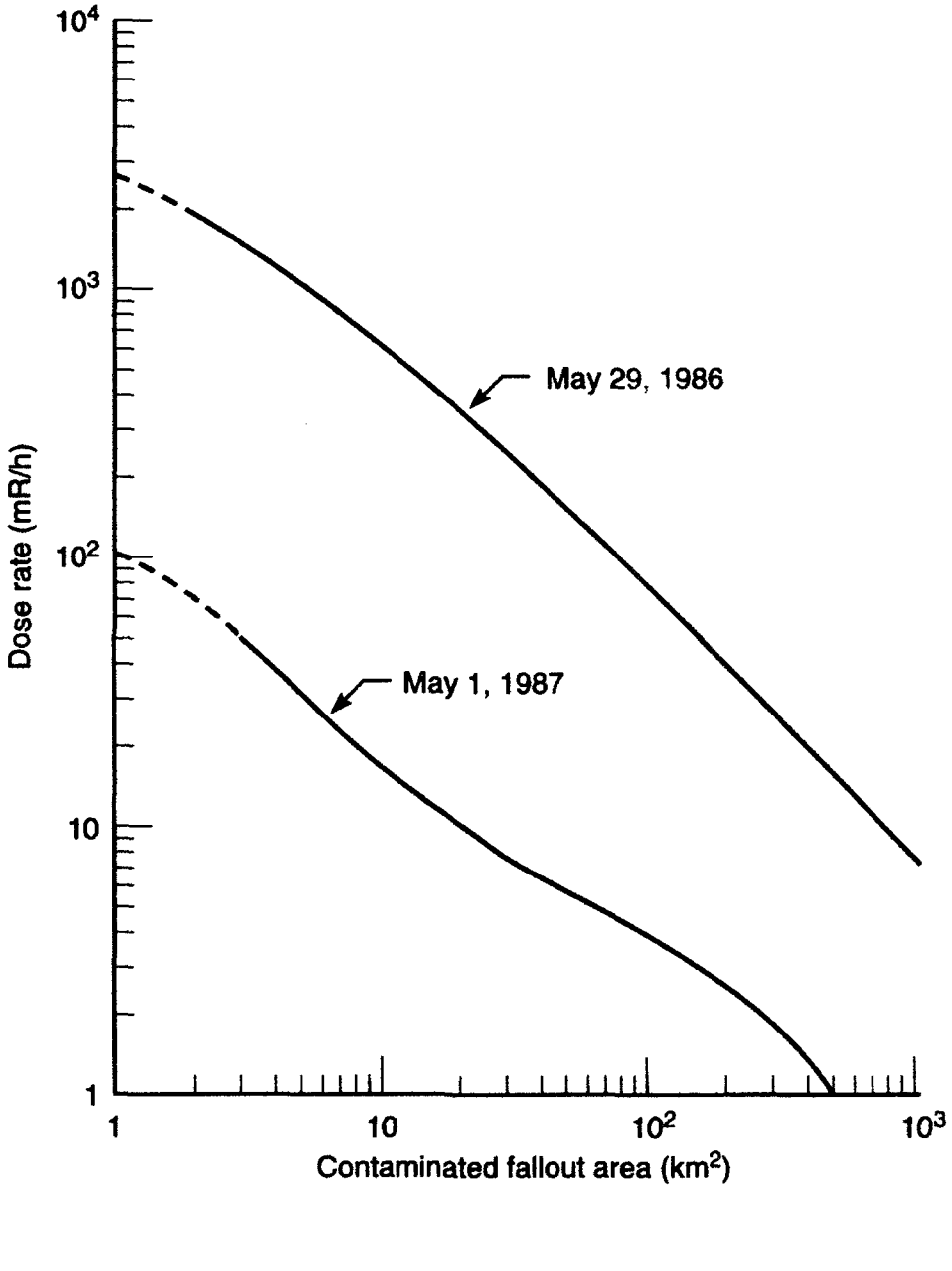

Figure 8-1. Dose rate measurements for close-in fallout contaminated areas for two different dates: May 29, 1986 (Izrael, Petrov and Severov, 1987) and May 1, 1987 (Asmolov et al., 1987).

Table 8-2 provides, in the second and fourth columns, values for selected contour dose rates read from Figure 8-1 for the two reference dates.

Table 8-2. Estimation of initial dose rates for contours enclosing specified areas.

Measurements of:	May 29, 1986[a]		May 1, 1987[b]	
Contaminated area within contour (km^2)	*Contour dose rate (mR/h)*	*Dose rate[c] on 4/26/86 (R/d)*	*Contour dose rate (mR/h)*	*Dose rate[c] on 4/26/86 (R/d)*
14.5	450	68		
4.0	1150	173	38	158
2.9	1450	218		
1.0	2500	376	100	416
0.8	3000	450		

[a]Measurements from Izrael, Petrov and Severov (1987).

[b]Measurements from Asmolov et al. (1987).

[c]Extrapolated back to date of accident according to Figure 8-2.

In order to obtain doses accumulated over the first three weeks after the accident, it is necessary know the time dependence of the dose rate. Figure 8-2 gives a plot of Soviet data for the change with time of the gamma dose rate in the close-in zone due to the decay and weathering of radioactive material. We have approximated the data with a smooth curve by fitting it with an empirical relationship,

$$F(t) = \exp\{-[\ln(1+t)]^2 / a\}, \qquad (8.1)$$

where, a = 6.7784 and postaccident time t is measured in days. Figure 8-2 plots the gamma dose rate in relative units normalized to the day of the accident (t = 0 on April 26, 1986); note that the abscissa is (1 + t). The dose rate values on the day of the accident are estimated with Equation 8.1 and shown in columns 3 and 5 of Table 8-2. The cumulative gamma dose for a postaccident exposure time t is determined for any initial dose rate R_0 by integrating Equation 8.1 over time, i.e.,

$$D(t) = R_0 \int_0^t F(t')dt'. \qquad (8.2)$$

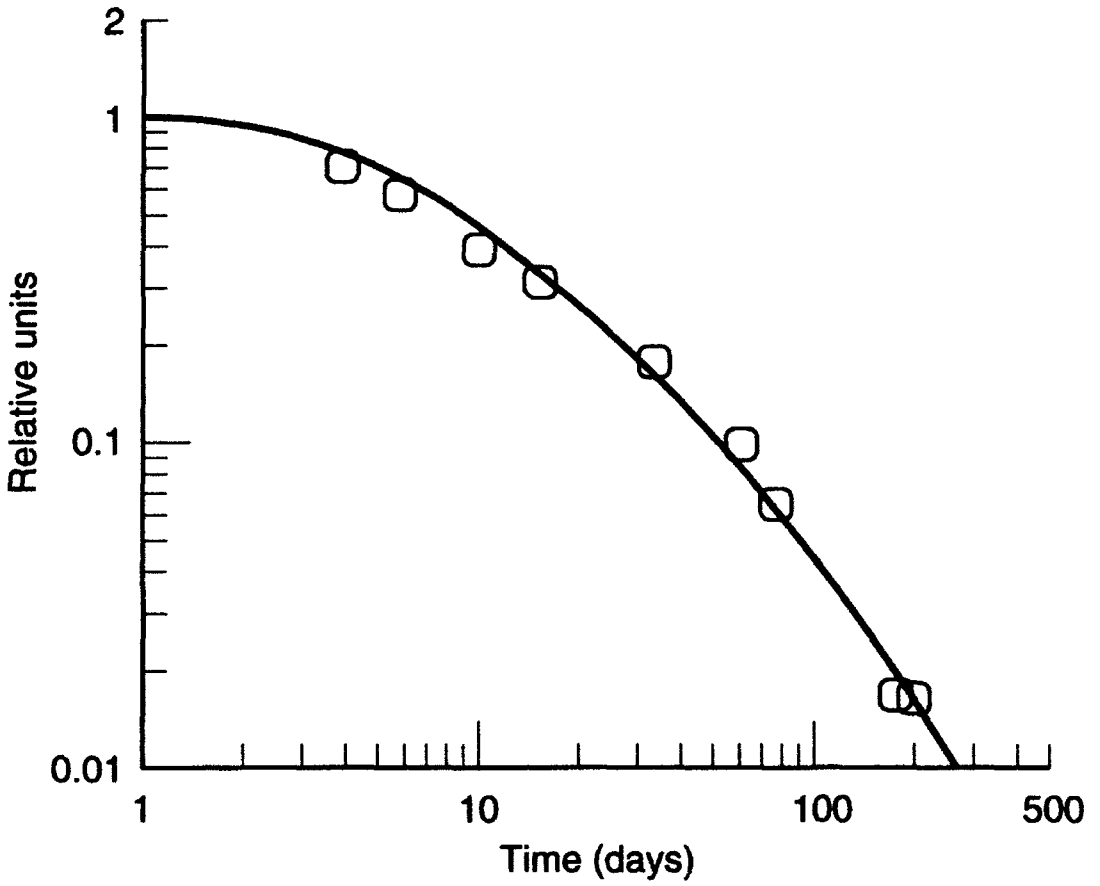

Figure 8-2. Change in gamma dose rate from radioactive materials in the close-in zone as a function of time based on aerographic surveys (data from Asmolov et al., 1987).

Figure 8-3 compares the 1-m gamma dose accumulated at the 1 km^2 and 4 km^2 contours as a function of postaccident time. The a and b curves reflect the Soviet measurements reported on May 1, 1987 and May 29, 1986, respectively. The middle curve, labeled 1 - 4 km^2, of Figure 8-3 plots the geometric mean dose for the 1 and 4 km^2 curves. Both the a and b curve pairs give essentially the same geometric mean value for the area between the 1 and 4 km^2 contours. The a and b curves are in good agreement considering the 11-month time difference of the data. We will use the earlier set for comparison with the satellite data since it is taken closer to the time of important exposure for the pine forest.

8.2.2 Close-in Foliage and 1-Meter Gamma Doses.

The analysis in Section 5 indicates an effective exposure time of about 3 weeks for the pine foliage around Chernobyl. This duration is based on the assumption that fallout initially retained in

the forest canopy makes an important dose contribution, especially the beta component. The effective duration of exposure is determined by the decay of radionuclides and the weathering of fallout particles from the foliage to the ground. Accordingly, radiobotanical data for exposure times of two to four weeks is used to derive radiation doses from the satellite imagery. With this point of view, the pine forest doses extracted from the imagery represent total doses received in about the first 21 days after the initial deposition.

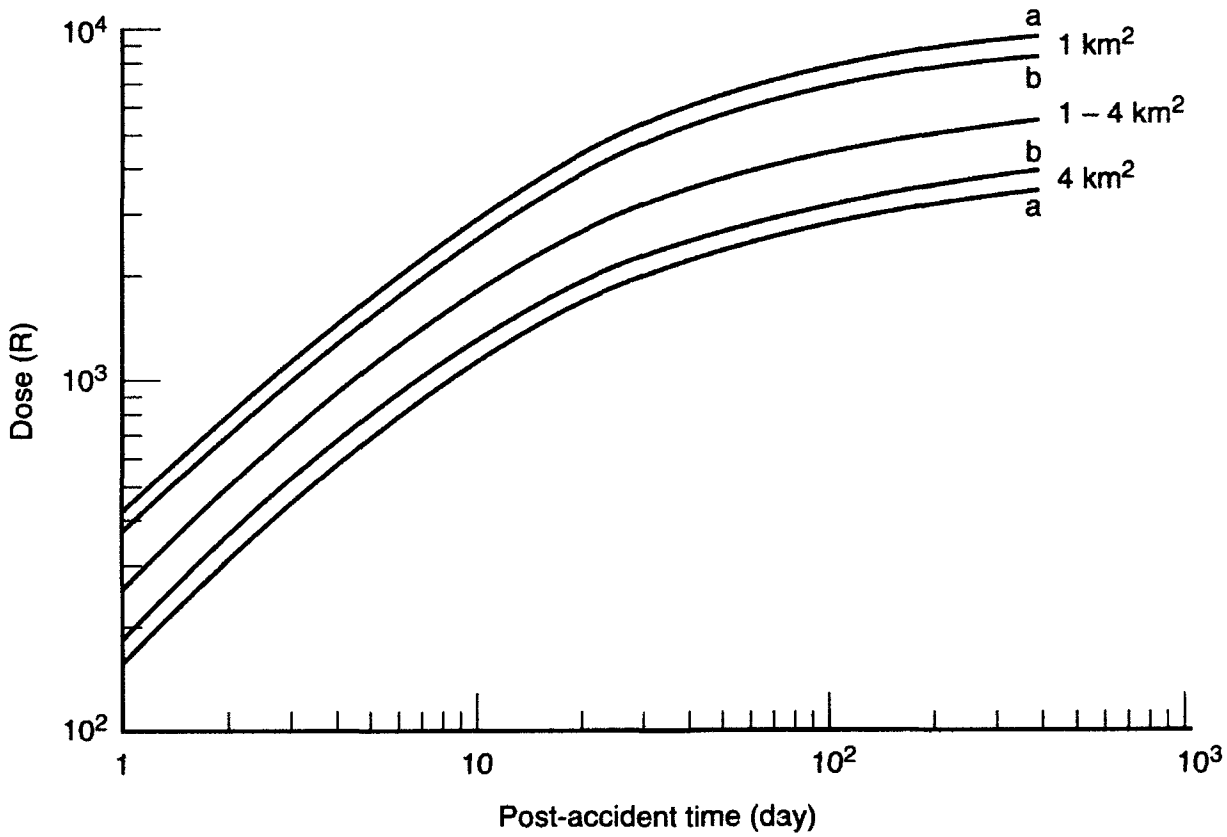

Figure 8-3. Accumulated close in fallout dose (1-m above ground) in 1 and 4 km^2 areas; a and b based on gamma field measurements (USSR, 1987) on 5/1/87 and 5/29/86 respectively; the middle curve is the geometric mean between 1 and 4 km^2.

Table 8-3 lists the pine forest foliage doses represented by the hand-drawn contours of Figure 7-8. For comparison, Table 8-3 lists the accumulated three week gamma dose one meter off the ground according to the survey data of May 29, 1986 (Izrael et al. 1987). These gamma doses are calculated with Equation 8.2 and the initial dose rates listed in Table 8-2. For each of the three

contours, the foliage dose exceeds the 1-m gamma dose. The ratios, also listed in Table 8-3, decrease from 2.9 at the lowest dose to 1.2 at the highest dose.

Table 8-3. The ratio of the pine canopy foliage dose to the gamma dose 1 m off the ground using satellite image and aerographic survey data.

Contour area (km^2)	*Foliage dose at contour (Table 7-2) (Gy)*	*1-m γ-dose (21 days) at contour (Gy)*	*Dose ratio (foliage/1-m γ)*
14.5	20.	6.9	2.9
2.9	30.	22.	1.4
0.8	54.	38.	1.2

8.2.3 Calculated Ratio of Foliage to 1-Meter Gamma Dose.

Section 5.3.2 presents calculations of the expected beta to gamma dose ratio for cylindrical pine foliage elements of various radii using the radiation transport calculations of Appendix A. The same assumptions and transport calculations provide an estimate of the ratio of the accumulated dose to foliage from beta and gamma rays to the accumulated 1-m gamma dose either under the canopy or in an open field. Figure 8-4 shows the resulting dose ratios as a function of accumulation time for foliage elements in the upper canopy. The physical parameters assumed for the canopy are given in Appendix A. We assume that a calculation of the gamma dose in an open field is the best analog for the Soviet survey data.

The dose ratios in Figure 8-4 are based on an assumed initial foliar intercept fraction of 0.60 and a weathering rate of 0.0495 per day as discussed in Section 5.5. Fallout decay rates are neglected. The measured ratios listed in Table 8-3 may be compared with the calculated ratios at 21 days postaccident from Figure 8-4b. The comparison shows that the two higher dose contours have measured dose ratios corresponding to foliage elements of about 0.4 cm in radius. The ratio for the lower dose contour corresponds to a foliage element of 0.10 cm radius.

The measured ratios are similar to the calculated ratios, although the indicated radii of foliage elements are somewhat larger than expected from the morphological discussion in Section 5. The apical meristematic tissue is estimated to be at a depth ranging from 0.01 to 0.12 cm in depth with a typical value of 0.04 cm. It is possible that other sensitive tissues at greater depths may contribute to the radiation response. For example, the new growth extension behind the apical meristem has a radius of about 0.15 cm and may be relatively sensitive to exposure early in the growing season.

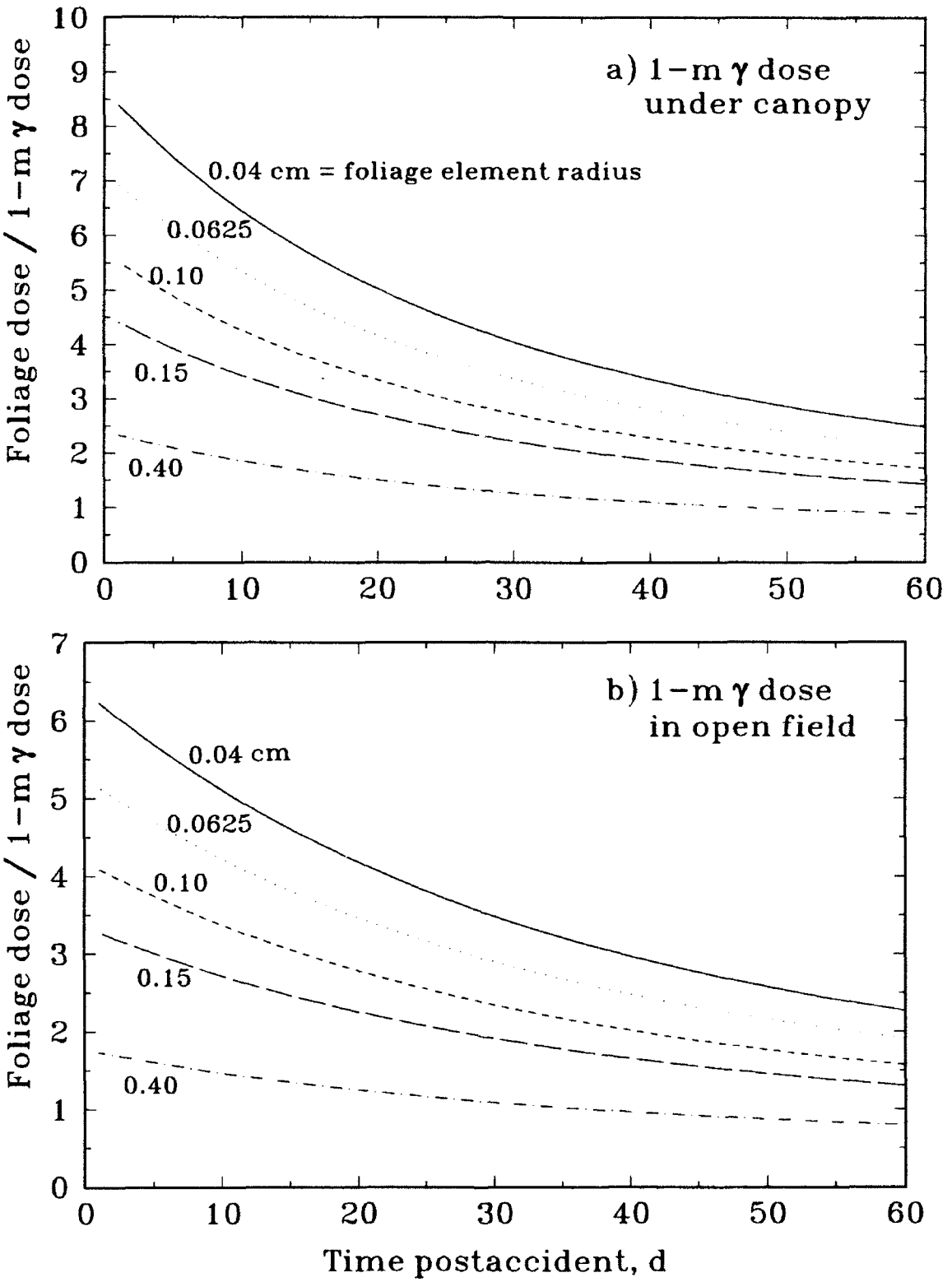

Figure 8-4. Ratio versus time of the accumulated dose (β and γ) at the center of cylindrical foliage elements at the top of pine forest canopy to the accumulated 1-m gamma dose a) under the canopy and b) in an open field for the same total fallout deposition.

It is noteworthy that the trend of the data in Table 8-3 is toward a higher ratio and an implied smaller depth of sensitive tissue for lower doses. This trend supports the conclusion in Section 5 that responses of pine trees to lower doses of radiation are likely to be more sensitive to beta exposure of apical meristems than are the responses at higher doses, which may be dominated by the systemic effects of more penetrating gamma rays.

8.3 COMPARISON WITH HUMAN EXPOSURE DATA.

Skin lesions from β-irradiation were an integral feature of the acute radiation syndrome suffered by the victims of the accident at the Chernobyl nuclear power plant (Barabanova and Osanov, 1990). About half of 115 patients who were exposed in and around the plant had radiation-induced lesions in addition to injury to the hematopoietic system. This significant contribution of β-dose to human injury in a fallout field parallels the importance of the β-dose to vegetation in a fallout field as emphasized in Section 5.

Table 8-4 lists typical β/γ dose ratios for four groups of accident victims at the Chernobyl. The patients are grouped according to mode of exposure as described in the footnotes to Table 8-4. Barabanova and Osanov (1990) describe the variations in occurrence and severity of skin lesions within these groups. The two depths at which dose ratios are presented in Table 8-4 correspond to 0.007 cm and 0.15 cm of unit density material. The smaller depth is essentially at the skin surface with little attenuation of beta dose. At 0.15 cm depth, however, beta dose is substantially attenuated as evidenced by the third column of Table 8-4. Even so, the β/γ dose ratio at 0.15 cm depth is still well above 1, especially when contact sources contribute or when only a few feet of air shields the skin from the beta source.

According to calculations presented in Section 5, the β/γ dose ratio at the center of a cylindrical element of pine foliage with radius 0.15 cm varies from about 5 to about 1 as the ground source fraction increases from 40% to 90% and the contact source fraction decreases correspondingly. This range agrees qualitatively with that in Table 8-4 at 150 mg/cm^2 for the more nearly planar geometry of human skin. Quantitative comparison would require accounting for any differences in assumed radionuclide mix and source distribution and the difference between cylindrical and planar geometry. Cylindrical geometry increases the β/γ ratio relative to the same depth in planar geometry.

The last column of Table 8-4 lists the range of gamma doses for the individuals in each patient group. Generally, these doses cannot be compared to the foliage doses derived from the satellite imagery because the victims were located in or very close to the Unit 4 reactor building rather than near the forests. However, the most severe case in Group II was an individual located 1.0 km downwind from the reactor site for about 1 hour following the reactor explosion. As reported by Barabanova and Osanov, his γ dose was 12.7 Gy and his β dose was about 30 Gy at a depth of

150 mg/cm^2. These doses should be somewhat comparable to those received by any nearby trees over the same exposure period.

Table 8-4. Summary of typical β/γ dose ratios for four groups of people who suffered radiation lesions in the skin at Chernobyl (Barabanova and Osanov, 1990).

Group[a]	*β/γ dose ratio (at 7 mg/cm^2)*	*β-dose attenuation*[b]	*β/γ dose ratio (at 150 mg/cm^2)*	*Range of γ doses (Gy)*
I	3 head (face)	3	1	2 - 5.8
	5 shoulder/chest		2	
	20 feet		7	
II	20 - 30	10	2 - 3	4 - 12.7
III	20	4	5	9 - 14
IV	(>13)[c]	3	(>4)	2 - 11.5

[a]Grouped according to characteristic patterns of irradiation:

Group I. Distant β-exposure (high energy); 15 patients exposed in and around the plant commencing 3 to 5 hours after explosion, little contact dose.

Group II. Deposition of thin source (relatively low energy); 6 patients exposed downwind by plume and by contact with fallout immediately after the explosion.

Group III. Exposure in cloud (fireman); 6 patients exposed on roof of Unit 4 for 30 to 40 minutes, clothing protected somewhat from β-rays.

Group IV. Deposition of thick source (various energies); 29 patients who were plant operators working in Unit 4 at the time of the explosion, wet clothing impregnated with radionuclides, various exposure modes.

[b]Attenuation factor from 7 mg/cm^2 to 150 mg/cm^2 skin tissue depth.

[c]Inferred from Table 1 of Barabanova and Osanov.

The γ dose of 12.7 Gy in about one hour implies a dose rate of about 30,000 R/d. This rate is one hundred times larger than the rates calculated from the aerographic surveys and listed in Table 8-2. If applied to a stationary pine tree for three weeks according to Equation 8.2, this initial dose rate would result in a dose about one hundred times higher than actually observed either from the satellite data or from the aerographic surveys. It seems likely then that the dose received by this individual was dominated by the airborne cloud dose for both beta and gamma rays as the

radioactive plume passed over and around him and not by fallout deposition. Since the cloud dose would affect the forest for only a limited time as well, this assumption avoids inconsistency in the dose calculations for the pine forest. It indicates, however, that the cloud dose may be a substantial contributor to the dose received by the pine forest since the doses received by this individual are as much as 20% or 30% of the doses estimated for the nearby pine forest. Occurring over a shorter exposure time, the cloud dose would also be weighted more strongly than the fallout dose in the induction of biological responses in the foliage.

8.4 UNCERTAINTIES IN THE IMAGE ANALYSIS.

The following uncertainties provide important caveats for the interpretation of the results presented in this report and equally important guides for future research:

1) Detectability of foliage radiation response.

There is little quantitative information available on radiation-induced spectral changes in pine foliage. Our assumptions regarding the detectability from orbit of morphological and biological changes based on visual descriptions in the literature are subject to uncertainty.

2) Seasonal variation of foliage response.

The seasonal variation in the detectability of radiation-induced damage to foliage needs better definition, especially for intermediate doses in the sublethal to mid-lethal range. For these intermediate doses, meristem damage may be obvious during the growing season but not cause observable spectral changes outside the growing season.

3) Relative biological effect (RBE).

Most of the published data for the time dependence of spectral changes of foliage are for gamma rays or mixed exposure to gamma rays and fission neutrons. Fallout involves mixed exposures of gamma and beta rays. Although beta and gamma rays have similar microdosimetry, differences in depth distribution of dose may influence observable spectral changes. Neutron exposure causes ionization tracks at higher average linear energy transfer (LET) than either beta or gamma rays. In mammals, the RBE of neutrons is sometimes unity but may vary upwards or downwards by a factor of two or more depending on the biological endpoint under consideration. We are not aware of published data on RBE for spectral changes in foliage.

4) Radiation transport in foliage.

We have not accounted for the full three dimensional, heterogeneous nature of the fallout deposition and radiation transport problem. This neglect will influence the relative importance of the exposure contribution from beta and gamma exposure.

5) Radionuclide release and fractionation.

Uncertainty in the radionuclide mix released from the reactor and fractionation during transport and deposition contributes to the uncertainty in the beta to gamma dose ratio for the sensitive tissues of the foliage at different distances from the reactor.

6) Cloud dose to the foliage.

We have little information regarding the contribution of the radioactive cloud to direct exposure of the foliage as it drifted over and about the trees within a few kilometers of the reactor.

7) Weathering of the fallout.

Weathering of fallout particles from the foliage to the ground and subsequent migration into the ground are important factors in the time dependence of the beta to gamma dose ratio and the effective exposure time for the foliage.

8) Physiological basis of pine tree response.

Analysis of the spectral response of pine tree foliage to irradiation, especially the time dependence of that response, requires a careful study of the physiology of pines, including the behavior of important radiosensitive tissues and their depth distribution. The change in the sequence of physiological events leading to mortality as the dose is increased above the LD_{50} is of particular importance and needs further elucidation.

9) Influence of decontamination and containment activities.

We know that helicopters sprayed polymers around the reactor site to immobilize fallout particles, but we do not know the timing, or location of such spraying and whether it influenced the satellite spectral observations for pine forest.

SECTION 9
CONCLUSION AND RECOMMENDATIONS

Our analysis of Landsat imagery of the area within a few kilometers of the Chernobyl nuclear reactor station provides maps of radiation dose to pine forest canopy resulting from the accident of April 26, 1986. Detection of the first date of significant, persistent deviation from normal of the spectral reflectance signature of pine foliage produces contours of radiation dose in the 20 to 80 Gy range extending up to 4 km from the site of the reactor explosion.

According to arguments presented in Section 5, the effective duration of the dominant exposure of the pine foliage is about 3 weeks. For this exposure time, the L_{50} of *Pinus sylvestris* (Scotch pine) is about 23 Gy. At this dose level, the onset of persistent deviation from normal for the spectral signature is delayed until about one year after exposure. Around twice the L_{50}, persistent deviation begins as soon as 4 to 5 weeks after the start of exposure. In a limited area, response of pine foliage was observed as soon as 12 days after the start of exposure, corresponding to a dose above 80 Gy.

A patch of forest about 2 km west and 1.5 km north of the Unit 4 reactor site showed a transient deviation from normal during the late growing season of 1986. This deviation is likely the result of a dose in the 7 to 15 Gy range, about 1/3 to 1/2 of the L_{50}. Accounting for such transient deviations, the practical threshold for remote detection of radiation dose to pine foliage with the Landsat Thematic Mapper is probably about 1/4 of the L_{50}.

These conclusions, stated relative to the L_{50}, should remain valid even if the effective exposure time for the pine forest at Chernobyl is found to be different than three weeks and our dose estimates are adjusted accordingly. The threshold of detectability by remote observation of foliage response relative to the L_{50} is likely to apply to other evergreen plant species, as well.

We believe that the results reported here contribute to an improved understanding of the effects of high levels of fallout radioactivity on vegetation and, especially, on the remote observation of radiation-induced foliage response and the extraction of dose estimates from those observations. The results may be used to gain an improved understanding of the radiation exposure consequences to personnel operating in an area contaminated by radioactive fallout and the impact of vegetation on that exposure.

The following recommendations build on the results of the present research:

1) Establish a cooperative effort with scientists of the former Soviet Union to better compare satellite data with ground studies made at specific locations within a few kilometers of the Chernobyl power plant.

2) Reexamine the question of the relative importance of specific pine tree tissues in causing outward manifestations of radiation injury, especially considering variations during the annual cycle.

3) Determine the contribution and impact of the airborne cloud exposure to the total dose received by the pine forest.

4) Perform calculations of the beta and gamma exposures of sensitive tissues in the pine tree using improved geometry and improved data on the appropriate radionuclide mix.

5) Analyze the satellite imagery to account for variations in seasonal observability of sublethal to midlethal damage.

6) Extract characteristic, time-dependent spectral signatures for the pine forest as a function of dose to the foliage as a guide for future observations.

7) Extend the methodology for dose estimation to include exposures during seasons other than spring.

SECTION 10
LITERATURE CITED

Aleksakhin, R.M., F.A. Tikhomirov and N.V. Kulikov, 1970, *Status and Problems of Forest Radioecology*, Soviet J. Ecology, 1:19-27.

Amiro, B.D. and J.R. Dugle, 1985, *Temporal Change in Boreal Forest Tree Canopy Cover Along A Gradient of Gamma Radiation*, Canadian J. Botany, 63:15-20.

Anno, G. H. and A. Laupa, 1989, *Chernobyl Accident Fatalities and Causes*, Technical Report DNA-TR-89-275, Defense Nuclear Agency, Washington, DC, February 1989.

Anonymous, 1962, *Atlas of the Ukrainian SSR and Maldavian SSR*, Central Administration of Geodesy and Cartography, Moscow (In Russian).

Asmolov, V.G., et. al., 1987, *The Accident at the Chernobyl Nuclear Power Plant: One Year After*, International Conference on Nuclear Power Performance and Safety, Vienna, 28 September-2 October 1987, IAEA-CN-48/63, International Atomic Energy Agency, Vienna (Translated from Russian).

Barabanova, A. and D. P. Osanov, 1990, *The Dependence Of Skin Lesions On The Depth-Dose Distribution From Beta-Irradiation Of People In The Chernobyl Nuclear Power Plant Accident*, Int. J. Radiation. Biol., Vol. 57, No. 4, 775-782.

Beck, H.L., 1980, *Exposure Rate Conversion Factors for Radionuclides Deposited on the Ground*, EML-378, Environmental Measurements Laboratory, U.S. Department of Energy. New York, NY.

Beck, H. and G. De Planque, 1968, *The Radiation Field in Air Due to Distributed Gamma-Ray Sources in the Ground*, HASL-195, Environmental Measurements Laboratory, U.S. Department of Energy, New York, NY.

Berg, L.S. 1950, *Natural Regions of the USSR* (O.A. Titelbaum, Translator), MacMillan Co., New York.

Biatobok, S. and W. Zelawski (eds.), 1976, *Outline of the Physiology of Scots (Scotch) Pine*, Foreign Scientific Publications, Department of the National Center for Scientific, Technical and Economic Information, Warsaw.

Borisov, A.A., 1965, *Climates of the USSR* (R. A. Ledward, translator), Aldine Publishing Co., Chicago, 225pp

Bohlen, C., 1987, *Chernobyl's Slow Recovery*, Washington Post, July 21, 1987:A1, A25.

Bostrack, J.M. and A.H. Sparrow, 1969, *Effects of Chronic Gamma Irradiation on the Anatomy of Vegetative Tissues of Pinus Rigida Mill*, Radiation Botany 9:367-374.

Bostrack, J.M. and A.H. Sparrow, 1970, *The Radiosensitivity of Gymnosperms, II, One the Nature of Radiation Injury and Cause of Death of Pinus Rigida and P. Strobus after Chronic Gamma Irradiation*, Radiation Botany 10:131-143.

Broido, A. and J.D. Teresi, 1961, *Analysis of the Hazards Associated with the Radioactive Fallout Material, I, Estimation of λ- and β-doses, Health Physics 5:63-69.*

Chamberlain, A.C., 1970, *Interception and Retention of Radioactive Aerosols by Vegetation*, Atmos. Env. 4:57-78.

Crist, E. P. and R. C. Cicone, 1984, *A Physically-Based Transformation of Thematic Mapper Data -- The TM Tasseled Cap*, IEEE Transactions on Geoscience and Remote Sensing, Vol. GE-22, No. 3, May 1984.

Crist, E. P., R. Laurin, and R. C. Cicone, 1986, *Vegetation and Soils Information Contained in Transformed Thematic Mapper Data*, Proceedings of IGARSS 1986 Symposium, Zurich, 8-11 September 1986, pp. 1465-1470.

DOE, 1987, *Health and Environmental Consequences of the Chernobyl Nuclear Power Plant Accident*, DOE/ER-0332, UC-41 and 48, National Technical Information Service, Springfield, VA 22161.

Dewdney, J.C., 1982, USSR in Maps, Holmes & Meier Publishers, Inc., New York.

Donini, B., 1967, *Effects of Chronic Gamma-Irradiation on Pinus Pinea and Pinus Halepensis*, Radiation Botany, 7:183-192.

Duda, R. O., and Hart, P. E., 1973, *Pattern Classification and Scene Analysis*, John Wiley & Sons.

Fridland, V.M., 1976, Patterns of Soil Cover, Israel Program for Scientific Translation, Jerusalem, 291 pp.

Fullard, H., 1972, Soviet Union in Maps, George Philip & Son Ltd., London.

Gamache, G., 1993, Private communication. Report in preparation for the Defense Nuclear Agency.

Golovina, L. P., M. N. Lysenko and T. I. Kisel., 1980, *Content and Distribution of Zinc in the Soil of the Ukrainian Poles'ye*, Soviet Soil Science 12(1):73-80

Hoffman, F.O. and C.F. Baes, III, 1979, *A Statistical Analysis of Selected Parameters for Predicting Food Chain Transport and Internal Dose of Radionuclides*, NUREG/CR-1004/ORNL/NUREGHM-282, Oak Ridge National Laboratory, Oak Ridge, TN 37830.

International Advisory Committee, 1991, *The International Chernobyl Project: An Overview*, International Atomic Energy Agency, Vienna.

Izrael, Y.A., V.N. Petrov and D.A. Severov, 1987, *Modeling Radioactive Fallout Near the Chernobyl Nuclear Power Plant Accident*, Meteorologiya i Gidrologiya 7:5-12.

IZVESTIYA, 1989, *Confession of a Veteran of Chernobyl. Written From a Hospital Bed*, 18001257 Moscow IZVESTIYA in Russian, 19 June 1989, Morning Edition, page 4. Reprinted in English in National Affairs, *Suffering From Chernobyl-Related Illness Continues*, FBIS-SOV-89-124, 29 June 1989, page 77-79.

Kantz, A.D., 1971, *Measurement of Beta Dose to Vegetation From Close-in Fallout*, pp. 56-70, In D.W. Benson and A.H. Sparrow (eds.), *Survival of Food Crops and Livestock in the Event of Nuclear War*, CONF-700909, National Technical Information Service, Springfield, VA.

Karaban, R.T., N.N. Mishenkov, B.S. Prister, R.M. Aleksakhin, F.N. Tikhomirov, G.N. Romanov, and M.A. Naryshkin, 1978, *Radiation Effects on Arboreal Plants During the First Year After Acute Gamma-Irradiation of a Forest*, Lesovedenii, 1:39-44.

Keller, B. A., 1927, *Distribution of Vegetation on the Plains of European Russia*, Journal of Ecology 15:189-233.

Kendrew, M. A., 1942, *The Climates of the Continents*, Oxford University Press, New York, 473 pp.

Klechkovskii, V.M., G.G. Polikarpov, and R.M. Aleksakhin, 1973, *Radioecology* (Translated from Russian by H. Kaner and H. Mills; translation edited by D. Greenberg, Israel Program for Scientific Translations, London), John Wiley and Sons, NY.

Krupskiy, N. K., V. P. Kuz'michev, and R. G. Derevyanko., 1970, *Humus Content in Ukrainian Soils*, Soviet Soil Science 2:278-288.

Lange, R., M.H. Dickerson and P.H. Gudiksen, 1987, *Dose Estimates from the Chernobyl Accident*, UCRL-96934 (preprint), Lawrence Livermore National Laboratory, Livermore, CA 94550.

Lysenko, M. N. and L. P. Golovina., 1982, *Boron Content and Distribution in the Soils of the Ukrainian Poles'ye*, Soviet Soil Science 14(1):89-97.

Mackin, J., S. Brown and W. Lane, 1971, *Measurement and Computational Techniques in Beta Dosimetry*, pp. 51-55. In D.W. Benson and A.H. Sparrow (eds.), *Survival of Food Crops and Livestock in the Event of Nuclear War*. CONF-700909. National Technical Information Service, Springfield, VA.

McClellan et al., 1992, *Chernobyl Doses: Volume 2 -- Conifer Stress Near Chernobyl Derived from Landsat Imagery*, Technical Report DNA-TR-92-37-V2, Defense Nuclear Agency, Washington, DC, December 1992.

McCormick, J.F., 1967, *Effects of Ionizing Radiation on a Pine Forest*, pp. 78-87. In D.J. Nelson and F.C. Evans, (eds.), *Symposium of Radioecology*, CONF-670503, U.S. Atomic Energy Comm., Div. Tech. Inform. Ext., Oak Ridge, TN.

Miller, G. L., 1968, *The Influence of Season on the Radiation Sensitivity of an Old Field Community*, Ph.D. Thesis, University of North Carolina, Chapel Hill, NC.

Monk, C.D., 1966, *Effects of Short-Term Gamma Irradiation on an Old Field*, Radiation Botany 6:329-335.

NEA, 1987, *The Radiological Impact of the Chernobyl Accident in OECD Countries*, Nuclear Energy Agency, Organisation for Economic Co-Operation and Development, Paris Cedex, France.

Oleynik, V. S., 1981, *Genetic Characteristics of Peat Soils in the Ukrainian Western Poles'ye*, Soviet Soil Science 13(4):32-37.

Osanov, D.P., J.J. Tissen, and G.B. Radzievsky, 1969, *Dose Distribution of β Radiation of Fission Products in the Tissue-Equivalent Material*, Health Physics 17:489-495.

Painter. E.L., F.W. Whicker, 1993, *Chernobyl Doses: Habitat and Vegetation Near the Chernobyl Nuclear Reactor Station*, Vol. 3, Defense Nuclear Agency, DNA-TR-92-37-V3.

Pedigo, R.A., 1963, *Effects of Ionizing Radiation on Pinus Taeda L*, pp. 295-299. In V. Schultz and A.W. Klement, Jr., (eds.), Radioecology, Van Nostrand-Reinhold, Princeton, NJ.

Platt, R.B., 1963, *Ionizing Radiation and Homeostasis of Ecosystems*, pp. 39-60. In G.M. Woodwell (ed.), *Ecological Effects of Nuclear War*, BNL-917 (C-43), Brookhaven national Laboratory, Upton, NY.

Public Health Service, 1960, *Radiological Health Handbook*, Division of Radiological Health, Public Health Service, U.S. Dept. of Health, Education, and Welfare, Washington, DC.

Rhoads, W.A., R.B. Platt, R.A. Harvey, and E.M. Romney, 1969, *Ecological and Environmental Effects from Local Fallout from Cabriolet, I, Radiation Doses and Short-Term Effects on the Vegetation from close-in Fallout*, USAEC Rept, PNE-956, EG&G, Inc., Goleta, CA.

Rodin, L.E., N.I. Bazilevich, and N.N. Rozov, 1975, *Productivity of the World's Main Ecosystems*, pp. 13-26. In *Productivity of World Ecosystems*, National Academy of Sciences, Washington, DC.

Sanbur, G. N. and I. I. Kovalenko., 1969, *Improvement and Rational Utilization of Lowland Saline Soils of the Southern Poles'ye and Northern Forest-Steppe of the Ukrainian SSR*, Soviet Soil Science 1:1401-1408.

Sheppard, M.I., D.H. Thibault, and J.E. Guthre, 1982, *Radiosensitivity and the Role of Pinus Sylvestris L. In the Revegetation of Radioactive Disposal Areas*, Environmental and Experimental Botany 22(2):193-198.

Sobdovych, E. V., V.P. Dudkin, S.N. Kireyev, N.N. Kaletnik, I.N. Los, V.V. Gudzenko, D.A. Bobyleva, and L.Y. Tabachny, 1992, *Chernobyl Catastrophe: Reasons and Consequences for Kiev, Minsk, and Moscow*. Ukrainian Academy of Sciences: Kiev.

Sparrow, A.H., A.F. Rogers, and S.S. Schwemmer, 1968, *Radiosensitivity Studies with Woody Plants - I. Acute Gamma Irradiation Survival for 28 Species and Predictions for 190 species*, Radiation Botany 8:149-186.

Sparrow, A.H., S.S. Schwemmer, and P.J. Bottino, 1971, *The Effects of External Gamma Radiation from Radioactive Fallout on Plants with Special Reference to Crop Production*, Radiation Botany 11:85-118.

Sukachev, V. N., 1928, *Principles of Classification of the Spruce Communities of European Russia*, Journal of Ecology, 16:1-18.

Symons, L., 1972, *Russian Agriculture: A Geographic Survey*, John Wiley and Sons, New York, 348 pp.

Szafer, W., 1966, *The Vegetation of Poland*, Pergamon Press, Oxford, 728 pp.

Takhtajan, A., 1986, *Floristic Regions of the World*, (T. J. Crovello, translator), University of California Press, Berkeley.

Tou, J. T. and R, C. Gonzalez, 1974, *Pattern Recognition Principles*, Addison-Wesley Publishing Company, Reading, Massachusetts, 1974

Ursino, D.J., A. Moss, and J. Stimac, 1974, *Changes in the Rates of Apparent Photosynthesis in 21% and 1% Oxygen and of Dark Respiration Following a Single Exposure of Three-year-old Pinus Strobus L. Plants to Gamma Radiation*, Radiation Botany 14:117-125.

USSR, 1986, *USSR State Committee on the Utilization of Atomic Energy: The Accident at the Chernobyl Nuclear Power Plant and its Consequences*, Information compiled for the IAEA experts' meeting, 25-29 August 1986, Vienna.

USSR, 1987, *The Accident at the Chernobyl Nuclear Power Plant: One Year After*, International Conference on Nuclear Power Performance and Safety, Vienna, Austria, 28 September-2 October 1987, IAEA-CN-48/63, International Atomic Energy Agency, Vienna.

Walter, H., 1978, *Vegetation of the Earth and Ecological Systems of the Geobiospher*, (J. Wieser, translator), Springer-Verlag, New York.

Whicker, F.W. and L. Fraley, Jr., 1974, *Effects of Ionizing Radiation on Terrestrial Plant Communities*, pp. 317-366. In *Advances in Radiation Biology*, Vol. 4, Academic Press, Inc.

Whicker, F.W. and T.B. Kirchner, 1987, *PATHWAY: A Dynamic Food Chain Model to Predict Radionuclide Ingestion After Fallout Deposition*, Health Physics 52(6):717-737.

Wolfe, W. L. and G. J. Zissis, eds., 1978, *The Infrared Handbook* (Environmental Research Institute of Michigan), p. 3-140.

Woodwell, G.M. and A.L. Rebuck, 1967, *Effects of Chronic Gamma Radiation on the Structure and Diversity of an Oak-Pine Forest*, Ecological Monographs, 37:53-69.

Woodwell, G.M. and A.H. Sparrow, 1963, *Effects of Ionizing Radiation on Ecological Systems*, pp. 20-38. In G.M. Woodwell (ed.), *Ecological Effects of Nuclear War*, BNL-917 (C-43). Brookhaven National Laboratory, Upton, NY.

Wulff, E. V., 1943, *An Introduction to Historical Plant Geography*, (E. Brissenden, translator), Chronica Botanica Co., Walham, Massachusetts, 223 pp.

Young, R. W., 1988, *Chernobyl in Retrospect*, in Pharmac. Ther. Vol. 00, Eds. J. F. Weiss and M. G. Simic, Pergamon Press, Great Britain , 1988

APPENDIX A

FALLOUT DOSE CALCULATIONS FOR PINE FOREST CANOPY

This appendix describes fallout beta and gamma radiation dose calculations in pine forest canopy for three dose points located 1, 7, and 12 meters above the ground, as indicated in Figure A-1. The 1-meter dose point is in air; the 7-meter point is in the middle of the canopy; and the 12-meter point is at the top of the canopy. Although we refer to dose calculations, the results are given in terms of dose rate, in cGy/h per unit source intensity.

Fallout radiation sources are assumed to be homogeneously distributed both in the canopy mass (leaves and twigs) and on a flat surface of the ground below. An homogenized canopy mass density of 0.0054 gm/cm^3 for medium density pine forest in mid-European latitudes, based on Kerr et al. (1971), is assumed to be of infinite extent laterally and finite vertically as indicated in Figure A-1. The dose calculations are all given in terms of the dose rate cGy/h per unit area or volume intensity, depending upon

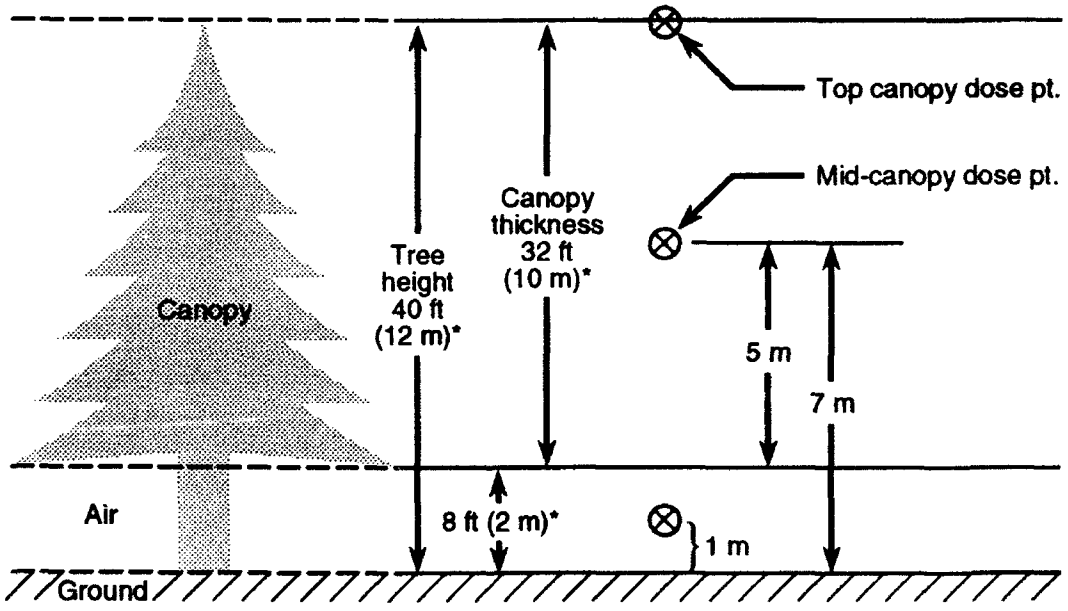

Figure A-1. Pine forest canopy model for dose calculations based on Kerr et al., 1971. Dose points are 1, 7, and 12 meters ground surface.

whether the fallout source is distributed over a surface (such as the ground) or within a space (such as the canopy), respectively.

The beta particle dose calculations are not explicitly performed for each beta decay spectral component, but rather are based on the mean and maximum beta energies according to a semiempirical beta dose relationship (discussed later in this Appendix). Accordingly, the convention we utilize to designate the unit source intensity for beta particles is β/cm^2-sec or β/cm^3-sec for radionuclide decay where "β" effectively represents all the beta decay spectra components from the excited radionuclide states.

For the gamma dose calculations, the explicit gamma ray energies and corresponding fractional yields associated with radionuclide decay are utilized. Accordingly, the convention we utilize to designate the unit source intensity for gamma rays is γ/cm^2-sec or γ/cm^3-sec where "γ" represents the frequency weighted effective gamma ray decay components.

GAMMA DOSES.

Gamma dose calculations for foliage (pine needles or budding meristems) at the canopy dose points indicated in Figure A-1 are done in three parts. The ground fallout source is treated as one part and the fallout retained in the canopy is divided into two parts, that due to fallout in direct contact with (deposited on) the foliage element whose dose is being calculated and that due to fallout deposited on the rest of the canopy. Parameters for the gamma dose calculations are listed by gamma energy in Table A-1. Calculations were first performed for each gamma energy and then the specific radionuclide source parameters listed in Table A-2 were applied to calculate the dose for the radionuclide source mix in Table A-2 based on weighting by the individual released source strength, Q(MCi).

The doses determined for each gamma energy in Table A-1 provide enough data to easily interpolate to find dose values for the radionuclide disintegration energies in Table A-2. Accordingly, if $R_{ij}(x)$ represents the gamma dose rate component for the i^{th} energy of the j^{th} radionuclide, the total dose rate at a dose point position x is

$$\dot{D}_\gamma(x) = \sum_j f_j \sum_i R_{ij}(x) Y_{ij} \qquad (A.1)$$

where, $f_j = Q_j / \sum_j Q_j$ and Y_{ij} is disintegration yield in Table A-2.

The gamma dose is determined by integrating a point source dose function G(r) over a surface or volume source region, $\Re$,

Table A-1. Parameters[1] for gamma dose calculations.

Gamma Energy E(MeV)	Canopy Fallout and Ground Source[2]				Ground Source Fallout/1 Meter Dose Point[3]			
	μ (cm^{-1})[4]	μ_{en}/ρ(cm^2/g)	a[5]	b[5]	μ/ρ(cm^{-1})	μ_{en}/ρ(cm^2/g)	a[5]	b[5]
0.1	8.91×10^{-4}	0.0280	5.71	0.121	0.1480	0.0227	5.93	0.113
0.15	7.99×10^{-4}	0.0274	4.71	0.125	0.1330	0.0247	4.70	0.121
0.2	7.29×10^{-4}	0.0295	4.11	0.117	0.1220	0.0265	3.94	0.113
0.3	6.37×10^{-4}	0.0319	3.13	0.096	0.1060	0.0287	3.10	0.094
0.4	5.72×10^{-4}	0.0328	2.63	0.080	0.0950	0.0294	2.61	0.079
0.5	5.22×10^{-4}	0.0331	2.30	0.068	0.0868	0.0298	2.29	0.067
0.6	4.83×10^{-4}	0.0328	2.07	0.058	0.0803	0.0295	2.05	0.058
0.8	4.24×10^{-4}	0.0319	1.73	0.045	0.0705	0.0287	1.71	0.045
1.0	3.82×10^{-4}	0.0310	1.51	0.035	0.0636	0.0278	1.50	0.035
1.5	3.10×10^{-4}	0.0283	1.17	0.021	0.0576	0.0254	1.16	0.021
2.0	2.66×10^{-4}	0.0260	0.98	0.013	0.0442	0.0234	0.97	0.013
3.0	2.14×10^{-4}	0.0227	0.76	0.004	0.0357	0.0205	0.75	0.005

[1]From Chilton, Shultis, and Faw (1984), *Principles of Radiation shielding.*
[2]Based on water.
[3]Based on dry air
[4]Homogenized canopy density, $\rho_C = 0.0054$ (g/cm^3).
[5]Parameters for Berger dose buildup factor.

Table A-2. Fallout radionuclides: Gamma-ray source disintegration energies E (MeV) and yields, Y.[1]

Radionuclides	Q (MCi)[2]	E	Y	E	Y	E	Y	E	Y	E	Y	E	Y
I-131	7.3	0.284	0.0606	0.364	0.8120	0.637	0.0730	0.722	0.0180				
Te-132	1.3	0.228	0.8820	0.144	0.0379								
Cs-134	0.5	0.605	0.9700	0.790	0.8700	0.569	0.1320	0.563	0.0853	0.802	0.0787	1.300	0.0548
Cs-137 + Ba-137	1.0	0.662	0.9000										
Mo-99 + Tc- 99m	3.0	0.141	0.9000	0.740	0.1380	0.181	0.0620	0.778	0.0480	0.366	0.0146		
Zr- 95 + Nb- 95m	3.8	0.757	0.5430	0.724	0.4350								
Ru-103 + Rh-103m	3.2	0.497	0.8900	0.610	0.0560								
Ru-106 + Rh-106	1.6	0.512	0.2100	0.622	0.0994	1.050	0.0148	0.745	0.0111				
Ba-140 + La-140	4.3	0.537	0.2380	0.163	0.0620	0.305	0.0450	0.424	0.0320	0.438	0.0210	0.563	0.0247
		1.600	0.9560	0.487	0.4500	0.816	0.2310	0.329	0.2100	0.871	0.1994	2.490	0.0416
Ce-141	2.8	0.145	0.4840										
Ce-144 + Pr-144	2.4	0.134	0.1100	0.696	0.0150	2.000	0.0103						
Np-239	1.2	0.326	0.0362	0.227	0.1140	0.200	0.0335	0.278	0.1400				
I-133	15.9	0.530	0.9000	0.875	0.0500	1.298	0.0233						
Sr- 89	2.2	0.	0.										
Sr- 90 + Y- 90	0.2	0.	0.										

[1]From NCRP Report No. 58 (1978), *A Handbook of Radioactivity Measurements Procedures*; Chilton, Shultis and Faw (1984), "Principles of Radiation Shielding."

[2]Estimated release of radioactivity from the Chernobyl reactor accident. (See Sections 4 and 5.5.)

$$\dot{D}_\gamma = KE_\gamma(\mu_{en}/\rho)S\int_{\Re} G(r)d\Re \quad .$$

where, E_γ is the gamma energy in MeV, (μ_{en}/ρ) is the energy absorption coefficient in cm^2/gm, S=1, is the unit gamma source strength per unit area or volume, and K is a dose conversion constant,

$$K = \frac{1.6\times10^{-6}\left(\frac{ergs}{MeV}\right)\times 3600\left(\frac{sec}{h}\right)}{100\left(\frac{ergs}{gm-cGy}\right)} = 5.76\times10^{-5}\left(\frac{gm-cGy-sec}{MeV-h}\right)$$

Then an energy dependent dose constant, $P_\gamma(E)$, is

$$P_\gamma(E) = 5.76\times10^{-5}E_\gamma(\mu_{en}/\rho) \quad ,$$

and the dose rate, $\dot{D}_\gamma$, will have units of $(cGy/h)/(\gamma/sec\text{-}cm^2$ or $cm^3)$.

Canopy Fallout Volume Source/12- and 7-Meter Dose Point. The calculational geometry for the canopy fallout source and dose point at the top of the canopy is shown below in Figure A-2.

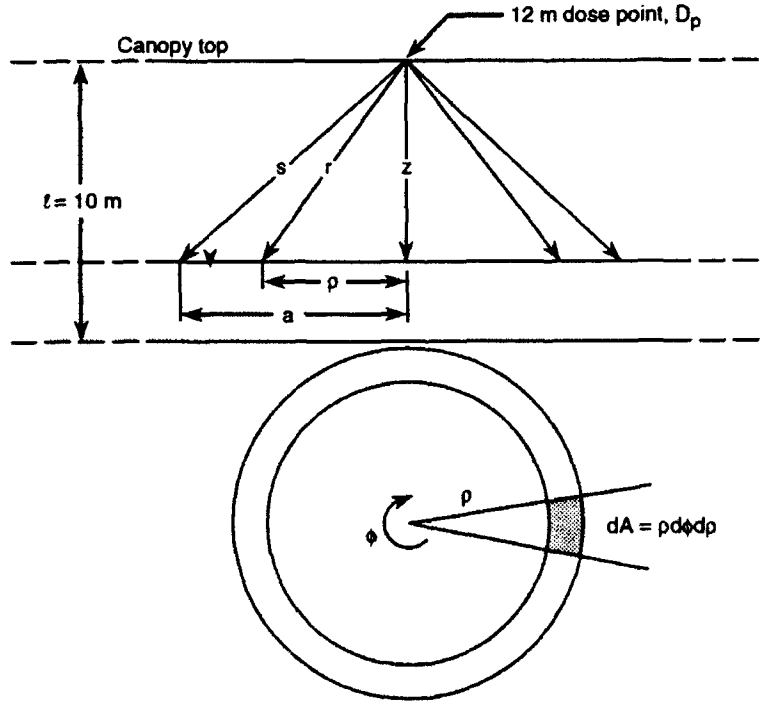

Figure A-2. Calculational geometry--canopy fallout volume source, dose point at 12 meters, side view upper panel, aerial view lower.

As shown in Figure A-2, a flat disk source of radioactive fallout material of radius a is imbedded in the homogenized canopy mass a distance z from the top of the canopy. The differential element of area is $dA=\rho d\phi d\rho$. The dose at the top of the canopy from disc source having unit gamma source intensity, $S_a=1\ \gamma/cm^2\text{-sec}$, is given by,

$$D_p = P_\gamma(E)S_a \int_0^{2\pi} d\phi \int_0^a \frac{B(\mu r)e^{-\mu r}}{4\pi r^2}\rho d\rho$$

$$= \frac{P_\gamma(E)S_a}{2}\int_0^a \frac{B(\mu r)e^{-\mu r}}{r^2}\rho d\rho \quad (cGy/h)/\left(\gamma/cm^2-sec\right). \qquad (A.2)$$

Since, $r^2=\rho^2+z^2$, and $rdr=\rho d\rho$,

$$D_p=\frac{P_\gamma(E)S_a}{2}\int_z^s \frac{B(\mu r)e^{-\mu r}}{r}dr \qquad (A.3)$$

Implementing the Berger's form of the dose buildup factor for gamma radiation given by,

$$B(\mu r) = 1+a\mu r e^{b\mu r} \quad , \qquad (A.4)$$

where a and b are fit constants given in Table A-1, the gamma dose integral becomes,

$$D_p = \frac{P_\gamma(E)S_a}{2}\left[\int_z^s \frac{e^{-\mu r}}{r}dr + a\mu\int_z^s e^{-(1-b)\mu r}dr\right] . \qquad (A.5)$$

The first term in the bracket, we call I(z,s) can be written as

$$I_1(z,s) = \int_{\mu z}^{\infty}\frac{e^{-u}}{u}du - \int_{\mu s}^{\infty}\frac{e^{-u}}{u}du \ .$$

These integrals are a specific form of the general exponential integral function,

$$E_n(b) \equiv b^{n-1}\int_b^{\infty}\frac{e^{-t}}{t}dt \quad .$$

Then $I(\mu z, \mu s) = E_1(\mu z) - E_1(\mu s)$

Integrating the second term in the bracket of Equation A.5 above, the dose, D_p, becomes,

$$D_p = \frac{P_\gamma(E)S_a}{2}\left\{E_1(\mu z) - E_1(\mu s) + \frac{a}{1-b}\left[e^{-(1-b)\mu z} - e^{-(1-b)\mu s}\right]\right\} . \qquad (A.6)$$

Assuming the radioactive fallout to be distributed over a homogenized volume of the canopy mass, a unit finite volume source element at a depth z in the canopy is $dS_v = S_a dz$. Then, dD_p

$$dD_p = \frac{P_\gamma(E)S_a}{2}\{\ \}dz \ . \qquad (A.7)$$

For purposes of integrating the disc source over the canopy mass volume, the source disc may be approximated by a radially infinite source plane were $s \to \infty$ and therefore, both $E_1(\mu s)$ and the exponential term, $\exp[-(1-b)\mu s]$, in Equations (A.6) and (A.7) are zero. Accordingly, the canopy mass is approximated as a homogeneous, vertically finite, laterally infinite slab source of radioactive material. Integrating Equation (A.7),

$$D_p = \frac{P_\gamma(E)S_v}{2}\left\{\int_o^\ell E_1(\mu z)dz + \frac{a}{1-b}\int_o^\ell e^{-(1-b)\mu z}dz\right\}$$

$$= \frac{P_\gamma(E)S_v}{2}\left\{\int_o^\ell E_1(\mu z)dz + \frac{a}{(1-b)^2\mu}\left[1 - e^{-(1-b)\mu\ell}\right]\right\} . \qquad (A.8)$$

Utilizing a property of exponential integral functions,

$$E_n(y) = -\frac{d}{dy}E_{n+1}(y) \ ,$$

the first integral in the bracket of Equation (A.8) is,

$$\int_o^\ell E_1(\mu z)dz = -\frac{1}{\mu}\int_o^{\mu\ell} dE_2(y) = \frac{1}{\mu}\left[1 - E_2(\mu\ell)\right] \ .$$

Employing the parameters given in Table A-1, the dose at the 12-meter point at the top of the canopy, for ℓ = 1000 cm, is then given by,

$$D_p = \frac{P\gamma(E)S_v}{2\mu}\left\{1 - E_2(\mu\ell) + \frac{a}{(1-b)^2}\left[1 - e^{-(1-b)\mu\ell}\right]\right\}$$

$$= 2.88\times10^{-5}E_\gamma(\mu_{en}/\rho)\{\ \} \ . \qquad (A.9)$$

Similarly, the dose at the 7-meter point, in the middle of the canopy (see Figure A-1), is given by Equation (A-9) for ℓ = 500 cm, and then doubled. Figure A-3 gives the calculated gamma dose rates per unit source, (cGy/h)/(γ/cm^3-sec) at the top (12 m dose point) and middle (7 m dose point) of the canopy for gamma energies from 0.1 to 3.0 MeV. The results are interpolated to obtain the dose rates, $R_{ij}(x)$, for the gamma-ray source, disintegration energies of the radionuclides in Table A-2. Then the source intensity-weighted gamma dose rate due to the homogenized canopy source at the two canopy dose points are given below employing Equation (A.1).

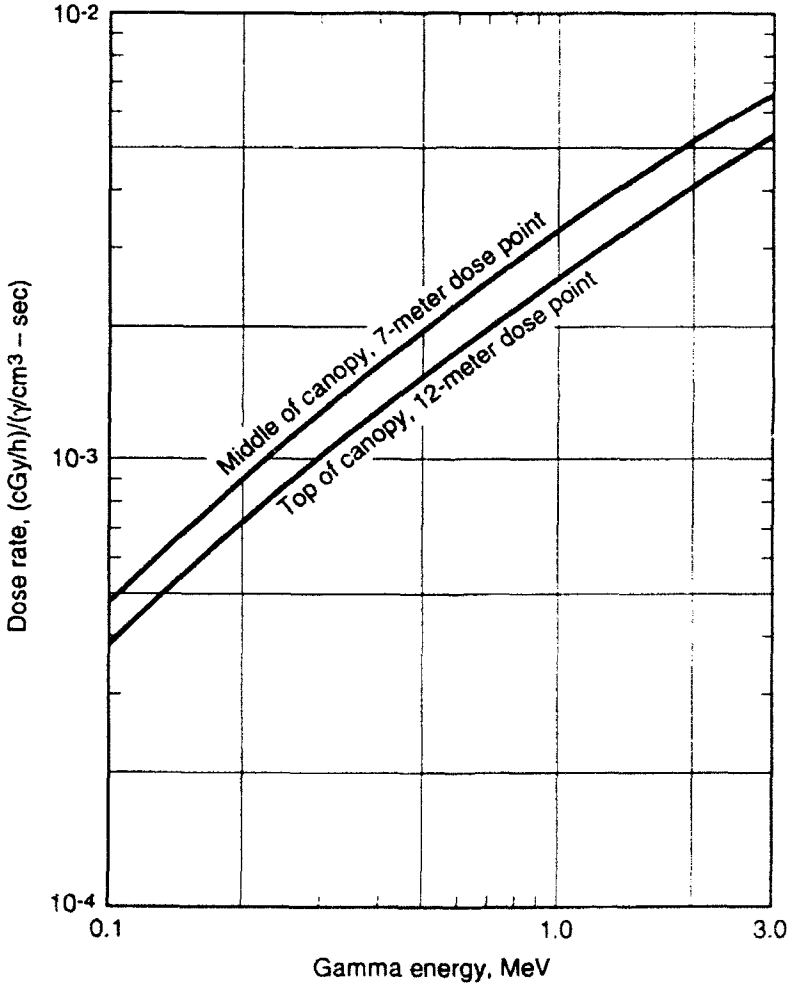

Figure A-3. Gamma dose rate in the canopy from canopy fallout volume source versus gamma energy.

Dose Point	Dose Rate, (cGy/h)/(γ/cm^3-sec)
Top of canopy 12-meters	1.651×10^{-3}
Middle of canopy 7-meters	2.064×10^{-3}

Ground Fallout Source/12- and 7-Meter Dose Points.

The calculational geometry for the ground fallout source for the dose point at the middle and top of the canopy is shown below in Figure A-4. In Figure A-4, a flat disc of radioactive material represents the ground fallout source a distance $\ell = 7$ m below the mid canopy dose point. The vertical air distance between the bottom of the canopy and the source disc is $\ell_1 = 2$ m; this region has an air density, $\rho_1 = 1.226 \times 10^{-3}$g/cm^3. The canopy thickness between the dose point and bottom of the canopy is $\ell = 5$ m; this region has a homogenized canopy density $\rho_2 = 0.0054$ g/cm^3.

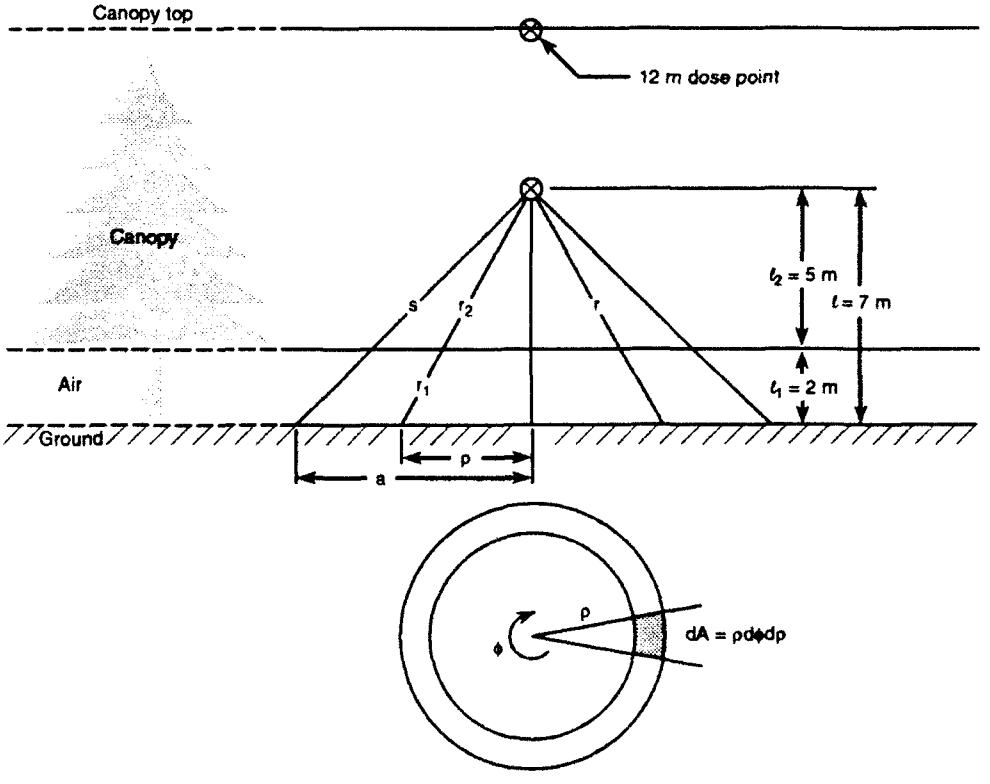

Figure A-4. Calculational geometry--ground fallout source/dose point at 7 meters.

The dose at the middle of the canopy from the disc source of unit source intensity (S_a = 1 γ/cm^2-sec) is given by,

$$D_p = P_\gamma(E) S_a \int_o^{2\pi} d\phi \int_o^a \frac{B(\Sigma\mu_i r_i)}{4\pi r^2} \exp(-\Sigma\mu_i r_i) \rho d\rho \ . \qquad (A.10)$$

Since $r^2 = \rho^2 + \ell^2$, and $rdr = \rho d\rho$, changing the variable of integration,

$$D_p = \frac{P_\gamma(E) S_a}{2} \int_\ell^s \frac{B(\Sigma\mu_i r_i)}{r^2} \exp(-\Sigma\mu_i r_i) r dr \ . \qquad (A.11)$$

Using Berger's form of the buildup factor, given by $B(\mu_i r_i) = 1 + a_i \mu_i r_i \exp(b_i \mu_i r_i)$ and combining with the exponential term in Equation (A.10),

$$B(\sum_i \mu_i r_i) \exp(-\sum_i \mu_i r_i) = \exp(-\sum_i \mu_i r_i) + \sum_i a_i \mu_i r_i \exp[-\sum_i (1 - b_i)\mu_i r_i] \ .$$

Then since $r_i = \ell_i r/\ell$, some of the summation terms can be simplified for purposes of integration, i.e.,

$$\sum_i \mu_i r_i = \frac{r}{\ell} \sum_i \mu_i r_i = \alpha r, \quad \alpha = \frac{1}{\ell} \sum_i \mu_i \ell_i \ ,$$

$$\sum_i a_i \mu_i r_i = \frac{r}{\ell} \sum_i a_i \mu_i \ell_i = \beta r, \quad \beta = \frac{1}{\ell} \sum_i a_i \mu_i \ell_i \ , \text{ and}$$

$$\sum_i (1 - b_i)\mu_i r_i = \frac{r}{\ell} \sum_i (1 - b_i)\mu_i \ell_i = \gamma r, \quad \gamma = \frac{1}{\ell} \sum (1 - b)\mu_i \ell_i \ ,$$

where, $\mu_i = (\mu/\rho)_i \rho_i$ and $(\mu/\rho)_1$ is the gamma mass attenuation coefficient for air (ρ_1 = 1.226 × 10^{-3}, g/cm^3); $(\mu/\rho)_2$ is that for the canopy (ρ_2 = 0.0054, g/cm^3).

Equation (A.11) can be rewritten as,

$$D_p = \frac{P_\gamma(E) S_a}{2} \int_\ell^s \left(e^{-\alpha r} + \beta r e^{-\gamma r}\right) \frac{dr}{r} \ . \qquad (A.12)$$

Integrating of first term in brackets results in the difference between two exponential integral functions: $E_1(\alpha\ell) - E_1(\alpha s)$. Integrating the second term in the brackets, the dose is given as,

$$D_p = \frac{P_\gamma(E) S_a}{2} \left[E_1(\gamma\ell) - E_1(\alpha s) + \frac{\beta}{\gamma}\left(e^{-\gamma\ell} - e^{-\gamma s}\right) \right]$$

Then assuming an infinitely extended ground source plane ($s \rightarrow \infty$), the dose in the canopy from the fallout source on the ground is,

$$D_p = 2.88 \times 10^{-5} E_\gamma (\mu_{en}/\rho) \left[E_1(\alpha \ell) + \frac{\beta}{\gamma} e^{-\gamma \ell} \right] \quad (cGy/h)/(\gamma/cm^2 - sec) \; . \qquad (A.13)$$

Employing Equation (A.13) with the parameters given in Table A-1, doses were determined for various gamma energies at the middle of the canopy for ℓ = 700 cm, ℓ_1 = 200 cm, and ℓ_2 = 500 cm; and at the top of the canopy for ℓ = 1200 cm, ℓ_1 = 200 cm,. and ℓ_2 = 1000 cm.

Figure A-5 gives the calculated gamma dose rates per unit fallout ground source (cGy/h)/(γ/cm^2-sec) at the 7-meter and 12-meter dose points as function of gamma energy ranging from 0.1 to 3.0 MeV.

Ground Fallout Dose at 1-Meter Height.

The same form as given by Equation (A.13) was employed to calculate the ground fallout source dose at 1 meter in air above the surface for ℓ = 100 m, $\alpha = (\mu/\rho)_1 \rho_1$, $\beta = a(\mu/\rho)_1$ and $\gamma = (1 - b)(\mu/\rho)_1$. Figure A-5 also gives the calculated gamma dose rates for the 1-meter dose as a function of gamma-ray energy.

The results of the ground fallout source dose rates at all three dose points, 1 meter, 7 meters, and 12 meters, were interpolated to obtain the dose rates, $R_{ij}(x)$, for the gamma-ray source, disintegration energies of the radionuclides in Table A-2. These values were then weighted and summed by the disintegration energy yields and radionuclide source intensity according to Equation (A.1), and given below.

Dose Point	Dose Rate (cGy/h)/(γ/cm^2-sec)
Top of canopy 12 meters	1.011×10^{-6}
Middle of canopy 7 meters	1.690×10^{-6}
1-meter height in air	2.936×10^{-6}

Canopy Fallout Contact Source/Dose to Foliage Elements.

Calculations were performed to estimate the fallout gamma dose at the center of cylindrical foliage elements such as a pine needle or a budding meristem due to fallout deposited directly on the foliage element in question. It is assumed that fallout material

is homogeneously deposited on the surface of a cylinder of length 2ℓ and radius ρ as shown in Figure A-6.

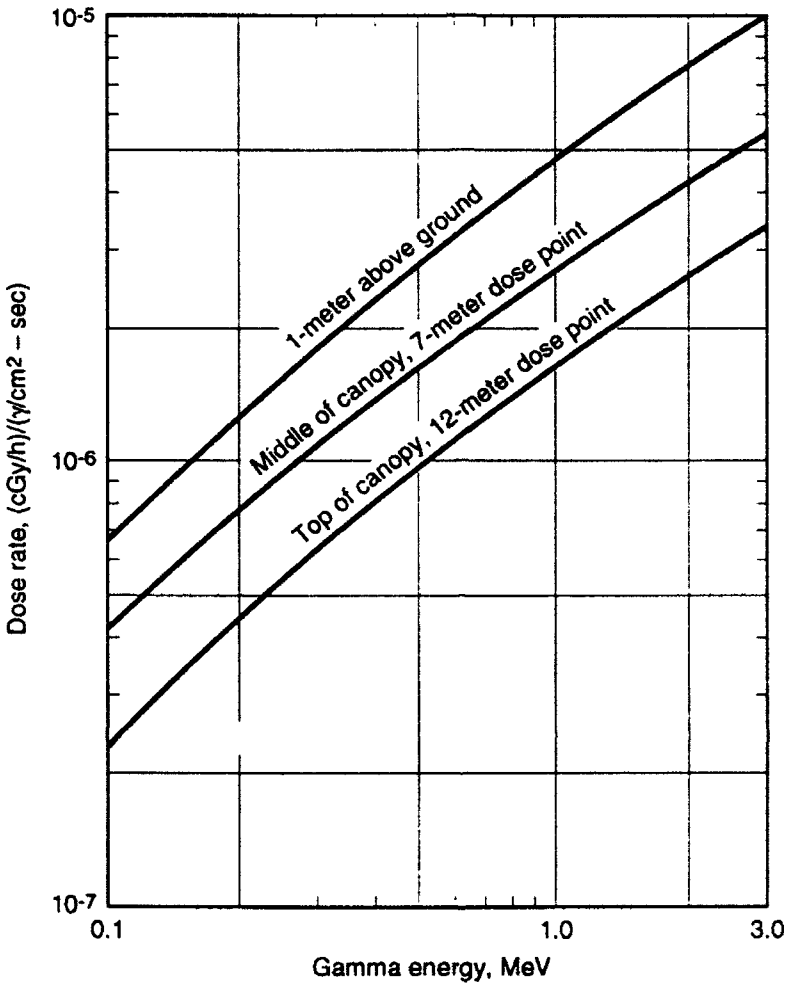

Figure A-5. Gamma dose rate from ground fallout source versus gamma energy.

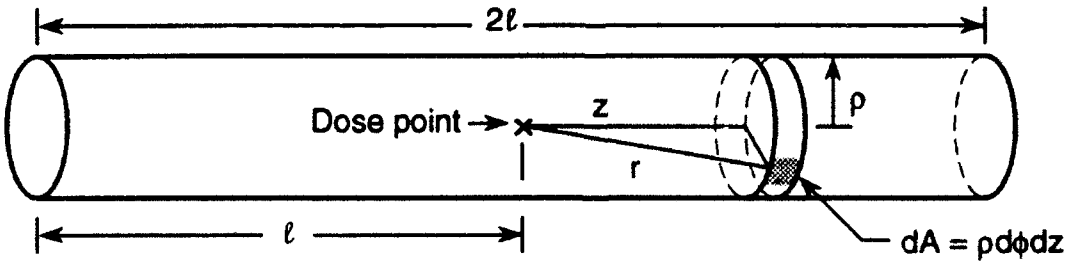

Figure A-6. Calculational geometry for canopy fallout contact source.

A point source gamma dose function at a small element of source area dA is integrated over the cylindrical surface to give the gamma dose at the dose point due to radionuclide fallout material on the surface.

$$D_\gamma = P_\gamma(E)S_a \int_0^{2\pi} d\phi \int_0^{\ell} \frac{e^{-\mu r}}{4\pi r^2} \rho d\phi dz \ . \qquad (A.14)$$

Changing the variable of integration $z \rightarrow r$, $r^2 = z^2 + \rho^2$, $dz = rdr/z$ and $z^2 = r^2 - \rho^2$,

$$D_\gamma = \frac{P_\gamma(E)\rho S_a}{2} \int_\rho^{\sqrt{\ell^2+\rho^2}} \frac{e^{-\mu r}}{r^2\sqrt{r^2-\rho^2}} r dr$$

$$= \frac{P_\gamma(E)\rho S_a}{2} \int_\rho^{\sqrt{\ell^2+\rho^2}} \frac{e^{-\mu r}}{r\sqrt{r^2-\rho^2}} dr \ . \qquad (A.15)$$

Since $\mu r << 1$, $e^{-\mu r} \approx 1 - \mu r$ and then,

$$D_\gamma = \frac{P_\gamma(E)\rho S_a}{2} \left[\int_\rho^{\sqrt{\ell^2+\rho^2}} \frac{dr}{r\sqrt{r^2-\rho^2}} - \mu \int_\rho^{\sqrt{\ell^2+\rho^2}} \frac{dr}{\sqrt{r^2-\rho^2}} \right] . \qquad (A.16)$$

Integrating Equation (A.16) and employing parameters in Table A-1, the gamma dose rate per unit source, (cGy/h)/(γ/cm^2-sec), for a given gamma ray energy is

$$D_\gamma = \frac{P_\gamma(E)S_a}{2} \left[\cos^{-1}\left(\frac{\rho}{\sqrt{\ell^2+\rho^2}} \right) - \mu\rho\ell n\left(\frac{\sqrt{\ell^2+\rho^2}+\ell}{\rho} \right) \right], \qquad (A.17)$$

where $S_a \equiv 1$ and $P_\gamma(E) = 5.76 \times 10^{-5}(\mu_{en}/\rho)E_\gamma$.

Interpolating the values obtained from Equation (A.17) and applying them in Equation (A.1) along with the values given in Table A-2, the gamma dose rate per unit fallout source, (cGy/h)/(γ/cm^2-sec), in a foliage element is obtained.

The size of a pine needle (*Pinus sylvestris*) of interest (assumed to be cylindrical) ranges from 2 to 7 cm in length and 2 mm in diameter (Painter and Wicker, 1993).

Calculations were based on an average length of 4.5 cm. For the budding meristem, the calculations were based on cylinders 0.04 and 0.0625 cm in diameter to simulate the dose depths discussed in Section 5.2. For horizontal orientation of the needle or meristem, the results obtained with Equation (A.17) should be doubled since the integration was over the half length ℓ. On the other hand, if fallout was only on the top surface of the cylinder the results would in turn be halved due to symmetry considerations. We assume that these two factors cancel. However, assuming a random directional orientation of the axis of the pine needle (or meristem) between $\pm\pi/2$ from the horizontal, the values obtained from Equation (A.17) were multiplied by the average value of the cosine, $\overline{\cos}\ (2/\pi)$ = 0.63662 to account approximately for the effective area seen by incident fallout particles. Accordingly, the gamma dose values for various foliage element dimensions are given below.

Dose Point		Dose Rate (cGy/h)γ/cm²-sec
Radius (ρ) cm	Length (2ℓ) cm	Random Orientation
0.04	4.5	5.13×10^{-7}
0.04	9.0	5.14×10^{-7}
0.0625	9.0	5.10×10^{-7}
0.10	4.5	4.983×10^{-7}
0.15	9.0	4.95×10^{-7}
0.40	2.0	3.783×10^{-7}

BETA DOSES.

Beta dose calculations were performed for the two dose points in the canopy indicated in Figure A-1 from fallout source radionuclide material dispersed in the canopy biomass. Beta dose calculations were also performed to estimate the dose in the foliage elements from radioactive fallout deposited on their surfaces. Because of the limited range of beta particles, the beta dose to the canopy dose points from fallout material on the ground surface was neglected.

Fallout radionuclide parameters for the beta dose calculations are listed in Table A-3. Beta doses were calculated for each radionuclide component and then weighted according to each radionuclide source intensity, Q(MCi), and summed to obtain the dose for the source mix. If $R_j(x)$ represents the beta dose rate component for the j^{th} radionuclide, the dose rate at position x is,

Table A-3. Fallout radionuclide parameters for beta dose calculations.*

Radionuclides	Q(MCi)	Maximum Beta Energy, E_0(Mev)	Average Beta Energy, E(Mev)	Maximum C.S.D.A. range, r_0(gm/cm^2)
I-131	7.3	0.810	0.180	0.300
Te-132	1.3	0.220	0.047	0.048
Cs-134	0.5	1.453	0.152	0.640
Cs-137 + Ba-137	1.0	1.167	0.195	0.490
Mo- 99 + Tc- 99m	3.0	1.215	0.398	0.540
Zr- 95 + Nb- 95m	3.8	1.130	0.115	0.480
Ru-103 + Rh-103m	3.2	0.710	0.062	0.255
Ru-106 + Rh-106	1.6	3.541	1.415	1.800
Ba-140 + La-140	4.3	2.200	0.490	1.050
Ce-141	2.8	0.580	0.144	0.190
Ce-144 + Pr-144	2.4	2.984	1.208	1.500
Np-239	1.2	0.723	0.135	0.260
I-133	15.9	1.540	0.418	0.716
Sr- 89	2.2	1.470	0.583	0.660
Sr- 90 + Y- 90	0.2	2.245	0.931	1.100

*From Hogan, Zigman, and Mackin (1964), "Beta Spectra II: Spectra of Individual Negatron Emitters"; Shlien and Terpilak (1984), *The Health Physics Radiological Handbook.*

$$\dot{D}_\beta(x) = \sum_j f_j R_j(x) \ , \qquad \text{(A.18)}$$

where, $f_j = Q_j / \sum_j Q_j$.

The beta dose calculations are based on integrating an energy dependent point source dose function over the source geometries of interest. The point source dose function J(r) is a semi-empirically derived relationship for beta particles given by Loevinger, Japha, and Brownell (1956),

$$J(r) = \frac{k}{(\nu r)^2}\left\{c\left[1-(\nu r/c)e^{1-(\nu r/c)}\right]+\nu r e^{1-\nu r}\right\} \qquad \text{(A.19)}$$

$$[\ ] \equiv 0, \quad r \geq c/\nu$$

where

$$k = \frac{1.6\times10^{-6}}{4\pi\times100}\rho^2\nu^3\bar{E}_\beta\alpha \ ,$$

$$= 1.273\times10^{-9}\rho^2\nu^3\bar{E}_\beta\alpha \ ,$$

$$\alpha = \left[3c^2-\left(c^2-1\right)e\right]^{-1} \ ,$$

$$c = 3.11e^{-0.55E_o} \ ,$$

$$\nu = \nu(E_o) = \frac{18.2}{(E_o-0.036)^{1.37}}\left(cm^2/g\right) \ , \text{ and}$$

r = source-to-detector distance, g/cm^2 ,

ρ = density, g/cm^3,

$\bar{E}_\beta$ = average beta energy, MeV ,

E_o = maximum beta energy, MeV ,

$\nu(E_o)$ = apparent absorption coefficient, cm^2/g .

Canopy Fallout Volume Source/12- and 7-Meter Dose Point.

The calculation procedure for canopy fallout source and canopy dose points is the same as that given for integrating the point source gamma dose function over the canopy volume of finite vertical width, and infinite lateral extent. Referring to the calculational geometry given in Figure A-2, the dose at the top of the canopy a vertical distance z from disc source of infinite radius imbedded in the canopy is,

$$D_p = \int_v J(r)dA = \int_0^{2\pi} d\phi \int_z^{\infty} J(r)rdr$$

$$= \frac{2\pi k}{\nu^2}\left\{\int_z^{c/\nu} \frac{c\left[1-(\nu r/c)e^{1-(\nu r/c)}\right]}{r^2} rdr + \int_z^{\infty} \frac{\nu r e^{1-\nu r}}{r^2} rdr\right\} \qquad (A.20)$$

$$[\ ] = 0\ ,\ r \geq c/\nu\ .$$

Carrying out the integration of Equation (A.20), we obtain,

$$D_p = P_\beta(E)\left\{c\left[1+\ell n(c/\nu z) - e^{1-(\nu z/c)}\right] + e^{1-\nu z}\right\}. \qquad (A.21)$$

Expressing D_p above as a dose rate per unit source, (cGy/h)/(β/cm^2-sec), $P_\beta(E) = 2.879 \times 10^{-5}\nu\bar{E}\beta\alpha(S_a \equiv 1)$.

In order to obtain the beta dose at the top of the canopy, the infinite disc source (Equation A.21) is integrated over the canopy source region of thickness ℓ = 1000 cm and of density ρ_C = 0.0054 g/cm. Furthermore, at that point, the beta dose is calculated at the center, x, of a pine needle of density ρ = 1 g/cm^3, and thickness 0.2 cm, where then, x = 0.1 gm/cm^2. The surface source of unit intensity S_a extends to a unit volume source S_v, i.e., $dS_v = S_a dz$. The volume integral is then,

$$D_p = \int_x^{x+\ell} S_v D_p(z)dz$$

$$= P_\beta(E)S_v\left\{\int_x^{c/\nu} c\left[1+\ell n(c/\nu z) - e^{1-(\nu z/c)}\right] + \int_x^{x+\ell} e^{1-\nu z}dz\right\}. \qquad (A.22)$$

For both dose points, 12 m or 7 m, , ℓ = 1000 cm (5.4 g/cm^2) and ℓ = 500 cm (2.7 g/cm^2) respectively, the canopy slab source is of infinite thickness since the distances exceed the maximum range, r_o, of the radionuclide disintegration betas given in Table A-3. Then given, $\ell \geq r_o$, and integrating Equation (A.22),

$$D_p(x,\infty) = 0.5D_\beta\alpha\left\{c^2\left[3 - e^{1-(\nu x/c)} - \frac{\nu x}{c}\left(2+\ell n\frac{c}{\nu x}\right)\right] + e^{1-\nu x}\right\}, \qquad (A.23)$$

$$[\ ] \equiv 0\ ,\ x \geq c/\nu\ ,$$

where, D_β is the beta particle dose in the interior of a large (infinite) source as is the case of the canopy slab source. The beta dose at the surface of the top of the canopy is $D_\beta/2$, as indicated in Equation (A.23), assuming negligible back scatter from the air above. Expressing D_p as the dose rate per unit source, (cGy/h)/(β/cm^3-sec), D_β is,

$$D_\beta = \frac{1.6\times10^{-6}(\text{ergs/g})\times\bar{E}_\beta(\text{MeV}/\beta)}{100\left(\frac{\text{ergs}}{\text{g}-\text{cGy}}\right)\times 0.0054\left(\frac{\text{g}}{\text{cm}^3}\right)}$$

$$= 1.0667\times10^{-2}\bar{E}_\beta \quad (\text{cGy/h})/\left(\beta/\text{cm}^3-\text{sec}\right). \tag{A.24}$$

The dose point given by Equation (A.23) is actually 0.1 cm above the canopy slab surface to account for penetration into the center of a pine needle. Locating the dose point 0.1 cm below the canopy slab surface just inside the canopy, the beta dose is

$$\dot{D}_\beta(x \text{ inside}, \infty) = D_\beta - D_p(x,\infty) \quad (\text{cGy/h})/\left(\beta/\text{cm}^3-\text{sec}\right). \tag{A.25}$$

Equation (A.25) is used to determine the beta dose rate at the top of the canopy (12-meter dose point). Then because of infinite slab thickness conditions of the canopy mass, the beta dose rate in the middle of the canopy (7-meter dose point) is obtained by doubling the value obtained from Equation (A.25) for the 12-m dose point. Calculations were performed for each radionuclide and weighted according to the source intensity and summed to obtain the beta dose rate for the radionuclide fallout mix; they are given below.

Dose Point	Beta Dose Rate (cGy/h)/(β/cm^3-sec)
Top of canopy 12 meters	3.345×10^{-3}
Middle of canopy 7 meters	6.69×10^{-3}

Canopy Fallout Contact Source/Dose to Foliage Elements.

Calculations were performed to estimate the fallout beta dose at the center of foliage elements such as a pine needle or a budding meristem. It is assumed that fallout material is homogeneously deposited on the surface of a cylinder of length 2ℓ and radius ρ as shown in Figure A-6.

The point source dose function, J(r), at the small element of source area, dA, is integrated over the cylindrical surface to give the beta dose at the dose point,

$$D_\rho = S_a \int_A J(r)\, 2\pi\rho dz \,. \tag{A.26}$$

Changing the variable of integration to r, $r^2 = z^2 + \rho^2$, dz = rdr/z, and $z = \sqrt{r^2 - \rho^2}$, the dose becomes

$$D_\beta = \frac{2\pi\rho k}{v^2} \int_\rho^{\sqrt{\ell^2+\rho^2}} \frac{J(r)rdr}{r^2\sqrt{r^2-\rho^2}}$$

$$= \frac{4\pi\rho k}{v^2}\left\{ \int_\rho^{\sqrt{\ell^2+\rho^2}} c\left[1-(vr/c)e^{1-(vr/c)}\right]\frac{dr}{r\sqrt{r^2-\rho^2}} + v\int_\rho^{\sqrt{\ell^2+\rho^2}} \frac{e^{1-vr}dr}{\sqrt{r^2-\rho^2}} \right\}. \tag{A.27}$$

Since in Equation (A.27) [ ] ≠ 0, $\sqrt{\ell^2+\rho^2} \geq c/v$, the integral of the first term in the [ ] brackets is $(1/\rho)\cos^{-1}(\rho/(c/v))$. Then the dose becomes,

$$D_\beta = P_\beta(E)S_a\left\{ c\left[\frac{1}{\rho}\cos^{-1}\left(\frac{\rho}{c/v}\right) - \frac{v}{c}\int_\rho^{UL}\frac{e^{1-(vr/c)}}{\sqrt{r^2-\rho^2}}dr\right] + v\int_\rho^{\sqrt{\ell^2+\rho^2}}\frac{e^{1-vr}}{\sqrt{r^2-\rho^2}}dr \right\}. \tag{A.28}$$

The two integrals in Equation (A.28) were evaluated numerically. Because of the conditions indicated above for the [ ] bracket, the upper limit, UL is subject to the conditions given as follows.

Condition	UL
$c/v > \sqrt{\rho^2+\ell^2} > \rho$	$\sqrt{\rho^2+\ell^2}$
$\sqrt{\rho^2+\ell^2} > c/v > \rho$	c/v
$\sqrt{\rho^2+\ell^2} > \rho > c/v$	0

Equation (A.28) gives the beta dose rate per unit source intensity (cGy/h)/(β/cm^2-sec) in the center of the foliage element where $P_\beta(E) = 2.879 \times 10^{-5}\ \rho v \bar{E}_\beta \alpha$.

The assumptions made for the calculations regarding dimensions, fallout source, surface symmetry, orientation, etc., are all discussed above under the subsection "Canopy Fallout Contact Source/Dose to Foliage Elements," which describes fallout gamma ray calculations parallel to those described here for beta radiation. Utilizing Equation (A.18) with the radionuclide fallout source intensity values in Table A-3, the beta dose rates obtained are as follows.

Dose Point		Dose Rate (cGy/h)γ/cm²-sec
Radius (ρ) cm	**Length (2ℓ) cm**	**Random Orientation**
0.04	4.5	3.02×10^{-5}
0.04	9.0	3.04×10^{-5}
0.0625	9.0	2.36×10^{-5}
0.10	4.5	1.73×10^{-5}
0.15	9.0	1.24×10^{-5}
0.40	2.0	0.32×10^{-5}

SUMMARY.

The various calculated beta and gamma dose components from fallout radiation are summarized in Table A-4. The dose rates are all expressed in terms of cGy/h per unit source either in the canopy or on the ground surface and reflect equal radionuclide fallout deposition in the canopy mass and on the ground surface below. Dose rates are given at three locations (see Figure A-1), two in the canopy and a third at 1 meter above the ground surface for reference. In the canopy mass, one dose point is located at the top, 12 meters above the ground, and another in the middle, 7 meters above the ground.

The results given for gamma and beta dose rates per unit volume source in the canopy reflect the adjustment made for the reference volume density in the canopy to be consistent with equal fallout deposition in the canopy mass and on the ground surface. That is, the fallout deposited in the canopy mass is assumed to be homogeneously distributed over the 1000 cm thickness of the canopy rather than on the plane surface of the ground, i.e., $S_v(\beta \text{ or } \gamma/cm^3\text{-sec}) = S_a(\beta \text{ or } \gamma/cm^2\text{-sec}) \times 10^{-3}$.

In addition to the dose rate contributions in the canopy from fallout radionuclide sources distributed in canopy mass and ground surface below, Table A-4 gives dose rates at these locations in the middle of cylindrical foliage elements from fallout radionuclides assumed to be deposited on their surfaces.

Table A-4. Summary of fallout dose rates (cGy/h)/unit source.

Dose Point	Fallout Source [a]			
	Canopy, Unit Source		Ground, Unit Source (γ or β/cm^2-sec)	
	Gamma	Beta	Gamma	Beta
Top of canopy (12 m)	1.65×10^{-6} [b]	3.34×10^{-6} [b]	1.01×10^{-6}	Negligible
Contact source, $\rho = 0.1$ cm	4.98×10^{-7} [c]	1.73×10^{-5} [c]	----	----
Contact source, $\rho = 0.4$ cm	3.78×10^{-7} [c]	3.20×10^{-6} [c]	----	----
Middle of canopy (7 m)	2.06×10^{-6} [b]	6.69×10^{-7} [b]	1.69×10^{-6}	Negligible
Contact source, $\rho = 0.1$ cm	4.98×10^{-7} [c]	1.73×10^{-5} [c]	----	----
Contact source, $\rho = 0.4$ cm	3.78×10^{-7} [c]	3.20×10^{-6} [c]	----	----
One meter above ground	----	----	2.94×10^{-6}	1.85×10^{-5} [d]

[a] Assumes 1/2 the fallout in the tree canopy and 1/2 on the ground surface.
[b] Reflects total fallout ground (surface) source and total fallout canopy (volume) source are equal; units are (cGy/h)/(γ or β/cm^3-sec).
[c] Assumes cylindrical foliage element randomly oriented $\pm \pi/2$ from horizontal; units are (cGy/h)/(γ or β/cm^2-sec).
[d] Based on beta/gamma dose ratio of 6.3 according to Barabanova (1990).

Inspection of Table A-4 indicates that the dominant dose component in canopy mass is beta radiation due to fallout deposition on the surface of foliage elements assuming that the fallout deposits equally in the canopy mass and on the ground surface below and that the surface density of fallout on the foliage elements is the same as that on the ground.

APPENDIX B
SPECTRAL DEVIATIONS FROM CLASS

This appendix presents our method for constructing a deviation vector for a pixel in standard units relative to a reference class of pixels.

Each pixel in a multispectral image is represented by a vector of its band intensities. The pixels belonging to a single class form a cluster in the hyperspace of band intensities. We assume that the cluster of pixels belonging to a reference site for the class may be approximated by a multivariate normal distribution. Let **u** be the mean vector of the pixels in the reference site and Σ be the covariance matrix for the reference site.

In Bayes decision theory, the distance of a pixel **x** from the mean of its class is called the *Mahalanobis* distance (Duda and Hart, 1973) when it is scaled relative to the covariance matrix Σ. The square of the Mahalanobis distance r is given by

$$r^2 = (\mathbf{x} - \mu)^T \Sigma^{-1} (\mathbf{x} - \mu). \qquad \text{(B-1)}$$

For a multivariate distribution, the Mahalanobis distance r is the equivalent of the normal deviate z used for a univariate normal distribution. It is a measure of the deviation of a pixel from its class mean in *standard units*. Since r is a scalar quantity, it provides no information regarding the direction of the deviation in hyperspace.

We have generalized the Mahalanobis distance to a Mahalanobis vector **m** that points in the direction of deviation and whose magnitude is the Mahalanobis distance r. For a pixel that deviates from its class, the magnitude r indicates the significance of the deviation. For a statistically significant deviation, the direction of the vector **m** carries information regarding the likely cause of the deviation.

Assume that a multispectral image has been transformed to Tasseled Cap space (TC space). In general, the cluster for a reference site will be hyperelliptical with its principle axes tilted with respect to the TC axes and with unequal variance along the principle axes. The upper panel of Figure B-1 illustrates a reference site cluster in two dimensions. The eigenvectors of the covariance matrix of the cluster lie along the principle component coordinate axes of the cluster. The eigenvalues are the variances of the cluster in the direction of these axes.

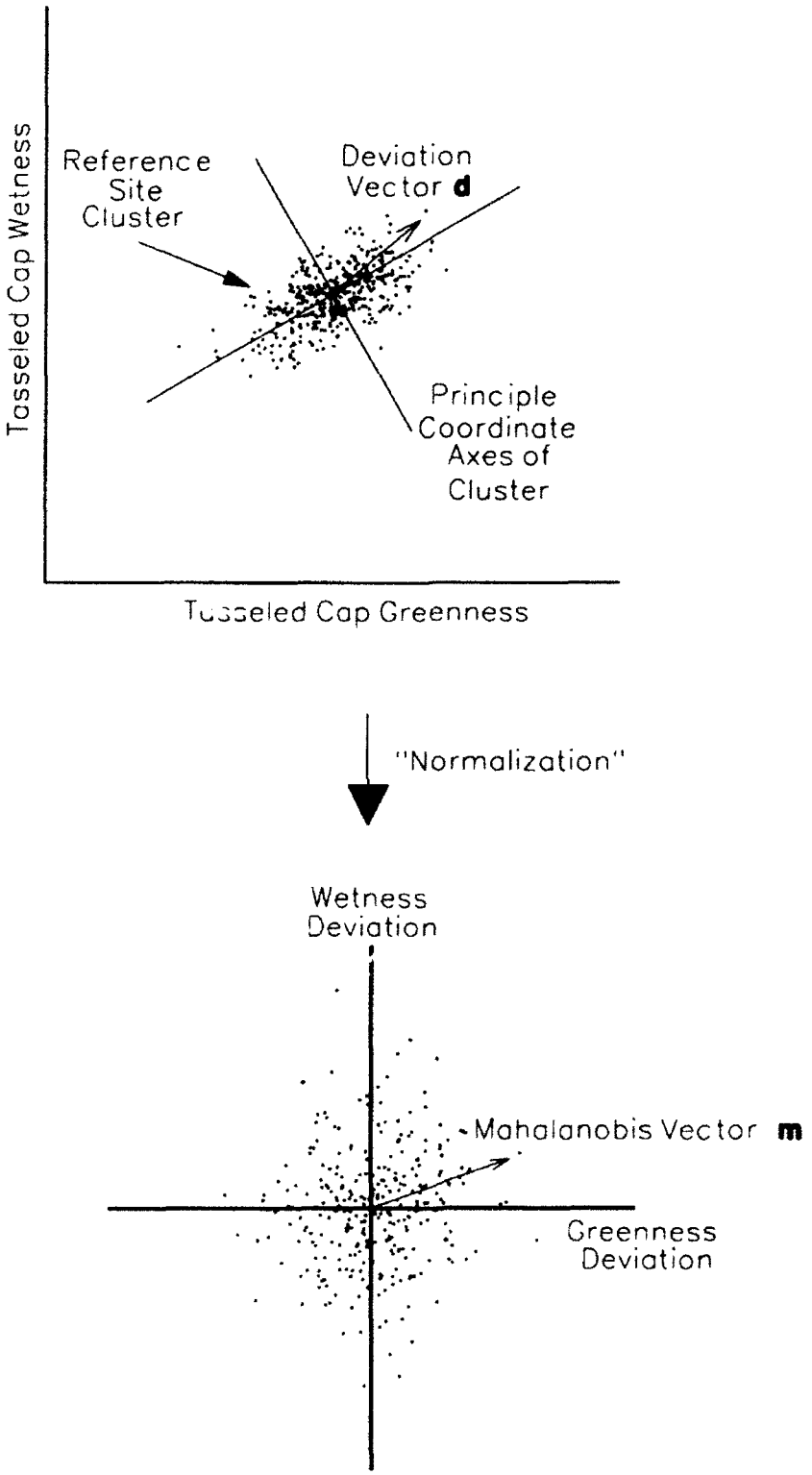

Figure B-1. The normalization procedure defined in Appendix B transforms the reference site cluster into a cluster with unit covariance matrix.

Let **U** be the matrix whose column vectors are the unit eigenvectors of the covariance matrix Σ. Let **x** be a pixel vector in TC space and $\mathbf{d} = \mathbf{x} - \mu$ be the deviation of the pixel from the reference site mean in TC space. The deviation **d** can be expressed in the principle component coordinate system of the reference site cluster by the transformation

$$\mathbf{d}_p = \mathbf{U}^T \mathbf{d}. \tag{B-2}$$

Likewise, the covariance matrix Σ_p of the cluster in the principle component coordinate system is

$$\Sigma_p = \mathbf{U}^T \Sigma \mathbf{U}. \tag{B-3}$$

Since **U** is constructed from the eigenvectors of Σ, the matrix Σ_p is diagonal with its diagonal components equal to the variance of the cluster along each of its principle axes. In fact, the usual procedure for finding the matrix **U** is to diagonalize Σ.

The reference site cluster may be scaled to a spherical distribution with unit variance along each of its axes in the principle component coordinate system by dividing each component of the pixel deviation vectors $\mathbf{d}_p$ by the standard deviations of the cluster along the corresponding principle axis. This scaling is accomplished by multiplication of each pixel deviation vector by a normalizing matrix $\mathbf{N}_p$:

$$\mathbf{m}_p \equiv \mathbf{N}_p \mathbf{d}_p. \tag{B-4}$$

The matrix $\mathbf{N}_p$ is a diagonal matrix given by

$$\mathbf{N}_p \equiv \Sigma_p^{-1/2}. \tag{B-5}$$

where the root is taken term-by-term on the right hand side of the equation. In other words, the diagonal terms of $\mathbf{N}_p$ are the inverses of the standard deviations of the reference site cluster along the principle axes.

The vector $\mathbf{m}_p$ given by Equation 4 for a pixel is the desired Mahalanobis vector expressed in the principle component coordinate system of the cluster. Since **U** is a unitary matrix, $\mathbf{U}^{-1} = \mathbf{U}^T$. So $\mathbf{m}_p$ may be expressed in the Tasseled Cap coordinate system by the transformation

$$\mathbf{m} = \mathbf{U} \mathbf{m}_p. \tag{B-6}$$

which is the inverse transformation of that in Equation 2.

Combining Equations 6, 4, 2, and the definition of **d**, we have

$$\mathbf{m} = \mathbf{U}\,\mathbf{N}_p\,\mathbf{U}^T(\mathbf{x} - \mu). \qquad \text{(B-7)}$$

Equation 7 shows that the normalizing matrix **N** for calculating Mahalanobis vectors in the TC coordinate system is

$$\mathbf{N} = \mathbf{U}\,[\mathbf{U}^T\,\Sigma\,\mathbf{U}]^{-1/2}\,\mathbf{U}^T. \qquad \text{(B-8)}$$

where the root on the square brackets is taken term-by-term. Finally, the desired Mahalanobis vector expressing the deviation vector of a pixel **x** from its class in standard units in Tasseled Cap space is

$$\mathbf{m} = \mathbf{N}(\mathbf{x} - \mu). \qquad \text{(B-9)}$$

This normalization, when applied to each pixel of the reference site cluster, results in a cluster with unit covariance matrix as illustrated in the lower panel of Figure B-1.

If the cluster is well approximated by a multivariate normal distribution, then the significance of the deviation of any given pixel from the mean of the cluster may be judged with a chi-squared test on the value of r^2 for the pixel. In practice, the usual procedure is to adjust a threshold of significance on r^2 by inspection of the resulting spatial and temporal patterns of significant deviations. The threshold is raised just enough to eliminated random spatial patterns of deviation or to eliminate deviations that occur before the time of a known stimulus.

APPENDIX C
CHRONOLOGY OF SELECTED EVENTS

SATURDAY, 26 APRIL 1986, 01:23

- two explosions of Unit 4; concrete, graphite, and debris escaped through roof; hole exposed graphite core (1)
- smoke and fumes with radioactive material rose in a hot plume about 1800 m high (1)
- heavier debris and particles fell near site (1)
- lighter particles to west and north (1)
- winds at 1500 m were 8-10 km/s from SE (1)
- plant firemen arrived within minutes (1)
- burning graphite on roof of Unit 3 (1)
- $\Delta t < 1$ h first case of acute radiation syndrome (1)
- $\Delta t \approx 1.5$ h Unit 3 shutdown (1)
- $\Delta t \approx 24$ h Units 1 & 2 shutdown (1)

26 APRIL 1986, 0500

First person report of Valeriy Fedorovich Zosimov (2)

> "Early in the morning, about 0500, I slipped into Kiev to meet my family. We returned in a private car. We reached Kopachy, not far from Pripyat, near the station. A captain with a portable radio gave us permission to leave the vehicle in Kopachy and from there walk home to Pripyat. So, we went.... My 10-year-old daughter, my wife, and me. Ahead and behind people were also walking, and from Kopachy the destroyed fourth unit could already be seen. Where the power transmission line crosses the road there was a long band of graphite smoke. I shook the light black flakes from my coat, and they immediately dispersed. We arrived home at night (later a large part of the forest around that path was declared hot and came under the ax—it was dangerous there! Just as it was when I walked along it with my family?)"

26 APRIL 1986, DAWN

- all fires extinguished except burning graphite in core (1)

27 APRIL 1986

1200 announcement of evacuation broadcast in Pripyat (1)

1400 - 1700 Pripyat evacuated with 1200 buses that had assembled in Chernobyl (1)

Line several kilometers long (1)

Some of population of Pripyat had already left, so the number transported was less than the 44,600 projected (1)

Population of Pripyat moved initially to surrounding towns and villages

2 MAY 1986

Evacuation of 30 km danger zone begun.

4 MAY 1986

High radiation levels force government headquarters from Pripyat to Chernobyl.

6 MAY 1986

End of atmospheric release of radioactivity from core (1)

6 MAY 1986

Evacuation of the danger zone (30 km radius) completed (1)

JUNE 1986

Start construction of hydraulic emergency structures (3)

Water Protection (1)

As part of the protection of rivers and the Kiev Reservoir, an effort was made to slow the movement of long-lived radionuclides through ground or surface water. Three major undertakings were:

- 140 dams and dikes to limit runoff from the site area into the cooling pond and the Pripyat river.
- existing silt traps at the bottoms of the rivers, the cooling pond, and the Kiev Reservoir were scoured.
- ground water barrier was built around the plant to prevent the flow of radioactive water towards the River Dnepr. The barrier was 8 km long and 30-35 m deep, down to the impermeable clay layer.

Hydraulic Emergency Structures (3)

- a filtration-proof wall in the soil along part of the perimeter of the site of the power plant and wells to lower the water table
- a drainage barrier for the cooling pond
- a drainage cutoff barrier on the right bank of the Pripyat river
- a drainage interception barrier in the south-west section of the plant
- drainage water purification facilities

MID-NOVEMBER 1986

Completion of *sarcophagus* (1)

APRIL 1987

Completion of work begun in May 1986 for protecting the water system. (1)

SOURCES

(1) International Advisory Committee, 1991.

(2) IZVESTIYA, 1989.

(3)

APPENDIX D
EVERGREEN SPECTRAL SIGNATURES BY CLASS AND DATE

E1. Spectral Signature of Classes on the Winter/Summer Composite Image COMP21

Name of class = FOREST1 Number of points in sample = 481

	Band 1	*Band 2*	*Band 3*	*Band 4*	*Band 5*	*Band 6*	*Band 7*
Min	45.00	124.00	150.00	57.00	138.00	111.00	147.00
Mean	53.53	134.61	160.67	65.30	147.03	128.89	151.16
Max	66.00	144.00	180.00	81.00	154.00	143.00	157.00

Covar	*Band 1*	*Band 2*	*Band 3*	*Band 4*	*Band 5*	*Band 6*	*Band 7*
Band 1	21.86	-19.39	24.98	17.52	-11.79	-19.44	6.87
Band 2	-19.39	19.16	-23.20	-16.96	12.02	19.46	-6.31
Band 3	24.98	-23.20	31.25	21.48	-14.66	-23.80	7.58
Band 4	17.52	-16.96	21.48	21.89	-13.55	-25.50	6.35
Band 5	-11.79	12.02	-14.66	-13.55	10.49	16.15	-4.39
Band 6	-19.44	19.46	-23.80	-25.50	16.15	35.48	-7.12
Band 7	6.87	-6.31	7.58	6.35	-4.39	-7.12	5.72

Name of class = FOREST2 Number of points in sample = 1945

	Band 1	*Band 2*	*Band 3*	*Band 4*	*Band 5*	*Band 6*	*Band 7*
Min	43.00	122.00	142.00	54.00	140.00	98.00	137.00
Mean	46.39	145.35	149.59	56.57	155.10	142.73	138.33
Max	74.00	150.00	179.00	93.00	160.00	149.00	142.00

Covar	*Band 1*	*Band 2*	*Band 3*	*Band 4*	*Band 5*	*Band 6*	*Band 7*
Band 1	6.73	-6.66	7.96	4.67	-1.90	-5.27	1.15
Band 2	-6.66	8.56	-9.37	-5.18	2.73	6.66	-1.33
Band 3	7.96	-9.37	12.41	6.27	-2.98	-7.82	1.60
Band 4	4.67	-5.18	6.27	6.25	-2.68	-7.18	1.03
Band 5	-1.90	2.73	-2.98	-2.68	3.63	4.37	-.66
Band 6	-5.27	6.66	-7.82	-7.18	4.37	11.86	-1.18
Band 7	1.15	-1.33	1.60	1.03	-.66	-1.18	1.06

Name of class = UNSUP CLASS 3

	Band 1	*Band 2*	*Band 3*	*Band 4*	*Band 5*	*Band 6*	*Band 7*
Min	42.00	126.00	146.00	58.00	123.00	89.00	125.00
Mean	55.32	132.61	158.74	71.12	147.73	118.98	152.09
Max	59.00	149.00	175.00	97.00	174.00	133.00	180.00

Covar	*Band 1*	*Band 2*	*Band 3*	*Band 4*	*Band 5*	*Band 6*	*Band 7*
Band 1	11.33	-5.84	9.35	-1.41	-.32	4.63	-.18
Band 2	-5.84	13.56	-6.40	1.01	1.20	1.15	.59
Band 3	9.35	-6.40	36.26	-9.20	-3.18	10.78	-1.46
Band 4	-1.41	1.01	-9.20	28.99	3.12	-15.72	-9.25
Band 5	-.32	1.20	-3.18	3.12	29.52	6.53	-6.79
Band 6	4.63	1.15	10.78	-15.72	6.53	34.63	-7.10
Band 7	-.18	.59	-1.46	-9.25	-6.79	-7.10	43.78

Name of class = UNSUP CLASS 4

	Band 1	*Band 2*	*Band 3*	*Band 4*	*Band 5*	*Band 6*	*Band 7*
Min	42.00	126.00	146.00	18.00	137.00	115.00	125.00
Mean	51.91	136.68	157.51	62.03	150.74	130.99	146.72
Max	59.00	151.00	174.00	78.00	163.00	147.00	174.00

Covar	*Band 1*	*Band 2*	*Band 3*	*Band 4*	*Band 5*	*Band 6*	*Band 7*
Band 1	10.17	-7.66	9.11	2.67	-.35	-1.66	-.85
Band 2	-7.66	11.74	-9.06	-1.64	1.08	2.31	2.28
Band 3	9.11	-9.06	18.57	.77	-.43	-1.17	-2.34
Band 4	2.67	-1.64	.77	10.25	-.39	-5.85	-1.02
Band 5	-.35	1.08	-.43	-.39	8.53	1.75	.19
Band 6	-1.66	2.31	-1.17	-5.85	1.75	12.17	-3.08
Band 7	-.85	2.28	-2.34	-1.02	.19	-3.08	23.89

Name of class = UNSUP CLASS 5

	Band 1	*Band 2*	*Band 3*	*Band 4*	*Band 5*	*Band 6*	*Band 7*
Min	42.00	126.00	146.00	5.00	113.00	125.00	34.00
Mean	46.82	142.92	151.21	56.30	154.12	140.47	139.67
Max	59.00	153.00	167.00	69.00	169.00	159.00	161.00

Covar	*Band 1*	*Band 2*	*Band 3*	*Band 4*	*Band 5*	*Band 6*	*Band 7*
Band 1	4.06	-2.71	2.70	.54	-1.26	-.32	-1.13
Band 2	-2.71	6.73	-4.05	-1.05	2.93	3.20	-.16
Band 3	2.70	-4.05	5.62	.61	-2.36	-2.30	.03
Band 4	.54	-1.05	.61	8.11	.89	-3.98	3.05
Band 5	-1.26	2.93	-2.36	.89	8.21	3.03	.50
Band 6	-.32	3.20	-2.30	-3.98	3.03	10.68	-6.14
Band 7	-1.13	-.16	.03	3.05	.50	-6.14	17.15

Name of class = UNSUP CLASS 6

	Band 1	*Band 2*	*Band 3*	*Band 4*	*Band 5*	*Band 6*	*Band 7*
Min	42.00	126.00	146.00	37.00	137.00	107.00	104.00
Mean	49.97	138.04	154.41	61.46	159.59	136.74	139.40
Max	59.00	151.00	168.00	77.00	176.00	156.00	156.00

Covar	*Band 1*	*Band 2*	*Band 3*	*Band 4*	*Band 5*	*Band 6*	*Band 7*
Band 1	7.19	-3.56	3.73	.41	-3.19	1.09	-1.35
Band 2	-3.56	8.94	-3.20	-.13	1.46	.59	3.31
Band 3	3.73	-3.20	10.78	-1.84	-5.09	.05	-.12
Band 4	.41	-.13	-1.84	8.30	2.24	-2.16	-3.38
Band 5	-3.19	1.46	-5.09	2.24	24.94	4.07	1.72
Band 6	1.09	.59	.05	-2.16	4.07	10.97	-3.73
Band 7	-1.35	3.31	-.12	-3.38	1.72	-3.73	20.67

Name of class = UNSUP CLASS 7

	Band 1	*Band 2*	*Band 3*	*Band 4*	*Band 5*	*Band 6*	*Band 7*
Min	42.00	126.00	146.00	57.00	147.00	109.00	114.00
Mean	55.18	131.70	159.84	67.61	163.87	130.24	142.73
Max	59.00	146.00	175.00	88.00	175.00	143.00	166.00

Covar	*Band 1*	*Band 2*	*Band 3*	*Band 4*	*Band 5*	*Band 6*	*Band 7*
Band 1	7.75	-3.97	4.85	1.18	-1.81	-1.14	.08
Band 2	-3.97	9.72	-4.55	-1.12	.80	1.79	2.22
Band 3	4.85	-4.55	24.13	-5.80	-1.34	1.59	.43
Band 4	1.18	-1.12	-5.80	18.08	1.04	-10.21	-.90
Band 5	-1.81	.80	-1.34	1.04	21.94	3.48	4.36
Band 6	-1.14	1.79	1.59	-10.21	3.48	17.77	-6.67
Band 7	.08	2.22	.43	-.90	4.36	-6.67	27.50

Name of class = UNSUP CLASS 8

	Band 1	*Band 2*	*Band 3*	*Band 4*	*Band 5*	*Band 6*	*Band 7*
Min	42.00	126.00	146.00	61.00	160.00	123.00	85.00
Mean	54.21	131.43	157.61	70.10	177.29	136.55	137.41
Max	59.00	146.00	173.00	82.00	193.00	157.00	155.00

Covar	*Band 1*	*Band 2*	*Band 3*	*Band 4*	*Band 5*	*Band 6*	*Band 7*
Band 1	11.00	-6.93	7.83	2.89	2.30	-2.29	-.01
Band 2	-6.93	12.81	-6.84	-4.95	-2.17	2.12	3.75
Band 3	7.83	-6.84	24.59	-.39	6.41	-3.94	4.62
Band 4	2.89	-4.95	-.39	11.97	4.68	-2.58	-5.08
Band 5	2.30	-2.17	6.41	4.68	27.57	3.32	4.10
Band 6	-2.29	2.12	-3.94	-2.58	3.32	13.36	-7.05
Band 7	-.01	3.75	4.62	-5.08	4.10	-7.05	24.94

Name of class = CLASS 3 REFERENCE SITE Number of points in sample = 70

	Band 1	*Band 2*	*Band 3*	*Band 4*	*Band 5*	*Band 6*	*Band 7*
Min	50.00	128.00	155.00	64.00	137.00	112.00	151.00
Mean	55.31	132.07	161.81	69.44	144.97	123.59	154.19
Max	59.00	137.00	169.00	77.00	153.00	131.00	158.00

Covar	*Band 1*	*Band 2*	*Band 3*	*Band 4*	*Band 5*	*Band 6*	*Band 7*
Band 1	3.96	-3.29	3.97	2.35	-.79	-2.21	1.26
Band 2	-3.29	3.82	-4.13	-2.76	1.92	3.27	-1.45
Band 3	3.97	-4.13	7.35	.88	-3.35	-.92	1.02
Band 4	2.35	-2.76	.88	9.79	-2.40	-9.56	2.70
Band 5	-.79	1.92	-3.35	-2.40	8.00	2.05	-.37
Band 6	-2.21	3.27	-.92	-9.56	2.05	13.70	-3.74
Band 7	1.26	-1.45	1.02	2.70	-.37	-3.74	2.72

Name of class = CLASS 4 REFERENCE SITE Number of points in sample = 253

	Band 1	*Band 2*	*Band 3*	*Band 4*	*Band 5*	*Band 6*	*Band 7*
Min	45.00	131.00	151.00	56.00	145.00	126.00	146.00
Mean	50.11	137.43	156.95	59.35	150.43	131.92	150.58
Max	56.00	143.00	164.00	63.00	156.00	138.00	157.00

Covar	*Band 1*	*Band 2*	*Band 3*	*Band 4*	*Band 5*	*Band 6*	*Band 7*
Band 1	4.94	-4.09	5.64	1.99	-.13	-2.06	-.36
Band 2	-4.09	6.30	-6.03	-2.09	1.09	3.31	-.51
Band 3	5.64	-6.03	9.20	2.77	-.80	-3.59	-.34
Band 4	1.99	-2.09	2.77	2.57	-.94	-3.21	.14
Band 5	-.13	1.09	-.80	-.94	4.22	2.96	-.39
Band 6	-2.06	3.31	-3.59	-3.21	2.96	7.45	-1.46
Band 7	-.36	-.51	-.34	.14	-.39	-1.46	6.83

Name of class = CLASS 5 REFERENCE SITE Number of points in sample = 664

	Band 1	*Band 2*	*Band 3*	*Band 4*	*Band 5*	*Band 6*	*Band 7*
Min	43.00	141.00	146.00	54.00	152.00	134.00	137.00
Mean	45.12	146.38	148.48	55.53	155.51	143.44	137.69
Max	50.00	150.00	155.00	59.00	160.00	147.00	140.00

Covar	*Band 1*	*Band 2*	*Band 3*	*Band 4*	*Band 5*	*Band 6*	*Band 7*
Band 1	.66	-.32	.40	.19	.11	-.15	.12
Band 2	-.32	1.48	-.80	-.27	.47	.61	-.20
Band 3	.40	-.80	1.58	.27	-.37	-.60	.19
Band 4	.19	-.27	.27	.61	-.13	-.47	.00
Band 5	.11	.47	-.37	-.13	2.19	1.20	-.40
Band 6	-.15	.61	-.60	-.47	1.20	2.57	-.41
Band 7	.12	-.20	.19	.00	-.40	-.41	.48

Name of class = CLASS 6 REFERENCE SITE Number of points in sample = 467

	Band 1	*Band 2*	*Band 3*	*Band 4*	*Band 5*	*Band 6*	*Band 7*
Min	46.00	131.00	146.00	57.00	149.00	130.00	132.00
Mean	48.29	138.08	154.12	61.14	157.37	137.04	136.99
Max	55.00	143.00	160.00	66.00	169.00	143.00	141.00

Covar	*Band 1*	*Band 2*	*Band 3*	*Band 4*	*Band 5*	*Band 6*	*Band 7*
Band 1	1.65	-.71	1.25	.70	-1.18	-1.55	.81
Band 2	-.71	2.89	-2.22	-.47	-.43	1.43	-.51
Band 3	1.25	-2.22	4.60	.06	-2.18	-2.50	.98
Band 4	.70	-.47	.06	2.47	2.56	-.32	-.71
Band 5	-1.18	-.43	-2.18	2.56	14.12	5.21	-3.63
Band 6	-1.55	1.43	-2.50	-.32	5.21	6.40	-2.39
Band 7	.81	-.51	.98	-.71	-3.63	-2.39	3.29

Name of class = CLASS 8 REFERENCE SITE Number of points in sample = 133

	Band 1	*Band 2*	*Band 3*	*Band 4*	*Band 5*	*Band 6*	*Band 7*
Min	48.00	126.00	147.00	63.00	169.00	134.00	135.00
Mean	53.65	131.73	158.92	67.95	177.39	138.28	137.26
Max	59.00	137.00	169.00	73.00	186.00	142.00	139.00

Covar	*Band 1*	*Band 2*	*Band 3*	*Band 4*	*Band 5*	*Band 6*	*Band 7*
Band 1	7.33	-5.52	8.04	3.90	6.26	-.40	-.01
Band 2	-5.52	6.96	-7.57	-3.83	-6.27	.29	-.14
Band 3	8.04	-7.57	12.63	4.63	7.68	-.53	-.04
Band 4	3.90	-3.83	4.63	4.42	6.75	-.32	-.13
Band 5	6.26	-6.27	7.68	6.75	14.60	1.02	-.72
Band 6	-.40	.29	-.53	-.32	1.02	2.27	.03
Band 7	-.01	-.14	-.04	-.13	-.72	.03	.40

E2. **Spectral Signatures for Five Evergreen Classes on each Date**

Class 3, Date 1; 6 JUN 85 Number of points in sample = 70

	Band 1	*Band 2*	*Band 3*	*Band 4*	*Band 5*	*Band 6*	*Band 7*
Min	64.00	137.00	112.00	119.00	152.00	159.00	151.00
Mean	69.44	144.97	123.59	121.96	156.47	160.17	154.19
Max	77.00	153.00	131.00	125.00	160.00	162.00	158.00

Covar	*Band 1*	*Band 2*	*Band 3*	*Band 4*	*Band 5*	*Band 6*	*Band 7*
Band 1	9.79	-2.40	-9.56	.28	-3.07	.17	2.70
Band 2	-2.40	8.00	2.05	-.66	1.66	-.29	-.37
Band 3	-9.56	2.05	13.70	.14	3.17	-.01	-3.74
Band 4	.28	-.66	.14	1.24	.19	.17	-.10
Band 5	-3.07	1.66	3.17	.19	2.73	-.21	-.90
Band 6	.17	-.29	-.01	.17	-.21	.49	-.09
Band 7	2.70	-.37	-3.74	-.10	-.90	-.09	2.72

Class 3, Date 2; 21 MAR 86 Number of points in sample = 72

	Band 1	*Band 2*	*Band 3*	*Band 4*	*Band 5*	*Band 6*	*Band 7*
Min	50.00	128.00	155.00	121.00	158.00	159.00	89.00
Mean	55.31	132.07	161.83	127.69	159.75	160.62	89.47
Max	59.00	137.00	169.00	134.00	162.00	162.00	90.00

Covar	*Band 1*	*Band 2*	*Band 3*	*Band 4*	*Band 5*	*Band 6*	*Band 7*
Band 1	3.88	-3.23	3.90	3.66	-.37	.12	-.14
Band 2	-3.23	3.73	-4.08	-3.73	.25	-.05	-.03
Band 3	3.90	-4.08	7.21	4.84	-.55	.09	.04
Band 4	3.66	-3.73	4.84	5.97	.03	.06	-.08
Band 5	-.37	.25	-.55	.03	.79	-.13	-.08
Band 6	.12	-.05	.09	.06	-.13	.50	.00
Band 7	-.14	-.03	.04	-.08	-.08	.00	.25

Class 3, Date 3; 29 APR 86 Number of points in sample = 72

	Band 1	*Band 2*	*Band 3*	*Band 4*	*Band 5*	*Band 6*	*Band 7*
Min	58.00	137.00	124.00	120.00	156.00	158.00	131.00
Mean	61.18	139.53	131.51	123.36	158.92	159.65	132.78
Max	66.00	143.00	136.00	126.00	161.00	162.00	136.00

Covar	*Band 1*	*Band 2*	*Band 3*	*Band 4*	*Band 5*	*Band 6*	*Band 7*
Band 1	3.23	-.68	-4.04	-.29	-.47	.23	.73
Band 2	-.68	1.94	.38	-.16	.23	-.26	-.42
Band 3	-4.04	.38	7.92	.53	.05	-.28	-1.18
Band 4	-.29	-.16	.53	1.43	-.01	-.08	.07
Band 5	-.47	.23	.05	-.01	1.28	-.16	.07
Band 6	.23	-.26	-.28	-.08	-.16	.49	.20
Band 7	.73	-.42	-1.18	.07	.07	.20	1.03

Class 3, Date 4; 8 MAY 86 Number of points in sample = 72

	Band 1	*Band 2*	*Band 3*	*Band 4*	*Band 5*	*Band 6*	*Band 7*
Min	57.00	139.00	119.00	117.00	155.00	159.00	140.00
Mean	62.51	143.28	127.58	120.69	158.74	160.43	143.69
Max	69.00	148.00	134.00	123.00	162.00	162.00	148.00

Covar	*Band 1*	*Band 2*	*Band 3*	*Band 4*	*Band 5*	*Band 6*	*Band 7*
Band 1	4.81	-1.96	-5.09	.43	-1.65	-.15	.53
Band 2	-1.96	4.01	1.87	-1.24	1.16	.29	-.39
Band 3	-5.09	1.87	8.80	.48	1.89	.50	-2.30
Band 4	.43	-1.24	.48	2.26	.00	.10	-.42
Band 5	-1.65	1.16	1.89	.00	1.86	.02	-.34
Band 6	-.15	.29	.50	.10	.02	.58	-.24
Band 7	.53	-.39	-2.30	-.42	-.34	-.24	3.81

Class 3, Date 5; 24 MAY 86 Number of points in sample = 72

	Band 1	*Band 2*	*Band 3*	*Band 4*	*Band 5*	*Band 6*	*Band 7*
Min	63.00	137.00	121.00	118.00	155.00	159.00	147.00
Mean	66.93	143.11	128.10	123.19	158.24	160.28	150.40
Max	73.00	150.00	134.00	126.00	161.00	162.00	154.00

Covar	*Band 1*	*Band 2*	*Band 3*	*Band 4*	*Band 5*	*Band 6*	*Band 7*
Band 1	4.56	-1.78	-4.53	.64	-1.55	.26	.89
Band 2	-1.78	5.02	2.63	-1.41	1.43	.02	-.86
Band 3	-4.53	2.63	8.51	-.24	2.03	.07	-1.97
Band 4	.64	-1.41	-.24	1.85	-.44	.14	.22
Band 5	-1.55	1.43	2.03	-.44	1.45	.06	-.31
Band 6	.26	.02	.07	.14	.06	.59	-.02
Band 7	.89	-.86	-1.97	.22	-.31	-.02	2.73

Class 3, Date 6; 31 MAY 86 Number of points in sample = 70

	Band 1	*Band 2*	*Band 3*	*Band 4*	*Band 5*	*Band 6*	*Band 7*
Min	63.00	136.00	124.00	124.00	154.00	159.00	151.00
Mean	67.59	140.59	131.67	126.63	158.56	160.57	154.63
Max	74.00	147.00	139.00	129.00	162.00	162.00	159.00

Covar	*Band 1*	*Band 2*	*Band 3*	*Band 4*	*Band 5*	*Band 6*	*Band 7*
Band 1	5.13	-1.37	-6.03	.62	-1.34	.66	1.03
Band 2	-1.37	3.74	2.94	-.32	.48	-.07	-.13
Band 3	-6.03	2.94	9.49	-.74	1.67	-.44	-1.84
Band 4	.62	-.32	-.74	1.21	-.02	.03	.07
Band 5	-1.34	.48	1.67	-.02	1.59	-.13	-.36
Band 6	.66	-.07	-.44	.03	-.13	.51	-.09
Band 7	1.03	-.13	-1.84	.07	-.36	-.09	3.32

Class 3, Date 7; 15 OCT 86 Number of points in sample = 72

	Band 1	*Band 2*	*Band 3*	*Band 4*	*Band 5*	*Band 6*	*Band 7*
Min	30.00	150.00	133.00	97.00	159.00	158.00	101.00
Mean	33.32	152.24	137.10	99.65	160.65	159.03	101.54
Max	36.00	155.00	141.00	101.00	163.00	161.00	102.00

Covar	*Band 1*	*Band 2*	*Band 3*	*Band 4*	*Band 5*	*Band 6*	*Band 7*
Band 1	1.55	.54	-.86	-.10	-.07	.09	.36
Band 2	.54	1.40	.25	-.17	-.07	.05	.19
Band 3	-.86	.25	2.54	.37	-.24	-.07	-.12
Band 4	-.10	-.17	.37	.76	-.03	.11	-.02
Band 5	-.07	-.07	-.24	-.03	.74	.10	-.08
Band 6	.09	.05	-.07	.11	.10	.53	-.01
Band 7	.36	.19	-.12	-.02	-.08	-.01	.25

Class 3, Date 8; 2 DEC 86 Number of points in sample = 72

	Band 1	*Band 2*	*Band 3*	*Band 4*	*Band 5*	*Band 6*	*Band 7*
Min	22.00	146.00	137.00	90.00	158.00	159.00	78.00
Mean	23.86	147.79	138.87	92.65	160.43	159.63	78.85
Max	26.00	149.00	141.00	95.00	162.00	161.00	79.00

Covar	*Band 1*	*Band 2*	*Band 3*	*Band 4*	*Band 5*	*Band 6*	*Band 7*
Band 1	.59	-.03	-.04	.08	.07	.20	.05
Band 2	-.03	.61	.03	.00	.07	-.03	-.03
Band 3	-.04	.03	.59	.22	.01	.08	.00
Band 4	.08	.00	.22	1.09	.06	.09	.02
Band 5	.07	.07	.01	.06	.76	-.04	-.01
Band 6	.20	-.03	.08	.09	-.04	.30	.05
Band 7	.05	-.03	.00	.02	-.01	.05	.13

Class 3, Date 9; 11 MAY 87 Number of points in sample = 72

	Band 1	*Band 2*	*Band 3*	*Band 4*	*Band 5*	*Band 6*	*Band 7*
Min	57.00	140.00	106.00	115.00	153.00	159.00	127.00
Mean	61.22	144.14	124.44	117.43	158.15	160.18	129.64
Max	74.00	147.00	131.00	120.00	162.00	162.00	132.00

Covar	Band 1	Band 2	Band 3	Band 4	Band 5	Band 6	Band 7
Band 1	9.06	-2.49	-10.47	.60	-2.95	.31	1.36
Band 2	-2.49	3.02	2.77	-.10	.72	.09	.16
Band 3	-10.47	2.77	16.02	.12	3.73	-.38	-2.24
Band 4	.60	-.10	.12	1.25	-.20	-.07	.38
Band 5	-2.95	.72	3.73	-.20	1.97	-.17	-.64
Band 6	.31	.09	-.38	-.07	-.17	.74	.23
Band 7	1.36	.16	-2.24	.38	-.64	.23	1.87

Class 3, Date 10; 7 SEP 87 Number of points in sample = 72

	Band 1	*Band 2*	*Band 3*	*Band 4*	*Band 5*	*Band 6*	*Band 7*
Min	50.00	141.00	134.00	114.00	158.00	158.00	124.00
Mean	52.53	144.90	140.28	116.81	159.93	159.42	126.14
Max	56.00	150.00	145.00	119.00	163.00	161.00	128.00

Covar	*Band 1*	*Band 2*	*Band 3*	*Band 4*	*Band 5*	*Band 6*	*Band 7*
Band 1	1.75	-.03	-1.84	-.09	-.20	.17	.48
Band 2	-.03	3.61	1.34	.15	.46	-.34	-.39
Band 3	-1.84	1.34	5.74	.87	.62	-.06	-.99
Band 4	-.09	.15	.87	1.47	.21	-.03	-.33
Band 5	-.20	.46	.62	.21	1.03	-.07	-.09
Band 6	.17	-.34	-.06	-.03	-.07	.35	-.06
Band 7	.48	-.39	-.99	-.33	-.09	-.06	.96

Class 3, Date 11; 28 MAY 88 Number of points in sample = 72

	Band 1	*Band 2*	*Band 3*	*Band 4*	*Band 5*	*Band 6*	*Band 7*
Min	52.00	146.00	103.00	108.00	150.00	158.00	145.00
Mean	56.49	149.96	123.54	112.11	156.17	159.93	148.24
Max	65.00	159.00	132.00	115.00	159.00	161.00	153.00

Covar	*Band 1*	*Band 2*	*Band 3*	*Band 4*	*Band 5*	*Band 6*	*Band 7*
Band 1	5.33	-.70	-7.86	.28	-2.02	.34	1.83
Band 2	-.70	7.13	1.28	-.84	-.33	-.86	-.23
Band 3	-7.86	1.28	16.69	1.04	3.29	-.40	-4.47
Band 4	.28	-.84	1.04	1.57	.21	.15	-.47
Band 5	-2.02	-.33	3.29	.21	2.42	-.07	-.42
Band 6	.34	-.86	-.40	.15	-.07	.52	.26
Band 7	1.83	-.23	-4.47	-.47	-.42	.26	4.22

Class 4, Date 1; 6 JUN 85 Number of points in sample = 253

	Band 1	*Band 2*	*Band 3*	*Band 4*	*Band 5*	*Band 6*	*Band 7*
Min	56.00	145.00	126.00	116.00	156.00	158.00	146.00
Mean	59.35	150.43	131.92	118.71	159.34	160.18	150.58
Max	63.00	156.00	138.00	122.00	162.00	162.00	157.00

Covar	*Band 1*	*Band 2*	*Band 3*	*Band 4*	*Band 5*	*Band 6*	*Band 7*
Band 1	2.57	-.94	-3.21	-.02	-.21	-.15	.14
Band 2	-.94	4.22	2.96	-.10	.14	-.04	-.39
Band 3	-3.21	2.96	7.45	.25	.41	.21	-1.46
Band 4	-.02	-.10	.25	1.23	.21	.09	-.29
Band 5	-.21	.14	.41	.21	1.10	.02	-.07
Band 6	-.15	-.04	.21	.09	.02	.54	.28
Band 7	.14	-.39	-1.46	-.29	-.07	.28	6.83

Class 4, Date 2; 21 MAR 86 Number of points in sample = 257

	Band 1	*Band 2*	*Band 3*	*Band 4*	*Band 5*	*Band 6*	*Band 7*
Min	45.00	131.00	151.00	118.00	157.00	158.00	88.00
Mean	50.12	137.42	156.96	123.72	159.64	160.58	89.24
Max	56.00	143.00	164.00	129.00	162.00	163.00	91.00

Covar	*Band 1*	*Band 2*	*Band 3*	*Band 4*	*Band 5*	*Band 6*	*Band 7*
Band 1	4.92	-4.07	5.62	3.72	-.25	.36	-.47
Band 2	-4.07	6.27	-6.03	-4.48	.27	-.28	.60
Band 3	5.62	-6.03	9.14	5.18	-.43	.41	-.81
Band 4	3.72	-4.48	5.18	5.15	-.12	.41	-.53
Band 5	-.25	.27	-.43	-.12	.73	.01	.07
Band 6	.36	-.28	.41	.41	.01	.70	-.04
Band 7	-.47	.60	-.81	-.53	.07	-.04	.68

Class 4, Date 3; 29 APR 86 Number of points in sample = 257

	Band 1	*Band 2*	*Band 3*	*Band 4*	*Band 5*	*Band 6*	*Band 7*
Min	51.00	139.00	132.00	119.00	159.00	158.00	127.00
Mean	53.91	143.06	137.56	121.47	160.78	160.02	129.60
Max	57.00	147.00	142.00	124.00	164.00	162.00	135.00

Covar	*Band 1*	*Band 2*	*Band 3*	*Band 4*	*Band 5*	*Band 6*	*Band 7*
Band 1	1.29	.09	-1.46	-.04	.02	.10	.29
Band 2	.09	1.84	.49	-.39	.03	-.18	-.22
Band 3	-1.46	.49	4.37	.33	.15	-.14	-.54
Band 4	-.04	-.39	.33	1.32	.03	.17	-.13
Band 5	.02	.03	.15	.03	.82	.04	-.10
Band 6	.10	-.18	-.14	.17	.04	.51	.03
Band 7	.29	-.22	-.54	-.13	-.10	.03	2.78

Class 4, Date 4; 8 MAY 86 Number of points in sample = 257

	Band 1	*Band 2*	*Band 3*	*Band 4*	*Band 5*	*Band 6*	*Band 7*
Min	51.00	144.00	126.00	115.00	157.00	159.00	135.00
Mean	55.02	148.54	133.40	118.34	160.17	160.18	140.12
Max	59.00	155.00	140.00	122.00	163.00	162.00	148.00

Covar	*Band 1*	*Band 2*	*Band 3*	*Band 4*	*Band 5*	*Band 6*	*Band 7*
Band 1	2.12	-.36	-2.71	-.13	-.18	.18	.61
Band 2	-.36	3.08	1.72	-.28	.03	-.29	-.64
Band 3	-2.71	1.72	6.50	.59	.24	-.23	-1.02
Band 4	-.13	-.28	.59	1.52	.18	.06	-.16
Band 5	-.18	.03	.24	.18	1.08	-.11	-.16
Band 6	.18	-.29	-.23	.06	-.11	.47	.20
Band 7	.61	-.64	-1.02	-.16	-.16	.20	5.98

Class 4, Date 5; 24 MAY 86 Number of points in sample = 257

	Band 1	*Band 2*	*Band 3*	*Band 4*	*Band 5*	*Band 6*	*Band 7*
Min	55.00	144.00	126.00	116.00	158.00	158.00	141.00
Mean	58.52	148.84	134.08	119.60	160.03	160.31	146.03
Max	63.00	155.00	140.00	122.00	163.00	162.00	153.00

Covar	*Band 1*	*Band 2*	*Band 3*	*Band 4*	*Band 5*	*Band 6*	*Band 7*
Band 1	2.17	-.28	-2.41	.02	-.13	.13	.36
Band 2	-.28	4.28	1.73	-.90	.01	.12	-.37
Band 3	-2.41	1.73	5.73	.21	.19	-.04	-.88
Band 4	.02	-.90	.21	1.44	.00	.10	-.51
Band 5	-.13	.01	.19	.00	1.01	-.02	-.38
Band 6	.13	.12	-.04	.10	-.02	.60	-.15
Band 7	.36	-.37	-.88	-.51	-.38	-.15	5.63

Class 4, Date 6; 31 MAY 86 Number of points in sample = 253

	Band 1	*Band 2*	*Band 3*	*Band 4*	*Band 5*	*Band 6*	*Band 7*
Min	57.00	141.00	131.00	122.00	156.00	158.00	143.00
Mean	60.10	145.17	138.00	125.03	160.02	160.02	147.70
Max	64.00	152.00	143.00	128.00	163.00	162.00	153.00

Covar	*Band 1*	*Band 2*	*Band 3*	*Band 4*	*Band 5*	*Band 6*	*Band 7*
Band 1	1.91	-.36	-2.14	-.23	-.11	.00	.59
Band 2	-.36	3.50	1.47	.05	.01	-.22	-.35
Band 3	-2.14	1.47	5.31	1.03	.11	.02	-1.54
Band 4	-.23	.05	1.03	1.33	.03	.01	-.45
Band 5	-.11	.01	.11	.03	1.17	-.06	-.27
Band 6	.00	-.22	.02	.01	-.06	.75	.09
Band 7	.59	-.35	-1.54	-.45	-.27	.09	3.19

Class 4, Date 7; 15 OCT 86 Number of points in sample = 257

	Band 1	*Band 2*	*Band 3*	*Band 4*	*Band 5*	*Band 6*	*Band 7*
Min	30.00	148.00	131.00	97.00	158.00	157.00	100.00
Mean	32.05	152.93	138.25	99.37	160.67	159.48	101.35
Max	36.00	156.00	142.00	102.00	164.00	162.00	103.00

Covar	*Band 1*	*Band 2*	*Band 3*	*Band 4*	*Band 5*	*Band 6*	*Band 7*
Band 1	1.28	.39	-.52	-.08	-.11	-.16	.04
Band 2	.39	2.20	1.26	-.20	-.01	-.07	-.01
Band 3	-.52	1.26	3.01	.15	-.03	.09	.03
Band 4	-.08	-.20	.15	.90	.02	.08	-.02
Band 5	-.11	-.01	-.03	.02	1.04	.10	.02
Band 6	-.16	-.07	.09	.08	.10	.69	.00
Band 7	.04	-.01	.03	-.02	.02	.00	.28

Class 4, Date 8; 2 DEC 86 Number of points in sample = 257

	Band 1	*Band 2*	*Band 3*	*Band 4*	*Band 5*	*Band 6*	*Band 7*
Min	22.00	146.00	136.00	89.00	159.00	158.00	79.00
Mean	23.41	148.33	138.48	91.72	160.47	159.38	79.39
Max	25.00	150.00	141.00	94.00	162.00	161.00	81.00

Covar	*Band 1*	*Band 2*	*Band 3*	*Band 4*	*Band 5*	*Band 6*	*Band 7*
Band 1	.44	.08	-.07	.11	.04	.09	-.01
Band 2	.08	.75	-.25	-.19	-.03	-.10	.01
Band 3	-.07	-.25	.74	.03	.05	.11	-.04
Band 4	.11	-.19	.03	1.09	.00	.07	.06
Band 5	.04	-.03	.05	.00	.54	.08	.00
Band 6	.09	-.10	.11	.07	.08	.38	.00
Band 7	-.01	.01	-.04	.06	.00	.00	.27

Class 4, Date 9; 11 MAY 87 Number of points in sample = 257

	Band 1	*Band 2*	*Band 3*	*Band 4*	*Band 5*	*Band 6*	*Band 7*
Min	50.00	143.00	126.00	113.00	157.00	158.00	125.00
Mean	54.30	148.23	132.39	115.82	159.75	159.70	127.62
Max	59.00	153.00	138.00	119.00	162.00	161.00	131.00

Covar	*Band 1*	*Band 2*	*Band 3*	*Band 4*	*Band 5*	*Band 6*	*Band 7*
Band 1	2.54	-.51	-2.76	-.05	-.21	.32	.13
Band 2	-.51	2.07	1.59	-.02	.02	-.24	-.21
Band 3	-2.76	1.59	6.08	.22	.18	-.19	-.28
Band 4	-.05	-.02	.22	1.02	.08	-.01	.05
Band 5	-.21	.02	.18	.08	.93	-.02	-.11
Band 6	.32	-.24	-.19	-.01	-.02	.57	.00
Band 7	.13	-.21	-.28	.05	-.11	.00	1.89

Class 4, Date 10; 7 SEP 87 Number of points in sample = 257

	Band 1	*Band 2*	*Band 3*	*Band 4*	*Band 5*	*Band 6*	*Band 7*
Min	47.00	142.00	138.00	113.00	158.00	157.00	123.00
Mean	49.09	145.98	142.65	116.34	160.18	159.33	124.18
Max	51.00	153.00	147.00	119.00	163.00	161.00	128.00

Covar	*Band 1*	*Band 2*	*Band 3*	*Band 4*	*Band 5*	*Band 6*	*Band 7*
Band 1	.81	-.07	-.86	.07	.16	.14	.14
Band 2	-.07	2.33	.86	-.07	-.16	-.18	.12
Band 3	-.86	.86	2.76	.34	-.33	.05	.05
Band 4	.07	-.07	.34	1.29	.15	.03	-.09
Band 5	.16	-.16	-.33	.15	1.00	.08	.01
Band 6	.14	-.18	.05	.03	.08	.60	.09
Band 7	.14	.12	.05	-.09	.01	.09	1.24

Class 4, Date 11; 28 MAY 88 Number of points in sample = 257

	Band 1	*Band 2*	*Band 3*	*Band 4*	*Band 5*	*Band 6*	*Band 7*
Min	47.00	149.00	120.00	108.00	153.00	157.00	139.00
Mean	50.36	153.25	130.41	110.87	157.78	159.98	142.70
Max	56.00	161.00	136.00	114.00	162.00	162.00	151.00

Covar	*Band 1*	*Band 2*	*Band 3*	*Band 4*	*Band 5*	*Band 6*	*Band 7*
Band 1	1.78	-.29	-2.01	.54	-.39	-.03	.40
Band 2	-.29	3.41	1.79	-.58	.07	-.07	-.61
Band 3	-2.01	1.79	5.96	.00	.61	.19	-1.55
Band 4	.54	-.58	.00	1.39	-.06	.08	.24
Band 5	-.39	.07	.61	-.06	1.34	-.02	-.09
Band 6	-.03	-.07	.19	.08	-.02	.58	.02
Band 7	.40	-.61	-1.55	.24	-.09	.02	4.43

Class 5, Date 1; 6 JUN 85 Number of points in sample = 664

	Band 1	*Band 2*	*Band 3*	*Band 4*	*Band 5*	*Band 6*	*Band 7*
Min	54.00	152.00	134.00	117.00	156.00	157.00	137.00
Mean	55.53	155.51	143.44	119.85	159.20	159.55	137.69
Max	59.00	160.00	147.00	123.00	161.00	162.00	140.00

Covar	*Band 1*	*Band 2*	*Band 3*	*Band 4*	*Band 5*	*Band 6*	*Band 7*
Band 1	.61	-.13	-.47	.06	.00	.03	.00
Band 2	-.13	2.19	1.20	-.03	-.11	-.06	-.40
Band 3	-.47	1.20	2.57	.25	-.09	.08	-.41
Band 4	.06	-.03	.25	1.33	.04	.04	-.07
Band 5	.00	-.11	-.09	.04	.78	.02	.06
Band 6	.03	-.06	.08	.04	.02	.61	-.03
Band 7	.00	-.40	-.41	-.07	.06	-.03	.48

Class 5, Date 2; 21 MAR 86 Number of points in sample = 665

	Band 1	*Band 2*	*Band 3*	*Band 4*	*Band 5*	*Band 6*	*Band 7*
Min	43.00	141.00	146.00	114.00	158.00	158.00	87.00
Mean	45.12	146.38	148.48	117.71	159.95	159.97	89.56
Max	50.00	150.00	155.00	122.00	163.00	162.00	91.00

Covar	*Band 1*	*Band 2*	*Band 3*	*Band 4*	*Band 5*	*Band 6*	*Band 7*
Band 1	.66	-.32	.40	.48	.05	.08	.07
Band 2	-.32	1.47	-.80	-.72	-.05	-.17	-.08
Band 3	.40	-.80	1.59	.65	-.03	.18	-.03
Band 4	.48	-.72	.65	1.59	.08	.10	-.01
Band 5	.05	-.05	-.03	.08	.66	-.02	.02
Band 6	.08	-.17	.18	.10	-.02	.47	-.03
Band 7	.07	-.08	-.03	-.01	.02	-.03	.51

Class 5, Date 3; 29 APR 86 Number of points in sample = 665

	Band 1	Band 2	Band 3	Band 4	Band 5	Band 6	Band 7
Min	52.00	143.00	138.00	119.00	158.00	158.00	123.00
Mean	54.00	145.96	144.03	122.73	160.86	159.72	123.80
Max	56.00	149.00	148.00	126.00	164.00	161.00	126.00

Covar	Band 1	Band 2	Band 3	Band 4	Band 5	Band 6	Band 7
Band 1	.40	-.01	-.25	.09	.01	.07	.08
Band 2	-.01	1.02	.23	-.29	.00	-.12	-.08
Band 3	-.25	.23	1.38	.23	.04	.00	-.15
Band 4	.09	-.29	.23	1.30	.06	.02	-.02
Band 5	.01	.00	.04	.06	.88	.04	-.02
Band 6	.07	-.12	.00	.02	.04	.41	.02
Band 7	.08	-.08	-.15	-.02	-.02	.02	.43

Class 5, Date 4; 8 MAY 86 Number of points in sample = 665

	Band 1	Band 2	Band 3	Band 4	Band 5	Band 6	Band 7
Min	52.00	147.00	136.00	116.00	157.00	158.00	128.00
Mean	53.75	151.02	141.14	119.68	160.28	159.86	129.90
Max	57.00	155.00	144.00	123.00	163.00	162.00	133.00

Covar	Band 1	Band 2	Band 3	Band 4	Band 5	Band 6	Band 7
Band 1	.52	-.15	-.36	.07	-.06	.12	.11
Band 2	-.15	1.29	.46	-.18	.07	-.18	-.25
Band 3	-.36	.46	1.67	.09	.21	.01	-.31
Band 4	.07	-.18	.09	1.17	.04	.03	.05
Band 5	-.06	.07	.21	.04	.81	-.03	-.05
Band 6	.12	-.18	.01	.03	-.03	.49	.03
Band 7	.11	-.25	-.31	.05	-.05	.03	.58

Class 5, Date 5; 24 MAY 86 Number of points in sample = 665

	Band 1	Band 2	Band 3	Band 4	Band 5	Band 6	Band 7
Min	54.00	149.00	136.00	116.00	157.00	158.00	134.00
Mean	55.49	152.51	142.02	119.99	160.08	159.60	135.21
Max	59.00	155.00	145.00	124.00	163.00	162.00	138.00

Covar	Band 1	Band 2	Band 3	Band 4	Band 5	Band 6	Band 7
Band 1	.57	-.11	-.22	.07	.01	.03	-.02
Band 2	-.11	1.43	.57	-.16	.06	-.09	-.31
Band 3	-.22	.57	1.64	.20	.04	.06	-.16
Band 4	.07	-.16	.20	1.40	.05	.11	-.02
Band 5	.01	.06	.04	.05	1.01	.03	-.07
Band 6	.03	-.09	.06	.11	.03	.50	.08
Band 7	-.02	-.31	-.16	-.02	-.07	.08	.95

Class 5, Date 6; 31 MAY 86 Number of points in sample = 665

	Band 1	*Band 2*	*Band 3*	*Band 4*	*Band 5*	*Band 6*	*Band 7*
Min	55.00	144.00	138.00	120.00	157.00	158.00	138.00
Mean	57.00	148.73	145.70	125.28	160.19	159.87	139.94
Max	60.00	152.00	149.00	129.00	164.00	162.00	142.00

Covar	*Band 1*	*Band 2*	*Band 3*	*Band 4*	*Band 5*	*Band 6*	*Band 7*
Band 1	.62	-.15	-.04	.37	.00	-.02	-.09
Band 2	-.15	1.46	.41	-.48	-.02	-.01	-.02
Band 3	-.04	.41	1.78	.46	.01	-.04	-.28
Band 4	.37	-.48	.46	1.96	.07	.01	-.19
Band 5	.00	-.02	.01	.07	.85	-.05	-.02
Band 6	-.02	-.01	-.04	.01	-.05	.60	.01
Band 7	-.09	-.02	-.28	-.19	-.02	.01	.72

Class 5, Date 7; 15 OCT 86 Number of points in sample = 665

	Band 1	*Band 2*	*Band 3*	*Band 4*	*Band 5*	*Band 6*	*Band 7*
Min	30.00	154.00	138.00	96.00	156.00	157.00	101.00
Mean	31.98	156.68	142.43	98.86	160.25	159.21	102.04
Max	34.00	160.00	146.00	103.00	163.00	161.00	103.00

Covar	*Band 1*	*Band 2*	*Band 3*	*Band 4*	*Band 5*	*Band 6*	*Band 7*
Band 1	.49	.26	-.02	.04	-.01	.01	-.01
Band 2	.26	1.23	.22	-.15	-.10	-.12	-.15
Band 3	-.02	.22	1.14	.13	-.10	.07	-.09
Band 4	.04	-.15	.13	.99	-.03	-.03	-.01
Band 5	-.01	-.10	-.10	-.03	.91	.00	.06
Band 6	.01	-.12	.07	-.03	.00	.72	.05
Band 7	-.01	-.15	-.09	-.01	.06	.05	.50

Class 5, Date 8; 2 DEC 86 Number of points in sample = 665

	Band 1	*Band 2*	*Band 3*	*Band 4*	*Band 5*	*Band 6*	*Band 7*
Min	21.00	147.00	137.00	89.00	157.00	158.00	78.00
Mean	23.39	149.57	139.48	91.70	160.22	159.31	78.58
Max	25.00	153.00	145.00	95.00	162.00	161.00	80.00

Covar	*Band 1*	*Band 2*	*Band 3*	*Band 4*	*Band 5*	*Band 6*	*Band 7*
Band 1	.33	.05	-.05	.10	.04	.04	.00
Band 2	.05	.79	-.06	-.17	-.07	-.05	.00
Band 3	-.05	-.06	.76	.07	-.05	.05	.03
Band 4	.10	-.17	.07	.99	.08	-.03	.01
Band 5	.04	-.07	-.05	.08	.59	-.01	-.02
Band 6	.04	-.05	.05	-.03	-.01	.32	-.01
Band 7	.00	.00	.03	.01	-.02	-.01	.29

Class 5, Date 9; 11 MAY 87 Number of points in sample = 673

	Band 1	*Band 2*	*Band 3*	*Band 4*	*Band 5*	*Band 6*	*Band 7*
Min	49.00	150.00	135.00	112.00	157.00	157.00	118.00
Mean	51.55	153.28	139.53	115.86	159.91	159.23	119.29
Max	55.00	157.00	143.00	120.00	163.00	161.00	122.00

Covar	*Band 1*	*Band 2*	*Band 3*	*Band 4*	*Band 5*	*Band 6*	*Band 7*
Band 1	.58	.01	-.30	.23	-.02	.08	.07
Band 2	.01	1.54	.82	-.25	-.06	-.10	-.29
Band 3	-.30	.82	2.23	.18	-.05	.02	-.40
Band 4	.23	-.25	.18	1.26	.12	.11	.03
Band 5	-.02	-.06	-.05	.12	.83	.02	.09
Band 6	.08	-.10	.02	.11	.02	.42	.02
Band 7	.07	-.29	-.40	.03	.09	.02	.60

Class 5, Date 10; 7 SEP 87 Number of points in sample = 665

	Band 1	*Band 2*	*Band 3*	*Band 4*	*Band 5*	*Band 6*	*Band 7*
Min	46.00	148.00	145.00	114.00	148.00	157.00	118.00
Mean	47.87	151.43	149.96	116.19	159.69	159.18	119.03
Max	64.00	193.00	169.00	119.00	164.00	162.00	121.00

Covar	*Band 1*	*Band 2*	*Band 3*	*Band 4*	*Band 5*	*Band 6*	*Band 7*
Band 1	.99	1.69	.72	.18	-.42	.10	-.02
Band 2	1.69	5.11	2.15	-.25	-1.19	.26	-.07
Band 3	.72	2.15	1.78	.13	-.67	.15	-.05
Band 4	.18	-.25	.13	1.29	.04	.03	-.05
Band 5	-.42	-1.19	-.67	.04	.94	-.10	-.01
Band 6	.10	.26	.15	.03	-.10	.47	-.01
Band 7	-.02	-.07	-.05	-.05	-.01	-.01	.24

Class 5, Date 11; 28 MAY 88 Number of points in sample = 665

	Band 1	*Band 2*	*Band 3*	*Band 4*	*Band 5*	*Band 6*	*Band 7*
Min	46.00	150.00	122.00	108.00	153.00	158.00	131.00
Mean	48.19	154.80	135.24	110.55	158.38	160.17	132.67
Max	52.00	158.00	139.00	115.00	168.00	162.00	135.00

Covar	*Band 1*	*Band 2*	*Band 3*	*Band 4*	*Band 5*	*Band 6*	*Band 7*
Band 1	.49	-.02	-.41	.16	.10	.07	.02
Band 2	-.02	1.19	.44	-.30	.09	-.14	-.22
Band 3	-.41	.44	2.07	.27	-.15	.03	-.20
Band 4	.16	-.30	.27	1.66	.06	.17	-.09
Band 5	.10	.09	-.15	.06	1.37	-.06	-.03
Band 6	.07	-.14	.03	.17	-.06	.35	-.07
Band 7	.02	-.22	-.20	-.09	-.03	-.07	.41

Class 6, Date 1; 6 JUN 85 Number of points in sample = 467

	Band 1	*Band 2*	*Band 3*	*Band 4*	*Band 5*	*Band 6*	*Band 7*
Min	57.00	149.00	130.00	118.00	157.00	158.00	13_.00
Mean	61.14	157.37	137.04	121.26	159.55	159.66	136.9?
Max	66.00	169.00	143.00	125.00	162.00	162.00	141.00

Covar	*Band 1*	*Band 2*	*Band 3*	*Band 4*	*Band 5*	*Band 6*	*Band 7*
Band 1	2.47	2.56	-.32	.62	-.14	.19	-.71
Band 2	2.56	14.12	5.21	-.55	-.34	.31	-3.63
Band 3	-.32	5.21	6.40	.61	-.54	.25	-2.39
Band 4	.62	-.55	.61	1.97	.00	.14	-.49
Band 5	-.14	-.34	-.54	.00	.99	-.06	.17
Band 6	.19	.31	.25	.14	-.06	.54	-.17
Band 7	-.71	-3.63	-2.39	-.49	.17	-.17	3.29

Class 6, Date 2; 21 MAR 86 Number of points in sample = 475

	Band 1	*Band 2*	*Band 3*	*Band 4*	*Band 5*	*Band 6*	*Band 7*
Min	46.00	131.00	146.00	120.00	158.00	159.00	86.00
Mean	48.29	138.10	154.11	123.77	160.13	160.48	87.53
Max	55.00	143.00	160.00	129.00	163.00	162.00	89.00

Covar	*Band 1*	*Band 2*	*Band 3*	*Band 4*	*Band 5*	*Band 6*	*Band 7*
Band 1	1.64	-.73	1.26	1.02	-.12	.08	.04
Band 2	-.73	2.92	-2.29	-1.60	.16	-.04	.17
Band 3	1.26	-2.29	4.63	1.95	-.32	.02	-.29
Band 4	1.02	-1.60	1.95	2.42	-.06	.12	-.07
Band 5	-.12	.16	-.32	-.06	.66	.01	.03
Band 6	.08	-.04	.02	.12	.01	.46	.01
Band 7	.04	.17	-.29	-.07	.03	.01	.39

Class 6, Date 3; 29 APR 86 Number of points in sample = 475

	Band 1	*Band 2*	*Band 3*	*Band 4*	*Band 5*	*Band 6*	*Band 7*
Min	53.00	139.00	131.00	121.00	159.00	158.00	124.00
Mean	55.68	142.57	140.01	124.55	161.25	159.84	126.26
Max	60.00	146.00	144.00	128.00	164.00	162.00	130.00

Covar	*Band 1*	*Band 2*	*Band 3*	*Band 4*	*Band 5*	*Band 6*	*Band 7*
Band 1	1.02	.12	-.84	.19	-.10	-.03	.39
Band 2	.12	1.33	.45	-.26	-.08	-.13	-.19
Band 3	-.84	.45	3.19	.31	.04	.02	-.47
Band 4	.19	-.26	.31	1.46	.01	.14	.06
Band 5	-.10	-.08	.04	.01	.89	.02	-.03
Band 6	-.03	-.13	.02	.14	.02	.56	.01
Band 7	.39	-.19	-.47	.06	-.03	.01	1.26

Class 6, Date 4; 8 MAY 86 Number of points in sample = 475

	Band 1	Band 2	Band 3	Band 4	Band 5	Band 6	Band 7
Min	52.00	146.00	128.00	117.00	158.00	158.00	130.00
Mean	55.11	150.67	137.15	120.04	160.66	159.91	133.41
Max	60.00	161.00	142.00	123.00	164.00	162.00	139.00

Covar	Band 1	Band 2	Band 3	Band 4	Band 5	Band 6	Band 7
Band 1	1.47	.83	-.91	-.13	-.10	.08	.27
Band 2	.83	5.07	2.04	-.16	-.21	-.22	-1.50
Band 3	-.91	2.04	4.06	.41	-.22	-.07	-1.48
Band 4	-.13	-.16	.41	1.30	-.02	-.08	-.10
Band 5	-.10	-.21	-.22	-.02	1.17	-.07	.02
Band 6	.08	-.22	-.07	-.08	-.07	.51	.22
Band 7	.27	-1.50	-1.48	-.10	.02	.22	2.18

Class 6, Date 5; 24 MAY 86 Number of points in sample = 475

	Band 1	Band 2	Band 3	Band 4	Band 5	Band 6	Band 7
Min	56.00	148.00	131.00	117.00	158.00	158.00	134.00
Mean	58.56	154.63	138.10	121.14	160.41	159.92	138.30
Max	66.00	169.00	144.00	125.00	163.00	162.00	143.00

Covar	Band 1	Band 2	Band 3	Band 4	Band 5	Band 6	Band 7
Band 1	2.32	2.18	-.12	.30	-.28	.14	-.06
Band 2	2.18	11.45	4.34	-.07	-.97	-.22	-3.25
Band 3	-.12	4.34	5.40	.44	-.50	.05	-2.14
Band 4	.30	-.07	.44	1.47	-.04	.15	-.14
Band 5	-.28	-.97	-.50	-.04	.89	-.03	.26
Band 6	.14	-.22	.05	.15	-.03	.64	-.02
Band 7	-.06	-3.25	-2.14	-.14	.26	-.02	3.52

Class 6, Date 6; 31 MAY 86 Number of points in sample = 467

	Band 1	Band 2	Band 3	Band 4	Band 5	Band 6	Band 7
Min	58.00	143.00	135.00	122.00	157.00	157.00	137.00
Mean	60.39	149.61	141.88	125.93	160.63	159.46	141.68
Max	65.00	160.00	147.00	130.00	163.00	162.00	147.00

Covar	Band 1	Band 2	Band 3	Band 4	Band 5	Band 6	Band 7
Band 1	1.51	1.51	-.62	-.03	-.17	.02	.05
Band 2	1.51	11.08	3.94	-.20	-.36	.23	-4.18
Band 3	-.62	3.94	4.46	.30	-.09	.31	-2.47
Band 4	-.03	-.20	.30	1.62	.18	.02	-.14
Band 5	-.17	-.36	-.09	.18	1.12	-.01	.09
Band 6	.02	.23	.31	.02	-.01	.67	-.24
Band 7	.05	-4.18	-2.47	-.14	.09	-.24	3.57

Class 6, Date 7; 15 OCT 86 Number of points in sample = 475

	Band 1	Band 2	Band 3	Band 4	Band 5	Band 6	Band 7
Min	29.00	151.00	130.00	95.00	158.00	157.00	97.00
Mean	32.05	154.14	138.69	99.49	160.63	159.66	99.03
Max	42.00	159.00	142.00	103.00	164.00	162.00	101.00

Covar	Band 1	Band 2	Band 3	Band 4	Band 5	Band 6	Band 7
Band 1	2.54	1.06	-1.49	-.31	-.16	-.02	.53
Band 2	1.06	1.69	-.04	-.24	-.10	-.07	.20
Band 3	-1.49	-.04	2.57	.33	.09	-.03	-.44
Band 4	-.31	-.24	.33	1.22	-.02	.06	-.13
Band 5	-.16	-.10	.09	-.02	1.01	-.04	-.02
Band 6	-.02	-.07	-.03	.06	-.04	.69	-.04
Band 7	.53	.20	-.44	-.13	-.02	-.04	.62

Class 6, Date 8; 2 DEC 86 Number of points in sample = 475

	Band 1	Band 2	Band 3	Band 4	Band 5	Band 6	Band 7
Min	21.00	143.00	136.00	88.00	158.00	141.00	78.00
Mean	23.51	148.73	138.72	91.85	160.43	159.20	78.95
Max	27.00	152.00	143.00	95.00	163.00	162.00	81.00

Covar	Band 1	Band 2	Band 3	Band 4	Band 5	Band 6	Band 7
Band 1	.67	.18	-.19	-.04	.02	-.16	.03
Band 2	.18	1.00	-.32	-.08	.09	.38	.02
Band 3	-.19	-.32	.88	.05	-.03	-.37	-.05
Band 4	-.04	-.08	.05	1.16	-.11	.22	-.06
Band 5	.02	.09	-.03	-.11	.62	.01	.01
Band 6	-.16	.38	-.37	.22	.01	2.38	.00
Band 7	.03	.02	-.05	-.06	.01	.00	.24

Class 6, Date 9; 11 MAY 87 Number of points in sample = 103

	Band 1	Band 2	Band 3	Band 4	Band 5	Band 6	Band 7
Min	51.00	147.00	123.00	113.00	157.00	158.00	124.00
Mean	54.75	151.17	130.56	115.37	159.68	159.65	125.47
Max	61.00	154.00	136.00	118.00	161.00	161.00	131.00

Covar	Band 1	Band 2	Band 3	Band 4	Band 5	Band 6	Band 7
Band 1	3.00	.09	-2.87	.22	.05	.18	1.16
Band 2	.09	1.99	.37	.01	.17	-.43	.21
Band 3	-2.87	.37	5.95	.12	-.21	-.21	-.70
Band 4	.22	.01	.12	1.23	.06	-.05	-.01
Band 5	.05	.17	-.21	.06	.75	-.09	-.11
Band 6	.18	-.43	-.21	-.05	-.09	.47	.19
Band 7	1.16	.21	-.70	-.01	-.11	.19	3.14

Class 6, Date 10; 7 SEP 87 Number of points in sample = 475

	Band 1	*Band 2*	*Band 3*	*Band 4*	*Band 5*	*Band 6*	*Band 7*
Min	47.00	143.00	143.00	114.00	158.00	157.00	117.00
Mean	49.52	147.73	146.81	117.94	160.93	159.17	119.07
Max	54.00	153.00	151.00	121.00	163.00	161.00	121.00

Covar	*Band 1*	*Band 2*	*Band 3*	*Band 4*	*Band 5*	*Band 6*	*Band 7*
Band 1	.89	.66	-.36	-.07	.04	.16	.14
Band 2	.66	2.71	.43	-.29	-.08	-.03	-.34
Band 3	-.36	.43	1.82	.12	-.14	.01	-.15
Band 4	-.07	-.29	.12	1.03	.00	.00	-.03
Band 5	.04	-.08	-.14	.00	.90	-.05	.03
Band 6	.16	-.03	.01	.00	-.05	.52	.10
Band 7	.14	-.34	-.15	-.03	.03	.10	.90

Class 6, Date 11; 28 MAY 88 Number of points in sample = 475

	Band 1	*Band 2*	*Band 3*	*Band 4*	*Band 5*	*Band 6*	*Band 7*
Min	48.00	153.00	126.00	107.00	154.00	158.00	129.00
Mean	50.45	159.47	133.48	110.87	158.31	159.78	134.19
Max	56.00	171.00	141.00	116.00	161.00	162.00	140.00

Covar	*Band 1*	*Band 2*	*Band 3*	*Band 4*	*Band 5*	*Band 6*	*Band 7*
Band 1	1.54	1.50	-.49	.20	-.08	.10	.13
Band 2	1.50	11.28	4.48	-.48	-.18	-.15	-3.76
Band 3	-.49	4.48	4.76	.20	.15	-.04	-2.16
Band 4	.20	-.48	.20	1.73	.08	.05	.19
Band 5	-.08	-.18	.15	.08	1.27	-.01	-.11
Band 6	.10	-.15	-.04	.05	-.01	.48	.09
Band 7	.13	-3.76	-2.16	.19	-.11	.09	3.86

Class 8, Date 1; 6 JUN 85 Number of points in sample = 133

	Band 1	*Band 2*	*Band 3*	*Band 4*	*Band 5*	*Band 6*	*Band 7*
Min	63.00	169.00	134.00	117.00	155.00	158.00	135.00
Mean	67.95	177.39	138.28	119.17	158.59	159.74	137.26
Max	73.00	186.00	142.00	122.00	161.00	162.00	139.00

Covar	*Band 1*	*Band 2*	*Band 3*	*Band 4*	*Band 5*	*Band 6*	*Band 7*
Band 1	4.42	6.75	-.32	-.20	-.54	.19	-.13
Band 2	6.75	14.60	1.02	-.88	-1.48	.24	-.72
Band 3	-.32	1.02	2.27	.15	-.32	.15	.03
Band 4	-.20	-.88	.15	.93	.09	-.04	.16
Band 5	-.54	-1.48	-.32	.09	1.27	.00	.18
Band 6	.19	.24	.15	-.04	.00	.68	.02
Band 7	-.13	-.72	.03	.16	.18	.02	.40

Class 8, Date 2; 21 MAR 86 Number of points in sample = 135

	Band 1	*Band 2*	*Band 3*	*Band 4*	*Band 5*	*Band 6*	*Band 7*
Min	48.00	126.00	147.00	120.00	157.00	159.00	88.00
Mean	53.65	131.71	158.93	126.55	159.76	161.13	89.21
Max	59.00	137.00	169.00	132.00	162.00	163.00	91.00

Covar	*Band 1*	*Band 2*	*Band 3*	*Band 4*	*Band 5*	*Band 6*	*Band 7*
Band 1	7.35	-5.55	8.06	5.49	-.86	.35	-.22
Band 2	-5.55	6.98	-7.57	-5.49	.37	-.46	.26
Band 3	8.06	-7.57	12.58	7.25	-1.13	.62	-.26
Band 4	5.49	-5.49	7.25	6.79	-.56	.47	-.22
Band 5	-.86	.37	-1.13	-.56	.76	-.03	.04
Band 6	.35	-.46	.62	.47	-.03	.52	-.03
Band 7	-.22	.26	-.26	-.22	.04	-.03	.27

Class 8, Date 3; 29 APR 86 Number of points in sample = 135

	Band 1	*Band 2*	*Band 3*	*Band 4*	*Band 5*	*Band 6*	*Band 7*
Min	56.00	143.00	119.00	117.00	158.00	158.00	126.00
Mean	61.39	147.63	130.09	120.01	160.72	160.01	127.68
Max	67.00	152.00	139.00	124.00	163.00	161.00	129.00

Covar	*Band 1*	*Band 2*	*Band 3*	*Band 4*	*Band 5*	*Band 6*	*Band 7*
Band 1	4.82	1.16	-5.01	-.65	.09	-.06	.14
Band 2	1.16	5.25	1.71	-.89	.41	-.31	.42
Band 3	-5.01	1.71	10.11	.77	-.15	-.16	.26
Band 4	-.65	-.89	.77	1.32	.02	.18	-.14
Band 5	.09	.41	-.15	.02	1.01	.05	-.09
Band 6	-.06	-.31	-.16	.18	.05	.41	-.14
Band 7	.14	.42	.26	-.14	-.09	-.14	.76

Class 8, Date 4; 8 MAY 86 Number of points in sample = 135

	Band 1	*Band 2*	*Band 3*	*Band 4*	*Band 5*	*Band 6*	*Band 7*
Min	57.00	151.00	121.00	116.00	156.00	158.00	131.00
Mean	62.92	160.24	131.91	118.81	159.69	159.92	132.87
Max	69.00	172.00	141.00	122.00	162.00	162.00	136.00

Covar	*Band 1*	*Band 2*	*Band 3*	*Band 4*	*Band 5*	*Band 6*	*Band 7*
Band 1	5.59	7.11	-1.56	-.51	-.63	-.50	.30
Band 2	7.11	22.16	9.40	-.30	-.81	-1.68	-.69
Band 3	-1.56	9.40	13.43	.51	-.18	-.76	-.96
Band 4	-.51	-.30	.51	1.01	.12	.14	-.22
Band 5	-.63	-.81	-.18	.12	1.26	-.09	-.11
Band 6	-.50	-1.68	-.76	.14	-.09	.56	.01
Band 7	.30	-.69	-.96	-.22	-.11	.01	.96

Class 8, Date 5; 24 MAY 86 Number of points in sample = 135

	Band 1	*Band 2*	*Band 3*	*Band 4*	*Band 5*	*Band 6*	*Band 7*
Min	60.00	162.00	135.00	117.00	157.00	158.00	134.00
Mean	67.19	172.80	139.22	120.01	159.32	159.76	135.54
Max	73.00	183.00	143.00	123.00	162.00	161.00	137.00

Covar	*Band 1*	*Band 2*	*Band 3*	*Band 4*	*Band 5*	*Band 6*	*Band 7*
Band 1	5.46	9.44	.73	.82	-.65	.37	.18
Band 2	9.44	20.93	3.54	1.45	-1.74	.62	.59
Band 3	.73	3.54	2.87	.53	-.52	.17	.21
Band 4	.82	1.45	.53	1.61	-.24	.17	.08
Band 5	-.65	-1.74	-.52	-.24	.94	-.03	-.11
Band 6	.37	.62	.17	.17	-.03	.50	.04
Band 7	.18	.59	.21	.08	-.11	.04	.54

Class 8, Date 6; 31 MAY 86 Number of points in sample = 133

	Band 1	*Band 2*	*Band 3*	*Band 4*	*Band 5*	*Band 6*	*Band 7*
Min	63.00	156.00	139.00	122.00	157.00	158.00	136.00
Mean	67.46	167.14	142.46	125.16	159.56	160.36	137.97
Max	72.00	174.00	147.00	129.00	162.00	162.00	143.00

Covar	*Band 1*	*Band 2*	*Band 3*	*Band 4*	*Band 5*	*Band 6*	*Band 7*
Band 1	3.83	5.87	-.22	.49	-.48	.04	.14
Band 2	5.87	11.65	.54	.45	-.90	.26	-.11
Band 3	-.22	.54	2.36	.16	-.30	.20	-.03
Band 4	.49	.45	.16	1.63	-.15	.24	.06
Band 5	-.48	-.90	-.30	-.15	1.04	-.03	.04
Band 6	.04	.26	.20	.24	-.03	.68	-.01
Band 7	.14	-.11	-.03	.06	.04	-.01	.95

Class 8, Date 7; 15 OCT 86 Number of points in sample = 135

	Band 1	*Band 2*	*Band 3*	*Band 4*	*Band 5*	*Band 6*	*Band 7*
Min	33.00	151.00	126.00	94.00	157.00	159.00	102.00
Mean	38.20	154.40	134.71	97.36	161.30	160.08	102.42
Max	45.00	158.00	138.00	101.00	163.00	162.00	103.00

Covar	*Band 1*	*Band 2*	*Band 3*	*Band 4*	*Band 5*	*Band 6*	*Band 7*
Band 1	4.72	1.40	-2.28	-1.05	.35	.29	-.12
Band 2	1.40	2.07	.29	-.44	-.27	-.02	.06
Band 3	-2.28	.29	4.18	.68	-.62	-.21	.25
Band 4	-1.05	-.44	.68	1.28	-.19	-.10	.07
Band 5	.35	-.27	-.62	-.19	.97	-.02	-.08
Band 6	.29	-.02	-.21	-.10	-.02	.39	-.02
Band 7	-.12	.06	.25	.07	-.08	-.02	.24

Class 8, Date 8; 2 DEC 86 Number of points in sample = 135

	Band 1	Band 2	Band 3	Band 4	Band 5	Band 6	Band 7
Min	23.00	145.00	134.00	90.00	158.00	158.00	77.00
Mean	24.68	147.41	137.64	92.24	160.64	160.04	77.73
Max	27.00	150.00	140.00	95.00	162.00	161.00	78.00

Covar	Band 1	Band 2	Band 3	Band 4	Band 5	Band 6	Band 7
Band 1	.51	.02	-.37	.06	.02	.06	-.01
Band 2	.02	.74	-.09	-.06	-.01	-.08	.09
Band 3	-.37	-.09	1.38	-.03	.17	.08	.04
Band 4	.06	-.06	-.03	1.20	.03	-.01	.00
Band 5	.02	-.01	.17	.03	.68	.01	-.05
Band 6	.06	-.08	.08	-.01	.01	.35	.01
Band 7	-.01	.09	.04	.00	-.05	.01	.20

Class 8, Date 9; 11 MAY 87 Number of points in sample = 94

	Band 1	Band 2	Band 3	Band 4	Band 5	Band 6	Band 7
Min	53.00	145.00	116.00	112.00	156.00	158.00	128.00
Mean	58.74	150.18	124.34	114.59	159.23	159.90	130.07
Max	65.00	157.00	132.00	118.00	162.00	161.00	133.00

Covar	Band 1	Band 2	Band 3	Band 4	Band 5	Band 6	Band 7
Band 1	6.32	2.59	-6.56	.02	-.71	.20	-.29
Band 2	2.59	7.78	2.23	-.03	.00	-.19	-.73
Band 3	-6.56	2.23	13.48	.22	1.05	-.09	.25
Band 4	.02	-.03	.22	1.05	.01	.02	-.18
Band 5	-.71	.00	1.05	.01	1.06	.00	.12
Band 6	.20	-.19	-.09	.02	.00	.58	.03
Band 7	-.29	-.73	.25	-.18	.12	.03	1.22

Class 8, Date 10; 7 SEP 87 Number of points in sample = 135

	Band 1	Band 2	Band 3	Band 4	Band 5	Band 6	Band 7
Min	51.00	151.00	139.00	114.00	158.00	158.00	120.00
Mean	54.83	156.87	143.07	117.13	160.37	159.62	120.24
Max	58.00	162.00	146.00	119.00	163.00	161.00	121.00

Covar	Band 1	Band 2	Band 3	Band 4	Band 5	Band 6	Band 7
Band 1	2.14	2.37	-1.12	-.25	.11	-.13	.07
Band 2	2.37	4.11	-.84	-.49	-.01	-.19	.01
Band 3	-1.12	-.84	2.38	.29	-.35	.13	-.01
Band 4	-.25	-.49	.29	1.03	-.02	.06	-.06
Band 5	.11	-.01	-.35	-.02	.75	.05	.00
Band 6	-.13	-.19	.13	.06	.05	.47	.00
Band 7	.07	.01	-.01	-.06	.00	.00	.19

Class 8, Date 11; 28 MAY 88 Number of points in sample = 135

	Band 1	*Band 2*	*Band 3*	*Band 4*	*Band 5*	*Band 6*	*Band 7*
Min	56.00	170.00	129.00	107.00	148.00	158.00	130.00
Mean	60.39	177.44	134.47	110.21	156.41	159.75	131.67
Max	65.00	187.00	149.00	114.00	160.00	161.00	135.00

Covar	*Band 1*	*Band 2*	*Band 3*	*Band 4*	*Band 5*	*Band 6*	*Band 7*
Band 1	5.39	8.15	.61	.24	-1.17	.13	.48
Band 2	8.15	17.00	4.27	-.64	-2.58	.20	1.20
Band 3	.61	4.27	7.07	.15	-2.22	.27	.86
Band 4	.24	-.64	.15	1.95	-.12	.10	-.13
Band 5	-1.17	-2.58	-2.22	-.12	2.95	-.15	-.26
Band 6	.13	.20	.27	.10	-.15	.49	.19
Band 7	.48	1.20	.86	-.13	-.26	.19	1.49

DISTRIBUTION LIST

DNA-TR-92-37-V1

DEPARTMENT OF DEFENSE

ARMED FORCES RADIOBIOLOGY RSCH INST
ATTN: DEPT OF RADIATION BIOCHEMISTRY
ATTN: BHS
ATTN: DIRECTOR
ATTN: EXH
ATTN: MRA
ATTN: PHY M WHITNALL
ATTN: RSD
ATTN: SCIENTIFIC DIRECTOR
ATTN: TECHNICAL LIBRARY

ASSISTANT SECRETARY OF DEFENSE
INTERNATIONAL SECURITY POLICY
ATTN: NUC FORCES & ARMS CONTROL PLCY

ASSISTANT TO THE SECRETARY OF DEFENSE
ATTN: EXECUTIVE ASSISTANT
ATTN: MIL APPL C FIELD

DEFENSE INTELLIGENCE AGENCY
ATTN: DB
5 CY ATTN: DB-4 RSCH RESOURCES DIV
ATTN: DB-5C
ATTN: DB-6B
ATTN: DB-6E
ATTN: DIW-4
ATTN: DN
ATTN: DT
ATTN: OFFICE OF SECURITY
ATTN: OS

DEFENSE INTELLIGENCE COLLEGE
ATTN: DIC/RTS-2
ATTN: DIC/2C

DEFENSE NUCLEAR AGENCY
ATTN: DFRA JOAN MA PIERRE
ATTN: NANF
ATTN: NASF
10 CY ATTN: RAEM
2 CY ATTN: TITL

DEFENSE SYSTEMS SUPPORT ORGANIZATION
ATTN: JNGO

DEFENSE TECHNICAL INFORMATION CENTER
2 CY ATTN: DTIC/OC

FIELD COMMAND DEFENSE NUCLEAR AGENCY
ATTN: FCPR
ATTN: FCPRT

FIELD COMMAND DEFENSE NUCLEAR AGENCY
ATTN: FCTO

NATIONAL DEFENSE UNIVERSITY
ATTN: ICAF TECH LIB
ATTN: NWCLB-CR
ATTN: LIBRARY
ATTN: STRAT CONCEPTS DIV CTR

NET ASSESSMENT
ATTN: DOCUMENT CONTROL

OASD
ATTN: DUSP/P
ATTN: USD/P

OFC OF MILITARY PERFORMANCE
ASSESSMENT TECHNOLOGY
2 CY ATTN: F HEGGE

STRATEGIC & SPACE SYSTEMS
ATTN: DR SCHNEITER

U S EUROPEAN COMMAND/ECJ-6-DT
ATTN: ECJ-6

U S EUROPEAN COMMAND/ECJ2-T
ATTN: ECJ-3
ATTN: ECJ2-T
ATTN: ECJ5-N
ATTN: ECJ5N

USSSTRATCOM/J531T
ATTN: J-521
ATTN: JPEP

3416TH TTS INTERSERVICE NUC WPNS SCHOOL
ATTN: TTV
2 CY ATTN: TTV 3416TH TTSQ

DEPARTMENT OF THE ARMY

ARMY RESEARCH LABORATORIES
ATTN: TECH LIB

COMBAT MATERIAL EVAL ELEMENT
ATTN: SECURITY ANALYST

DEP CH OF STAFF FOR OPS & PLANS
ATTN: DAMO-SWN
ATTN: DAMO-ZXA

NUCLEAR EFFECTS DIVISION
ATTN: STEWS-NE-T

TEXCOM
ATTN: D PACE

U S ARMY AIR DEFENSE ARTILLERY SCHOOL
ATTN: COMMANDANT

U S ARMY ARMOR SCHOOL
ATTN: ATSB-CTD
ATTN: TECH LIBRARY

U S ARMY BALLISTIC RESEARCH LAB
ATTN: AMSRL-SL-BS DR KLOPCIC
ATTN: AMSRL-SL-BS E DAVIS
ATTN: SLCBR-D
ATTN: SLCBR-DD-T
ATTN: SLCBR-TB

U S ARMY CHEMICAL SCHOOL
ATTN: CRAL FRAKER

U S ARMY COMBAT SYSTEMS TEST ACTIVITY
ATTN: JOHN GERDES
ATTN: MIKE STANKA

U S ARMY COMD & GENERAL STAFF COLLEGE
ATTN: ATZL-SWJ-CA
ATTN: ATZL-SWT-A

U S ARMY CONCEPTS ANALYSIS AGENCY
ATTN: TECHNICAL LIBRARY

U S ARMY FIELD ARTILLERY SCHOOL
ATTN: ATSF-CD

U S ARMY FORCES COMMAND
ATTN: AF-OPTS

U S ARMY FOREIGN SCIENCE & TECH CTR
ATTN: C WARD

U S ARMY INFANTRY CENTER
ATTN: ATSH-CD-CSO

U S ARMY ITAC
ATTN: IAX-Z

U S ARMY LABORATORY COMMAND
ATTN: DIRECTOR
ATTN: DR D HODGE

U S ARMY NUCLEAR & CHEMICAL AGENCY
4 CY ATTN: MONA-NU DR D BASH
ATTN: MONA-NU MAJ BLISS

U S ARMY TEST & EVALUATION COMMAND
ATTN: STECS-NE

U S ARMY VULNERABILITY/LETHALITY
ATTN: AMSLC-VL-NE DR J FEENEY

U S ARMY WAR COLLEGE
ATTN: LIBRARY
ATTN: STRATEGIC STUDIES INSTITUTE

U S MILITARY ACADEMY
ATTN: DEPT BEHAVORIAL SCI & LEADERSHIP
ATTN: COL J G CAMPBELL
ATTN: SCIENCE RESEARCH LAB

US ARMY MATERIEL SYS ANALYSIS ACTVY
ATTN: DRXSY-DS

US ARMY MEDICAL RESEARCH &
DEVELOPMENT COMMAND
ATTN: SGRD-PLE

US ARMY MODEL IMPROVEMENT STUDY
MANAGEMENT AGENCY
ATTN: E VISCO

WALTER REED ARMY MEDICAL CENTER
ATTN: G RIPPLE

DEPARTMENT OF THE NAVY

MARINE CORPS
ATTN: CODE PPO
ATTN: PSI G RASP

NAVAL OCEAN SYSTEMS CENTER
ATTN: CODE 9642-B

NAVAL PERSONNEL RES & DEV CENTER
ATTN: CODE P302

NAVAL POSTGRADUATE SCHOOL
ATTN: CODE 52 LIBRARY

NAVAL RESEARCH LABORATORY
ATTN: CODE 1240
ATTN: CODE 5227

NAVAL SEA SYSTEMS COMMAND
ATTN: PMS-423
ATTN: SEA-07R

NAVAL SURFACE WARFARE CENTER
ATTN: CODE F-31
ATTN: G RIEL

NAVAL TECHNICAL INTELLIGENCE CTR
ATTN: NTIC-DA30

NAVAL WAR COLLEGE
ATTN: CODE E-11
ATTN: CTR FOR NAV WARFARE STUDIES
ATTN: DOCUMENT CONTROL
ATTN: LIBRARY
ATTN: STRATEGY DEPT

NAWCWPNSDIV DETACHMENT
ATTN: CLASSIFIED LIBRARY

NUCLEAR WEAPONS TNG GROUP ATLANTIC
ATTN: CODE 222
ATTN: DOCUMENT CONTROL

NUCLEAR WEAPONS TNG GROUP PACIFIC
ATTN: CODE 32

OPERATIONAL TEST & EVALUATION FORCE
ATTN: COMMANDER

PLANS, POLICY & OPERATIONS
ATTN: CODE-P
ATTN: CODE-POC-30

STRATEGY AND POLICY DIVISION
ATTN: N 51
ATTN: NIS-22
ATTN: NOP 50
ATTN: NOP 603
ATTN: NOP 91
ATTN: NUC AFFAIRS & INT'L NEGOT BR
ATTN: N455

DEPARTMENT OF THE AIR FORCE

AFIS/INT
ATTN: INT

AIR UNIVERSITY
ATTN: STRATEGIC STUDIES

AIR UNIVERSITY LIBRARY
ATTN: AUL-LSE
ATTN: LIBRARY

ARMSTRONG LABORATORY
ATTN: AL/CFBE DR F S KNOX

ASSISTANT CHIEF OF STAFF
ATTN: AFSAA/SAMI

DEPUTY CHIEF OF STAFF FOR PLANS & OPERS
ATTN: AFXOOSS

HQ ACC/XP-JSG
ATTN: ACC/XP-JSG

HQ USAFA/DFSELD
ATTN: LIBRARY

NATIONAL AIR INTELLIGENCE CENTER
ATTN: CCN
ATTN: SDA

USAF NUCLEAR CRITERIA GROUP SERETARIAT
ATTN: AFWL/NTN R SUDER

DEPARTMENT OF ENERGY

DEPARTMENT OF ENERGY
ATTN: DR T JONES

DPEARTMENT OF ENERGY
ATTN: B SANTORO
ATTN: G KERR
ATTN: J WHITE
ATTN: W RHOADES

LAWRENCE LIVERMORE NATIONAL LAB
ATTN: A WARSHAWSKY
ATTN: Z DIVISION LIBRARY

LOS ALAMOS NATIONAL LABORATORY
ATTN: D STROTTMAN
ATTN: REPORT LIBRARY

SANDIA NATIONAL LABORATORIES
ATTN: TECH LIB 3141

OTHER GOVERNMENT

CENTRAL INTELLIGENCE AGENCY
ATTN: COUNTER-TERRORIST GROUP
ATTN: DIRECTOR OF SECURITY
ATTN: MEDICAL SERVICES
ATTN: NIO-T
ATTN: N1O STRATEGIC SYS

FEDERAL EMERGENCY MANAGEMENT AGENCY
ATTN: CIVIL SECURITY DIVISION
ATTN: NP-CP
ATTN: OFC OF CIVIL DEFENSE

U S DEPARTMENT OF STATE
ATTN: PM/STM

U S NUCLEAR REGULATORY COMMISSION
ATTN: DIR DIV OF SAFEGUARDS
ATTN: S YANIV

DEPARTMENT OF DEFENSE CONTRACTORS

ARES CORP
2 CY ATTN: A DEVERILL

ARI
ATTN: JOHN LOCKHART

EAI CORPORATION
ATTN: MILLARD MERSHON
ATTN: DENNIS METZ
ATTN: KRISTIN GAVLINSKI

FULTON FINDINGS
ATTN: WES FULTON

HORIZONS TECHNOLOGY INC
ATTN: F GREY

HORIZONS TECHNOLOGY, INC
ATTN: J MARSHALL-MIES

INSTITUTE FOR DEFENSE ANALYSES
ATTN: DOUGLAS SCHULTZ
ATTN: J ORLANSKY
ATTN: M FINEBERG

JAYCOR
ATTN: CYRUS P KNOWLES

KAMAN SCIENCES CORP
ATTN: DASIAC

KAMAN SCIENCES CORPORATION
ATTN: R STOHLER

KAMAN SCIENCES CORPORATION
ATTN: DASIAC

LOCKHEED MISSILES & SPACE CO, INC
ATTN: WE-YOUNG WOO

LOGICON R & D ASSOCIATES
ATTN: DOCUMENT CONTROL
ATTN: DOUGLAS C YOON

LOGICON R & D ASSOCIATES
ATTN: S WOODFORD

MASSACHUSETTS INSTITUTE OF TECHNOLOGY
ATTN: DUNCAN C MILLTER

MICRO ANALYSIS AND DESIGN
ATTN: N LAVINE
ATTN: R LAUGHERY
ATTN: T ROTH

PACIFIC-SIERRA RESEARCH CORP
2 CY ATTN: F W WHICKER
2 CY ATTN: G ANNO
20 CY ATTN: G E MCCLELLAN
ATTN: H BRODE

PACIFIC-SIERRA RESEARCH CORP
ATTN: D GORMLEY
2 CY ATTN: G MCCLELLAN

PSYCHOLOGICAL RESEARCH CENTER
ATTN: L GAMACHE

SCIENCE APPLICATIONS INTL CORP
ATTN: D KAUL
ATTN: E SWICK
ATTN: L HUNT
ATTN: R J BEYSTER
ATTN: W WOOLSON

SCIENCE APPLICATIONS INTL CORP
ATTN: J MCGAHAN
ATTN: J PETERS
ATTN: P VERSTEEGEN
ATTN: W LAYSON

SCIENCE APPLICATIONS INTL CORP
ATTN: R CRAVER

TECHNICO SOUTHWEST INC
ATTN: S LEVIN

TRW INC
ATTN: TIC

TRW OGDEN ENGINEERING OPERATIONS
ATTN: D C RICH

TRW S I G
ATTN: DR BRUCE WILSON

UNIVERSITY OF CINCINNATI MEDICAL CENTER
ATTN: E SILBERSTEIN

DIRECTORY OF OTHER

UNIV OF ILLINOIS-WILLIARD AIRPORT
ATTN: H L TAYLOR